University of Groningen

Modelling of optical response properties

Jensen, Lasse

IMPORTANT NOTE: You are advised to consult the publisher's version (publisher's PDF) if you wish to cite from it. Please check the document version below.

Document Version
Publisher's PDF, also known as Version of record

Publication date:
2004

Link to publication in University of Groningen/UMCG research database

Citation for published version (APA):
Jensen, L. (2004). *Modelling of optical response properties: Application to nanostructures*. s.n.

Copyright
Other than for strictly personal use, it is not permitted to download or to forward/distribute the text or part of it without the consent of the author(s) and/or copyright holder(s), unless the work is under an open content license (like Creative Commons).

The publication may also be distributed here under the terms of Article 25fa of the Dutch Copyright Act, indicated by the "Taverne" license. More information can be found on the University of Groningen website: https://www.rug.nl/library/open-access/self-archiving-pure/taverne-amendment.

Take-down policy
If you believe that this document breaches copyright please contact us providing details, and we will remove access to the work immediately and investigate your claim.

Downloaded from the University of Groningen/UMCG research database (Pure): http://www.rug.nl/research/portal. For technical reasons the number of authors shown on this cover page is limited to 10 maximum.

Download date: 06-06-2022

Modelling of Optical Response Properties:

Application to Nanostructures

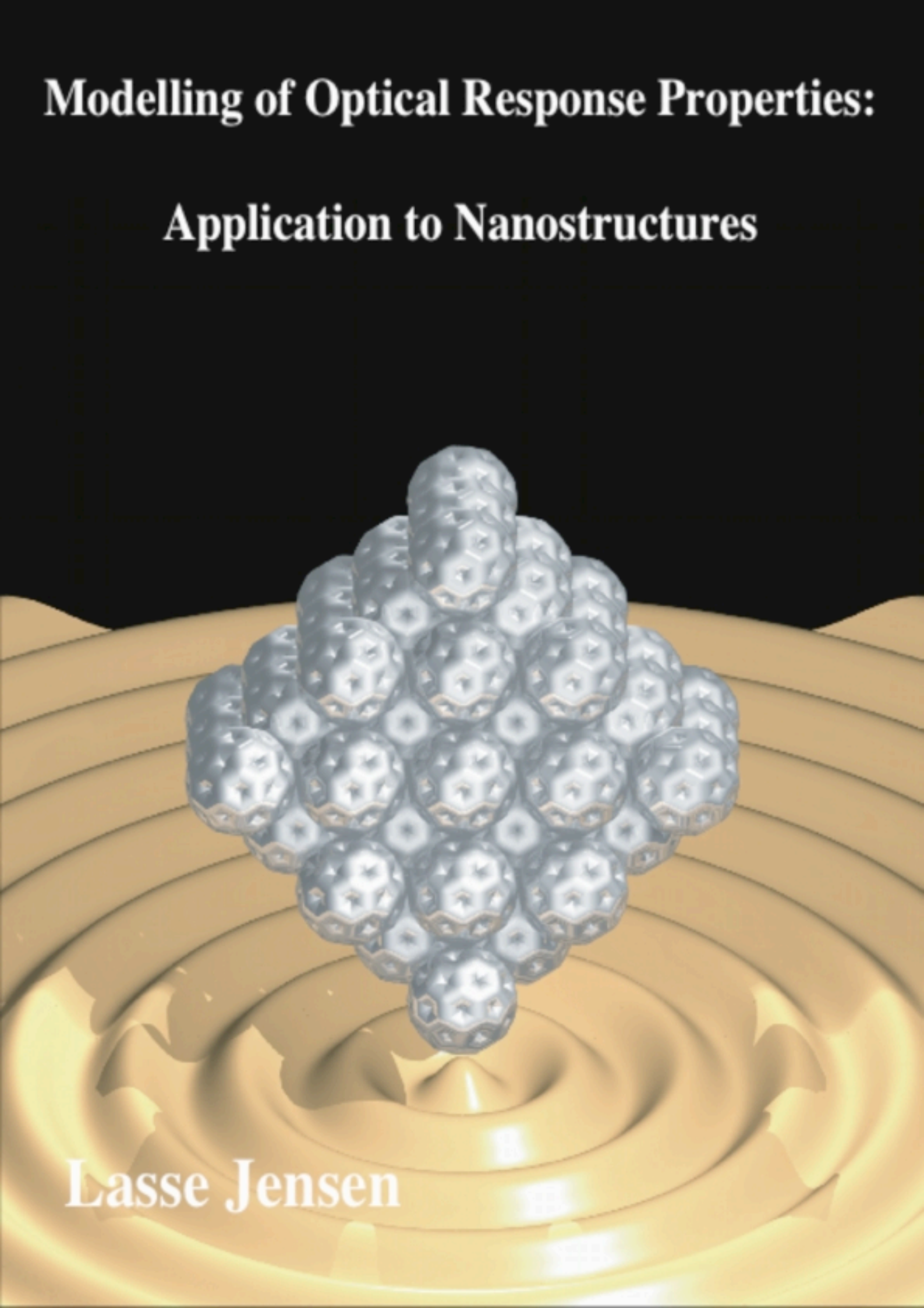

Lasse Jensen

Modelling of optical response properties: Application to nanostructures

Lasse Jensen

Front cover: Structure of a face-centered cubic cluster of 63 C_{60} molecules. (Chapter 7)

The work described in this thesis was performed in the Theoretical Chemistry Group of the Materials Science Centre at the University of Groningen, Nijenborgh 4, 9747 AG Groningen, The Netherlands.

Lasse Jensen,

Modelling of optical response properties: Application to nanostructures,

Proefschrift Rijksuniversiteit Groningen.

© L. Jensen, 2004

RIJKSUNIVERSITEIT GRONINGEN

Modelling of optical response properties: Application to nanostructures

PROEFSCHRIFT

ter verkrijging van het doctoraat in de
Wiskunde en Natuurwetenschappen
aan de Rijksuniversiteit Groningen
op gezag van de
Rector Magnificus, dr. F. Zwarts,
in het openbaar te verdedigen op
vrijdag 13 februari 2004
om 14.45 uur

door

Lasse Jensen

geboren op 10 september 1974
te Gentofte (Denemarken)

Promotores:

Prof. dr. J. Knoester
Prof. dr. ing. P.Th. van Duijnen

Beoordelingscommissie:

Prof. dr. K. Duppen

Prof. dr. E. J. Baerends
Prof. dr. B. Champagne

Acknowledgment

The work presented in this thesis is the results of four years of research in the theoretical chemistry group at Rijksuniversiteit Groningen. During this period I have meet, talked and worked with several people who has directly or indirectly contributed to the completion of this thesis.

First I would like to thank my supervisor and promoter Prof. Dr. Ing. P. Th. van Duijnen. Piet, thank you for inviting me to Groningen to do my Ph.D. research. I am grateful for the freedom to pursue the research that I found interesting and the many conversation about science, life, and everything. In particular the discussions about the local field problems springs to mind. Sadly and untimely my first promoter Prof. Dr. J. G. Snijders died before the finish of my thesis. His always interesting comments and questions during talks, discussions, and writing of articles are remembered and missed. I am therefore grateful that Prof. Dr. J. Knoester took the job of being my first promoter. Jasper, I appreciate all the comments and correction to the manuscript even though the time was short.

I am also grateful to my Danish contact person Prof. Dr. K. V. Mikkelsen. Kurt, thank you for establishing the contact with Piet and supporting me in going to Groningen. I am grateful for the continuing contact with KU, the collaboration on several papers included in this thesis, and, the suggestion to go to Northwestern University for a Post. Doc. position with Prof. Dr. G. Schatz. Also, the collaboration with Prof. Dr. P.-O. Åstrand, where several papers are included in this thesis, is highly appreciated. Per-Olof, I want to thank you for my stays in Trondheim. I enjoyed very much working together on the project(s), the numerous visits to restaurants and the trips to Tromsø. Unfortunately, one project was more difficult than we thought and the time too limited.

I have also had the pleasure of collaborating with several other people, which have always been very inspiring. Thanks to Prof. Dr. D.P. Chong, Dr. R.-H Xie, Prof. Dr. V.H. Smith Jr., and Dr. K.-O. Sylvester-Hvid.

The members of the reading committee, Prof. Dr. K. Duppen, Prof. Dr. E. J. Baerends, and Prof. Dr. B. Champagne are thanked for reading and commenting the manuscript.

I would like to thank old and new members of the theoretical chemistry group. Alex, Alexandrina, Arjan, Freddie, Henriette, Johan, Liviu, Marcel, Meta, Nienke, Nils, Olena, Paul, Pina, Ria, Robert, Rosanna, Thomas, Wim, thank you all for making the group a nice place to work, always having time to answer and fix problems either small or big, and all the fun times away from the lab. Thomas, thanks for the help with all the small problems and that I could stay at your place the first month in Groningen. Having you gone through many of the same problems before me, helped me a lot. Marcel, I hope that we can continue working together since I think we have many goals in common. Arjan and Pina, thanks to both of your for being my "paranimfen".

Thanks to family and friends for making my stay in Groningen fun and enjoyable.

Finally, I would like to thank the Danish Research Training Council and the Materials Science Centre for financial support.

Lasse Jensen
Groningen, 2004

Contents

Chapter 1

General introduction

1.1 Abstract

In this chapter we will provide a general introduction to this thesis. An introduction to the theoretical methodology adopted in this thesis and the long term goals of the work are presented. This includes a brief description of the methods used and developed in this work and some of the results obtained with these theoretical models. In the end of this chapter an outline of the thesis is presented.

1.2 Introduction

As a child one of my favourite toys was LEGO. The simple idea that from a bag of small building blocks one could construct large complex structures fascinated me, and still does. The same concept is now holding the promise to revolutionize our lives by means of nanotechnology and nanoscience.[1–6] Nanoscience is the study of molecules and structures with at least one dimension $\sim 1 - 100$ nm, so-called nanostructures, and Nanotechnology is the application of these nanostructures into nanoscale devises.[1] In the vision of nanotechnology the LEGO blocks are replaced by atoms and molecules and complex devices or new materials are constructed by arranging the molecules or the atoms with nanoscale precision. This, constructing materials at the molecular level, is often called the "bottom-up" approach and was first introduced by Feynman in his famous and highly visionary talk "There's Plenty of Room at the Bottom"[7] The idea is not that the nanostructures are constructed by putting one atom at a time, this would require too much time to make a macroscopic sample,[6] but rather that the nanostructures are assembled from larger molecular building blocks.[3] Within nanotechnology and nanoscience the prospects are great but the challenges even greater.

The interest in nanostructures stems from the fact that at the nanoscale the properties of materials change and start to exhibit size and shape dependent features. From a technological point of view this size-dependence enables for making nanostructures having specific tailored properties, which could not have been arrived at from the bulk properties. From a scientific point of view a detailed understanding of nanostructures and in particular of how the properties of nanostructures depend on size, shape and the individual building blocks is of fundamental interest. If we want to design nanostructures at the molecular level we need to understand the building blocks, how different building blocks interact and how the properties of the building blocks change when assembled into a nanostructure. Therefore, at the heart of nanoscience lies modelling and theory. If we want to achieve an efficient rational design of nanostructures, a combined theoretical and experimental understanding is required.[1,5]

An area receiving a lot of interest, and not only within nanoscience, is the development of new functional materials exhibiting nonlinear optical (NLO) effects. This is due to their potential for future application in electronics and photonics.[8–11] An important prospect is the utilization of the intensity dependence of the refractive index in all-optical switching devices, an essential element in future information processing technology.[8,10,11] Because the refractive index is governed by the linear susceptibility, $\chi^{(1)}$ (at the molecular level the linear dipole-dipole polarizability, α), and the intensity dependence of the refractive index by the third-order susceptibility, $\chi^{(3)}$ (where the molecular second hyperpolarizability, γ, is the corresponding microscopic property), an in-depth understanding of these properties is required.[8,12,13]

One promising class of materials are the so-called molecular materials, *i.e.* materials consisting of molecular entities. [8] The optical response properties of this class of materials are to a large extent governed by the properties of the individual molecules and to some extent by the interactions with the neighboring molecules. These new materials will be

designed on a molecular scale and carbon-based materials provide numerous possibilities to design molecular functionality because of the large variety of molecules that can be synthesized in organic chemistry. Consequently, a detailed understanding of the electronic structure of the molecular building blocks, the dependence of the microscopic optical response properties on the molecular structure, and the differences between the properties of isolated molecules and molecules embedded in the actual macroscopic devices are of fundamental importance.[8,12,14–22] Therefore, it has been conjectured that applied quantum chemistry will play a central role in the development of such new NLO materials.[18,23]

This thesis deals with the theoretical modelling of nonlinear optical response properties and the application of these models to nanostructures. The strategy taken can be considered as a sort of molecular "bottom-up" approach. We want to understand the NLO properties of complex materials like nanostructures, liquids and molecules in solution from the point of view of molecules. This means an first understanding of the NLO properties of the isolated molecule. Then to investigate how the properties of molecules change when going from the isolated case to the case of many interacting molecules in the condensed phase. Finally, the properties of the molecules in the condensed phase should then be related to the macroscopic response of the material which can be measured.

This chapter provides an introduction to the theoretical methodology adopted in this thesis and describes briefly the methods used and some of the results obtained. In section 1.3 we introduce the concepts of nonlinear optical properties and especially how one can relate the macroscopic properties measured in experiments to the microscopic molecular properties calculated using quantum chemical methods. In section 1.4 we describe briefly time-dependent density functional theory and its application to the calculation of the NLO properties. A study of the nonlinear optical properties of heterofullerenes using time-dependent density functional theory are discussed in section 1.5. The theory of an electrostatic interaction model for calculating NLO properties of large molecules or assemplies of molecules are discribed in section 1.6 and in section 1.7 the application of this model to carbon nanostructures such as nanotubes and fullerene clusters is presented. A discrete solvent reaction field model for the calculation of molecular response properties and the application of the model to water in aqueous solution are presented in section 1.8. Finally, an outline of the rest of the thesis is presented in section 1.9.

1.3 Nonlinear optical properties

When a material interacts with an electromagnetic field, either optical or static, the charge distribution of the material changes, the system becomes polarized, and the propagation of the electromagnetic field trough the media is altered. Even new electromagnetic fields can be generated exhibiting different behavior than the original field, e.g. oscillating at two or three times the frequency of the original field, i.e. showing a different color. Depending on the strength of the electromagnetic field the polarization will depend either linearly or nonlinearly on the applied electromagnetic field. Here we will use a semi-classical radiation theory, meaning that the electromagnetic field will be treated as a classical field

described by Maxwell's equations and the material system will be treated by quantum mechanics described by the Schödinger equation. Furthermore, the interactions between the quantum system and the electromagnetic field will be considered within the electric dipole approximation which means that we can treat the material as a (nonlinear) dielectric medium subjected to an electric field.[24] In this work we will restrict the treatment to purely electronic polarization, meaning that vibrational contributions are not calculated and rotations are considered by classical isotropic averaging.[15,25,26] This is not to say that vibrational contributions are insignificant and safely can be ignored but rather that these effects should be considered separately.[15,25] In the literature several different conventions exist for describing nonlinear optical properties[27] which differ in the numerical coefficients used. Therefore, in order to compare values obtained in different conventions it is important to correct for the differences in the numerical factors used. This has been clearified by Willetts *et al.*[27] but remains a problem, since often it is not stated explicitly which convention is used. In this work we will use a perturbation series expansion for the macroscopic polarization, which is often used for experimental properties, and a Taylor series expansion for the microscopic polarization, which frequenctly is used for theoretical properties.

1.3.1 The macroscopic polarization

The macroscopic polarization of a material in the presence of a macroscopic electric field, F^{mac}, is expressed as power series in the field strength as[8,10]

$$\mathcal{P}_I(t) = \mathcal{P}_I^0 + \chi_{IJ}^{(1)} F_J^{mac}(t) + \chi_{IJK}^{(2)} F_J^{mac}(t) F_K^{mac}(t) + \chi_{IJKL}^{(3)} F_J^{mac}(t) F_K^{mac}(t) F_L^{mac}(t) + \cdots \quad (1.1)$$

where $\mathcal{P}^0$ is the permanent polarization, $\chi^{(1)}$ the linear optical susceptibility, $\chi^{(2)}$ the second-order nonlinear optical susceptibility, and $\chi^{(3)}$ the third-order nonlinear optical susceptibility. The subscripts $I, J, K, L, ...$ denotes space-fixed axes and the Einstein summation convention is used for repeated subscripts. If we consider the macroscopic field to be a superposition of a static and an optical component,

$$F_J^{mac}(t) = F_{0,J}^{mac} + F_{\omega,J}^{mac} \cos(\omega t), \quad (1.2)$$

the macroscopic polarization can be expressed as[8,10]

$$\mathcal{P}_I(t) = \mathcal{P}_I^0 + \mathcal{P}_I^{\omega} \cos(\omega t) + \mathcal{P}_I^{2\omega} \cos(2\omega t) + \mathcal{P}_I^{3\omega} \cos(3\omega t) + \cdots . \quad (1.3)$$

The Fourier amplitudes of the polarization are then given in terms of the frequency-dependent susceptibilities as[8,10]

$$\begin{aligned} \mathcal{P}_I^{\omega_s} &= \delta_{\omega_s,0}\mathcal{P}_I^0 + \chi_{IJ}^{(1)}(-\omega_s;\omega_s) F_{\omega_s,J}^{mac} + K(-\omega_s;\omega_a,\omega_b)\chi_{IJK}^{(2)}(-\omega_s;\omega_a,\omega_b) F_{\omega_a,J}^{mac} F_{\omega_b,K}^{mac} \\ &+ K(-\omega_s;\omega_a,\omega_b,\omega_c)\chi_{IJKL}^{(3)}(-\omega_s;\omega_a,\omega_b,\omega_c) F_{\omega_a,J}^{mac} F_{\omega_b,K}^{mac} F_{\omega_c,L}^{mac} + \cdots , \end{aligned} \quad (1.4)$$

where the output frequency is given as the sum of input frequencies $\omega_s = \sum_a \omega_a$. The numerical coefficients $K(-\omega_s;\omega_a,\cdots)$ arise from the Fourier expansion of the electric field

and polarization and ensures that all susceptibilities of the same order have the same static limit. A tabulation of the coefficients can be found in Ref. 14, 28. The frequency-dependent susceptibilities can then be found from Eq. 1.4 by differentiation which gives the linear susceptibility

$$\chi^{(1)}_{IJ}(-\omega_s;\omega_s) = \left.\frac{\partial \mathcal{P}^{\omega_s}_I}{\partial F^{\mathrm{mac}}_{\omega_s,J}}\right|_{F^{\mathrm{mac}}=0}, \tag{1.5}$$

the second-order nonlinear susceptibility

$$\chi^{(2)}_{IJK}(-\omega_s;\omega_a,\omega_b) = K^{-1}(-\omega_s;\omega_a,\omega_b)\left.\frac{\partial^2 \mathcal{P}^{\omega_s}_I}{\partial F^{\mathrm{mac}}_{\omega_a,J}\partial F^{\mathrm{mac}}_{\omega_b,K}}\right|_{F^{\mathrm{mac}}=0}, \tag{1.6}$$

and the third-order nonlinear susceptibility

$$\chi^{(3)}_{IJKL}(-\omega_s;\omega_a,\omega_b,\omega_c) = K^{-1}(-\omega_s;\omega_a,\omega_b,\omega_c)\left.\frac{\partial^3 \mathcal{P}^{\omega_s}_I}{\partial F^{\mathrm{mac}}_{\omega_a,J}\partial F^{\mathrm{mac}}_{\omega_b,K}\partial F^{\mathrm{mac}}_{\omega_c,L}}\right|_{F^{\mathrm{mac}}=0}. \tag{1.7}$$

Each of the frequency-dependent susceptibilities corresponds to different physical processes,[8,10] e.g $\chi^{(1)}(-\omega;\omega)$ governs the refractive index, $\chi^{(2)}(-2\omega;\omega,\omega)$ the second harmonic generation (SHG), $\chi^{(3)}(-3\omega;\omega,\omega,\omega)$ the third harmonic generation (THG) and, $\chi^{(3)}(-\omega;\omega,\omega,-\omega)$ the degenerate four-wave mixing (DFWN) or the intensity-dependence of the refractive index.

1.3.2 The microscopic polarization

In a similar way as for the macroscopic polarization we can expand the microscopic polarization (dipole moment) in terms oscillating at different frequencies as[27,29]

$$\mu_\alpha(t) = \mu^0_\alpha + \mu^\omega_\alpha \cos(\omega t) + \mu^{2\omega}_\alpha \cos(2\omega t) + \mu^{3\omega}_\alpha \cos(3\omega t) + \cdots . \tag{1.8}$$

The microscopic dipole moment is then usually given by a Taylor expansion as[27,29]

$$\begin{aligned}\mu^{\omega_s}_\alpha &= \delta_{\omega_s,0}\mu^0_\alpha + \alpha_{\alpha\beta}(-\omega_s;\omega_s)F^{\mathrm{tot}}_{\omega_s,\beta} + \frac{1}{2}K(-\omega_s;\omega_a,\omega_b)\beta_{\alpha\beta\gamma}(-\omega_s;\omega_a,\omega_b)F^{\mathrm{tot}}_{\omega_a,\beta}F^{\mathrm{tot}}_{\omega_b,\gamma} \\ &+ \frac{1}{6}K(-\omega_s;\omega_a,\omega_b,\omega_c)\gamma_{\alpha\beta\gamma\delta}(-\omega_s;\omega_a,\omega_b,\omega_c)F^{\mathrm{tot}}_{\omega_a,\beta}F^{\mathrm{tot}}_{\omega_b,\gamma}F^{\mathrm{tot}}_{\omega_c,\delta} + \cdots \end{aligned} \tag{1.9}$$

where μ^0_α is the permanent electric dipole moment, $\alpha_{\alpha\beta}(-\omega_s;\omega_s)$ is the polarizabillity, $\beta_{\alpha\beta\gamma}(-\omega_s;\omega_a,\omega_b)$ is the first hyperpolarizability and, $\gamma_{\alpha\beta\gamma\delta}(-\omega_s;\omega_a,\omega_b,\omega_c)$ is the second hyperpolarizability. The numerical coefficients $K(-\omega_s;\omega_a,\cdots)$ are the same as for the macroscopic polarization and again this ensures that all (hyper)polarizabilities of the same order have the same static limit. The subscripts $\alpha,\beta,\gamma,\cdots$ denote molecule-fixed axes and again the Einstein summation convention is used for repeated subscripts. The microscopic polarization is expanded in terms of the actual total electric field, $F^{\mathrm{tot}}_{\omega_b,\gamma}$, felt by the molecule.

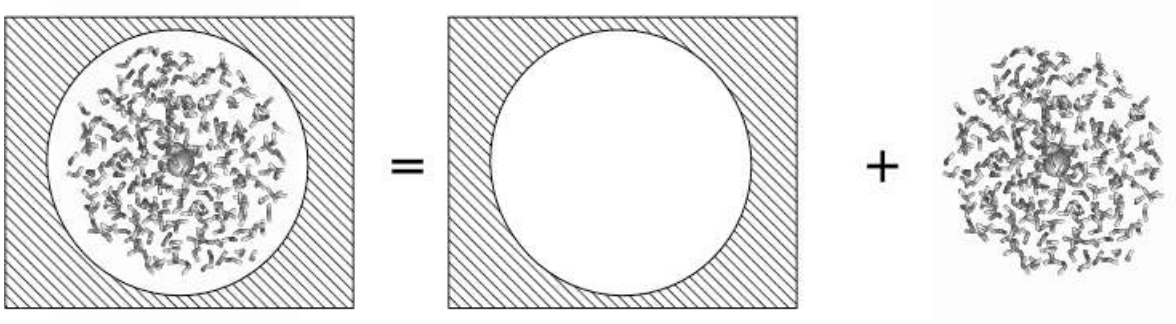

FIGURE 1.1: *Separation of the total system into a macroscopic region far from the central molecule and a microscopic region close to the molecule. In the microscopic region the actual electric field felt by the molecule should be considered in detail.*

In the condensed phase the actual electric field felt by the molecule is different from the macroscopic electric field. Therefore, in order to express the macroscopic properties in terms of the microscopic properties we need to relate the actual electric field at a molecule to the macroscopic electric field.

The concept of relating the actual electric field, often called the internal or local field, to the macroscopic field dates back to the work of Lorentz.[30,31] Lorentz[30] derived a simple relation between the internal electric field, the macroscopic electric field and the macroscopic polarization of the system, and due to its simplicity Lorentz local field theory is still used.[8,10,26,31] The central idea is that only close to the molecule we need to consider explicitly the field from nearby molecules, so the total system is separated into a macroscopic region far from the molecule and microscopic region close to the molecule. This separation is illustrated in Figure 1.1. The molecules in the region far from the central molecule can then be described by the average macroscopic properties. Therefore, inside a macroscopically small, but microscopically large, virtual cavity V we subtract the contribution from the macroscopic electric field and replace it by the correct discrete local field,

$$F^{tot}_{\omega_s,\alpha} = F^{mac}_{\omega_s,\alpha} - F^{pol}_{\omega_s,\alpha} + F^{disc}_{\omega_s,\alpha}(\Omega), \tag{1.10}$$

where $F^{pol}_{\omega_s,\alpha}$ is the macroscopic electric field in the cavity V and $F^{disc}_{\omega_s,\alpha}(\Omega)$ is the discrete electric field field in the cavity V which depends on the local configuration, Ω, of the molecules inside the cavity. Since we are not allowing the macroscopic region to adjust to the presence of the cavity the polarization remains homogeneous.[31] This approach neglects that a static electric field tends to orient molecules with a permanent dipole[31,32] and therefore a correction due to Onsager[32] is often used for static electric fields.

What Lorentz[30] did was to show that for a cubic arrangement of identical particles the discrete field was zero. This is also true on average for a completely random distribution where there is no correlation between the induced dipoles and the position of the molecules.[31] For a spherical cavity the macroscopic field is simply given in terms of the

macroscopic polarization[30,31] and the total electric field can be written as

$$F^{tot}_{\omega_s,\alpha} = F^{mac}_{\omega_s,\alpha} + \frac{4\pi}{3}\mathcal{P}^{\omega_s}_{\alpha} + F^{ind}_{\omega_s,\alpha}(\Omega) + F^{perm}_{\alpha}(\Omega) \tag{1.11}$$

where we have split the discrete electric field, F^{disc}, into two different contributions, F^{ind} and F^{perm}. The first term arises from the interactions of the macroscopic electric field with the other molecules in the cavity, i.e. accounts for the induced polarization of the surrounding molecules due to the electric field. The second term accounts for the interactions between the molecules when there is no electric field present, i.e. arises from the permanent charge distribution of the surrounding molecules. However, depending on the theoretical model used for describing the microscopic region, this spitting of the discrete electric field is not always possible nor necessary. Since the last two terms depend strongly on the local configuration of the molecules in the cavity and are inherently microscopic in nature it is better to treat these fields explicitly within the microscopic model used.

Therefore, instead of expanding the induced dipole moment in terms of the total field, Eq. 1.9, we expand it in terms of an effective macroscopic electric field

$$F^{eff}_{\omega_s,\alpha} = F^{mac}_{\omega_s,\alpha} + \frac{4\pi}{3}\mathcal{P}^{\omega_s}_{\alpha}. \tag{1.12}$$

This expansion in terms of the effective field defines the so-called effective properties[29] as

$$\begin{aligned}
\mu^{\omega_s}_{\alpha} &= \delta_{\omega_s,0}\mu^{0}_{\alpha} + \alpha^{eff}_{\alpha\beta}(-\omega_s;\omega_s)F^{eff}_{\omega_s,\beta} \\
&+ \frac{1}{2}K(-\omega_s;\omega_a,\omega_b)\beta^{eff}_{\alpha\beta\gamma}(-\omega_s;\omega_a,\omega_b)F^{eff}_{\omega_a,\beta}F^{eff}_{\omega_b,\gamma} \\
&+ \frac{1}{6}K(-\omega_s;\omega_a,\omega_b,\omega_c)\gamma^{eff}_{\alpha\beta\gamma\delta}(-\omega_s;\omega_a,\omega_b,\omega_c)F^{eff}_{\omega_a,\beta}F^{eff}_{\omega_b,\gamma}F^{eff}_{\omega_c,\delta} + \cdots .
\end{aligned} \tag{1.13}$$

These effective properties give an induced dipole moment due to the effective macroscopic electric field which is identical to the induced dipole moment in Eq. 1.9 and are the properties which we will relate to the experimental susceptibilities. This means that the microscopic contributions to the total field are incorporated into the effective properties. These effective properties could be compared with experimental results corrected for differences between the total field and the macroscopic electric field by the Lorentz local field method.[29]

Since we have separated the discrete field into the two contributions mentioned above we can also choose to expand the induced dipole moment in terms of the field arising directly from the macroscopic electric field,

$$F^{sol}_{\omega_s,\alpha} = F^{mac}_{\omega_s,\alpha} + \frac{4\pi}{3}\mathcal{P}^{\omega_s}_{\alpha} + F^{ind}_{\omega_s,\alpha}(\Omega), \tag{1.14}$$

where the field arising from the interactions between the molecules when there is no macroscopic field is incorporated into the properties. This gives an expansion which defines

the so-called solute properties[29] as

$$\begin{aligned}\mu_\alpha^{\omega_s} &= \delta_{\omega_s,0}\mu_\alpha^0 + \alpha^{sol}_{\alpha\beta}(-\omega_s;\omega_s)F^{sol}_{\omega_s,\beta} \\ &+ \frac{1}{2}K(-\omega_s;\omega_a,\omega_b)\beta^{sol}_{\alpha\beta\gamma}(-\omega_s;\omega_a,\omega_b)F^{sol}_{\omega_a,\beta}F^{sol}_{\omega_b,\gamma} \\ &+ \frac{1}{6}K(-\omega_s;\omega_a,\omega_b,\omega_c)\gamma^{sol}_{\alpha\beta\gamma\delta}(-\omega_s;\omega_a,\omega_b,\omega_c)F^{sol}_{\omega_a,\beta}F^{sol}_{\omega_b,\gamma}F^{sol}_{\omega_c,\delta} + \cdots . \end{aligned} \tag{1.15}$$

These solute properties relate to the macroscopic properties corrected for the field from the dipoles of all other molecules induced by the macroscopic field in addition to the Lorentz local field. This corresponds to a thought experiment where the macroscopic field is allowed to propagate inside the cavity without being modified by interactions with the molecules.

1.3.3 Relating the macroscopic and the microscopic polarization

The macroscopic polarization is related to the average microscopic dipole moment per molecule by[10,26]

$$\mathcal{P}_I^{\omega_s} = N_d \left\langle \mu_\alpha^{\omega_s} \right\rangle_I \tag{1.16}$$

where N_d is the number density and the brackets, $\langle\rangle$, denote orientational averaging and relate the molecule-fixed axes to the space-fixed axes.[25,26] Inserting the expansion of the dipole moment in terms of the effective macroscopic field, Eq. 1.13, we can express the macroscopic polarization in terms of the effective (hyper)polarizabilities as,

$$\begin{aligned}\mathcal{P}_I^{\omega_s} &= N_d \left\langle \delta_{\omega_s,0}\mu_\alpha^0 \right\rangle_I + N_d \left\langle \alpha^{eff}_{\alpha\beta}(-\omega_s;\omega_s)F^{eff}_{\omega_s,\beta} \right\rangle_I \\ &+ \frac{1}{2}K(-\omega_s;\omega_a,\omega_b)N_d \left\langle \beta^{eff}_{\alpha\beta\gamma}(-\omega_s;\omega_a,\omega_b)F^{eff}_{\omega_a,\beta}F^{eff}_{\omega_b,\gamma} \right\rangle_I \\ &+ \frac{1}{6}K(-\omega_s;\omega_a,\omega_b,\omega_g)N_d \left\langle \gamma^{eff}_{\alpha\beta\gamma\delta}(-\omega_s;\omega_a,\omega_b,\omega_c)F^{eff}_{\omega_a,\beta}F^{eff}_{\omega_b,\gamma}F^{eff}_{\omega_c,\delta} \right\rangle_I \\ &+ \cdots . \end{aligned} \tag{1.17}$$

We see that the averaging is done on the product of the (hyper)polarizabilities and the effective fields. This is exactly the reason why the total electric field was split into an effective macroscopic part and a microscopic part which was incorporated into the (hyper)polarizabities in Eq. 1.13 by expanding the dipole moment in terms of the effective field. Since the effective field is macroscopic we can take it outside the averaging and express the macroscopic polarization in terms of orientational averages of the effective (hyper)polarizabilities as

$$\begin{aligned}\mathcal{P}_I^{\omega_s} &= N_d \left\langle \delta_{\omega_s,0}\mu_\alpha^0 \right\rangle_I + N_d \left\langle \alpha^{eff}_{\alpha\beta}(-\omega_s;\omega_s) \right\rangle_{IJ} F^{eff}_{\omega_s,J} \\ &+ \frac{1}{2}K(-\omega_s;\omega_a,\omega_b)N_d \left\langle \beta^{eff}_{\alpha\beta\gamma}(-\omega_s;\omega_a,\omega_b) \right\rangle_{IJK} F^{eff}_{\omega_a,J}F^{eff}_{\omega_b,K} \\ &+ \frac{1}{6}K(-\omega_s;\omega_a,\omega_b,\omega_c)N_d \left\langle \gamma^{eff}_{\alpha\beta\gamma\delta}(-\omega_s;\omega_a,\omega_b,\omega_c) \right\rangle_{IJKL} F^{eff}_{\omega_a,J}F^{eff}_{\omega_b,K}F^{eff}_{\omega_c,L} \\ &+ \cdots . \end{aligned} \tag{1.18}$$

By combinging the definitions of the susceptibilities in Eqs. 1.5, 1.6, and 1.7 with the expression for the macroscopic polarization in terms of the effective (hyper)polarizabilities we can obtain a link between the macroscopic and the microscopic properties. In order to illustrate this we first consider the ZZ component of the linear susceptibility for a pure isotropic system. By inserting the definition of the effective field, Eq. 1.12, into Eq. 1.18 and using the definition of the susceptibilitiy, Eq. 1.5, we obtain

$$\chi^{(1)}_{ZZ}(-\omega_s;\omega_s) = N_d \left\langle \alpha^{eff}_{\alpha\beta}(-\omega_s;\omega_s) \right\rangle_{ZZ} \left(1 + \frac{4\pi}{3}\chi^{(1)}_{ZZ}(-\omega_s;\omega_s)\right). \tag{1.19}$$

The isotropic orientation average of the polarizability, often refered to as the mean polarizability, is given by[25]

$$\left\langle \alpha^{eff}_{\alpha\beta} \right\rangle_{ZZ} = \overline{\alpha}^{eff} = \frac{1}{3}(\alpha^{eff}_{xx} + \alpha^{eff}_{yy} + \alpha^{eff}_{yy}). \tag{1.20}$$

and denoted $\overline{\alpha}$. The linear susceptibility can then be written in terms of the mean effective polarizability by rewriting Eq. 1.19 as,

$$\chi^{(1)}_{ZZ}(-\omega_s;\omega_s) = \frac{N_d \overline{\alpha}^{eff}(-\omega_s;\omega_s)}{1 - \frac{4\pi}{3} N_d \overline{\alpha}^{eff}(-\omega_s;\omega_s)} \tag{1.21}$$

which is the standard expression for the susceptibility corrected for the Lorentz local field.[10,33] The susceptibility can be related to the refractive index or dielectric constant of the system as

$$n^{(1)}(\omega_s) = \sqrt{\epsilon^{(1)}(\omega_s)} = \sqrt{1 + 4\pi\chi^{(1)}_{ZZ}(-\omega_s;\omega_s)} = \sqrt{\frac{1 + \frac{8\pi}{3} N_d \overline{\alpha}^{eff}(-\omega_s;\omega_s)}{1 - \frac{4\pi}{3} N_d \overline{\alpha}^{eff}(-\omega_s;\omega_s)}} \tag{1.22}$$

which is the familar Lorentz-Lorenz or Clausius-Mossotti equation.[30,31,33]

As an expample of a nonlinear susceptibility we will consider the third-order nonlinear susceptibility corresponding to the third-harmonic generation experiments. We will look at the $ZZZZ$ component of a pure isotropic sample where the individual molecules are centrosymmetric, an example could be crystalline C_{60}. The fact that the molecules are centrosymmetric allows us to ignore cascading contributions[34,35] since the molecules have no intrinsic first hyperpolarizability. The THG susceptibility can then be obtained by inserting Eq. 1.12 into Eq. 1.18 and using the definition of the susceptibilitiy, Eq. 1.7, as

$$\begin{aligned} \chi^{(3)}_{ZZZZ}(-3\omega;\omega,\omega,\omega) &= N_d \left\langle \alpha^{eff}_{\alpha\beta}(-3\omega;3\omega) \right\rangle_{ZZ} \left(\frac{4\pi}{3}\chi^{(3)}_{ZZZZ}(-3\omega;\omega,\omega,\omega)\right) \\ &+ \frac{1}{6} N_d \left\langle \gamma^{eff}_{\alpha\beta\gamma\delta}(-3\omega;\omega,\omega,\omega) \right\rangle_{ZZZZ} \left(1 + \frac{4\pi}{3}\chi^{(1)}_{ZZ}(-\omega;\omega)\right)^3 \end{aligned} \tag{1.23}$$

We see that we have a contribution both from the linear susceptibility and from the third-order nonlinear susceptibility. The isotropic orientation average of the second hyperpolarizability, often refered to as the mean or parallel second hyperpolarizability, is given

by[25]

$$\left\langle \gamma^{eff}_{\alpha\beta\gamma\delta} \right\rangle_{ZZZZ} = \overline{\gamma}^{eff} = \frac{1}{15}\sum_{\alpha\beta}(\gamma^{eff}_{\alpha\alpha\beta\beta} + \gamma^{eff}_{\alpha\beta\beta\alpha} + \gamma^{eff}_{\alpha\beta\alpha\beta}) \tag{1.24}$$

The THG susceptibility can then be written as

$$\begin{aligned} \chi^{(3)}_{ZZZZ}(-3\omega;\omega,\omega,\omega) &= \frac{1}{6}N_d\overline{\gamma}^{eff}(-3\omega;\omega,\omega,\omega) \\ &\times \left(1 - \frac{4\pi}{3}N_d\overline{\alpha}^{eff}(-3\omega;\omega)\right)^{-1}\left(\frac{\epsilon^{(1)}(\omega)+2}{3}\right)^3 \end{aligned} \tag{1.25}$$

where we have used the relation between the linear susceptibility and the dielectric constant in Eq. 1.22. Using Eq. 1.21 we can express the term with the effective polarizability in terms of the dielectric constant at 3ω. This allows us to express the third-order nonlinear susceptibility as

$$\chi^{(3)}_{ZZZZ}(-3\omega;\omega,\omega,\omega) = \frac{1}{6}N_d\overline{\gamma}^{eff}(-3\omega;\omega,\omega,\omega)\left(\frac{\epsilon^{(1)}(3\omega)+2}{3}\right)\left(\frac{\epsilon^{(1)}(\omega)+2}{3}\right)^3 \tag{1.26}$$

which is the form for the nonlinear susceptibility well known from standard Lorentz local field theory with $n+1$ local field corrections, where n is the number of applied fields.

1.4 (Time-dependent) Density Functional Theory

The use of quantum chemical methods[36] enable accurate calculations of molecular response properties like the electronic excitations and frequency-dependent (hyper)polarizabilities.[15] However, due to very high computational demands the most accurate of these methods can only be used for small systems containing few atoms. Therefore, it is of fundamental importance to extend the use of these quantum chemical methods to treat large systems containing many atoms. A method which has attracted considerable interest, especially within recent years, is Time-Dependent Density Functional Theory (TD-DFT).[37–41] The main reason for this is that (TD-)DFT provides a level of accuracy which in most cases is sufficient at a lower computational requirement than other methods. The use of TD-DFT for calculating molecular response properties in the gas-phase has been shown to be accurate for small and medium size (< 20 atoms) molecules, especially if one uses recently developed density functionals.[42–51]

1.4.1 The Kohn-Sham equations

Ground state density functional theory is based on the Hohenberg-Kohn theorems[52] which states that there is a one-to-one correspondence between the ground state density and the external potential and that the exact ground-state density of a system in an external potential can be found by minimizing an energy functional. The energy functional for a

system of interacting particles moving in a field arising from the fixed nuclei (often referred to as the external potential), $v(r)$, is given by[52]

$$E[\rho] = \int dr\rho(r)v(r) + F_{HK}[\rho], \tag{1.27}$$

where ρ is the density and $F_{HK}[\rho]$ is a universal functional of the density. The universal functional is, however, not known and practical DFT involves finding approximate forms for the functional.[53] Most DFT approaches use the method of Kohn and Sham[54] for constructing the functional. In the Kohn-Sham (KS) approach [54] the functional is split as

$$F_{HK}[\rho] = T_s[\rho] + \frac{1}{2}\int\int drdr'\frac{\rho(r)\rho(r')}{|r-r'|} + E_{xc}[\rho], \tag{1.28}$$

where the first term, $T_s[\rho]$, is the kinetic energy of a non-interacting system, the second term is the Coulomb interaction and the last term is the unknown part called the exchange-correlation (xc) energy functional. The central assumption is that for any ground state density of an interacting system there exists a noninteracting system with the same ground state density. We can then find the ground-state density by minimizing the energy functional[52]

$$0 = \frac{\delta}{\delta\rho(r)}\left[E[\rho] - \mu\int dr\rho(r)\right] = \frac{\delta T_s[\rho]}{\delta\rho(r)} + v(r) + \int dr'\frac{\rho(r')}{|r-r'|} + v_{xc}[\rho](r) - \mu \tag{1.29}$$

where μ is a Lagrange multiplier ensuring the correct number of electrons. The functional derivative of the unknown xc-functional, the xc-potential,

$$v_{xc}[\rho](r) = \frac{\delta E_{xc}[\rho]}{\delta\rho(r)]}, \tag{1.30}$$

has been introduced. This is identical to what one finds for a system of non-interacting particles moving in an effective potential, $v_s(r)$, the KS-potential, given by[54]

$$v_s(r) = v(r) + \int dr'\frac{\rho(r')}{|r-r'|} + v_{xc}[\rho](r). \tag{1.31}$$

We can therefore find the ground state density of the interacting system by solving a set of effective one-particle equations, the KS equations, given by

$$\left[-\frac{1}{2}\nabla^2 + v(r) + \int dr'\frac{\rho(r')}{|r-r'|} + v_{xc}[\rho](r)\right]\phi_i(r) = \epsilon_i\phi_i(r). \tag{1.32}$$

where $\phi_i(r)$ is a KS orbital and ϵ_i is the corresponding orbital energy. The density of the system is given as the sum of the occupied KS orbitals

$$\rho(r) = \sum_i^N n_i|\phi_i(r)|^2. \tag{1.33}$$

where n_i is the occupation number. If the xc-potential is exact the density will be the exact density of the interacting system. Therefore in the KS approach the problem of finding an approximation to the universal functional, F_{HK}, is reduced to finding an approximation to the xc-functional. It should however be noted that the name xc-energy is slightly misleading since it also contains a small part of the kinetic energy, i.e the difference between the kinetic energy of the true interacting system and the kinetic energy of the non interacting system.

1.4.2 The Time-dependent Kohn-Sham equations

Since we are interested in calculating frequency-dependent properties we have to consider a time-dependent formalism. The time-dependent extension of the KS equations was derived by Runge and Gross.[37] As in the ground state we have to assume that a potential, $\upsilon_s(r,t)$, exists that reproduces the time-dependent density of the interacting system. The density of the interacting system can then be found from[37–41] the time-dependent KS equations

$$i\frac{\partial}{\partial t}\phi_i(r,t) = \left(-\frac{\nabla^2}{2} + \upsilon_s[\rho](r,t)\right)\phi_i(r,t). \tag{1.34}$$

The time-dependent KS potential is written as,

$$\upsilon_s[\rho](r,t) = \upsilon(r) + \upsilon^{\mathrm{per}}(r,t) + \int dr' \frac{\rho(r',t)}{|r-r'|} + \upsilon_{xc}(r,t) \tag{1.35}$$

where $\upsilon(r)$ is the field of the nuclei, $\upsilon^{\mathrm{per}}(r,t)$ is an external time-dependent perturbation, the third term is the Columb term and the last term is the time-dependent xc-potential. The time-dependent xc-potential, $\upsilon_{xc}(r,t)$, is usually adopted within the adiabatic aproximation $\upsilon_{xc}(r,t) \simeq \upsilon_{xc}(r)$. The time-dependent density is then given by the sum of the occupied time-dependent KS orbitals as

$$\rho(r,t) = \sum_i^N n_i |\phi_i(r,t)|^2. \tag{1.36}$$

where n_i is the occupation number. We are interested in calculating properties due to a perturbation by an external time-dependent electric field. Within the dipole approximation this time-dependent perturbation is given by

$$\upsilon^{\mathrm{per}}(r,t) = \hat{\mu}F(t) = \hat{\mu}(F_0 + F_\omega \cos(\omega t)), \tag{1.37}$$

where $\hat{\mu}$ is the dipole operator and $F(t)$ is the electric field. The total electronic dipole moment of the system in the presence of the electric filed can be calculated from the density as[55]

$$\mu_\alpha(t) = -\int d^3r \hat{\mu}_\alpha \rho(r,t) = -Tr[H^\alpha P(t)], \tag{1.38}$$

where Tr denotes the trace. The time-dependent density matrix is given by

$$\rho(r,t) = \sum_{pq} \phi_p^*(r)\phi_q(r)P_{pq}(t) \tag{1.39}$$

and the elements of the dipole moment matrix, H^{α}, are given by

$$H^{\alpha}_{pg} = \langle \phi_p | \, \hat{\mu}_{\alpha} \, | \phi_q \rangle \, . \tag{1.40}$$

We can then expand the density matrix in a Taylor series as[56]

$$P = P^0 + P^{\beta} F_{\beta} + \frac{1}{2!} P^{\beta\gamma} F_{\beta} F_{\gamma} + \cdots \, , \tag{1.41}$$

where P^0 is the unperturbed density matrix, P^{β} the linear response and $P^{\beta\gamma}$ the quadratic response. Inserting this expansion into Eq. 1.38 and comparing with Eq. 1.9 allows us to identify the dipole moment, the frequency-dependent polarizability, and the frequency-dependent first hyperpolarizabillity as

$$\mu_{\alpha} = -Tr[H^{\alpha} P^0] \tag{1.42}$$

$$\alpha_{\alpha\beta}(-\omega;\omega) = -Tr[H^{\alpha} P^{\beta}(\omega)], \tag{1.43}$$

$$\beta_{\alpha\beta\gamma}(-\omega_s;\omega_a,\omega_b) = -Tr[H^{\alpha} P^{\beta\gamma}(\omega_a,\omega_b)], \tag{1.44}$$

where $\omega_s = \omega_a + \omega_b$. We can then by using time-dependent linear response theory obtain a set of self-consistent equations for the first order density response,[37–41]

$$P_{st}(\omega) = \frac{\Delta n_{st}}{(\epsilon_s - \epsilon_t) - \omega} \delta \upsilon^{eff}_{st}(\omega), \tag{1.45}$$

where ϵ_s is the orbital energy, Δn_{st} is the difference in occupation numbers, i.e. 1 for $st = ai$ and -1 for $st = ia$, where a denotes virtual orbitals and i denotes occupied orbitals. The change in the effective potential, $\delta \upsilon^{eff}_{st}$, is dependent on the first order change in the density, $\delta\rho$, and is given by

$$\begin{aligned} \delta \upsilon^{eff}_{st}(\omega) &= \delta \upsilon^{per}_{st}(\omega) \\ &+ \int dr \phi^*_s(r) \left[\upsilon_{Coul}[\delta\rho](r,\omega) + \upsilon_{xc}[\delta\rho](r,\omega) \right] \phi_t(r). \end{aligned} \tag{1.46}$$

The first term is the matrix elements of the time-dependent perturbation and the second term consist of the Coulomb part given by

$$\upsilon_{Coul}[\delta\rho](r,\omega) = \int dr' \frac{\delta\rho(r',\omega)}{|r - r'|}, \tag{1.47}$$

and the xc part, often called the xc-kernal, given by

$$\upsilon_{xc}[\delta\rho](r,\omega) = \int dr' \frac{\delta \upsilon_{xc}(r)}{\delta\rho(r')} \delta\rho(r',\omega). \tag{1.48}$$

Since the effective potential in Eq. 1.46 depends on the first-order density matrix through the potentials $\upsilon_{Coul}[\delta\rho](r,\omega)$ and $\upsilon_{xc}[\delta\rho](r,\omega)$ a self-consistent solution of Eq. 1.45 is required. In a manner similar to the linear response a set of equations for the solution of

the higher order density response can be constructed.[49–51,57,58] However, a more efficient approach is to take advantage of the (2n+1) rule which allows for the quadratic response properties to be rewritten in terms of quantities obtained from a solution of the first order response equations. Within TD-DFT van Gisbergen *et al.* have shown how this is done for the frequency-dependent first hyperpolarizability[57] in an approach similar to the TD-HF approach of Karna and Dupuis.[56]

1.5 NLO properties of heterofullerenes as studied by TD-DFT

Quantum chemical studies of structure-property relations for the first hyperpolarizability of organic molecules have helped synthetic organic chemist to develop better organic chromophores for use in electrooptical materials.[12,17,19,21,22] Similar to the first hyperpolarizability structure-properties relationship for the second hyperpolarizability are emerging but to a much lesser degree than for the first hyperpolarizability.[13,20,59,60] Although much progress has been made, the search for organic chromophores with large hyperpolarizabilities still continues. Among the molecules of interest are conjugated organic molecules with delocalized electron systems like polymers and fullerenes. Since the discovery of the C_{60} fullerene[61] there have been numerous theoretical and experimental investigations of its linear and nonlinear optical properties, see *e.g.* Ref. 62–66 and references therein. However, both experiments[67,68] and theory[64,65,69] have shown that the third-order nonlinearity of C_{60} is smaller than first assumed. For this reason the third-order nonlinearity of chemical functionalized C_{60} have been experimentally investigated and found to provide a large increase in the nonlinearity compared with the pure C_{60}, see *e.g* Ref. 62, 68, 70, 71. Substitution of carbon atoms in C_{60} with boron or nitrogen atoms has theoretically been suggested as a way of increasing the nonlinearity by several orders of magnitude.[72,73] These studies were done using an extended Su-Schrieffer-Heeger (SSH) model[74] which for the pure fullerene[72] predicts a much larger second hyperpolarizability than found with DFT and SCF. [64,65,69] Therefore, we investigated the effects of substitute-dope C_{60} with 2 B, 2 N and BN on the second hyperpolarizability component along the doping-axis using TD-DFT.[75] This work is presented in Chapter 2 and some of the results are summarised in Table 1.1. We found,

	C_{60}[76]	$C_{58}N_2$[75]	$C_{58}B_2$[75]	$C_{58}BN$[75]	$C_{48}N_{12}$[76]	$C_{48}B_{12}$[77]
γ_{zzzz}	137950	130147	155430	208470	232970	470190
$\overline{\gamma}$	137950	-	-	-	215222	387628

TABLE 1.1*: Static second hyperpolarizability for $C_{48}N_{12}$, $C_{48}N_{12}$ and C_{60} in a.u calculated using TD-DFT.*

in contrast to the results obtained with a SSH model,[72,73,78] only small differences when comparing the 2 N- and 2 B-substituted C_{60} with the pure C_{60} molecule. Substituting with 2 N decreases the second hyperpolarizability with about 5% and substituting with

2 B increases it with about 12%. Although an increase with 50% was found when doping C_{60} with both B and N the effect of doping was in general found to be very small. We also calculated the second hyperpolarizability of the newly synthesized[79] aza-fullerene $C_{48}N_{12}$[76] and the theoretically proposed[80] boron analog $C_{48}B_{12}$.[77] The structure of the aza-fullerene $C_{48}N_{12}$ is shown in Figure 1.2. This study was part of a computational characterization of the structural, electronic, vibrational and magnetic properties of these new heterofullerenes.[76,77] The results for the second hyperpolarizability of the heterofullerenes are presented in Table 1.1. For $C_{48}B_{12}$ the second hyperpolarizability is $\sim 180\%$ larger that for C_{60} and for $C_{48}N_{12}$ it is increased with ~ 55 %. It is therefore seen that these new heterofullerenes can have a second hyperpolarizability which is significant larger than that of C_{60}. However, a comparison of the hyperpolarizabilites of heterofullerenes and chemical functionalized fullerenes is required in order to determine which systems are the more interesting.

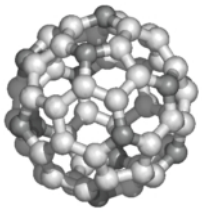

FIGURE 1.2: *Structure of the aza-fullerene $C_{48}N_{12}$. Dark atoms nitrogen and light atoms carbon.*

1.6 An interaction model for the (hyper)polarizability of large molecules

Sophisticated quantum chemical methods can be applied only on rather small molecules, even though considerable effort has been devoted to calculate NLO properties at the SCF level for relatively large molecules like fullerenes.[81] Furthermore, the use of conventional DFT, which in general gives improved accuracy over the Hartree-Fock approximation at similar or lower computational cost, gives relatively poor results for nonlinear optical properties of large conjugated molecular chains.[82,83] Although some recent advances within DFT have been presented for the linear polarizability of conjugated polymers[83–86] not much have been done in the case of the nonlinear polarizabilitites. Therefore, for large molecules and assemblies of molecules, modelling is currently restricted to less sophisticated methods.

An alternative approach to quantum chemical methods is based on representing the molecule as a set of interacting induced point dipoles,[87–89] a model exploited extensively

by Applequist and coworkers.[90,91] In an external field, atomic dipole moments are induced which interact with each other. A molecular polarizability tensor is thus obtained even though isotropic(atom-type) atomic polarizabilities are adopted in the model. The molecular $\boldsymbol{\gamma}$ is obtained analogously by including also an atomic γ in the interaction model.[92] It has furthermore been demonstrated that damping of the interatomic interactions at short distances is crucial.[93] We have developed an interaction model along these lines based on a parametrization of molecular polarizabilities obtained from quantum chemical calculations. The model includes the frequency dependence of $\boldsymbol{\alpha}$, an improved damping term, and the molecular $\boldsymbol{\gamma}$.[63,94–96] In chapter 3 we describe the dipole interaction model for the linear polarizability including the frequency-dependent molecular polarizability, the improved damping term and some initial applications of the model to the polarizability of molecular clusters. The dipole interaction model for the second hyperpolarizability is presented in chapter 4. Here the theory is briefly outlined.

In a system of N point polarizabilities, $\alpha_{I,\alpha\beta}$, the atomic induced dipole moment of atom I, $\mu^{\text{ind}}_{I,\alpha}$ is given as

$$\mu^{\text{ind}}_{I,\alpha} = \alpha_{I,\alpha\beta} F^{\text{tot}}_{I,\beta} + \frac{1}{6}\gamma_{I,\alpha\beta\gamma\delta} F^{\text{tot}}_{I,\beta} F^{\text{tot}}_{I,\gamma} F^{\text{tot}}_{I,\delta} \tag{1.49}$$

where $F^{\text{tot}}_{I,\beta}$ is the total microscopic electric field given by[31,33]

$$F^{\text{tot}}_{I,\beta} = F^{\text{eff}}_{\beta} + F^{\text{disc}}_{I,\beta} = F^{\text{mac}}_{\beta} + \frac{4\pi}{3}\mathcal{P}_{\beta} + \sum_{J\neq I}^{N} T_{IJ,\beta\gamma}\mu^{\text{ind}}_{J,\gamma} \tag{1.50}$$

The term $T_{IJ,\beta\gamma}\mu^{\text{ind}}_{J,\gamma}$ is the electric field of the induced dipole moment at site J calculated at atom I. $F^{\text{disc}}_{I,\beta}$ is thus the electric field at site I from all other induced dipole moments and corresponds to the discrete local field in Eq. 1.10 in a dipole approximation. The solutions of the set of coupled linear equations in Eq. 1.49 may be expressed in terms of a two-atom relay tensor, $B^{(2)}_{IJ,\alpha\beta}$, and a four-atom relay tensor $B^{(4)}_{IJKL,\alpha\beta\gamma\delta}$ as[92,95]

$$\mu^{\text{ind}}_{I,\alpha} = \sum_{J}^{N} B^{(2)}_{IJ,\alpha\beta} F^{\text{eff}}_{J,\beta} + \frac{1}{6}\sum_{J,K,L}^{N} B^{(4)}_{IJKL,\alpha\beta\gamma\delta} F^{\text{eff}}_{L,\delta} F^{\text{eff}}_{K,\gamma} F^{\text{eff}}_{J,\beta} \ , \tag{1.51}$$

where $B^{(2)}_{IJ,\alpha\beta}$ gives the induced dipole moment at atom I from an effective electric field on atom J. Analogously, $B^{(4)}_{IJKL,\alpha\beta\gamma\delta}$ gives the induced dipole moment at atom I from effective electric fields on atoms J, K, and L. The resulting molecular polarizability, $\alpha^{\text{mol}}_{\alpha\beta}$, and molecular second hyperpolarizability, $\gamma^{\text{mol}}_{\alpha\beta\gamma\delta}$, are given as

$$\alpha^{\text{mol}}_{\alpha\beta} = \sum_{IJ}^{N} B^{(2)}_{IJ,\alpha\beta} \ , \tag{1.52}$$

and

$$\gamma^{\text{mol}}_{\alpha\beta\gamma\delta} = \sum_{IJKL}^{N} B^{(4)}_{IJKL,\alpha\beta\gamma\delta} \ . \tag{1.53}$$

We show in chapter 3 that, by adopting two parameters for each element, a polarizability, α_P, and a damping parameter, Φ_P, good results are obtained for example for the polarizability of large molecular clusters.[63] As shown in chapter 4 a parametrization of the molecular γ includes an atomic γ parameter, γ_P, in addition to the parameters adopted for the molecular polarizability.[95]

The point dipole interaction (PDI) model described in chapter 3 and 4 can be used to calculate the properties of large molecules and cluster of molecules. When considering molecular cluster the properties calculated corresponds to properties of the total cluster or supermolecule. We can therefore use this model, or any supermolecular method, to calculate the effective molecular properties defined in Eq. 1.13. This can be done by calculating the molecular properties per molecule and extend the cluster until no changes are observed in the properties. However, if one is interested in obtaining the molecular properties of the individual members of the cluster the total response has to be distributed over the molecules. In chapter 5 we discuss possible ways of partitioning the total polarizability into local contributions. Three general partitioning schemes are described and a localized dipole interaction model is presented. Here we will shortly summarize the localized dipole interaction model.

To calculate the (hyper)polarizability of the individual molecules (or subgroups) in a cluster, we utilize the localized point-dipole interaction model (LPDI) described in chapter 5.[97] The partitioning is carried out by first decomposing the two-atom matrix into a block diagonal form with M blocks, $\hat{B}^{(2)}_{I,PQ,\alpha\beta}$, corresponding to a relay tensor for the I'th molecule or subgroup, where M is the total number of molecules or subgroups in the cluster. In the decomposition of the relay matrix, the interaction blocks $B^{(2)}_{P\in IQ\in J,\alpha\beta}$, where atom P belongs to molecule I and atom Q to molecule J, is assigned to the diagonal blocks $B^{(2)}_{P\in IQ\in I,\alpha\beta}$ where both atom P and Q belong to molecule I. This assignment is a more less arbitrary procedure but can be done similarly to the Mulliken population analysis.[98] Therefore, we have for molecule I,

$$\hat{B}^{(2)}_{I,PQ,\alpha\beta} = B^{(2)}_{P\in IQ\in I,\alpha\beta} + \frac{1}{2}\sum_{J\neq I}^{M}\left(B^{(2)}_{P\in IQ\in J,\alpha\beta} + B^{(2)}_{P\in JQ\in I,\alpha\beta}\right) \ . \tag{1.54}$$

The polarizability and second hyperpolarizabilty can subsequently be calculated by Eqs. 1.52 and 1.53 using the diagonal blocks of the decomposed relay matrix, $\hat{B}^{(2)}_{I,PQ,\alpha\beta}$. They will give the polarizability and hyperpolarizability of each of the M individual molecules in the molecular cluster.

1.7 NLO properties of large carbon nanostructures

An important concept in the design of new nonlinear optics materials is the scaling behaviour of the optical properties with increasing size. In the limit of infinitely long chains, both the polarizability, $\boldsymbol{\alpha}$, and the second hyperpolarizability, $\boldsymbol{\gamma}$, will scale linearly with the length of the chain. In particular, the so-called saturation length, i.e. where the property

($\boldsymbol{\alpha}$ or $\boldsymbol{\gamma}$) starts to scale linearly with increasing size of the system, is of interest. We have used the PDI model described in the chapters 3, 4, and 5 to calculate the polarizability and second hyperpolarizability of large carbon nanostructures such as carbon nanotubes and clusters of fullerene molecules. In chapter 6 we present a characterization of the scaling behavior and saturation of the second hyperpolarizability for carbon nanotubes as the length of the tube increases. For the C_{60} fullerene clusters we have investigated the size dependences of a linear chain, a mono-layer film, and a face-centered cubic (FCC) crystal cluster and the results are presented in chapter 7. We have also calculated the corresponding linear and third-order susceptibilities, $\chi^{(1)}$ and $\chi^{(3)}$ for the FCC cubic cluster in order to compare with experimental results. We will here discuss some of the results and present some results which have not been presented elsewhere.[99]

In order to validate the PDI model for the carbon nanostructures we compared the PDI results for $\overline{\alpha}$ and $\overline{\gamma}$ for C_{60} and C_{70} with the available SCF and experimental results. These results for C_{60} and C_{70} are presented in Table 1.2. The parameters, α_C and Φ_C,

	C_{60}		C_{70}	
	$\overline{\alpha}$	$\overline{\gamma}$	$\overline{\alpha}$	$\overline{\gamma}$
PDI	77.5	115.2	91.5	145.5
SCF	75.1	109.2	89.8	149.7
Exp	76.5 ± 8	-	102 ± 14	-

TABLE 1.2*: Mean polarizability and mean second hyperpolarizability of small fullenerenes. Polarizability in* $\AA^3$ *and second hyperpolarizability in* 10^3*a.u.*

used are the general parameters obtained in chapter 3. [63] These parameters were shown to give good results for α^{mol} for nanotubes[100] and in chapter 3 for the fullerene clusters.[63] The last parameter γ_C has been chosen to describe γ^{mol} of C_{60} obtained from Hartree-Fock calculations taken from Ref. 65. The reason for not choosing the general γ_C parameter obtained in chapter 4 is the problem of describing both α^{mol} and γ^{mol} with the same damping parameters. From Table 1.2 we see that we obtain good results for $\overline{\alpha}$ and $\overline{\gamma}$ for the small fullerenes, especially $\overline{\alpha}$ is in good agreement with both SCF and experimental results.

The molecular α and γ have been calculated for [5,5] and [9,0] open-ended carbon nanotubes as a function of the tube length and the results for γ are presented in chapter 6.[96] The largest tubes studied corresponds to $\sim$ 6000 atoms and a length of $\sim$ 75 nm. All of the results have been characterized by fitting the results to the expression $\frac{\chi(N)}{N} = \chi^{\infty} - C\exp\left(-\frac{N}{N^{\mathrm{sat}}}\right)$, where χ represents either α or γ. This allows for a description of α (γ) in terms of three parameters which are independent of the chain length. The parameter χ^{∞} represents the asymptotic value and N^{sat} represents the onset of which the saturation starts. The scaling parameters obtained for the nanotubes are in Table 1.3 compared with results for conjugated organic oligomers[101] obtained using the semiemperical INDO/S method. We see that the saturation length of γ is significant larger than for α both for the oligomers and for the nanotubes. It is found that the magnitude of γ with respect to the

	$N^{sat}(\alpha)$	α_{zz}^{∞}	$N^{sat}(\gamma)$	γ_{zzzz}^{∞}
Oligomers	1.4-4 nm	32.9-84.9 a.u/Å	2-8 nm	$6 \times 10^4 - 1.2 \times 10^6$a.u/Å
Nanotubes	4.5 nm	238.2 a.u/Å	7.5 nm	1.8×10^6 a.u/Å

TABLE 1.3*: Comparison of the saturation characteristics for the polarizability and second hyperpolarizability of carbon nanotubes and oligomers. Oligomers results taken from Ref. 101.*

length of carbon nanotubes is comparable with that of conjugated polymers whereas for α it is larger. For this reason, carbon nanotubes are demonstrated to be a valid alternative to conjugated polymers for constructing new materials for use in nonlinear optical devices, especially considering the possibilities of enhancing the nonlinearities of carbon nanotubes by means of either endohedral, exohedral or substitutional doping (see *e.g.* ref. 62, 71).

For the fullerene clusters studied in chapter 7 we found that the effects of the surrounding molecules on the molecular α and γ were large, in particular for the chain and the film because of the anisotropic surroundings, and that large clusters are required to obtain converged results. In Table 1.4 we present a comparison between the linear, $\chi^{(1)}$, and the nonlinear, $\chi^{(3)}$, susceptibilities calculated using three different local field models. The first model corresponds to a non-interacting model and the susceptibilities are simply obtained from the gas phase polarizability and second hyperpolarizability. The second model is a Lorentz-Lorenz model. Here the linear susceptibility is calculated from the gas phase polarizability. From the linear susceptibility the refractive index is calculated and used together with the gas phase second hyperpolarizability to calculate the nonlinear susceptibility. Finally the interacting model from chapter 7, where $\chi^{(1)}$ and $\chi^{(3)}$ have been calculated using a modified local-field theory which include the induced dipole moments of the surrounding molecules explicitly. We see that as expected the noninteracting

Local field model	$\chi^{(1)}$	$\chi^{(3)}$
Non interacting	0.11	0.14×10^{-13}esu
Lorentz-Lorenz	0.20	1.7×10^{-13}esu
Interacting	0.24	3.2×10^{-13}esu
Exp.	0.24-0.29	$16.1 - 36 \times 10^{-13}$esu

TABLE 1.4*: Linear and nonlinear susceptibilities for C_{60} fullerene cluster calculating using different local field models.*

susceptibilites are significant smaller than in the other models, especially the nonlinear susceptibility is smaller by an order of magnitude. If we compare the Lorentz-Lorenz model with the interacting model we see that for $\chi^{(1)}$ the difference is only $\sim 15\%$ whereas for $\chi^{(3)}$ it is $\sim 50\%$. The corresponding refractive index and dielectric constant compare well with experiments whereas the experimental nonlinear susceptibility is significant larger. However, one should realize that the comparison of $\chi^{(3)}$ with experiments is complicated by dispersion and vibrational contributions.

1.8 A discrete solvent reaction field model for molecular properties

The calculation of molecular properties of molecules in the condensed phase is a fundamental and important theoretical problem which still remains problematic. Most experimental measurements of NLO properties of organic chromophores are made in the condensed phase. Therefore, if we want to relate the microscopic properties calculated to the experimental quantities measured we need to consider the condensed phase explicitly. Furthermore, since molecular properties like (hyper)polarizabilities are sensitive to the local environment accurate calculations of these properties could serve as a test for the molecular models used in describing intermolecular forces. This will not only help develop rational design strategies for new NLO materials but also improve the general understanding of condensed phase materials at the molecular level.

Accurate calculation of molecular properties requires a quantum mechanical treatment which currently, due to high computational cost, are limited to small systems. Although, the size of these "small" systems grows steadily due to an increases in computational power and highly efficient software using parallel computing and linear scaling techniques. If we are for example interested in calculating the NLO properties of a chromophore in solution. Assuming unlimited computation powers we could calculate these properties using the supermolecular cluster approach. We keep on extending the cluster by adding more and more solvent molecules until the properties are converged. However, this approach means that most of our computational resources are used for calculating the properties of the solvent and not the chromophore we were interested in. Another example is proteins, where often the interest is in a small part of the protein, the active site, and the rest of the protein is consider as a "solvent". Therefore the most successful methods divide the total system into the molecular system of interest, which is treated with a quantum mechanical method, and another part which contains the rest of the system which is treated by a much simpler method, usually a classical description.[102–116] This separation of the system into two parts is illustrated in Figure 1.3.

Among these methods are the combined quantum mechanical and classical mechanics models (QM/MM).[105–116] In the QM/MM method the solvent molecules (MM) are treated with a classical force field and the interactions between the solute and solvent are described with an effective operator. In the QM/MM method the total (effective) Hamiltonian for the system is written as[105–116]

$$\hat{H} = \hat{H}_{QM} + \hat{H}_{QM/MM} + \hat{H}_{MM} \tag{1.55}$$

where $\hat{H}_{QM}$ is the quantum mechanical Hamiltonian for the solute, $\hat{H}_{QM/MM}$ describes the interactions between solute and solvent and $\hat{H}_{MM}$ describes the solvent-solvent interactions. We have recently developed such a method for studying solvent effect on molecular properties which we denoted the Discrete Solvent Reaction Field model (DRF) [Ref. 117–119, Chaps. 8, 9, 10] where the QM part is treated using DFT. Within the Discrete Solvent

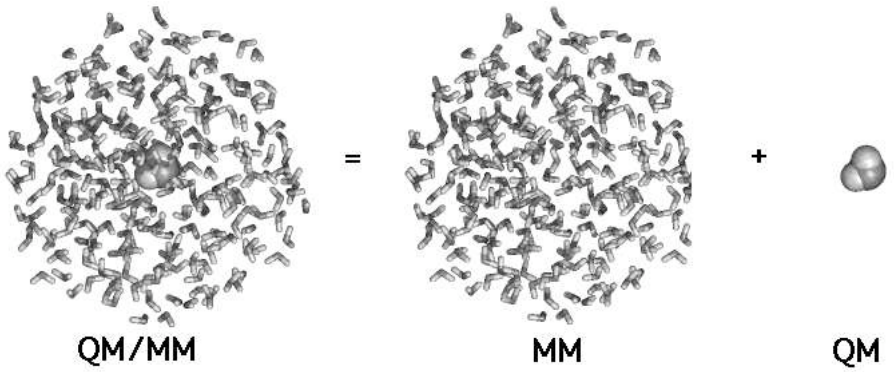

FIGURE 1.3: *An illustration of the separation of the total system into two subsystem used in the QM/MM model.*

Reaction Field model the QM/MM operator at a point r_i is given by

$$\hat{H}_{QM/MM} = \sum_i v^{DRF}(r_i, \omega) = \sum_i v^{el}(r_i) + \sum_i v^{pol}(r_i, \omega), \tag{1.56}$$

where the first term, v^{el}, is the electrostatic operator and describes the Coulombic interaction between the QM system and the permanent charge distribution of the solvent molecules. The second term, v^{pol}, is the polarization operator and describes the many-body polarization of the solvent molecules, *i.e.* the change in the charge distribution of the solvent molecules due to interaction with the QM part and other solvent molecules. The charge distribution of the solvent is represented by atomic point charges and the many-body polarization term is represented by induced atomic dipoles at the solvent molecules. The QM/MM interactions are introduced into the Kohn-Sham equations and all interactions are solved self-consistently, thereby allowing for the solute to be polarized by the solvent. Furthermore, the inclusion of polarizabilities in the MM part allows the solvent molecules to be polarized by the solute and by interactions with other solvent molecules. The advantage of including polarizabilities in the MM part is that all parameters can be obtained from gas phase properties. In general it is expected that a distributed polarizability approach will give better results than an approach using only an (anisotropic) polarizability located at a single site, especially when the size of the solvent molecule increases.[120] In Chapter 8 we describe the DRF model and the implementation within ground state DFT.[117] The treatment of linear response properties of molecules in solution using the DRF model within TD-DFT is presented in chapter 9.[118] The application of the DRF model to calculate the frequency-dependent hyperpolarizability of a molecule in solution within TD-DFT is described in chapter 10.[119]

Before we start discussing the results a small comment on the molecular properties actually calculated in the DRF approach, is required. The DRF operator in Eq. 1.56 represents the interaction between the solvent molecules and the solute when there is no external electric field present. That was exactly the reason for splitting the local discrete

field in Eq. 1.10 into two distinct parts. The second term, F^{perm}, in Eq. 1.11 arises from the permanent charge distribution of the surrounding molecules, which is described by Eq. 1.56 and now incorporated directly into the microscopic description through the effective Hamiltonian. Therefore, the properties which we calculate are the solute properties defined in Eq. 1.15. The first term, F^{ind}, in Eq. 1.11 which accounts for the induced polarization of the surrounding molecules due to the external electric field are therefore not included in the present description. The inclusion of this term in the microscopic treatment would require a coupling of the external electric field with the polarization operator, v^{pol}, in Eq. 1.56. This extension is required if we want to make a realistic comparison between experimental properties and calculated properties.

So far we have used the DRF model to study the molecular properties of a water molecule in a cluster of 127 classical water molecules. We have chosen water not because we consider it an interesting molecule with respect to its NLO properties, although the experimentally observed sign change in the first hyperpolarizability upon solvation is interesting. The reason is rather that for this particular cluster of water molecules there existed uncorrelated and correlated wave function QM/MM results. This enabled us to assess approximate xc-potentials for calculating molecular response properties in solution. This water cluster corresponds to an average water structure (AWS) obtained from MD simulations and should in an average way represent the local environment around the water molecule. Here we will extend the comparison between the DFT/DRF model and an accurate wave function QM/MM method to include results which have not been available before. In Table 1.5 we summarise the results for the dipole moment, polarizability,

		μ	$\overline{\alpha}(-\omega;\omega)$	$\overline{\beta}(-2\omega;\omega,\omega)$	$\overline{\gamma}(-2\omega;\omega,\omega,0)$
Gas					
	CCSD [a]	0.73	9.52	-19.26	1942
	DFT [b]	0.71	9.97	-20.42	2021.3
	Exp. [c]	0.73	9.83	-19.2±0.9	1800±150
Liquid					
AWS	CCSD/MM[a]	1.07	10.04	12.21	2169
AWS	DFT/DRF[b]	1.04	10.13	8.57(12.77)	2117.6
DWS	DFT/DRF [d]	1.09±6%	10.61±1%	12.51±48%	2230.36±7%

[a]Results are taken from: μ) Ref. 121, α) Ref. 122, β) Ref. 123, and γ) Ref. 124.
[b]Results are taken from: μ) Ref. 117, α) Ref. 118, β) Ref. 119, and γ) Ref. 119.
[c]Results are taken from: μ) Ref. 125, α) Ref. 126, β) Ref. 127, and γ) Ref. 127.
[d]Results are taken from Ref. 128

TABLE 1.5: *A comparison of the molecular properties of water in the gas phase and in the liquid phase. All results presented are in a.u. and the frequency used is* $\omega = 0.0428$ *a.u.*

first hyperpolarizability and the second hyperpolarizability of water in the gas phase and in solution. In the gas phase we compare the DFT results with Couple Cluster Singles Doubles (CCSD) wavefunction and experimental results. For the AWS we compare the

DFT/DRF results with the CCSD/MM results. If we compare the gas phase results we see that for all the properties there is a good agreement between the DRF and the CCSD results and that both methods are in good agreement with the gas phase experimental results. Therefore, we see that both DFT and CCSD can reproduce the experimetal results of water in the gas phase, indicating that vibrational contributions to these properties are small. If we compare the results for the AWS again we see a good agreement between the DFT/DRF and the CCSD/MM results. The only exception seems to be the first hyperpolarizability where the DFT/DRF result is smaller than that of CCSD/MM. However, as discussed in chapter 10 the cause was that at short distances the DRF operator in Eq. 1.56 is damped. The first hyperpolarizability calculated without the short range damping is also presented in Table 1.5 and seen to be in good agreement with the CCSD/MM results. For the other properties only small changes were found by ignoring the damping which indicated that especially the first hyperpolarizability was sensitive the the local molecular environment. In order to investigate this sensitivity of the molecular properties to changes

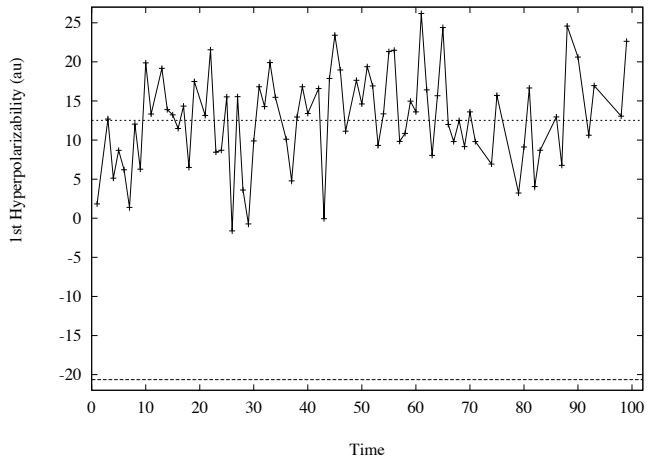

FIGURE 1.4*: The first hyperpolarizability of water in liquid water as a function of time in the MD simulation. Each point corresponds to a single DFT/DRF calculation of the first hyperpolarizability. The time separation between points is 0.5 ps. The lower horizontal line corresponds to the value of the first hyperpolarizability in the gas phase and the upper line to the average value in the liquid phase.*

in the local environment we performed[128] a new MD simulation. From this MD simulation we selected 101 different water structures (DWS) each containing 256 water molecules, *i.e.*, snapshots of the local molecular environment, well separated in time. We then performed a DFT/DRF calculation for each of the configurations and averaged the molecular properties obtained from these calculations. The average results are presented in Table 1.5. We see that the results obtained from AWS are in good agreement with the results from DWS except for the first hyperpolarizability. The standard deviation given in Table 1.5 represents the average fluctuation in the property. We see that except for the first hyper-

polarizability the fluctuations in the properties are small. The strong fluctuations in the first hyperpolarizability are illustrated in Figure 1.4, where the first hyperpolarizability is plotted for all 101 configurations. Therefore, in order to obtain a realistic description of molecular properties in solution a proper sampling of the local environment is crucial.

1.9 Outline of this thesis

In this chapter we have discussed several aspects of theoretical modelling of nonlinear optical response properties and the application of these models to nanostructures. The focus has been in particular on how to relate the calculated microscopic properties and the macroscopic properties measured in experiments. We have briefly described the method developed during this work and some of the results obtained using these models. However, a more detailed description of the models and the application of the models are described in the following chapters. In chapter 2 we describe the application of TD-DFT to study the nonlinear optical properties of substitute-doped fullerenes. The theory and application of a dipole interaction model to the polarizability of molecular clusters are presented in chapter 3. The extension of this model to the second hyperpolarizability is described in chapter 4. A localized dipole interaction model is described in chapter 5 and the application of the model to investigate the microscopic polarization in liquids is presented. The application of the dipole interaction model to investigate the saturation behavior of the second hyperpolarizability of carbon nanotubes is described in chapter 6. An investigation of the microscopic and macroscopic polarization in large fullerene cluster using the dipole interaction model are described in chapter 7. The discrete solvent reaction field model to describe molecular properties in solution and the application of the model to describe the dipole and quadrupole moments of water in the liquid phase are described in chapter 8. The extension of the discrete solvent reaction field model to time-dependent density functional theory is described in chapter 9. Finally, in chapter 10 the application of the discrete solvent reaction field model to calculate the nonlinear optical response properties of molecules in solution is presented.

Chapter 2

TD-DFT study of the second hyperpolarizability of substituted C_{60}

L. Jensen, P. Th. van Duijnen, J. G. Snijders, and D. P. Chong "Time-dependent density functional study of the second hyperpolarizability of BB-, NN- and BN-substituted C_{60}" *Chem. Phys. Lett.* **359**, 524-529, 2002.

2.1 Abstract

In this work we have investigated the effects of substituting carbon atoms with B and N on the second hyperpolarizability of C_{60} using time-dependent density functional theory. We have calculated the second hyperpolarizability of the double substitute-doped fullerenes C_{58}NN, C_{58}BB and C_{58}BN. For C_{60} only small changes in the second hyperpolarizability were found when doping with either 2B or 2N. However, by doping C_{60} with both B and N, creating an donor-acceptor system, an increase in the second hyperpolarizability with about 50% was found.

2.2 Introduction

Molecules which exhibit large nonlinear optical (NLO) response properties are of great technological importance. They define a new generation of compounds useful in information technology, where rapid communication processes are based on optical methods rather than electronics.[8,14] Conjugated organic molecules with delocalized electron systems are interesting because of their potentially large optical response properties. Fullerenes and carbon nanotubes have an extended π-system and are therefore promising candidates for new photonic materials.

Recently both experiments[67,68] and theory[64,65,69] have shown that the third-order nonlinearity of C_{60} is smaller than first assumed. For this reason the third-order nonlinearity of derivatives of C_{60} have been experimentally investigated and found to provide a large increase in the nonlinearity compared with the pure C_{60}, see e.g. Ref. 68,70. Theoretically, substitute-doping of the fullerene C_{60} with B or N has been suggested as another way of increasing the nonlinearity of the fullerenes.[72,73] These studies have been done using an extended Su-Schrieffer-Heeger (SSH) model[74] and show that doping enlarges the second hyperpolarizability by several orders of magnitude compared to the pure fullerenes, suggesting B-, N-, and BN-doped fullerenes as serious candidates for photonic devices. Since the SSH model predicts results[72] for the pure fullerene which are larger than that predicted with first-principle methods such as DFT and *ab initio* SCF[64,65,69] it is interesting also to investigate the effects of substitute-doping on the second hyperpolarizability of the fullerenes using DFT.

In this work we will investigate the effects of substitute-doped C_{60} with 2 B, 2 N and BN on the second hyperpolarizability component along the doping-axis. The calculation of the second hyperpolarizability will be done using time-dependent density functional theory (TD-DFT).

2.3 Computational details

Here we use TD-DFT for the calculations of the second hyperpolarizability, γ, as described in Ref. 57, 64, 129. First the first hyperpolarizability, β, is calculated analytically in the presence of a small electric field. The second hyperpolarizability can then be obtained by finite-field differentiation of the analytically calculated first hyperpolarizability as

$$\gamma_{\alpha\beta\gamma\delta}(0;0,0,0) = \lim_{E_\delta \to 0} \frac{\beta_{\alpha\beta\gamma}(0;0,0)|_{E_\delta}}{E_\delta}. \tag{2.1}$$

For all the TD-DFT calculations we used the RESPONSE code [57,130] in the Amsterdam Density Functional (ADF) program.[131–135] The ADF program uses basis sets of Slater functions where in this work a triple zeta valence plus polarization (in ADF basis set IV) were chosen as basis. The basis set was then augmented with field-induced polarization (FIP) functions of Zeiss *et al.*[136] They chose the exponents based on results of an exact

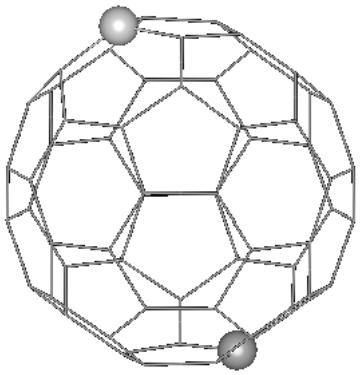

FIGURE 2.1: *Position of substituted atoms in C_{60}.*

analysis of field induced changes in hydrogen atom orbitals. We use both first- and second-order FIP functions since for the calculation of γ the second-order FIP functions are needed in order to get good results.[137] This basis set will here be denoted as IV++ ([6s4p2d1f] for C,N,B and [4s2p1d] for H). In order to test the quality of this basis set we also calculated γ for benzene and borazine using a large even-tempered basis set with additional diffuse functions ([8s6p4d4f] for C,N,B and [4s3p3d] for H), here called ET.

For the calculations of γ for the fullerenes we used the local density approximation (LDA) and the calculations were restricted to the static γ_{zzzz} component, which is the component along the doping-axis. This was done for two reasons. The first is to keep the computational burden as low as possible and the second is that the aim was to investigate the effects on γ by doping the fullerene not obtaining highly accurate results. However, in order to assess the validity of LDA we also tested three different exchange-correlation (xc) potentials, the Becke-Lee-Yang-Parr (BLYP),[138,139] the Perdew-Wang (PW91)[140] and the van Leeuwen-Baerends (LB94)[141] potentials for the calculations of γ for the benzene molecule.

All molecular geometries were optimized using the PW91 xc-potential. The benzene and borazine molecules are placed in the xy-plane. All geometries are available from the authors on request. The location of the doping atoms in the fullerene are illustrated in Fig. 2.1. For C_{60} the doping atoms are on opposite sides of the carbon cage and are identical to the (1,60) doping configuration of Xu *et al.*[73] The z-axis is taken along the direction from the pentagon in the bottom to the pentagon on the top. This configuration of the doping atoms were previously found to give the largest doping effects on the second hyperpolarizability[73] and is therefore the configuration used in this work.

	LDA/ET	LDA/IV	LDA	BLYP	PW91	LB94	SCF [a]	MP2[a]
α_{xx}	84.46	80.43	84.05	84.03	82.11	81.19	74.21	76.02
α_{zz}	45.46	39.68	45.42	46.37	44.46	36.76	39.47	41.28
γ_{xxxx}	21878	9459	16251	19530	17302	8540	14190	19332
γ_{yyyy}	21875	9417	16216	18875	17317	8550	14190	19332
γ_{xxyy}	7288	3142	5419	6899	5767	2851	4728	6402
γ_{zzzz}	16050	2381	14863	18190	16323	3724	12480	15708
γ_{yyzz}	8506	2140	7369	9276	7974	2190	6456	8688
γ_{xxzz}	8506	2140	7369	9276	7974	2190	6456	8688
$\overline{\gamma}$ [b]	21681	7220	17529	21499	18874	7055	15228	20386
$\overline{\gamma}$ [c]			19000	23800	-	12900	-	-

[a] From Ref. 142
[b] $\overline{\gamma} = \frac{1}{15}\sum_{i,j}(\gamma_{iijj} + \gamma_{ijij} + \gamma_{ijji})$.
[c] real-space results from Ref. 49.

TABLE 2.1: *Static polarizability and second hyperpolarizability for benzene (in au).*

2.4 Results

2.4.1 Second hyperpolarizability of benzene and borazine

The results for the static polarizability and second hyperpolarizability tensor for benzene and borazine are displayed in Tables 2.1 and 2.2, respectively. The errors introduced in adopting the combination of single-side finite-field and analytical techniques can be estimated from the differences between γ_{xxxx} and γ_{yyyy} which by symmetry arguments should be identical for both benzene and borazine. It is found that the difference between γ_{xxxx} and γ_{yyyy} is very small, especially using LDA. With LDA we performed calculations both with the IV, IV++ and the ET basis sets. In general there is reasonable agreement between the results obtained with the IV++ and the ET basis sets, especially for the polarizability. The IV basis set clearly underestimates the second hyperpolarizability most noticeable in the direction perpendicular to the ring, i.e. γ_{zzzz}, which illustrates the importance of the FIP's. Comparing the results obtained with IV++ and ET the largest deviation, around 25%, is found for the γ_{xxxx} and γ_{yyyy} components of benzene. However, comparing the mean hyperpolarizability, $\overline{\gamma}$, for benzene with the recent results of Iwata *et al.*[49] we only find around an 8% deviation. In their work they use a real-space TD-DFT method which gives results for the second hyperpolarizability in agreement with TD-DFT results close to the basis-set limit.[49] We therefore believe that the basis-set (IV++) used here, captures most features of the second hyperpolarizability and is adequate for the study on larger systems where the basis-set effect are expected to be smaller.

In Table 2.1 we also present the polarizability and second hyperpolarizability for benzene calculated using the basis set IV++ and various xc-potentials. First it is noted that the effect of using a GGA functional (PW91,BLYP) gives an increase in the second hyperpolarizability but the effect is very small. This is in good agreement with studies of

	LDA/ET	LDA/IV	LDA	SCF [a]	MP2[a]
α_{xx}	76.45	72.20	76.66	66.85	75.64
α_{zz}	48.51	40.83	46.53	40.39	44.31
γ_{xxxx}	21814	12273	17745	-	-
γ_{yyyy}	21654	12128	17606	-	-
γ_{xxyy}	7213	4042	5865	-	-
γ_{zzzz}	13203	4221	13901	-	-
γ_{yyzz}	5874	1775	5565	-	-
γ_{xxzz}	5874	1775	5565	-	-
$\overline{\gamma}$	18919	8761	16648	-	-

[a]From Ref. 143.

TABLE 2.2*: Static polarizability and second hyperpolarizability for borazine (in au).*

the second hyperpolarizability for small molecules.[49,129,137] Secondly, the effect of using a xc-potential which has the correct asymptotic behavior (LB94) on the second hyperpolarizability is large. The results using the LB94 potential is between 2 and 4 times smaller than the LDA results. This finding is in agreement with the results of van Gisbergen *et al.* using the same functional.[129] However, the LDA results for the second hyperpolarizability for benzene obtained here is in good agreement with both the SCF and MP2 results of Perrin *et al.*[142] Also, the static polarizability for benzene and borazine calculated using LDA are larger than the MP2 and SCF results in good agreement with previous findings.[144] Therefore, to improve the LDA results a functional which provides both correct inner and outer parts of the xc-potential is needed.[45]

2.4.2 Second hyperpolarizability of C_{60}

The static second hyperpolarizability components along the z-axis for the fullerene C_{60} are presented in Table 2.3. For C_{60} there is only one independent component and γ_{zzzz} is therefore equal to the average second hyperpolarizability. Also presented in Table 2.3 are three recent theoretical predictions of the second hyperpolarizablility of C_{60}. A comparison with experiments are difficult due to the large differences in the experimental results[64,65,69] and the comparison will therefore only be made with theoretical results. In this work we have neglected vibrational, dispersion and solvent effect and these factors have to be considered when comparing with experiments. Karna *et al.* also discussed other problems in relating calculated values with experimental results for benzene.[145] Our results for the second hyperpolarizability of C_{60} is about 35% larger than the previously reported LDA result[64] but is in reasonable good agreement with the recent real-space LDA result[49] and the SCF result.[65] This again supports the notion that the basis set used here is adequate to study the second hyperpolarizability of large systems, especially, because of the agreement with our results and the real-space results both for benzene and C_{60}.

	C_{60}	$C_{58}N_2$	$C_{58}B_2$	$C_{58}BN$
β_{zzz}	-	-	-	-602.01
γ_{zzzz}	137950	130147	155430	208470
γ_{zzzz} [a]	124000			
γ_{zzzz} [b]	87438			
γ_{zzzz} [c]	113765			

[a]Real-space LDA result from Ref. 49
[b]LDA result from Ref. 64
[c]SCF results from Ref. 65

TABLE 2.3: *Second hyperpolarizability of pure and substituted fullerenes(in au).*

2.4.3 Second hyperpolarizability of substituted C_{60}

In Table 2.3 the results for the first and second hyperpolarizability of B,N-substituted C_{60} are displayed. Only the BN substituted fullerene has a first hyperpolarizability which is different from zero. We find only small differences in the second hyperpolarizability between the 2N- and 2B-substituted C_{60} and the pure C_{60} molecule. Substituting with 2N decreases the second hyperpolarizability with about 5% and substituting with 2B increases the second hyperpolarizability with about 12%. This is in contrast to the results obtained with a SSH model[72,73,78] where increases by several orders of magnitude were found both by substituting with B and with N. This increase in the second hyperpolarizability were found both for mono-substituted C_{60}[72] and double substituted C_{60}[73] where the largest increase were found for two B-substituted C_{60}. From populations analysis it was found that N acts as an electron acceptor and B as an electron donor in the doubly substituted fullerene [1] which was also found in a previously study.[146] Therefore, the effects of doping C_{60} with either B or N will affect the π-electron density in different ways and therefore also the nonlinear optical properties. For this reason we also calculated the second hyperpolarizability of C_{60} substituted with both B and N creating a donor-acceptor system with B as donor and N as acceptor. For this system it is found that the second hyperpolarizability is increased with around 50% compared with the undoped system. Also, the first hyperpolarizability is of the same order as that of p-nitroaniline calculated with SCF, see e.g. 147. However, in general the doping effect on the hyperpolarizabilties of C_{60} found here is very small compared with that found for fullerene derivatives.[68,70] Since the hyperpolarizabilities are expected to increase with an increase in the distance between the donor and acceptor it would be interesting to investigate the scaling behaviour of the hyperpolarizability of doped fullerenes as a function of the cage size. Also, in push-pull derivatives of C_{60} a relationship between the conjugation path length between donor/acceptor groups and the first hyperpolarizability was found.[148] For pure carbon structures it is found that the carbon nanotubes have larger second hyperpolarizabilities than the fullerenes with the

[1]The Mulliken charge on B in $C_{58}B_2$ was 0.97 and the charge on N in $C_{58}N_2$ was -0.53. In $C_{58}BN$ the charge on B was 0.93 and on N -0.52.

same number of atoms[149] and the effect of substituting nanotubes instead of fullerenes as a way of increasing the second hyperpolarizability would also be interesting.

2.5 Conclusion

We have used TD-DFT to calculate the second hyperpolarizability of the doubly substitute-doped fullerenes $C_{58}NN$, $C_{58}BB$ and $C_{58}BN$ after testing the procedure on benzene and borazine. Reasonable good agreement is found with previously results for benzene, borazine and C_{60}, especially considering the small size of the basis set used in this work. Only small changes in the second hyperpolarizability were found when doping C_{60} with either 2B or 2N. However, an increase with 50% was found when doping C_{60} with both B and N. We therefore propose BN-doped fullerenes as an interesting starting point for further investigations of the hyperpolarizabilities of doped fullerenes and carbon nanotubes.

Acknowledgment

The Danish Research Training Council is gratefully acknowledged for financial support of L.J.

Chapter 3

A dipole interaction model for the polarizability

L. Jensen, P.-O. Åstrand, A. Osted, J. Kongsted, and K. V. Mikkelsen "Polarizability of molecular clusters as calculated by a dipole interaction model" *J. Chem. Phys.* **116**, 4001-4010, 2002.

3.1 Abstract

We have developed and investigated a dipole interaction model for calculating the polarizability of molecular clusters. The model has been parametrized from the frequency-dependent molecular polarizability as obtained from quantum chemical calculations for a series of 184 aliphatic, aromatic and hetero-cyclic compounds. A damping of the interatomic interaction at short distances is introduced in such a way as to retain a traceless interaction tensor and a good description of the damping over a wide range of interatomic distances. By adopting atomic polarizabilities in addition to atom-type parameters describing the damping and the frequency-dependence, respectively, the model is found to reproduce the molecular frequency-dependent polarizability tensor calculated with *ab initio* methods. A study of the polarizability of four dimers has been carried out: the hydrogen fluoride, methane, benzene and urea dimers. We find in general good agreement between the model and the quantum chemical results over a wide range of intermolecular distances. To demonstrate the power of the model, the polarizability has been calculated for a linear chain of urea molecules with up to 300 molecules and one- and two-dimensional clusters of C_{60} with up to 25 molecules. Substantial intermolecular contributions are found for the polarizability anisotropy, whereas the effects are small for the mean polarizability. For the mean polarizability of C_{60}, we find good agreement between the model and experiments both in the case of an isolated molecule and in a comparison of a planar cluster of 25 C_{60} molecules with experimental results on thin films.

3.2 Introduction

The design of new carbon-based materials for potential use in optoelectronic and photonic devices is of great technological importance. These new materials will lead to a new generation of information technology where optical methods are the basis for rapid communication processes.[8,9,11] One promising class of materials is the so-called molecular materials, *i.e.*, materials consisting of molecular entities. The optical response properties of this class of materials are to a large extent governed by the properties of the individual molecules and to some extent by the interactions with the neighboring molecules. Therefore, understanding the response properties of the bulk materials, the molecular response properties and the perturbations caused by environmental interactions are needed in order to achieve an efficient procedure for designing optical molecular materials at the atomistic level.[8,12,14–18] From a theoretical point of view, the molecular response to an external electromagnetic field is calculated most efficiently by applying quantum chemical response theory.[150] Accurate quantum chemical calculations of molecular properties can, however, only be carried out for rather small molecules due to the large requirements of computer resources. Furthermore, the use of conventional density functional theory, which in general gives improved accuracy over the Hartree-Fock approximation at a similar or lower computational cost, gives relatively poor results for nonlinear optical properties of large conjugated molecular chains.[82,83] Therefore, for large molecules and assemblies of molecules, modeling is currently restricted to less sophisticated methods.

The isotropic part of the molecular polarizability is to a good extent an additive property, indicating that the polarizability can be calculated from a sum of transferable atomic or bond contributions. However, perfect additivity can only occur if the subunits are non-interacting, which obviously is not the case for atoms in molecules. Therefore, as pointed out by Silberstein,[87] the molecular polarizability is not additive unless the chemical environment of each atom is considered in detail. The chemical environment was first introduced by using bond polarizability models,[151,152] which were quite successful in reproducing the static mean polarizability (the isotropic part of the polarizability tensor) of alkanes.[152] Different methods using the additivity concept have also been proposed[153–155] and these models are in general successful in reproducing the molecular mean polarizability. Recently, the additivity model was adopted for the static polarizability tensors of organic molecules[156,157] and also for both the static and frequency-dependent polarizability tensors of halogen derivatives of benzene[158] using atomic polarizability tensor elements. However, since the molecular polarizability is a tensor, also the atomic contributions have to be tensors in an additive model leading to a larger number of parameters to be determined.

A more elaborate model, but yet very simple compared with quantum chemical calculations, is the dipole interaction model of Applequist *et al.*[90,91,159] based on the early work of Silberstein.[87–89] In the interaction model, the atoms of a molecule in an external field interact by means of their atomic induced dipole moments according to classical electrostatics. Even if the atomic parameters are isotropic polarizabilities, an anisotropy of the molecular polarizability is introduced by the electric fields from the surrounding atoms. An important extension of the interaction model was to include overlap effects on the internal

electric fields,[93,160,161] *i.e.*, the electric field at the nucleus is damped. In particular, the model of Thole[93] has turned out to be successful in predicting the molecular polarizability tensor using model atomic polarizability parameters independent of the chemical environment of the atom. Thole's model has recently been investigated in more detail[94,162–166] and also extended to include atom-type damping parameters and the treatment of the frequency-dependent polarizability tensor.[94,166]

However, despite the success of the Thole model, a problem arises from the introduction of the damping term into the interaction tensor. The modification of the interaction tensor leads to a tensor which, in contrast to the undamped tensor, is not traceless. In addition, the most promising damping function suggested by Thole[93] is not continuous. This discontinuity may give problems at small intermolecular distances and is therefore not suitable for investigating intermolecular interactions.[165]

In this study, we present a way of introducing a damping of the interaction tensor which preserves the traceless property of the interaction tensor. The formulae will in principle be valid for all terms of the interaction tensor in the multipole expansion. Furthermore, the way that atom-type damping parameters are introduced is given a more firm theoretical base than the more *ad hoc* approach adopted previously.

Both in the additivity and interaction models, the model atomic (or bond) polarizabilities are fitted to the molecular polarizabilities of a trial set of molecules. Therefore, the quality of the data in the trial set will affect the accuracy and the actual values of the model parameters. In particular, experimental molecular polarizabilities also include zero-point vibrational and pure vibrational contributions that most probably are not negligible.[25,167,168] It is therefore preferred to use quantum chemical calculations of molecular electronic polarizabilities for the parameterization. Here, we extend the set of aromatic and aliphatic molecules employed previously[94] to also include hetero-monocyclic compounds containing B, N, and C atoms and we parameterize the model from *ab initio* frequency-dependent molecular polarizabilities. The obtained model will be used to study the interaction polarizability of four dimers, the HF, methane, benzene and urea dimers. Since the aim of the work is to treat large molecular assemblies, we also present results for one-dimensional urea chains with up to 300 molecules and for one- and two-dimensional C_{60} clusters with up to 25 molecules. To our knowledge, this is the first theoretical study of the polarizability of C_{60} clusters and it gives the possibility of comparing with the polarizability obtained from experiment on thin films. The additional boron parameters are used in a separate work on boron nitride nanotubes.[100]

3.3 The Dipole Interaction Model

Considering a set of N interacting atomic polarizabilities, the atomic induced dipole moment, μ_p^{ind}, due to an external electric field, E^{ext}, is given by

$$\mu_{p,\alpha}^{\text{ind}} = \alpha_{p,\alpha\beta}\left(E_\beta^{\text{ext}} + \sum_{q\neq p}^{N} T_{pq,\beta\gamma}^{(2)}\mu_{q,\gamma}^{\text{ind}}\right), \tag{3.1}$$

where $T^{(2)}_{pq,\beta\gamma}$ is the so-called dipole interaction tensor given as

$$T^{(2)}_{pq,\beta\gamma} = \frac{3r_{pq,\beta}r_{pq,\gamma}}{r^5_{pq}} - \frac{\delta_{\beta\gamma}}{r^3_{pq}}. \tag{3.2}$$

In Eq. 3.1 the Einstein summation convention for repeated indices has been employed, and it is used throughout this work. The molecular polarizability can be written as[90]

$$\alpha^{\mathrm{mol}}_{\alpha\beta} = \sum_{p,q}^{N} B_{pq,\alpha\beta}, \tag{3.3}$$

where $\mathbf{B}$ is the relay matrix defined in a supermatrix notation as

$$\mathbf{B} = \left(\boldsymbol{\alpha}^{-1} - \mathbf{T}^{(2)}\right)^{-1}. \tag{3.4}$$

If we consider two interacting atoms, p and q, the polarizability parallel, $\alpha_\parallel$, and perpendicular, $\alpha_\perp$, to the axes connecting the atoms are given by Silberstein's equations[89]

$$\alpha_\parallel = \frac{\alpha_p + \alpha_q + 4\alpha_p\alpha_q/r^3}{1 - 4\alpha_p\alpha_q/r^6}, \tag{3.5}$$

$$\alpha_\perp = \frac{\alpha_p + \alpha_q - 2\alpha_p\alpha_q/r^3}{1 - \alpha_p\alpha_q/r^6}. \tag{3.6}$$

Inspection of Eqs. 3.5 and 3.6 shows that when r approaches $(4\alpha_p\alpha_q)^{1/6}$, $\alpha_\parallel$ goes to infinity and it becomes negative for even shorter distances. Thole avoided this "polarizability catastrophe" by modifying the dipole interaction tensor using smeared-out dipoles.[93] The interaction tensor was first rewritten in terms of a reduced distance $u_{pq,\beta} = r_{pq,\beta}/(\alpha_p\alpha_q)^{1/6}$ as

$$T^{(2)}_{pq,\beta\gamma} = (\alpha_p\alpha_q)^{1/2} t(u_{pq}) = (\alpha_p\alpha_q)^{1/2} \frac{\partial^2\phi(u_{pq})}{\partial u_{pq,\beta}\partial u_{pq,\gamma}} \tag{3.7}$$

where $\phi(u_{pq})$ is a spherically symmetric potential of some model charge distribution ρ. Thole considered several different forms of the charge distribution and obtained the most promising results using an interaction tensor of the form,

$$T^{(2)}_{pq,\beta\gamma} = \frac{3\upsilon^4_{pq}r_{pq,\beta}r_{pq,\gamma}}{r^5_{pq}} - \frac{(4\upsilon^3_{pq} - 3\upsilon^4_{pq})\delta_{\beta\gamma}}{r^3_{pq}} \tag{3.8}$$

where $\upsilon_{pq} = \frac{r_{pq}}{s_{pq}}$ if $r_{pq} < s_{pq}$, otherwise $\upsilon_{pq} = 1$ and the normal dipole interaction tensor is recovered. Thole originally defined $s_{pq} = a(\alpha_p\alpha_q)^{1/6}$ with a global damping parameter a. We recently investigated a slightly modified definition, namely $s_{pq} = (\eta_p\eta_q)^{\frac{1}{4}}$ where η_p is a fitting parameter assumed to be proportional to the atomic second order moment,[94] thereby introducing in an *ad hoc* fashion atom-type damping parameters. Here, this model will be termed the IM-MT model, where IM denotes interaction model and MT denotes modified Thole.

The modification of the interaction tensor in Eq. 3.8 leads to a tensor with a trace different from zero. The undamped interaction tensor is traceless and the importance of this can be illustrated by considering the molecular quadrupole moment. The quadrupole moment is often chosen as being traceless,[169] and one reason for this is that its trace does not contribute to the interaction energy according to classical electrostatics. This is noticed from regarding the interaction between a test charge and a quadrupole moment, $\frac{1}{3}q_A T^{(2)}_{AB,\alpha\beta} Q_{B,\alpha\beta}$ and adding a small contribution Δ to each of the diagonal components of $Q_{B,\alpha\beta}$. The additional contribution from Δ to the interaction energy is obtained as

$$\frac{1}{3}q_A \Delta \left(T^{(2)}_{AB,xx} + T^{(2)}_{AB,yy} + T^{(2)}_{AB,zz} \right) \tag{3.9}$$

which normally is zero because $T^{(2)}_{AB,\alpha\beta}$ is traceless. The non-traceless tensor will in principle not give wrong polarizabilities, but the choice will affect the obtained values of the fitted parameters. However, in order to retain the property of $T^{(2)}$ as being traceless, we introduce the damping in a different way. In particular, this will be of importance if the interaction model is extended to molecular dipole-quadrupole polarizabilities and dipole-dipole hyperpolarizabilities. For example, the leading term to an interaction model for the first hyperpolarizability, β, arises from an atomic dipole-quadrupole hyperpolarizability,[170] and includes normally a traceless definition of the quadrupole moment. However, the traceless definition of the quadrupole moment has been criticized because some electromagnetic observables apparently become origin-dependent for this choice of definition.[171]

Damping may be included by modifying the distance r_{pq} to obtain a scaled distance, s_{pq},

$$s_{pq} = v_{pq} r_{pq} = f(r_{pq}), \tag{3.10}$$

where v_{pq} is a scaling factor and $f(r_{pq})$ is an appropriately chosen function of r_{pq}. Furthermore, if each component of r_{pq} also is scaled by v_{pq}, the reduced distance becomes,

$$s_{pq} = \sqrt{s_{pq,\alpha} s_{pq,\alpha}} = v_{pq} \sqrt{r_{pq,\alpha} r_{pq,\alpha}} = v_{pq} r_{pq}, \tag{3.11}$$

which is consistent with the definition in Eq. 3.10. The interaction tensor can thus be obtained from

$$T^{(n)}_{pq,\alpha_1 \ldots \alpha_n} = \nabla_{\alpha_1} \ldots \nabla_{\alpha_n} \left(\frac{1}{s_{pq}} \right), \tag{3.12}$$

which is equivalent to replacing r_{pq} by s_{pq} and $r_{pq,\alpha}$ by $s_{pq,\alpha}$ in the regular formulae for the interaction tensor.

To derive explicit formulas for the scaling function $f(r_{pq})$ we consider the interaction between two spherical Gaussian charge distributions with exponents Φ_p and Φ_q and normalized to one. The interaction energy is given by[172,173]

$$V = \iint \frac{\rho_p(r_1)\rho_q(r_2)}{r_{12}} dr_1 dr_2 = \frac{erf(\sqrt{a} r_{pq})}{r_{pq}}. \tag{3.13}$$

where a is the reduced exponent $a = \Phi_p \Phi_q / (\Phi_p + \Phi_q)$ and $erf(\sqrt{a} r_{pq})$ is the regular error function. As the exponent $\sqrt{a} r_{pq}$ tends to infinity, the error function tends to 1 and we

recover the usual expression for a point charge. This leads to a scaling function of the form,

$$f(r_{pq}) = \frac{r_{pq}}{\mathrm{er}f(\sqrt{a}r_{pq})}. \tag{3.14}$$

The components of the scaled distance vector, $s_{pq,\alpha}$, are calculated as $v_{pq}r_{pq,\alpha}$, where v_{pq} is obtained from Eq. 3.10 as

$$v_{pq} = \frac{f\left(r_{pq}\right)}{r_{pq}} \ . \tag{3.15}$$

However, due to the relatively complex form of the error function we have also investigated two approximations of this function,[174] namely

$$f(r_{pq}) = \sqrt{r_{pq}^2 + \frac{\pi}{4a}} \tag{3.16}$$

and

$$f(r_{pq}) = \left(r_{pq}^4 + \frac{\pi^2}{16a^2}\right)^{1/4}. \tag{3.17}$$

The approximations in Eqs. 3.16 and 3.17 can be realized considering the limits of Eq. 3.13 at $r_{pq} \to 0$ and $r_{pq} \to \infty$, *i.e.*

$$\lim_{r_{pq}\to\infty} \frac{\mathrm{er}f(\sqrt{a}r_{pq})}{r_{pq}} = \frac{1}{r_{pq}} \tag{3.18}$$

and

$$\lim_{r_{pq}\to 0} \frac{\mathrm{er}f(\sqrt{a}r_{pq})}{r_{pq}} = \frac{1}{\sqrt{\frac{\pi}{4a}}}. \tag{3.19}$$

To give the correct limiting behavior, the combination of Eqs. 3.18 and 3.19 may lead to either Eq. 3.16 or Eq. 3.17. The three different models will be denoted according to the scaling function used, *i.e.*, IM-ERF, IM-SQRT or IM-QDRT if, respectively, Eq. 3.14, Eq. 3.16 or Eq. 3.17 is used. It is noted that in particular the form of the damping in Eq. 3.16 would be efficient in molecular dynamics simulations of condensed phases because in principle it only involves an extra addition in the calculation of the distance.

Well below the first electronic absorption, the frequency-dependence of the molecular polarizability is often approximated with an Unsöld-type of expression.[15] Here we assume that the atomic polarizability has a similar frequency-dependence,[94]

$$\alpha_p(-\omega;\omega) = \alpha_p(0;0) \times \left[\frac{\overline{\omega_p}^2}{\overline{\omega_p}^2 - \omega^2}\right] \ , \tag{3.20}$$

where $\overline{\omega}_p$ is an atom-type parameter and ω is the frequency.

3.4 Quantum chemical calculation

The quantum chemical computations of frequency-dependent polarizabilities were carried out with the DALTON program package[175] as described in Refs. 150, 176, 177 using linear response functions at the self-consistent field (SCF) level. The basis set of Sadlej[178] was employed because it has been shown previously that it gives good results for polarizabilities considering its limited size.[158] The following frequencies have been used: $\omega(a.u.)/\lambda(nm) = 0.0/\infty$, 0.02389/1907, 0.04282/1064 and 0.0774/589 (1 a.u. = 27.21 eV). A series of 74 molecules has been generated from four disubstituted six-membered hetero-monocyclic compounds containing B, N, and C atoms.[179] The hetero-rings investigated were borazine, 1,3,5-triborate, hexahydro-1,3,5-triazine and hexahydro-1,4-diboro-2,5-diazine where the nomenclature used is the extended Hantzsch-Widman system.[180] The geometry of the substituted hetero-rings were optimization at the PM3 level with the GAUSSIAN 94 program package.[181] The set of 74 hetero-rings were added to the set of 113 molecules (the original set of 115 molecules apart from the two biphenyls) used in the previous study of aliphatic and aromatic molecules.[94] The geometry of the molecules in the original set were generated adopting standard bond lengths and bond angles taken from Refs 182, 183. We have not included olephines in the trial set since in this case intramolecular charge-transfer effects are important, and these effects cannot be modeled on the basis of atomic polarizabilities only.[184–186] It is noted that we use different kinds of molecular geometries for different molecules. The obtained atomic parameters should, however, be independent of the choice of molecular geometry because the geometry dependence is included explicitly in the $T^{(2)}$ tensor (see Eq. 3.2). In contrast, for applications the choice of molecular geometries can be crucial in the comparison of model results with experimental data. A crucial test of the atomic parameters would be to calculate polarizability derivatives and thereby Raman scattering parameters in line with the work by Applequist and Quicksall.[91,187]

The parameters describing the frequency-dependent polarizabilities have been optimized using the same scheme as in Ref 94. For the static polarizability, the root-mean-square (rms) of the differences between the quantum chemical molecular polarizability tensors, $\alpha^{QC}_{\alpha\beta,i}$, and the model molecular polarizability tensors, $\alpha^{model}_{\alpha\beta,i}$, are minimized as

$$rms = \sqrt{\frac{\sum_{i=1}^{N}\sum_{\alpha,\beta=1}^{3}\left(\alpha^{model}_{\alpha\beta,i} - \alpha^{QC}_{\alpha\beta,i}\right)^2}{N-1}}, \tag{3.21}$$

where N is the number of molecules.

The parameters describing the frequency-dependence of the molecular polarizability have been optimized by minimizing

$$rms = \sqrt{\frac{\sum_{i=1}^{N}\sum_{\alpha,\beta=1}^{3}\left[\left(\alpha^{model}_{\alpha\beta,i}(\omega) - \alpha^{model}_{\alpha\beta,i}(0)\right) - \left(\alpha^{QC}_{\alpha\beta,i}(\omega) - \alpha^{QC}_{\alpha\beta,i}(0)\right)\right]^2}{N-1}}, \tag{3.22}$$

i.e. we parameterize the frequency-dependence only and do not attempt to correct for errors introduced in the parameterization of the static polarizability.

The *interaction* polarizability, $\Delta\alpha$, was calculated as the difference between the dimer polarizability and twice the monomer polarizability as

$$\Delta\alpha = \alpha^{dimer} - 2\alpha^{monomer}, \tag{3.23}$$

and for the SCF calculations on the complexes, we corrected for basis set superposition errors (BSSE) by the counterpoise method.[188] Four different kinds of dimers were included in the study. The HF dimer has a single hydrogen bond whereas the linear urea dimer forms two hydrogen bonds. In addition, two nonpolar complexes, the methane and benzene dimers, are included where the attractive part of the interaction is dominated by dispersion interactions. In the case of the benzene dimer, it was arranged such that the π-electrons are perturbed which is not the most likely orientation but it serves as a severe test of the model. The relative orientations of the molecules in the dimers are displayed in Fig. 3.1.

(a) HF dimer (b) Methane dimer (c) Benzene dimer (d) Urea dimer

FIGURE 3.1*: Relative orientation of the four dimers.*

It should be noted that the interaction polarizabilities are often rather small compared with the molecular polarizability and they will therefore be critical tests of the model. The HF, methane and benzene molecules have been included in the training-set described above, whereas the urea molecule was not included. The geometry of the urea molecules was taken from Ref. 189. For the calculations on the urea chains, the intermolecular distance between the centre-of-mass of the urea molecules in the planar urea chains is 9.5 bohr which corresponds to the equilibrium distance of the linear dimer.[190] The structure of the C_{60} molecule was taken from our previous work.[94] Solid C_{60} exhibits a face-centered-cubic structure with a lattice vector a_0 = 14.17 Å giving a nearest-neighbor distance of a = 10.02. Å[191] The one- and two-dimensional clusters were constructed using this nearest-neighbor distance and the two-dimensional structure is illustrated in Fig. 3.2.

3.5 Results

The optimized parameters describing the static polarizability for the IM-MT, IM-ERF, IM-QDRT, and IM-SQRT models are given in Table 3.1, where also the parameters from our previous work[94] on the IM-MT model are included. A detailed comparison with the

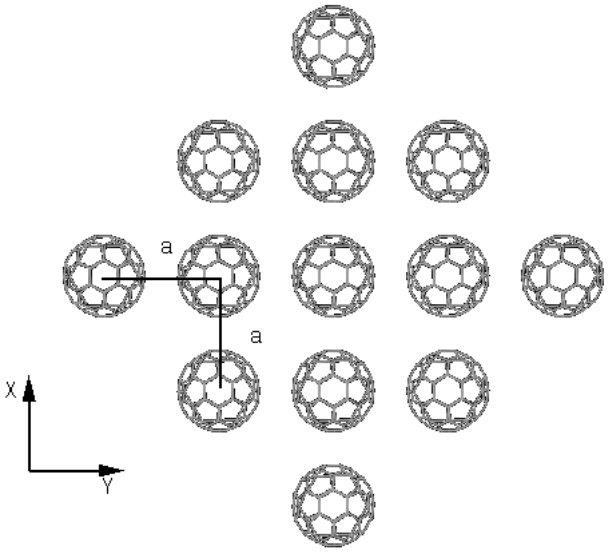

FIGURE 3.2: *The 2-dim. C_{60}-cluster with 13 molecules. The distance between nearest molecules is a = 10.02 Å.*

Applequist model and the Thole model has not been carried out here but can be found in, *e.g.*, Ref. 94.

For the IM-MT model, which includes the additional heterocyclic molecules in comparison with our previous work, we find that the inclusion of the heterocyclic molecules in the training set does not reduce the accuracy of the model. However, the actual values of the parameters change considerably, and in particular the damping parameters are different. For the polarizability parameters, the largest changes are found for α_N. The reason is that all added molecules contain BN-ring systems, which means that we have added a new type of nitrogen-containing molecules. This indicates that damping is especially important for ring-systems which is also discussed by Applequist[185] in his *partial neglect of ring interactions* (PNRI) approximation for aromatic molecules. In the PNRI approximation, C is assigned an anisotropic polarizability (components parallel and perpendicular to the ring) and interactions between carbon atoms in the same conjugated system are neglected. The PNRI approximation is required in the Applequist model in order to get a reasonable description of the polarizability perpendicular to the ring in aromatic molecules.

As noticed in Table 3.1, the values of the polarizability parameters are lowered for the approaches included here (IM-ERF, IM-QDRT, IM-SQRT), but this is compensated by modifying the damping parameters. In general, it seems like the damping parameters are more affected by the choice of training set, optimizing procedure, etc. than the atomic polarizabilities. Both the polarizability and damping parameters are very similar for all three models as expected due to the similarity of the damping functions. The best fit is obtained for the simplest model, IM-SQRT, although no significant difference between the IM-SQRT model and the IM-QDRT model is found. Compared with the IM-MT model,

Damping	IM-MT				IM-ERF		IM-QDRT		IM-SQRT	
Atom	α_p	Φ_p	α_p [a]	Φ_p [a]	α_p	Φ_p	α_p	Φ_p	α_p	Φ_p
H	2.118	1.090	1.84	2.75	1.335	0.267	1.310	0.336	1.280	0.358
B	10.612	9.475	-	-	8.782	0.047	8.611	0.075	8.649	0.074
C	11.111	7.600	11.52	20.99	8.405	0.083	8.415	0.124	8.465	0.124
N	8.365	6.491	10.55	26.55	5.994	0.177	6.127	0.274	6.169	0.268
O	6.982	3.825	5.64	12.16	3.626	2.794	3.805	2.649	3.754	4.103
F	2.603	1.752	2.25	4.78	1.967	1.667	1.937	1.653	1.907	1.468
Cl	15.342	4.921	16.08	17.64	13.101	0.185	13.084	0.468	13.081	0.453
rms [b]	6.29		6.67		5.71		5.30		5.29	
mae [c]	4.98 ± 2.98 %		-		3.71 ± 2.66 %		3.50 ± 2.56 %		3.55 ± 2.60 %	

[a] See Ref. 94. Fitted to 115 aliphatic and aromatic molecules.
[b] Optimized error, see Eq. 3.21.
[c] Mean absolute error in diagonal components.

TABLE 3.1: *Atomic parameters fitted to model the static polarizability (in a.u., 1 a.u.=0.1482 Å^3).*

the IM-SQRT model gives an improvement of around 15% which is substantial considering that only the damping function has been changed and no additional fitting parameters have been included.

The relative mean absolute error (*mae*) in the diagonal components is also presented in Table 3.1. It should be noted that the *rms* includes both diagonal and off-diagonal components. The IM-QDRT model gives the lowest *mae* but again there is little difference between the IM-SQRT and IM-QDRT models. The IM-SQRT is therefore expected to give results which are within 6% of the SCF results.

If the atomic parameters are compared, it is found for the IM-MT model that α_B is slightly smaller than α_C, which is unphysical. In contrast, for the three new models α_B is slightly larger than α_C. The differences are, however, small and changes in the α-parameters may be compensated by modifying the Φ-parameters. For the three new models, it is also noted that in particular Φ_O but also Φ_F are considerably larger than the other Φ-parameters. This can be understood since the damping term $\frac{1}{a}$ can be rewritten as $\frac{1}{a} = \frac{1}{\Phi_p} + \frac{1}{\Phi_q}$ and therefore the smallest damping parameter will to a large extent determine the damping. Even if one may regard the Φ-parameters as a measure of an atomic second moment, it is, as already mentioned, our experience that the actual values of the Φ-parameters are sensitive to the optimization procedure. Presently, it is therefore difficult to regard the Φ-parameters as anything else than fitting parameters.

In Table 3.2, we present the parameters describing the frequency-dependence of the polarizability. As in our previous work,[94] we find a significant improvement by dividing the molecules in the training set into three groups, *i.e.* aliphatic, aromatic and molecules containing the element B. It is interesting that improvements were found by separating the BN-rings into its own group. It may be related to the special electrooptic properties found

	all molecules		aliphatic		aromatic		boron
Atom	$\overline{\omega}_p$	$\overline{\omega}_p$ [a]	$\overline{\omega}_p$	$\overline{\omega}_p$ [a]	$\overline{\omega}_p$	$\overline{\omega}_p$ [a]	$\overline{\omega}_p$
H	0.471	0.605	0.413	0.414	0.341	0.351	1.081
B	0.446	-	-	-	-	-	0.467
C	0.541	0.445	0.784	0.714	0.447	0.396	0.596
N	0.811	0.342	0.658	0.432	0.295	0.223	0.649
O	0.386	0.561	0.493	0.430	1.773	1.339	0.408
F	0.311	0.404	0.896	0.973	1.934	1.085	1.149
Cl	0.461	0.441	0.532	0.530	0.544	0.432	0.535
rms	1.286	0.809	0.375	0.424	0.559	0.712	0.582

[a] Taken from Ref. 94.

TABLE 3.2: *Parameters describing the frequency-dependence of molecular polarizabilities (in a.u.).*

for boron-nitride tubes (see, *e.g.*, Ref. 90, 100 and references therein). The *rms* values are reduced by almost a factor of two for all three groups as compared to including all molecules in one group. In general, we find good agreement with the results from our previous work.[94] For the aliphatic molecules the largest changes are found for the $\overline{\omega}^N$ parameter. This is due to that the hexahydro-1,3,5-triazine rings have been added to this group. The fact that the rest of the parameters are only slightly affected illustrates the transferability of the parameters. In the case of the group of aromatic molecules, large changes are found for $\overline{\omega}^O$ and $\overline{\omega}^F$ parameters. Since the set of aromatic molecules employed in this work are the same as in the previous study, the changes are due to minor differences in the optimization routine used. The reason for this is that $\overline{\omega}^O$ and $\overline{\omega}^F$ have the largest values. Therefore, they give an almost negligible contribution to the total frequency-dependence of the polarizability (see Eq. 3.20) and are not very well determined in the optimization. It is demonstrated that the frequency-dependence of the molecular polarizability for the hetero-rings can also be described with atom-type parameters. However, for the boron group in particular the H parameter is different from the other groups. Equivalently to the discussion above, $\overline{\omega}_H$ has become that large that it is not contributing to the frequency dependence. Qualitatively, it should not be expected that the electrons related to the hydrogen atoms contribute to the frequency dependence for these molecules because the most important absorption band is related to the ring structure.

3.5.1 Dimers

The interaction polarizabilities of the HF, methane, benzene and urea dimers are displayed in Figure 3.3, 3.4, 3.5 and 3.6, respectively. The interaction polarizability calculated with the IM-SQRT model is compared with SCF results. For the HF dimer (Figure 3.3), the results of the IM-MT model are also included in order to illustrate the discontinuous

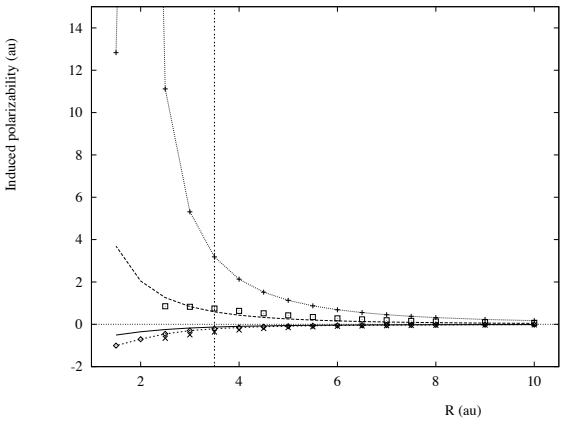

FIGURE 3.3: *Interaction polarizability of the HF dimer in a.u. R is the intermolecular distance between H and F as indicated in Fig. 3.1(a). SCF results : (□) $\alpha_{\parallel}$ and (×) $\alpha_{\perp}$. IM-MT results : (· · ·, +) $\alpha_{\parallel}$ and (· · ·, ◇) $\alpha_{\perp}$. IM-SQRT results : (- -) $\alpha_{\parallel}$ and (—) $\alpha_{\perp}$. Vertical line indicate equilibrium distance taken from Ref. 192.*

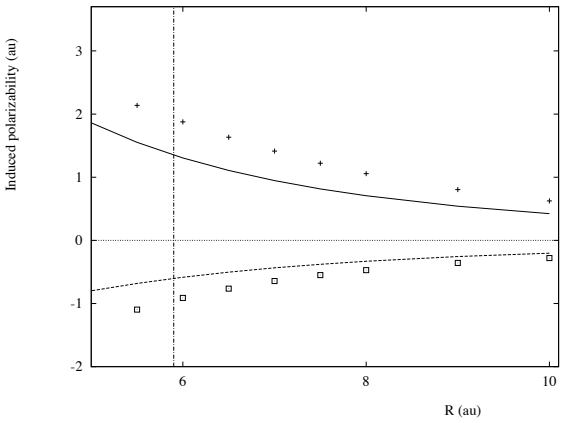

FIGURE 3.4: *Interaction polarizability of the Methane dimer in a.u. R is the intermolecular distance between C and H as indicated in Fig. 3.1(b). SCF results : (+) $\alpha_{\parallel}$ and (□) $\alpha_{\perp}$. IM-SQRT results : (—) $\alpha_{\parallel}$ and (- -) $\alpha_{\perp}$. Vertical line indicate equilibrium distance taken from Ref. 193.*

damping function of the IM-MT model. From the discontinuity in Figure 3.3, we see that in the IM-MT model there is no damping for distances larger than 2 bohr. This is expected since the IM-MT model is optimized to reproduce damping effects at typical bond distances for covalent bonds and not at typical intermolecular distances. Using the IM-SQRT model improves the damping greatly at short intermolecular distances for the HF dimer. Although the discontinuity in the IM-MT models only occurs at very short intermolecular distances, it may still not be suitable for being used in molecular dynamics simulations as discussed by Burnham *et al.*[165] For the other three dimers (Figures 3.4, 3.5 and 3.6) the IM-SQRT model slightly overestimates the intermolecular damping which again is due to that the IM-SQRT model is optimized to describe damping at intramolecular bond distances. Furthermore, it is observed that the SCF results predict that the interaction polarizability of the benzene and HF dimer parallel to the separation axes become almost stationary around the equilibrium distance. This behavior cannot be reproduced with the damping function employed here.

In spite of the chemical difference of the four dimers studied some general trends are found for the interaction polarizability. The interaction polarizability of the dimers increases in the direction along the axes connecting the the molecules ("dimer axes") and decreases in the directions perpendicular to the dimer axes which is expected from Eqs. 3.5 and 3.6. The mean polarizability is, however, almost unchanged by the intermolecular interactions. That the isotropic part of the polarizability is almost additive for a linear dimer may be realized from Eqs. 3.5 and 3.6. If a diatomic molecule, consisting of atoms

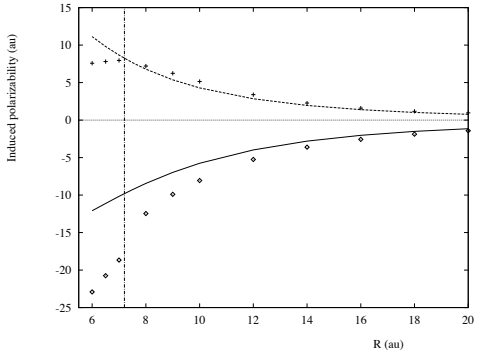

FIGURE 3.5: *Interaction polarizability of the Benzene dimer in a.u. R is the intermolecular distance between mass center as indicated in Fig. 3.1(c). SCF results : (+) $\alpha_{\parallel}$ and ($\diamond$) $\alpha_{\perp}$. IM-SQRT results : (- -) $\alpha_{\parallel}$ and (—) $\alpha_{\perp}$. Vertical line indicate equilibrium distance taken from Ref. 194.*

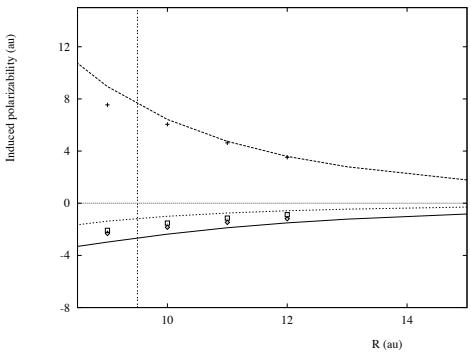

FIGURE 3.6: *Interaction polarizability of the Urea dimer in a.u. R is the intermolecular distance between mass center as indicated in Fig. 3.1(d). SCF results : (+) $\alpha_{\parallel}$, ($\diamond$) $\alpha_{\perp}$ in plane and ($\square$) $\alpha_{\perp}$ out of plane. IM-SQRT results : (– –) $\alpha_{\parallel}$, (—) $\alpha_{\perp}$ in plane and (- - -) $\alpha_{\perp}$ out of plane. Vertical line indicate equilibrium distance taken from Ref. 190.*

p and q, is considered, the isotropic part of the polarizability is $\alpha = \frac{1}{3}\left(\alpha_{\parallel} + 2\alpha_{\perp}\right)$, which becomes $\alpha = \alpha_p + \alpha_q$ if the short-range $1/r^6$-terms in the denominator of Eqs. 3.5 and 3.6 are neglected. The agreement between the IM-SQRT model and the SCF results are in general reasonable over a wide range of intermolecular distances. The largest discrepancy is found at short distances for the benzene dimer perpendicular to the separation axes (see Figure 3.1). This was expected due to the non-classical effects arising from perturbations of the π-system in the benzene dimer at short distances. At large intermolecular distances, the difference between the SCF results and the IM-SQRT model becomes small. This indicates that the long-range induced polarizability at the SCF level is well described in terms of dipole-induced-dipole interactions in good agreement with the result on the He dimer.[195] The results for the interaction polarizability of the HF dimer compare well with that obtained from the equilibrium structure of the HF dimer which is bent compared with the linear dimer structure adopted here.[196] Similar trends for the interaction polarizability are also observed for the linear acetylene dimer,[197] the linear dimer of H_2NO,[198] the water dimer,[199] the linear dimer of urea[200] and parallel chains of polyacetylene oligomers.[201] Also, since a similar behavior is observed for the second hyperpolarizability[197,201,202] this indicates a general scheme for enhancing the (hyper)polarizability of assemblies of molecules by aligning the molecules along the axes with the largest polarizability. Furthermore, interactions between different chains should be minimized since these interactions tend to lower the polarizability.[201] However, further studies of the interaction (hyper)polarizability are needed in order to determine the usefulness of this type of alignment schemes.

N	α_{xx} [a]	α_{zz} [a]	α_{yy} [a]	$\overline{\alpha}$ [a]
1	39.68	22.09	38.23	33.33
2	76.69 (-3.4)	43.01 (-2.6)	84.03 (9.9)	67.91 (1.9)
4	149.97 (-5.5)	84.59 (-4.3)	179.51 (17.4)	138.02 (3.5)
6	223.03 (-6.3)	126.11 (-4.9)	276.10 (20.4)	208.41 (4.2)
8	296.03 (-6.7)	167.60 (-5.2)	372.97 (21.9)	278.87 (4.6)
10	369.01 (-7.0)	209.09 (-5.3)	469.94 (22.9)	349.35 (4.8)
15	551.42 (-7.4)	312.79 (-5.6)	712.55 (24.3)	525.59 (5.1)
20	733.81 (-7.5)	416.49 (-5.7)	955.27 (24.9)	701.86 (5.3)
30	1098.55 (-7.7)	623.87 (-5.9)	1440.79 (25.6)	1054.40 (5.5)
50	1828.01 (-7.9)	1038.63 (-6.0)	2411.94 (26.2)	1759.53 (5.6)
100	3651.61 (-8.0)	2075.51 (-6.0)	4839.99 (26.6)	3522.37 (5.7)
200	7298.78 (-8.0)	4149.26 (-6.1)	9696.18 (26.8)	7048.07 (5.7)
300	10945.95 (-8.0)	6223.00 (-6.1)	14552.39 (26.9)	10573.78 (5.7)

[a]Percent deviation from additivity in parentheses

TABLE 3.3: *Polarizability of urea chains calculated using IM-SQRT (in au). N is the number of molecules in the chain. Y-axes is along the chain, X-axes is perpendicular to the chain but in the plane and Z-axes is perpendicular to the plane*

3.5.2 Chain of urea molecules

The polarizability of chains of urea molecules with increasing number of molecules in the chain and their deviation from additivity are presented in Table 3.3. The mean polarizability, $\overline{\alpha}$, is defined as $\overline{\alpha} = \frac{1}{3}(\alpha_{xx} + \alpha_{yy} + \alpha_{zz})$. With increasing number of molecules, we find that the polarizability parallel to the chain increases more than expected from an additive model and perpendicular to the chain it increases less rapidly than an additive model. A significant deviation from additivity is found for the tensor component along the chain which amount to around 25%. For the mean polarizability, however, the largest deviation from additivity is around 5%. These results are in good agreement with the *ab initio* study of Perez and Dupuis[200] on urea dimers and trimers. A chain length of around 100 molecules is needed before the deviation from additivity becomes stationary. Since the polarizability is converging slowly with respect to the number of molecules in the chain, extrapolation schemes are often employed to get the polarizability in the infinite limit. However, the polarizability for infinitely long chains is dependent on both the adopted extrapolation scheme and the total number of entities.[203]

3.5.3 C_{60} clusters

For C_{60}, we have investigated the polarizability both for one- and two-dimensional clusters. The results are presented in Table 3.4 and again the deviation from additivity is given in parentheses. The polarizability components parallel to the chain and in the plane of the film increase more rapidly with the number of molecules than expected from an additive

	one-dimensional cluster			two-dimensional cluster		
N	$\alpha_\perp$ [a]	$\alpha_\parallel$ [a]	$\overline{\alpha}/N$ [a]	$\alpha_\perp$ [a]	$\alpha_\parallel$ [a]	$\overline{\alpha}/N$ [a]
1	522.62	522.62	522.62	-	-	-
2	981.71(-6.1)	1231.67(17.8)	532.52(1.9)	-	-	-
3	1434.69(-8.5)	1994.32(27.2)	540.41 (3.4)	-	-	-
5	2336.31(-10.6)	3568.27(36.6)	549.39(5.1)	2273.72(-13.0)	2919.66(11.7)	540.87(3.5)
7	3236.09(-11.5)	5162.48(41.1)	554.03(6.0)	-	-	-
13	5932.65(-12.7)	9971.86(46.8)	559.93(7.1)	5410.12(-20.4)	8118.21(19.5)	555.04(6.2)
25	11323.15(-13.3)	19612.55(50.1)	563.45(7.8)	9879.24(-24.4)	16284.52(24.6)	565.98(8.3)

[a] Percent deviation from additivity in parentheses

TABLE 3.4: *Polarizability of C_{60} calculated using IM-SQRT (in au). N is the number of molecules in the cluster.*

model, whereas the components perpendicular to the chain and out of the plane increase less rapidly than an additive model. The deviation from additivity is larger for the chain than for the film. It is around 50 % along the chain and around -15 % perpendicular to the chain. In the case of the two-dimensional cluster the relative deviations from additivity perpendicular to the plane and in the plane are nearly identical but with different sign. The largest deviation from additivity in the mean polarizability is around 8 % both for the chain and the film.

The mean polarizability of the isolated C_{60} molecule is calculated to 77.5 Å^3 which agrees well with the experimental result of 76.5±8 Å^3 (Ref. 204) and an accurate SCF result of 75.1 Å^3.[205] In addition, good agreement is found between the results of the largest two-dimensional cluster of 83.9 Å^3 and experimental results on thin films where the results range between 80.5 and 91.9 Å^3.[206–211] The experimental estimate of the vibrational contribution to the polarizability is only about 2 Å^3,[211] indicating that our model gives reasonable results for C_{60} clusters as compared to experiments.

3.6 Conclusions

In this work, we have investigated an approach for modeling the damping contribution in the dipole interaction model. In contrast to the Thole model, the interaction tensors in this approach remain traceless. The modification discussed here also gives a significant improvement compared with the models adopted in previous work, even though also heterocyclic compounds have been included in the model. Although the model can describe the frequency-dependent molecular polarizability with one parameter for each element describing the frequency-dependence, a significant improvement is found by dividing the molecules into aliphatic, aromatic and molecules containing the element B.

The interaction polarizability of four dimers has also been studied. We find in general good agreement between the model and the SCF results over a wide range of intermolecular distances. Polarizabilities of linear chains of urea molecules and one- and two-dimensional

clusters of C_{60} molecules have also been calculated. The effects of neighboring molecules on the polarizability anisotropy are substantial, whereas the effects are smaller on the mean polarizability. For the mean polarizability of C_{60}, we find good agreement between the model and experiments both in the case of an isolated molecule and a model of a thin film.

Acknowledgment

L.J. thanks Prof. Paolo Lazzeretti for kindly supplying the Sadlej basis-set for boron. L.J. gratefully acknowledges The Danish Research Training Council for financial support. K.V.M. thanks Statens Naturvidenskabelige Forskningsråd (SNF), Statens Teknisk-Videnskabelige Forskningsråd (STVF) and the EU-network:MOLPROP for support.

Chapter 4

A dipole interaction model for the second hyperpolarizability

L. Jensen, K. O. Sylvester-Hvid, P.-O. Å]strand, and K. V. Mikkelsen "A dipole interaction model for the molecular second hyperpoalrizability" *J. Phys. Chem. A* **107**, 2270-2276, 2003.

4.1 Abstract

A dipole interaction model (IM) for calculating the molecular second hyperpolarizability, γ, of aliphatic and aromatic molecules has been investigated. The model has been parametrized from quantum chemical calculations of γ at the self-consistent field (SCF) level of theory for 72 molecules. The model consists of three parameters for each element p: an atomic polarizability, an atomic second hyperpolarizability, and an atomic parameter, Φ_p, describing the width of the atomic charge distribution. The Φ_p parameters are used for modeling the damping of the interatomic interactions. Parameters for elements H, C, N, O, F and Cl were determined and typical differences between the molecular γ derived from quantum chemical calculations and from the IM are below 30% and on average around 10%. As a preliminary test, the dipole interaction model was applied to the following molecular systems not included in the training set: the urea molecule, linear chains of urea molecules, and C_{60}. For these molecules deviations of the IM result for the molecular γ from the corresponding SCF value were at most around 30% for the individual components, which in all cases is a better performance than obtained with semi-empirical methods.

4.2 Introduction

The current development of carbon-based functional materials holding a potential for future applications in electronics and photonics has sparked a revolution in materials science.[8,9] An important prospect is the utilization of the intensity dependence of the refractive index in all-optical switching devices, an essential element in future information processing technology.[8] Since the intensity dependence of the refractive index is governed by the third-order nonlinearity, materials with a large third-order optical susceptibility, $\chi^{(3)}$ (where the molecular second hyperpolarizability, γ, is the corresponding microscopic property) are suitable candidates for optical switching components.[8,12,13] These new materials are intended to be designed on a molecular scale and thus a detailed understanding of their electronic structure is indispensable. Therefore, it has been conjectured that applied quantum chemistry will play a central role in the development of such new nonlinear optical (NLO) materials.[18,23]

Accordingly, γ has been investigated extensively both theoretically and experimentally for a variety of molecular systems including conjugated polymers,[59,212–226] near-infrared dyes,[17,227,228] fullerenes,[229–238] and nanotubes.[239,240]

Sophisticated quantum chemical methods can be applied only on rather small molecules, even though considerable effort has been devoted to calculate NLO properties at the SCF level for relatively large molecules like fullerenes.[81] In addition, methods based on density-functional theory (DFT) are subject to problems in the calculation of molecular (hyper)polarizabilities, although some recent advances have been presented.[83,84] Hence, to a large extent modeling optical properties for large molecules and molecular clusters is restricted to less sophisticated methods. An example is the empirical Su-Schrieffer-Heeger model,[241,242] which has been applied to describe γ of conjugated polymers,[243] fullerenes,[72] and carbon nanotubes.[149,244–247]

It is of fundamental importance to seek suitable representations of the molecular electronic structure. A successful representation of a molecular response property, in terms of for example atomic parameters, provides an understanding of its behavior in addition to an often computationally attractive scheme for extrapolation to large systems. An example is the derivation of intermolecular potentials from molecular wave functions which can be used for molecular dynamics simulations of liquids and solutions.[248]

Considering the isotropic part of the molecular polarizability, it has been known for a long time that to a good degree it can be described by an additive scheme, *i.e.*, a summation of transferable atom- or bond-type parameters.[151,152] Also recently, an additive scheme has been used for modeling the static polarizability tensor of organic molecules[156,157] and for the frequency-dependent polarizability tensor of halogen-derivatives of benzene.[158] To model the anisotropy of the polarizability tensor within an additive scheme, however, also the atomic contributions have to be tensors, rendering the model less attractive due to the increased number of parameters thus introduced.

An alternative model, introduced by Silberstein[87] and to a large extent developed by Applequist and co-workers,[90,249] is the so-called dipole interaction model (IM). In this approach, a set of atomic polarizabilities, α, interact with each other according to clas-

sical electrostatics in the limit of a vanishing external electrical field. If the molecular α is modeled by a set of isotropic atomic polarizabilities, the anisotropy of the molecular α is introduced by the interatomic interactions. Consequently, the isotropic part of the molecular α to a large degree can be modeled by an additive model for atomic polarizabilities whereas its anisotropy is determined entirely by the geometrical arrangement of the atoms. Similarly, because the atomic first hyperpolarizability, β, is zero for almost all atoms, also the molecular β is entirely determined by the interatomic interactions.[250] In fact, the leading term in the IM for β arises from atomic dipole-quadrupole hyperpolarizabilities.[170] Considering the molecular γ, the components $\gamma_{\alpha\alpha\alpha\alpha}$ and $\gamma_{\alpha\alpha\beta\beta}$ (α, $\beta = x$, y or z) are nonzero for atoms[250] and consequently, these components may to a good degree be modeled by an additive model.[251] To model the molecular β is thus in principle equally difficult as calculating the anisotropies of α and γ.

Dipole interaction models have been used extensively, and in particular to model the polarizability.[159,162,165,252,253] In addition, we have recently studied the polarizability of carbon nanotubes,[166] boron nitride nanotubes,[100] and fullerene clusters. [Ref. 63, Chap. 3] Examples of other molecular properties studied by the IM include optical rotation,[254,255] Raman scattering,[187,256] absorption,[257,258] circular dichroism,[259,260] and hyperpolarizabilities.[170,261,262] Generalized dipole interaction models for electronic polarization have also been discussed.[249,263]

From a computational point of view the IM is very attractive since computational times are many orders of magnitude faster than the corresponding quantum chemical methods. The approximations posed by the IM are at the same level as in accurate force fields calculations used to derive intermolecular interaction energies, even though interactions within a molecule are considered here.

An important extension of the IM for the molecular polarizability is the inclusion of a damping term for the interatomic interactions.[93,160] In particular, the Thole model has been investigated in detail,[94,163] and recently a new model for the damping was investigated which improved the IM considerably. [Ref. 63, Chap. 3] In the present work, we extend this approach to an IM for the molecular γ and present some initial applications.

4.3 Theory

The molecular response to an external electric field, E_β^{ext}, may be written in terms of an induced molecular dipole moment, μ_α^{ind}, as[169,250]

$$\mu_\alpha^{ind} = \alpha_{\alpha\beta} E_\beta^{ext} + \frac{1}{2}\beta_{\alpha\beta\gamma} E_\gamma^{ext} E_\beta^{ext} + \frac{1}{6}\gamma_{\alpha\beta\gamma\delta} E_\delta^{ext} E_\gamma^{ext} E_\beta^{ext} + \dots \ , \tag{4.1}$$

where $\alpha_{\alpha\beta}$ is the molecular polarizability, $\beta_{\alpha\beta\gamma}$ the molecular first hyperpolarizability and $\gamma_{\alpha\beta\gamma\delta}$ the molecular second hyperpolarizability with (α, β, γ, δ) designating Cartesian coordinates. In Eq. 4.1 and elsewhere in this paper, the Einstein summation convention for repeated indices is employed.

For a set of N atom-like interacting particles, we may write the induced atomic dipole moment, $\mu_{i,\alpha}^{ind}$ as

$$\mu_{i,\alpha}^{ind} = \alpha_{i,\alpha\beta} E_{i,\beta}^{tot} + \frac{1}{6}\gamma_{i,\alpha\beta\gamma\delta} E_{i,\delta}^{tot} E_{i,\gamma}^{tot} E_{i,\beta}^{tot} \ , \tag{4.2}$$

where $\alpha_{i,\alpha\beta}$ is the polarizability and $\gamma_{i,\alpha\beta\gamma\delta}$ the second hyperpolarizability of atom i. The total electric field at atom i, $E_{i,\beta}^{tot}$, is given by the external field and the electric fields from all other atoms as

$$E_{i,\beta}^{tot} = E_{\beta}^{ext} + \sum_{j\neq i}^{N} T_{ij,\beta\gamma}^{(2)} \mu_{j,\gamma}^{ind} \ , \tag{4.3}$$

where $T_{ij,\beta\gamma}^{(2)}$ is the so-called interaction tensor given as

$$T_{ij,\beta\gamma}^{(2)} = \frac{3R_{i,\beta}R_{j,\gamma}}{R_{ij}^5} - \frac{\delta_{\beta\gamma}}{R_{ij}^3} \ . \tag{4.4}$$

$R_{i,\beta}$ is a Cartesian coordinate component for atom i and R_{ij} the distance between atoms i and j. We have not included an atomic β in Eq. 4.2 since β is zero for spherically symmetric particles. Similarly, the same symmetry properties are assumed for the atomic α,

$$\alpha_{i,\alpha\beta} = \alpha_i \delta_{\alpha\beta} \ , \tag{4.5}$$

and the atomic γ,[250]

$$\gamma_{i,\alpha\beta\gamma\delta} = \frac{1}{3}\gamma_i \left(\delta_{\alpha\beta}\delta_{\gamma\delta} + \delta_{\alpha\gamma}\delta_{\beta\delta} + \delta_{\beta\gamma}\delta_{\alpha\delta}\right) \ , \tag{4.6}$$

where $\delta_{\alpha\beta}$ is the usual Kroenecker delta function. Alternatively, if the electric field at each atom is regarded as an independent variable, the atomic induced dipole moment may be expanded in terms of relay tensors in a Taylor expansion as[92]

$$\mu_{i,\alpha}^{ind} = \sum_{j}^{N} \mathcal{B}_{ij,\alpha\beta}^{(2)} E_{j,\beta}^{ext} + \frac{1}{2}\sum_{j,k}^{N} \mathcal{B}_{ijk,\alpha\beta\gamma}^{(3)} E_{k,\gamma}^{ext} E_{j,\beta}^{ext} + \frac{1}{6}\sum_{j,k,l}^{N} \mathcal{B}_{ijkl,\alpha\beta\gamma\delta}^{(4)} E_{l,\delta}^{ext} E_{k,\gamma}^{ext} E_{j,\beta}^{ext} + \dots \ , \tag{4.7}$$

where the n-atom relay tensor $\mathcal{B}_{i_1 i_2 \dots i_n,\alpha_1\alpha_2\dots\alpha_n}^{(n)}$ is defined as

$$\mathcal{B}_{i_1 i_2 \dots i_n,\alpha_1\alpha_2\dots\alpha_n}^{(n)} = \frac{\partial^{(n-1)}\mu_{i_1,\alpha_1}^{ind}}{\partial E_{i_2,\alpha_2}^{ext} \dots \partial E_{i_n,\alpha_n}^{ext}} \ , \tag{4.8}$$

in the limit of vanishing external fields. The molecular induced dipole moment, μ_{α}^{ind}, is simply the sum of the atomic induced dipole moments in Eq. 4.7, and if it is furthermore assumed that the external field is homogeneous, *i.e.* $E_{j,\beta}^{ext} = E_{\beta}^{ext}$ for all j, we have

$$\begin{aligned} \mu_{\alpha}^{ind} &= \left(\sum_{i,j}^{N} \mathcal{B}_{ij,\alpha\beta}^{(2)}\right) E_{\beta}^{ext} + \frac{1}{2}\left(\sum_{i,j,k}^{N} \mathcal{B}_{ijk,\alpha\beta\gamma}^{(3)}\right) E_{\gamma}^{ext} E_{\beta}^{ext} \\ &+ \frac{1}{6}\left(\sum_{i,j,k,l}^{N} \mathcal{B}_{ijkl,\alpha\beta\gamma\delta}^{(4)}\right) E_{\delta}^{ext} E_{\gamma}^{ext} E_{\beta}^{ext} + \dots \ . \end{aligned} \tag{4.9}$$

By comparison of Eqs. 4.1 and 4.9, the molecular (hyper)polarizabilities may be identified. The two-atom relay tensor, $\mathcal{B}^{(2)}_{ij,\alpha\beta}$, may be obtained from the regular approach for a dipole interaction model for the molecular polarizability as

$$\mathcal{B}^{(2)}_{ij,\alpha\beta} = \alpha_{i,\alpha\gamma}\left(\delta_{ij}\delta_{\gamma\beta} + \sum_{k\neq i}^{N} T^{(2)}_{ik,\gamma\delta}\mathcal{B}^{(2)}_{kj,\delta\beta}\right) \ , \tag{4.10}$$

which in supermatrix notation is cast into[90,93]

$$\mathcal{B}^{(2)} = \left(\boldsymbol{\alpha}^{-1} - \mathbf{T}^{(2)}\right)^{-1} \ . \tag{4.11}$$

The three- and four-atom relay tensors can be obtained by the scheme deviced by Sundberg.[92] The four-atom relay tensor is defined as

$$\mathcal{B}^{(4)}_{ijkl,\alpha\beta\gamma\delta} = \frac{\partial^3 \mu^{ind}_{i,\alpha}}{\partial E^{ext}_{j,\beta}\partial E^{ext}_{k,\gamma}E^{ext}_{l,\delta}} \ , \tag{4.12}$$

which is obtained by differentiating Eq. 4.2. As demonstrated in section 4.8, the four-atom relay tensor for a system of spherically symmetric particles may be written as

$$\mathcal{B}^{(4)}_{ijkl,\alpha\beta\gamma\delta} = \sum_{m}^{N} \gamma_{m,\lambda\mu\nu\xi}\widetilde{\mathcal{B}}^{(2)}_{ml,\xi\delta}\widetilde{\mathcal{B}}^{(2)}_{mk,\nu\gamma}\widetilde{\mathcal{B}}^{(2)}_{mj,\mu\beta}\widetilde{\mathcal{B}}^{(2)}_{mi,\lambda\alpha} \ , \tag{4.13}$$

where $\widetilde{\mathcal{B}}^{(2)}_{ij,\alpha\beta}$ is defined as

$$\widetilde{\mathcal{B}}^{(2)}_{ij,\alpha\beta} = \delta_{ij}\delta_{\alpha\beta} + \sum_{k\neq i}^{N} T^{(2)}_{ik,\alpha\gamma}\mathcal{B}^{(2)}_{kj,\gamma\beta} \ . \tag{4.14}$$

Since the electronic charge distribution is smeared out, the electric field at a nucleus will be damped by the charge distribution.[93,160] The damping may be modeled by modifying the distance R_{ij} to obtain a scaled distance S_{ij}, [Ref. 63, Chap. 3]

$$S_{ij} = v_{ij}R_{ij} = f(R_{ij}) \ , \tag{4.15}$$

where v_{ij} is a scaling factor and $f(R_{ij})$ an appropriately chosen function of R_{ij}. Furthermore, if each component of R_{ij} also is scaled by v_{ij}, the reduced distance becomes,

$$S_{ij} = \sqrt{S_{ij,\alpha}S_{ij,\alpha}} = v_{ij}\sqrt{R_{ij,\alpha}R_{ij,\alpha}} = v_{ij}R_{ij} \ , \tag{4.16}$$

consistent with the definition in Eq. 4.15. The damped interaction can thus be obtained by modifying the interaction tensors only,

$$T^{(n)}_{ij,\alpha_1\ldots\alpha_n} = \nabla_{\alpha_1}\ldots\nabla_{\alpha_n}\left(\frac{1}{S_{ij}}\right) \ , \tag{4.17}$$

which is equivalent to replacing R_{ij} by S_{ij} and $R_{ij,\alpha}$ by $S_{ij,\alpha}$ in the regular formulae for the interaction tensor. The form of the scaling function employed here is [Ref. 63, Chap. 3]

$$f\left(R_{ij}\right) = \sqrt{R_{ij}^2 + \frac{\pi}{4a_{ij}}}\ , \tag{4.18}$$

where a_{ij} is given by $a_{ij} = \Phi_i\Phi_j/(\Phi_i + \Phi_j)$, and Φ_i is the damping parameter for atom i. This particular form of the scaling function was obtained by approximating the interaction between two Gaussian charge distributions on atoms i and j with exponents Φ_i and Φ_j.

4.4 Quantum chemical calculation

To obtain highly accurate values of γ, it is necessary to consider both electron correlation and large basis sets with many diffuse functions.[142,264–267] Because the aim of this work has been to investigate a dipole interaction model for γ, the quantum chemical computations have been invoked at the SCF level using the DALTON program package[175] as described in Refs. 268,269. The polarization basis set by Sadlej[178] is used since it has been shown previously that it gives reasonable results for (hyper)polarizabilities considering its limited size[158,267,270–272] and further is consistent with our previous work on the molecular polarizability. [Ref. 63, Chap. 3] Obviously, the choice of method will affect the results and in particular the ratio between tensor components. For example, the out-of-plane component, γ_{zzzz}, of benzene is, unrealistically, larger than the in-plane component, γ_{xxxx}, obtained with the Sadlej basis set at the SCF level. This is due to the fact that the basis set is tailored to describe the dipole moment and polarizability by including the first-order polarized functions whereas a highly accurate description of γ also requires second-order polarized functions.[267,270] In the present work, the SCF calculations of the γ tensor have been restricted to the components contributing to the average γ,

$$\overline{\gamma} = \frac{1}{15}\sum_{\alpha,\beta} \gamma_{\alpha\alpha\beta\beta} + \gamma_{\alpha\beta\alpha\beta} + \gamma_{\alpha\beta\beta\alpha}, \tag{4.19}$$

and we have carried out SCF calculations for 72 molecules[273] adopting standard bond lengths and angles taken from Refs. 182,183.

Geometries of the molecules not included in the training set, *i.e.* urea, linear chains of urea molecules and C_{60} are all taken from [Ref. 63, Chap. 3]. We will in this work use atomic units (a.u.) for γ but the conversion factor to cgs units is : 1 a.u. $= 5.03670 \times 10^{-40}$ esu. The molecular geometries are available from [Ref. 63, Chap. 3], and the quantum chemical molecular γ are made available as supporting informations.

4.5 Optimization procedure

The parameters describing γ have been optimized by minimizing the root-mean-square, rms, of the difference between the components of the SCF tensor, $\gamma^{SCF}_{\alpha\beta\gamma\delta,n}$, and the IM

tensor, $\gamma^{IM}_{\alpha\beta\gamma\delta,n}$, as

$$rms = \sqrt{\frac{\sum_{n=1}^{N}\sum_{\alpha,\beta,\gamma,\delta}\left(\gamma^{IM}_{\alpha\beta\gamma\delta,n} - \gamma^{SCF}_{\alpha\beta\gamma\delta,n}\right)^2}{N-1}}, \tag{4.20}$$

where N is the number of molecules in the training set. It should be noted that in the second sum in Eq. 4.20, only components have been included which contribute to $\overline{\gamma}$ in Eq. 4.19, implying that the sum includes in total 21 terms per molecule.

4.6 Results

4.6.1 Optimization of the training set

We have performed in all two types of optimizations : The parameters in the first optimization (A) have been obtained by optimizing the atomic γ_p, keeping the atomic polarizabilities, α_p and damping parameters, Φ_p, constant. In the second optimization (B), also the Φ_p parameters were optimized. A third optimization was tried in which all parameters, i.e. α_p, Φ_p, and γ_p were optimized. This gave only a small improvement on the results compared with the second optimization although one extra parameter was included for each element. For this reason this optimization was not considered in more details. The values of α_p used in (A) and (B) and Φ_p used in (A) are taken from a previous study [Ref. 63, Chap. 3] where the parameters were optimized to describe the molecular polarizability for 187 molecules in a similar fashion. The 72 molecules of the present study were among these 187 molecules.

	(A)			(B)		
Atom	α_p [a]	Φ_p [a]	γ_p	α_p [a]	Φ_p	γ_p
H	1.280	0.358	350.309	1.280	0.0909	-211.0525
C	8.465	0.124	233.335	8.465	0.0211	2194.3233
N	6.169	0.269	111.169	6.169	0.0499	888.8899
O	3.754	4.103	-80.050	3.754	14.4795	-233.4550
F	1.907	1.468	-49.390	1.907	2.0271	-1666.8621
Cl	13.081	0.453	732.170	13.081	0.2921	820.2538
rms [b]		8971.54			4434.98	
mean absolute div. in $\overline{\gamma}$ [c] (%)		18.57			12.70	
mean absolute div. in $\gamma_{\alpha\beta\gamma\delta}$ (%)		38.15			21.44	

[a] Parameters taken from Ref. 63,Chap. 3 (not optimized)
[b] Optimized error
[c] $\overline{\gamma} = \frac{1}{15}\sum_{\alpha\beta}\gamma_{\alpha\alpha\beta\beta} + \gamma_{\alpha\beta\alpha\beta} + \gamma_{\alpha\beta\beta\alpha}$

TABLE 4.1: *Atomic parameters fitted to model the static second hyperpolarizability (in a.u.).*

The optimized parameters describing the molecular γ are presented in Table 4.1 and the results from (A) and (B) displayed in Figures 4.1 and 4.2, respectively, where the SCF

tensor components have been plotted against the corresponding IM tensor. A reasonable description of the molecular γ is obtained by procedure (A) by using only one additional parameter per element, γ_p (see Table 4.1). However, large deviations are found for the aromatic molecules in the γ components perpendicular to the ring. These components have been singled out in Figure 4.1. The ratios between the diagonal components in the plane ($\gamma_{xxxx} = \gamma_{\mathrm{ip}}$) and perpendicular to the plane ($\gamma_{zzzz} = \gamma_{\perp}$) in the IM are determined by the interactions between the atoms. At small distances the interatomic interactions, and therefore also the ratio $\gamma_{\mathrm{ip}}/\gamma_{\perp}$, is determined to a large extent by the damping. In the limit of infinitely large damping, *i.e.* infinitely small Φ_p parameters, the model becomes additive and the γ_{ip} and $\gamma_{\perp}$ components identical. If the SCF/Sadlej results for benzene are considered, the ratio $\gamma_{\mathrm{ip}}/\gamma_{\perp}$ is nearly unity whereas the ratio between the polarizability components, $\alpha_{\mathrm{ip}}/\alpha_{\perp}$, is about two. Therefore, to predict $\gamma_{\perp}$ for aromatic compounds, the damping of the interactions has to be modified as compared to a description for polarizability only. The limitations pertinent to the IM for describing the polarizability of π-conjugated systems correctly have been discussed elsewhere[186] and also the importance of damping in predicting the polarizability component perpendicular to the ring has been discussed previously. [Ref. 63, 185, Chap. 3] On the other hand, in a theoretical study of benzene including electron correlation and larger basis set, it is found that γ_{ip} is around 40% larger than $\gamma_{\perp}$.[265]

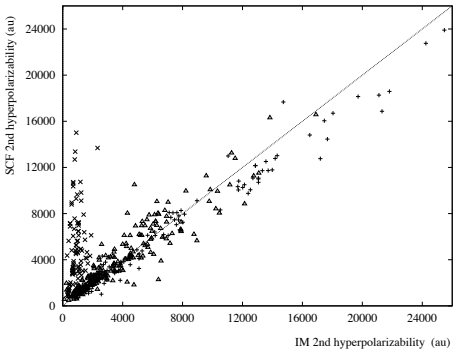

FIGURE 4.1*: Comparison between the second hyperpolarizability tensor components obtained with the IM and with the SCF/Sadlej method. IM results obtained with parameters from (A) (only γ_p is optimized). (△) indicates aliphatic molecules and (+,×) aromatic molecules, respectively. For the aromatic molecules tensor components with an axis perpendicular to the ring are displayed with (×) and other components with (+).*

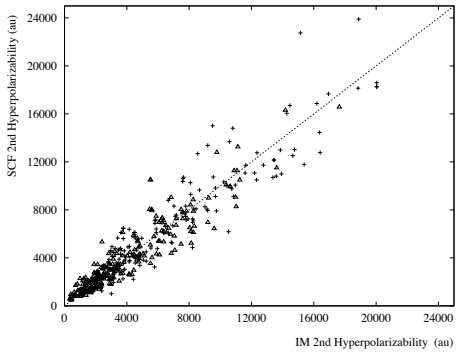

FIGURE 4.2*: Comparison between the second hyperpolarizability tensor components obtained with the IM and with the SCF/Sadlej method. IM results obtained with parameters from (B) (γ_p and Φ_p are optimized). (△) indicates aliphatic molecules and (+) aromatic molecules, respectively.*

To improve the description of $\gamma_{\perp}$ for the aromatic molecules, a second optimization (B) was carried out where also Φ_p was included in the optimization. From the results

in Table 4.1 and Figure 4.2, it is clear that a substantial improvement in reproducing the SCF/Sadlej results is obtained. The *rms* is reduced by a factor of two and also the mean absolute deviation in the γ components are reduced by nearly a factor of two. In addition, and foremost, from Figure 4.2 it is seen that the description of $\gamma_\perp$ for the aromatic molecules is improved considerably. As a consequence the values of the atomic parameters have also changed considerably. As expected, the damping parameters, except for O and F, are much smaller than the parameters used in (A). The reason that the parameters for O and F still are large is that the damping term, $\frac{1}{a_{ij}}$, can be written as $\frac{1}{a_{ij}} = \frac{1}{\Phi_i} + \frac{1}{\Phi_j}$, and therefore dominated by the smallest parameters. The contribution to the damping from Φ_F and Φ_O are thus small and accordingly these parameters are not well determined in the optimization.

Since optimization procedure (A) and (B) utilize identical α_p (previously optimized to reproduce molecular SCF polarizabilities [Ref. 63, Chap. 3]) the stronger damping enforced by procedure (B) implies that the molecular α and γ cannot both be well described using the parameters of optimization (B). Furthermore, for this reason it is not possible to obtain a good description of both the molecular α and γ by *e.g.* optimizing all the parameters. The molecular α derived IM from parameters of optimization (B) become almost nearly isotropic due to exaggerated damping (in terms of describing polarizabilities). Using the benzene molecule as example, the ratio $\alpha_{\rm ip}/\alpha_\perp$ is 1.1 calculated with the IM and 1.8 with the SCF/Sadlej method. However, the mean polarizability predicted with the IM is still within 15% of the SCF/Sadlej results.

Optimization procedure (B) also implies large changes for the γ_p parameters and in general they become larger. Since the interatomic interactions are more strongly damped in (B), larger γ_p parameters are necessary in order to describe the same molecular γ. If the γ_p values from (B) are compared with the results obtained from an additive model for $\overline{\gamma}$,[251] good agreement is found with respect to both sign and magnitude of the parameters. This again reflects the stronger damping obtained for the parameters in (B). In addition, in contrast to (A), the magnitude of γ_H is smaller than γ_C which is to be expected from the small number of electrons in H.

The IM has previously been used to model the experimental $\overline{\gamma}$ of a set of 16 small haloalkanes,[262] but this work differs in several ways, and a detailed comparison will not be sought. In terms of comparison with experimental data the IM is subject to the same limitations as the *ab initio* methods from which the parameters are derived;, *i.e.*, standard SCF derivations of γ do not include vibrational contributions and various solvent-induced effects. Also, the present study addresses γ in the static limit only, and a proper comparison with experiment will require the dispersion to be evaluated as well. In a previous study of α, the IM approach was extended to include the frequency dependence,[94] and a similar approach for γ may be adopted.

4.6.2 Test on molecules not in the training set

As a test of the model, we have also performed calculations for some molecules which were not included in the training set, *i.e.* urea, linear chains of urea molecules and the

fullerene C_{60}. The reason for choosing these molecules is the large body of previous studies using both semi-empirical and first-principle methods thus allowing for comparisons on equal levels of theory. For the urea chains there has only been an *ab initio* study of the urea dimer and trimer.[200] The larger chains have been included to illustrate the effects of increasing the chain length.

	IM	SCF/Sadlej [a]	MNDO[a]	PM3[a]
γ_{xxxx}	3537.84	4447.95	16956.47	2960.25
γ_{yyyy}	2922.62	4095.59	7317.23	-89.80
γ_{zzzz}	2424.22	3380.39	41.69	11.23
γ_{xxyy}	1096.38	1576.34	5126.71	1335.80
γ_{xxzz}	979.22	1622.84	341.57	4.81
γ_{yyzz}	899.92	1582.75	112.25	205.26
$\overline{\gamma}$	2967.15	4296.04	7095.93	1194.68

[a]Taken from. Ref. 274

TABLE 4.2*: Static second hyperpolarizability of urea (in a.u.): Y axis parallel to the C-O bond, X-axis perpendicular to this bond but in the plane. Z axis perpendicular to the molecular plane. For the IM calculation, parameters from (B) were used.*

The results for the urea molecule are presented in Table 4.2 and compared with *ab initio* and semi-empirical results taken from Ref. 274. The γ tensor components calculated with the IM are between 20-40% lower than the corresponding SCF values yielding a $\overline{\gamma}$ which is 30% too low as compared with the SCF results. However, the general agreement between the IM and SCF methods are better than the agreement between semi-empirical and SCF methods. For semi-empirical methods, in particular the components with an axis perpendicular to the plane are underestimated.

N [a]	1	2	4	6	8	10
γ_{xxxx}	3537.84	6631.92(-6.3)	12642.51(-10.7)	18602.53(-12.4)	24548.19(-13.3)	30487.78(-13.8)
γ_{yyyy}	2922.62	6618.94(13.2)	14672.84(25.5)	22965.15(31.0)	31324.29(34.0)	39709.98(35.9)
γ_{zzzz}	2424.22	4578.63(-5.6)	8781.06(-9.4)	12952.30(-11.0)	17114.64(-11.8)	21273.21(-12.2)
γ_{xxyy}	1096.38	2281.60(4.1)	4712.26(7.5)	7162.60(8.9)	9618.31(9.7)	12076.16(10.1)
γ_{xxzz}	979.22	1843.23(-5.9)	3525.13(-10.0)	5193.71(-11.6)	6858.48(-12.4)	8521.66(-13.0)
γ_{yyzz}	899.92	1880.89(4.5)	3896.91(8.3)	5930.62(9.8)	7969.17(10.7)	10009.65(11.2)
$\overline{\gamma}$	2967.15	5968.19(0.6)	12073.00(1.7)	18218.76(2.3)	24375.81(2.7)	30537.18(2.9)

[a]Number of urea molecules in chain.

TABLE 4.3*: Static second hyperpolarizability (in a.u.) of linear urea-chains calculated with the IM using (B) parameters. Percent deviation from additivity in parentheses. Y axis along the chain, X axis perpendicular to the chain but in the plane. Z axis perpendicular to the molecular plane*

In Table 4.3, γ for linear chains of urea molecules with an increasing number of molecules in the chain along with its deviation from molecular additivity are presented. We find that γ parallel to the chain increases more than expected from an additive model with increasing chain length, whereas perpendicular to the chain, γ decreases as expected from an additive model. The largest deviation from additivity is found for the component parallel to the chain and it is around 35%. For $\overline{\gamma}$, the deviation is only about 3%. The results for the urea chains are in agreement with *ab initio* results found elsewhere for the urea dimer and trimer,[200] however, a larger deviation from additivity was observed in that study.

Method	$\overline{\gamma}$	Ref.
IM	132044	This work
LDA	124000	49
SCF	113765	65
PM3	49834	275
SOS-VEH	49040	237
INDO	58967	66

TABLE 4.4*: Mean static second hyperpolarizability for C_{60} (in a.u.). IM results calculated using (B) parameters.*

Results for C_{60} are presented in Table 4.4 and are compared with semi-empirical and quantum-chemical calculations of γ. A comparison with experiment is difficult due to the large differences in the experimental results[64,65,69] but also since we in this work have neglected vibrational, dispersion and solvent effects. We find good agreement between the IM results and the quantum chemical results. The IM value of 132044 a.u. is 16% larger than the SCF result of 113765 a.u.[65] and 7% larger than the DFT result of 124000 a.u.,[49] respectively. The semi-empirical results,[66,237,275] are in good agreement with each other but are about 50% smaller than the SCF result.

4.7 Conclusion

In this work, we have investigated and parametrized a model for the molecular γ tensor of aliphatic and aromatic molecules based on a dipole interaction model. The model consists of three parameters for each element: an atomic polarizability, an atomic second hyperpolarizability, and a parameter, Φ_p, describing the damping of the interatomic interactions. By utilizing atomic polarizabilities and damping parameters obtained in a previous study of the molecular polarizability, it is demonstrated that γ is modeled reasonably well with only one extra parameter per element. However, for the aromatic molecules the components perpendicular to the ring are underestimated as compared to the SCF calculations. This was corrected for by additionally optimizing the damping parameters. Preliminary application of the model to urea, linear chains of urea molecules and C_{60} in general shows

good agreement with SCF results and clearly illustrates the usefulness of the interaction model to model γ for large molecules and molecular aggregates.

Acknowledgment

L.J. gratefully acknowledges The Danish Research Training Council for financial support. KSH is indebted to Østed∗DTU, Electromagnetic Systems, DTU for providing computational resources. K.V.M. thanks Statens Naturvidenskabelige Forskningsråd (SNF), Statens Teknisk-Videnskabelige Forskningsråd (STVF), Danish Center for Scientific Computing and the EU-network: MOLPROP for support.

Supporting Information Available: Tables containing the quantum chemical molecular γ tensor for the 72 molecules studied in this work. This material is available free of charge via the Internet at http://pubs.acs.org.

4.8 The four-atom relay tensor

The four-atom relay tensor, $\mathcal{B}^{(4)}_{ijkl,\alpha\beta\gamma\delta}$, is obtained from Eq. 4.12,

$$\mathcal{B}^{(4)}_{ijkl,\alpha\beta\gamma\delta} = \frac{\partial^3 \mu^{ind}_{i,\alpha}}{\partial E^{ext}_{j,\beta} \partial E^{ext}_{k,\gamma} E^{ext}_{l,\delta}} \ , \tag{4.21}$$

by differentiating the atomic induced dipole moment, $\mu^{ind}_{i,\alpha}$, in Eq. 4.2,

$$\mu^{ind}_{i,\alpha} = \alpha_{i,\alpha\beta} E^{tot}_{i,\beta} + \frac{1}{6} \gamma_{i,\alpha\beta\gamma\delta} E^{tot}_{i,\delta} E^{tot}_{i,\gamma} E^{tot}_{i,\beta} \ , \tag{4.22}$$

repeatedly with respect to the external field, $E^{ext}_{i,\alpha}$. The straightforward approach is to adopt partial differentiation by noting that the total electric field, $E^{tot}_{i,\alpha}$ in Eq. 4.3,

$$E^{tot}_{i,\alpha} = E^{ext}_{i,\alpha} + \sum_{j \neq i}^{N} T^{(2)}_{ij,\alpha\beta} \mu^{ind}_{j,\beta} \ , \tag{4.23}$$

may be differentiated with respect to the external field as

$$\frac{\partial E^{tot}_{i,\alpha}}{\partial E^{ext}_{k,\gamma}} = \delta_{ik}\delta_{\alpha\gamma} + \sum_{j \neq i}^{N} T^{(2)}_{ij,\alpha\beta} \mathcal{B}^{(2)}_{jk,\beta\gamma} \ , \tag{4.24}$$

which we in Eq. 4.14 denoted as $\widetilde{\mathcal{B}}^{(2)}_{ik,\alpha\gamma}$. Furthermore,

$$\frac{\partial^2 E^{tot}_{i,\alpha}}{\partial E^{ext}_{k,\gamma} \partial E^{ext}_{l,\delta}} = \sum_{j \neq i}^{N} T^{(2)}_{ij,\alpha\beta} \mathcal{B}^{(3)}_{jkl,\beta\gamma\delta} \ , \tag{4.25}$$

which is denoted as $\widetilde{\mathcal{B}}^{(3)}_{ikl,\alpha\gamma\delta}$, and

$$\frac{\partial^3 E^{tot}_{i,\alpha}}{\partial E^{ext}_{k,\gamma} \partial E^{ext}_{l,\delta} \partial E^{ext}_{m,\epsilon}} = \sum_{j \neq i}^{N} T^{(2)}_{ij,\alpha\beta} \mathcal{B}^{(4)}_{jklm,\beta\gamma\delta\epsilon} \ , \tag{4.26}$$

which is denoted as $\widetilde{\mathcal{B}}^{(4)}_{iklm,\alpha\gamma\delta\epsilon}$. Repeated differentiation yields

$$\begin{aligned}
\mathcal{B}^{(4)}_{ijkl,\alpha\beta\gamma\delta} &= \gamma_{i,\alpha\lambda\mu\nu} \widetilde{\mathcal{B}}^{(2)}_{ij,\lambda\beta} \widetilde{\mathcal{B}}^{(2)}_{ik,\mu\gamma} \widetilde{\mathcal{B}}^{(2)}_{il,\nu\delta} \\
&+ \left(\alpha_{i,\alpha\lambda} + \frac{1}{2} \gamma_{i,\alpha\lambda\mu\nu} E^{tot}_{i,\nu} E^{tot}_{i,\mu} \right) \widetilde{\mathcal{B}}^{(4)}_{ijkl,\lambda\beta\gamma\delta} \\
&+ \gamma_{i,\alpha\lambda\mu\nu} E^{tot}_{i,\nu} \left(\widetilde{\mathcal{B}}^{(3)}_{ijk,\mu\beta\gamma} \widetilde{\mathcal{B}}^{(2)}_{il,\lambda\delta} + \widetilde{\mathcal{B}}^{(3)}_{ijl,\mu\beta\delta} \widetilde{\mathcal{B}}^{(2)}_{ik,\lambda\gamma} + \widetilde{\mathcal{B}}^{(3)}_{ikl,\mu\gamma\delta} \widetilde{\mathcal{B}}^{(2)}_{ij,\lambda\beta} \right) \ .
\end{aligned} \tag{4.27}$$

Because $\widetilde{\mathcal{B}}^{(4)}_{ijkl,\lambda\beta\gamma\delta}$ contains $\mathcal{B}^{(4)}_{mjkl,\epsilon\beta\gamma\delta}$, Eq. 4.27 is recast in non-iterative form as

$$\begin{aligned}\mathcal{B}^{(4)}_{mjkl,\epsilon\lambda\mu\nu} &= \sum_i \Big(\gamma_{i,\alpha\beta\gamma\delta}\widetilde{\mathcal{B}}^{(2)}_{il,\delta\nu}\widetilde{\mathcal{B}}^{(2)}_{ik,\gamma\mu}\widetilde{\mathcal{B}}^{(2)}_{ij,\beta\lambda}\widetilde{\mathcal{B}}^{(2)}_{im,\alpha\epsilon} \\ &+ \gamma_{i,\alpha\beta\gamma\delta}E^{tot}_{i,\delta}\widetilde{\mathcal{B}}^{(2)}_{im,\alpha\epsilon}\Big(\widetilde{\mathcal{B}}^{(2)}_{ij,\beta\lambda}\widetilde{\mathcal{B}}^{(3)}_{ikl,\gamma\mu\nu} + \widetilde{\mathcal{B}}^{(2)}_{ik,\beta\mu}\widetilde{\mathcal{B}}^{(3)}_{ijl,\gamma\lambda\nu} + \widetilde{\mathcal{B}}^{(2)}_{il,\beta\nu}\widetilde{\mathcal{B}}^{(3)}_{ijk,\gamma\lambda\mu}\Big)\Big) \quad (4.28)\end{aligned}$$

which apart from notation and definitions is equivalent to the four-atom relay tensor given by Sundberg.[92] For a system of (hyper)polarizabilities the total field, $E^{tot}_{i,\beta}$, vanishes when the external field, $E^{ext}_{i,\beta}$ approaches zero, and thus the second term in Eq. 4.28 vanishes and the final result for the four-atom relay tensor becomes

$$\mathcal{B}^{(4)}_{mjkl,\epsilon\lambda\mu\nu} = \sum_i \gamma_{i,\alpha\beta\gamma\delta}\widetilde{\mathcal{B}}^{(2)}_{il,\delta\nu}\widetilde{\mathcal{B}}^{(2)}_{ik,\gamma\mu}\widetilde{\mathcal{B}}^{(2)}_{ij,\beta\lambda}\widetilde{\mathcal{B}}^{(2)}_{im,\alpha\epsilon} \ . \quad (4.29)$$

Chapter 5

A localized dipole interaction model

L. Jensen, M. Swart, P. Th. van Duijnen, and J. G. Snijders "Medium perturbations on the molecular polarizability calculated within a localized dipole interaction model" *J. Chem. Phys.* **117**, 3316-3320, 2002.

5.1 Abstract

We have studied the medium effects on the frequency-dependent polarizability of water by separating the total polarizability of water clusters into polarizabilities of the individual water molecules. A classical frequency-dependent dipole-dipole interaction model based on classical electrostatics and an Unsöld dispersion formula has been used. It is shown that the model reproduces the polarizabilities of small water clusters calculated with time-dependent density functional theory. A comparison between supermolecular calculations and the localized interaction model illustrates the problems arising from using supermolecular calculations to predict the medium perturbations on the solute polarizability. It is also noted that the solute polarizability is more dependent on the local geometry of the cluster than on the size of the cluster.

5.2 Introduction

Since the factors determining the linear and nonlinear optical (NLO) response properties of single molecules are becoming more clear and the existence of highly accurate methods to calculate these properties the design of new NLO-materials at the molecular level is becoming feasible.[12,14,15,276] However, in molecular crystals, molecules in solution and polymeric materials the properties of the individual molecules are perturbed by interactions with the surrounding medium. These intermolecular effects can have significant influence on the (hyper-) polarizabilities of the molecules.[195,200,202,277–279] [Ref. 63, Chap. 3]

The presence of a medium (solvent) will affect the molecule (solute) in two ways. First, the externally applied fields are modified and, second, there is an explicit solute-solvent interaction. The modulation of the applied fields is in general treated by means of local field factors, which will not be discussed here, but the reader is referred to *e.g.* Refs. 29,280,281. The solute-solvent interactions are most commonly taken into account by adopting the so called continuum model, see *e.g.* Refs. 102, 277, 278, 282. The greatest disadvantage of the continuum models is the neglect of the explicit microscopic structure of the solvent. In a supermolecular calculation the solvent molecules are taken into account explicitly and treated at the same level of theory as the solute. This type of brute force method allows only the nearest neighbor molecules to be included. An alternative is a combination of the continuum model and a supermolecular calculations, the so called semi-continuum model.[277,283,284]

Although the supermolecular methods are accurate (within the chosen model) the properties obtained are for the total supermolecule or cluster. Unless the molecular property of interest is additive the problem of partitioning the total response into local contributions remains. This resembles the problem of extracting information about molecular properties from experimental macroscopic properties. Therefore, understanding the response properties of the bulk materials, the individually molecules and the perturbations caused by environmental interactions are needed in order to achieve an efficient procedure for designing optical molecular materials at the atomic level.[8,12,14,15]

Therefore we will in this paper discuss possible ways of partitioning the total polarizability into local contributions. Three general partitioning schemes for any supermolecular type of calculation will be discussed. Also, a classical localized model in which the medium effect on the molecular polarizability can be calculated is presented. The method is a modification of a classical dipole interaction model[90,93,94,163] for calculating the molecular polarizability. The results from the model will be compared with time-dependent DFT calculations.

5.3 Distributed polarizabilities of interacting molecules

5.3.1 General partitioning schemes

In general a proper partitioning scheme should be additive,[285] *i.e.*, the sum of effective properties of the individual molecules in the total aggregate. The simplest way of constructing the effective polarizabilities is treating all molecules as identical, *i.e.*, to calculate the polarizability per molecule (PPM) α/N. Since the PPM model gives an average quantity it is useless for retrieving information about a specific member in the cluster such as a solute molecule in solution. A simple alternative to the PPM model is the "differential shell" approach (DSA).[277,286] In DSA the solute polarizability is defined as the difference between the polarizability of the cluster and the polarizability of the solvent. Information about a specific member of the cluster can be obtained at the expense of one extra calculation. Therefore, the model can also be used for systems where the solute molecule is different from the surrounding solvent molecules.

If we expand the total polarizability, α^{tot}, in a cluster sum[287,288] we can write the interaction polarizability as

$$\Delta\alpha^{\mathrm{tot}} = \alpha^{\mathrm{tot}} - \sum_i \alpha^i = \sum_{i<j} \Delta^{ij}\alpha^{(2)} + \sum_{i<j<k} \Delta^{ijk}\alpha^{(3)} + \cdots , \tag{5.1}$$

where α^i is the polarizability of the isolated monomers and $\Delta^{ij}\alpha^{(2)}$ is the induced polarizability arising from interaction between molecule i and j. Similarly $\Delta^{ijk}\alpha^{(3)}$ is the nonadditive three-body polarizability of molecules i, j and k. Using the above expansion of the interaction polarizability we can define a partitioning of the cluster polarizability into a many-body corrected polarizability, α^{MBP}, as

$$\alpha^{\mathrm{MBP}} = \alpha^p + \sum_j W^{(2)}_{pj}\Delta^{pj}\alpha^{(2)} + \sum_{j,k} W^{(3)}_{pjk}\Delta^{pjk}\alpha^{(3)} + \cdots , \tag{5.2}$$

where $W^{(2)}_{pj}$ and $W^{(3)}_{pjk}$ are appropriate weight factors chosen such that Eq. 5.1 is fulfilled. A simple choice of weights would be to divide the interaction polarizability equally among the molecules. Another, more general method but also more difficult, is a weighted assignment. The weighting could e.g. be done with the vacuum polarizabilities of the isolated molecules as

$$W^{ij}_{\alpha\beta} = \frac{\left|\alpha^j_{\alpha\beta}\right|}{\left|\alpha^j_{\alpha\beta}\right| + \left|\alpha^i_{\alpha\beta}\right|}. \tag{5.3}$$

This weigting scheme is dependent on the different types of molecules involved and also on the orientation of the molecules. A major drawback of the MBP approach is that it requires many calculations in order to determine the interaction polarizabilities. However, for pure liquids, such as water, the two different weighting schemes will be nearly identical and the method can be used as a test of other partitioning schemes.

5.3.2 The localized dipole-dipole interaction model

An elaborate model, but yet very simple compared with quantum chemical calculations, is the dipole interaction model of Applequist *et al.*[90,91] based on the earlier work of Silberstein.[87–89] In the interaction model (IM), the atoms of a molecule in an external field interact by means of their atomic induced dipole moments according to classical electrostatics. Even if the atomic parameters are isotropic polarizabilities, an anisotropy of the molecular polarizability is introduced by interactions with the surrounding atoms.

Considering a set of N interacting atomic polarizabilities, the atomic induced dipole moment due to an external electric field, E^{ext}, is given by

$$\mu_{p,\alpha}^{\text{ind}} = \alpha_{p,\alpha\beta}\left(E_{\beta}^{\text{ext}} + \sum_{q\neq p}^{N} T_{pq,\beta\gamma}^{(2)}\mu_{q,\gamma}^{\text{ind}}\right), \tag{5.4}$$

where $T_{pq,\alpha\beta}^{(2)}$ is the interaction tensor which has been modified according to Thole[93] to include a damping term

$$T_{pq,\alpha\beta}^{(2)} = \frac{3f_{pq}^{T}r_{pq,\alpha}r_{pq,\beta}}{r_{pq}^{5}} - \frac{f_{pq}^{E}\delta_{\alpha\beta}}{r_{pq}^{3}}. \tag{5.5}$$

The screening functions in Eq. 5.5 are given by[163]

$$f_{pg}^{E} = 1 - \left[1 + s_{pq} + \frac{1}{2}s_{pq}^{2}\right]\exp(-s_{pq}) \text{ and } f_{pg}^{T} = f_{pg}^{E} - \frac{1}{6}s_{pq}^{3}\exp(-s_{pq}), \tag{5.6}$$

where the term s_{pq} is given by $s_{pq} = ar_{pq}/(\alpha_p\alpha_q)^{1/6}$, with a the screening length, and α_p the atomic polarizability of atom p.

The molecular polarizability can be written as[90]

$$\alpha_{\alpha\beta}^{\text{mol}} = \sum_{p,q}^{N} B_{pq,\alpha\beta}, \tag{5.7}$$

where $\mathbf{B}$ is the relay matrix defined in supermatrix notation as

$$\mathbf{B} = \left(\boldsymbol{\alpha}^{-1} - \mathbf{T}^{(2)}\right)^{-1}. \tag{5.8}$$

Well below the first electronic absorption, the frequency-dependence of the molecular polarizability is often approximated with an Unsöld-type of expression.[15] Here we assume that the atomic polarizability has a similar frequency dependence[94]

$$\alpha_p(-\omega;\omega) = \alpha_p(0;0) \times \left[\frac{\overline{\omega_p}^2}{\overline{\omega_p}^2 - \omega^2}\right]. \tag{5.9}$$

where $\overline{\omega_p}$ is an atomic parameter describing the frequency-dependence.

In order to calculate the polarizability of the solute molecule in the presence of the solvent molecules we utilize a localized interaction model (LIM). This is done first by

decomposing the relay matrix into a block diagonal form with blocks, $\tilde{B}_{ii}$, corresponding to a relay tensor for the i'th molecule or subgroup. In the decomposition of the relay matrix an assignment of the interaction blocks $B_{i\neq j}$ to the diagonal blocks B_{ii} is needed. This is arbitrary but can be done similarly to the weighing in the MBP approach. Therefore, we have for molecule i

$$\alpha^i_{\alpha\beta} = \sum_{pq\in i}\left(B^{ii}_{pq,\alpha\beta} + \sum_{j\neq i} W^{ij}_{\alpha\beta} B^{ij}_{pq,\alpha\beta}\right), \tag{5.10}$$

where W^{ij} is a weight factor either equal to $\frac{1}{2}$ or given by Eq. 5.3. The scheme where $W^{ij} = \frac{1}{2}$ is denoted LIM-1 and the scheme where the weights are given by Eq. 5.3 is denoted LIM-2.

5.4 Computational methods

The atomic parameters α_p and $\overline{\omega_p}$ are obtained by fitting to the frequency-dependent polarizability of a single water molecule. The screening length parameter $a = 2.130$ was taken from Ref. 163. For the benzene molecule only the carbon parameter, α_C, was optimized, leaving the hydrogen parameter to that obtained from water. The polarizabilities were obtained by TD-DFT calculations which are described in more details below. The optimized atomic parameters are, $\alpha_O = 8.3955$ au, $\alpha_H = 0.3118$ au, $\alpha_C = 14.0775$ au, $\overline{\omega}_O = 0.5426$ au and $\overline{\omega}_H = \infty$. The frequency parameter for hydrogen indicates that all the frequency-dependence in water is due to the oxygen atom.

For all the DFT calculations we used the RESPONSE code [57,130,289] in the Amsterdam Density Functional (ADF) program.[131–134,290] The ADF program uses basis sets of Slater functions. Here we used a triple zeta valence plus polarization and extra diffuse s, p, d functions (TZ2P+, in ADF basis set VI) were used. The van Leeuwen-Baerends (LB94) exchange-correlation potential[141] was used because of its correct asymptotic behavior.

The intra-molecular geometry of the water molecules was that in gas phase, *i.e.* R_{O-H} = 0.958 Å and $\angle_{HOH} = 104.5°$. The solute water molecule was placed in the xz-plane with the z-axis bisecting the H-O-H angle. Experimental evidence[291,292] indicates that a tetrahedrally coordinated water molecule is present in liquid water and therefore we constructed a cluster containing the 1st solvation shell from Ref. 277. This tetrahedral structure has 2 donor hydrogen bonds and 2 acceptor hydrogen bonds (see Fig. 5.1). The O-O distance is $R_{O-O} = 2.85$ Å. The geometry of the larger clusters ($N > 5$) was obtained by MD-simulations keeping the 1st solvation shell fixed. The geometry of the benzene molecule was taken with standard bond lengths and angles from Ref 182 and is placed in the xy-plane with the x-axis along a 2-fold axis. The cluster containing benzene molecules was generated by MD-simulations with one fixed solute in the center and 41 solvent molecules. The MD-simulations were performed with the DRF90-program[293] which uses a polarizable force field, consistent with the model used in this work. The MD-simulation was done with the canonical NVT ensemble at a temperature of 298.15 K and a density of 0.9982 g/cm^3. The structure of the clusters was generated by first a 20 ps equilibration run followed by

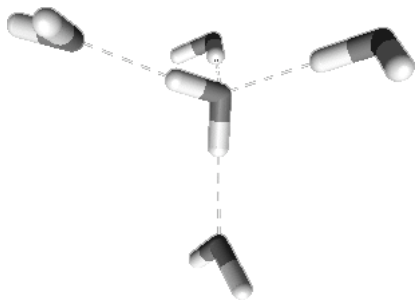

FIGURE 5.1: *A model of the structure of a water molecules and the 1st solvation shell. The symmetry of the cluster is* C_{2v}.

a 100 ps production run from which the lowest energy configuration was chosen.

5.5 Results and discussion

In order to evaluate how well the dipole interaction model represents the polarizability of larger water clusters TD-DFT calculations were performed for the $N = 5$ and $N = 13$ clusters. These results are compared with the results obtained from the IM in Table 5.1. We find in general good agreement between the TD-DFT results and the IM calculations. The largest deviations are for the N=13 cluster and are about 3% both in the static and frequency-dependent case. Especially for the results of the 1st solvation shell ($N = 4$) there is excellent agreement between the two methods. This indicate that the "not so close" interaction is particular well described. At small distance basis sets superposition errors (BSSE) start to influence the TD-DFT results and accounts for some of the deviations. Therefore, the results in Table 5.1 clearly illustrate that the dipole interaction model

		$\omega = 0.0000$ au				$\omega = 0.0656$ au			
Method	N[a]	$\overline{\alpha}$	α_{xx}	α_{yy}	α_{zz}	$\overline{\alpha}$	α_{xx}	α_{yy}	α_{zz}
IM	1	9.15	9.83	8.40	9.21	9.28	9.97	8.53	9.34
TD-DFT	1	9.15	9.84	8.41	9.19	9.28	9.95	8.56	9.32
IM	4	36.65	34.78	39.36	35.81	37.17	35.28	39.91	36.32
TD-DFT	4	36.67	34.85	39.42	35.73	37.19	35.43	39.87	36.28
IM	5	46.40	45.39	48.24	45.57	47.06	46.05	48.92	46.22
TD-DFT	5	46.88	46.18	49.00	45.45	47.58	46.93	49.66	46.14
IM	13	116.56	115.27	117.98	116.43	118.15	116.85	119.56	118.04
TD-DFT	13	118.82	118.71	119.90	117.84	120.45	120.79	120.77	119.80

[a]Number of water molecules in cluster

TABLE 5.1: *Frequency-dependent mean polarizability and polarizability tensor components of water clusters (in au).*

accounts for the static and frequency-dependent polarizability of these clusters and is therefore also capable of describing larger clusters.

	$\overline{\alpha}$	α_{xx}	α_{yy}	α_{zz}
		Water in water		
vacuum	9.15	9.83	8.40	9.21
LIM-1	8.95	9.72	8.49	8.65
LIM-2	8.96	9.72	8.50	8.66
		Benzene in benzene		
vacuum [a]	69.49	82.36	82.36	43.75
LIM-1	63.67	66.67	76.84	47.49
LIM-2	63.91	67.96	77.09	46.67
		Water in benzene		
vacuum	9.15	9.83	8.40	9.21
LIM-1	8.62	10.56	7.63	7.66
LIM-2	7.99	10.88	6.88	6.21
		Benzene in water		
vacuum [a]	69.49	82.36	82.36	43.75
LIM-1	69.94	82.36	80.01	47.44
LIM-2	72.78	86.39	85.61	46.34

[a]The TD-DFT results are : $\alpha_{xx} = \alpha_{yy} = 82.36$ au and $\alpha_{zz} = 41.89$ au.

TABLE 5.2: *Comparison between LIM-1 and LIM-2 for calculating* α^{solute}. *All calculations were performed with the dipole interaction model and are given in au. The clusters contains 1 solute molecule and 41 solvent molecules.*

The convergence of the MBP scheme was checked for the water pentamer. The calculations were done with the IM approach since it involves quite many calculations, i.e. 5 dimers, 5 trimers, 3 tetramers and 1 pentamer. If TD-DFT were used, extensive corrections for BSSE would also have to be considered. It was found that the expansion converged by correcting for the three-body contributions. Also, the polarizability components changed by no more than 0.02 au as the MBP expansion is taken beyond the pair-wise terms. The tetramer contributions are an order of magnitude smaller than the trimer corrections and therefore it is to be expected in general that trimer contributions will be sufficient. To determine the differences between the two partitioning schemes within LIM we also performed calculations on water in benzene, benzene in water and benzene in benzene. The results are displayed in Table 5.2. As expected, the results obtained with LIM-1 and LIM-2 are nearly identical for pure liquids. For the "solutions" the largest differences were found for water in benzene. If the polarizability of the solvent is much larger than that of the solute the weight factors in Eq. 5.3 become nearly unit and LIM-2 will give large differences compared with LIM-1. Therefore, the LIM-2 partitioning scheme should be used whenever the polarizability of the solute and solvent are different. However, in the rest of the work we only consider water and will therefore not distinguish between LIM-1 and LIM-2. The results of comparing LIM with PPM, DSA and MBP is presented in Table 5.3, they are

	$\overline{\alpha}$	α_{xx}	α_{yy}	α_{zz}	$\overline{\alpha}$	α_{xx}	α_{yy}	α_{zz}
vacuum	9.15	9.83	8.40	9.21				
		N = 5[a]				N = 13[a]		
LIM	9.55	10.33	8.74	9.58	9.21	9.91	8.17	9.56
PPM	9.28	9.08	9.65	9.11	8.97	8.87	9.08	8.96
DSA	9.75	10.61	8.88	9.76	8.98	9.60	7.73	9.60
MBP-3	9.46	10.24	8.66	9.49	-	-	-	-

[a]Number of water molecules in the cluster.

TABLE 5.3: *Comparison between LIM, PPM, DSA and MBP for calculating* α^{solute}. *All calculations were performed with the dipole interaction model and are given in au.*

all calculated with the IM approach. The MBP results for the water pentamer shows an increase in all polarizability components compared with the vacuum results. There is a good agreement between LIM and MBP results indicating that LIM gives an accurate description of the "solvation" shift. The increase in the polarizability components predicted by DSA is about a factor of 2 larger than that predicted with MBP and for PPM the XX and ZZ components decreases while the increase in the YY component is almost 5 times larger than the MBP result. Therefore, we used the LIM model as a reference for comparing with results for the $N = 13$ cluster for which the MBP approach becomes very tedious. For the $N = 13$ cluster the LIM results predicts a decrease in all polarizability components compared with the results obtained if only the 1st solvation shell is included. This trend is also found with DSA, however, the decrease in the polarizability components is much larger. Using PPM a decrease in all components is also found, but the polarizability is nearly isotropic in contrast to the results from both LIM and DSA. Therefore, in order to get an accurate description of the solvent shift in the polarizability tensor it is clearly necessary to go beyond simple models like PPM and DSA. In Fig. 5.2 we display the mean polarizability of a solute water molecule in water clusters as a function of the size of the cluster. The calculation has been performed with the LIM-2 method and the PPM scheme. To check the influence of the nearest neighbor molecules we also performed a MD simulation where the structure of the 1st solvation shell was relaxed. The solute polarizability was again calculated with LIM and is also displayed in Fig. 5.2, which clearly illustrates that the solute polarizability is dependent on the size of the cluster. Both for LIM and PPM, large fluctuations are found for the smaller clusters, whereas the results are reasonably converged at a cluster size around $N = 21$. The result for the cluster with the relaxed 1st solvation shell shows a large decrease of the mean polarizability. This indicates that the solute polarizability is more dependent on the local geometry of the cluster than on the actual size. Therefore it might be more important to include a larger number of different clusters than increasing the size of the individual clusters. In order to get a better description of the local solvent structure we performed a MD simulation of 100 ps from which 100 randomly chosen configurations were picked. We used as starting configuration the $N = 41$ cluster with the fixed 1st solvation shell. The solute polarizability

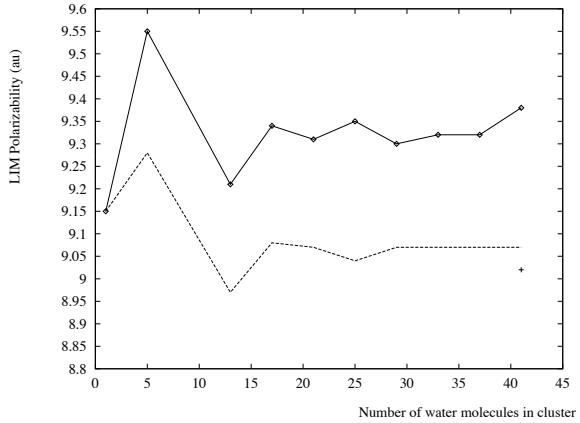

FIGURE 5.2*: Mean polarizability of a solute water molecule as a function of cluster size (in au). All calculation were calculated with LIM-2 and PPM schemes. (–,◇) LIM-2, (- -) PPM and (+) indicates the LIM-2 result for the* $N = 41$ *cluster with the structure of the 1st solvation shell relaxed.*

was then calculated as an average over the 100 configurations. The results are displayed in Table 5.4, both for the static and the frequency-dependent polarizability at frequency $\omega = 0.0656$. The mean polarizability of water is lowered by around 1.5% in going from vacuum to the cluster both in the static and in the frequency-dependent case. The largest changes, around 4%, were found in the X direction. This was also found for the static mean polarizability in an *ab initio* approach at the MP2 level where molecular interaction was accounted for by coulombic interactions, although a lowering of around 4.6% was found.[279] The main difference in the two results can be explained from the difference in the vacuum polarizabilities predicted by respectively MP2 and TD-DFT.

ω		$\overline{\alpha}$	α_{xx}	α_{yy}	α_{zz}
0.0000	vac.	9.15	9.83	8.40	9.21
	solv.	9.02 ± 0.08	9.47 ± 0.29	8.53 ± 0.36	9.05 ± 0.37
	Δ [a]	-1.4	-3.7	1.5	-1.8
0.0656	vac.	9.28	9.97	8.53	9.34
	solv.	9.14 ± 0.07	9.59 ± 0.30	8.63 ± 0.35	9.17 ± 0.38
	Δ^a	-1.5	-3.8	1.2	-1.8

[a]Solvent shift as percentage.

TABLE 5.4*: Polarizability and solvation shift of a water molecule averaged over 100 randomly chosen solvent configurations with* $N = 41$*. Calculated with the LIM-2 method. The results are in au.*

5.6 Conclusion

In this work we have discussed the problems arising from using supermolecular calculations to predict the medium effect on a solute polarizability. Three different schemes for partitioning the polarizability of a cluster into local contribution are discussed. Within the dipole interaction model a partitioning scheme has been suggested which allows solvation effects on the molecular polarizability to be studied with a computationally cheap method. Results from small water clusters have been used to compare the different partitioning schemes which clearly illustrate the problems with supermolecular calculations. Also, the effect of different weighting schemes were examined using clusters where the solute molecule was different from the solvent molecules. The results from large water clusters indicate that the polarizability is more dependent on the local geometry of the solvent than on the actual size of the cluster. However, it is important to include more than the first solvation shell in the calculations.

Acknowledgment

The Danish Research Training Council is gratefully acknowledged for financial support of L.J.

Chapter 6

Saturation of the third-order polarizability of carbon nanotubes

L. Jensen, P.-O. Åstrand, and K. V. Mikkelsen, "Saturation of the third-order polarizability of carbon nanotubes characterized by a dipole interaction model" *Nano Lett.* **3**, 661-665, 2003.

6.1 Abstract

An atomic dipole interaction model has been used for calculating the second hyperpolarizability of carbon nanotubes on the length scale up to 75 nm. It is demonstrated that an atomistic representation of mesoscale systems like nanotubes can be used to obtain a cubic response property up to a size of the system where the property scales linearly with increasing size. In particular, it demonstrates that atomistic models are useful also for designing nonlinear molecular materials, where local modifications may give large macroscopic contributions. The saturation length has been calculated for carbon nanotubes. It is found that carbon nanotubes are comparable to conjugated polymers with respect to the magnitude of the second hyperpolarizability and is therefore as promising as a candidate for future nonlinear optical materials.

6.2 Introduction

The prospect of utilizing optical nonlinearities of materials in constructing all-optical devices holds great promises. Particular promising is the exploitation of the intensity-dependence of the refractive index due to the second hyperpolarizabilities for constructing all-optical switching devices, which provides the basis for an all-optical information technology.[8] This requires novel materials exhibiting large nonlinearities characterized at the macroscopic level by the third-order optical susceptibility, $\chi^{(3)}$, and at the microscopic level by the third-order polarizability or second hyperpolarizability γ. It has been conjectured that computer modelling will play an essential role in the development of new materials.[23] In particular, the modeling of new nonlinear optical materials will require a detailed model of the electronic structure and its response to an external electric field.[18] Since the discovery of fullerenes[61] and later carbon nanotubes,[294] they have been strong candidates for the next generation of functional materials. The reason that these all-carbon molecules are of interest in nonlinear optical application is their extended π-system and that no absorption occurs due to C-H bonds.[62,71]

An important concept for designing new materials is the scaling behaviour of the nonlinear optical properties of the molecule with increasing system size and in particular the saturation limit, *i.e.* where the property scales linearly with increasing size. For polyenes it is well-known that for small chain lengths, N, the molecular γ obey a power law $\gamma \sim N^a$ with a between 3 and 6.[101,295,296] At large N, γ/N will saturate and the scaling exponent a will tend towards one. Obviously, the reason is that the most long-range interaction behaves as $1/R$ and thus approaches zero when R goes to infinity.

A cubic response property like the second hyperpolarizability is, however, a challenge to determine accurately both theoretically and experimentally. Considering γ of fullerenes, experimental results show large variations with respect to the choice of structure and experimental conditions.[62,71] The third-order polarizability of carbon nanotubes or tubular fullerenes have been studied both theoretical and experimentally to a much lesser degree than the small fullerenes.[62,71] However, in general it is found theoretically that the third-order polarizability varies strongly with the length, diameter and symmetry of the nanotubes, see *e.g.* Ref. 71. Theoretically, a scaling law for the third-order polarizability for small nanotubes was found using a Su-Schrieffer-Heeger model with the Coulomb interaction included[297] but the saturation limit was not investigated. *Ab initio* quantum chemical calculations would in principle be a valuable tool to study γ of these kinds of systems, but currently they are too computer-demanding to be used systematically to study for example the scaling of γ with respect to the length of a carbon nanotube. It is noted, however, that accurate calculations have been carried out for γ of the smallest fullerenes at the Hartree-Fock level.[65]

An alternative approach is based on representing the molecule as a set of interacting point polarizabilities,[88,89] a model which has been exploited extensively by Applequist and coworkers.[91] In a system of N interacting point polarizabilties, $\alpha_{I,\alpha\beta}$, the atomic induced dipole moment of atom I, $\mu^{\mathrm{ind}}_{I,\alpha}$ is given as

$$\mu_{I,\alpha}^{\text{ind}} = \alpha_{I,\alpha\beta}\left(E_{I,\beta}^{\text{ext}} + \sum_{J\neq I}^{N} T_{IJ,\beta\gamma}\mu_{J,\gamma}^{\text{ind}}\right) \tag{6.1}$$

where $E_{I,\beta}^{\text{ext}}$ is the external electric field at atom I and $T_{IJ,\beta\gamma}\mu_{J,\gamma}^{\text{ind}}$ is the electric field of the induced dipole moment at site J calculated at atom I. Greek suffices denote the Cartesian coordinates, x, y, or z and the Einstein summation convention is used for repeated indices.

If the atoms are regarded as spherically symmetric particles, $\alpha_{P,\alpha\beta} = \alpha_P\delta_{\alpha\beta}$, where the isotropic atomic polarizabilities, α_P, are atom-type parameters. It has been demonstrated that accurate parameters are obtained if they are parametrized from a training set of molecular polarizabilities obtained from quantum chemical calculations instead of experimental data.[94] The reasons are that experimental polarizabilities also include large vibrational contributions in addition to the electronic polarization included in Eq. 6.1. In addition, experimental results are often obtained from condensed phases and thus include also solvent effects.

An improved parametrization is obtained if the contributions from a smeared-out charge distribution is included in terms of a damping of the interaction in Eq. 6.1 by modifying the $T_{IJ,\alpha\beta}$ tensor.[93] Consequently, by adopting two parameters for each element, a polarizability, α_P, and a damping parameter, Φ_P, good results have been obtained for example for the polarizability of large molecular clusters. [Ref. 63, Chap. 3]

The solutions of the coupled set of linear equations in Eq. 6.1 may be expressed in terms of a two-atom relay tensor, $B_{IJ,\alpha\beta}^{(2)}$, as[92]

$$\mu_{I,\alpha}^{\text{ind}} = \sum_{J}^{N} B_{IJ,\alpha\beta}^{(2)} E_{J,\beta}^{\text{ext}} \tag{6.2}$$

where $B_{IJ,\alpha\beta}^{(2)}$ gives the induced dipole moment at atom I from an external field on atom J. The molecular second hyperpolarizability, $\gamma_{\alpha\beta\gamma\delta}^{\text{mol}}$, may be obtained by including higher-order terms in Eq. 6.1,

$$\mu_{I,\alpha}^{\text{ind}} = \alpha_{I,\alpha\beta}E_{I,\beta}^{\text{tot}} + \frac{1}{6}\gamma_{I,\alpha\beta\gamma\delta}E_{I,\delta}^{\text{tot}}E_{I,\gamma}^{\text{tot}}E_{I,\beta}^{\text{tot}} \tag{6.3}$$

where the total electric field, $E_{I,\beta}^{\text{tot}}$, is the sum of the external field and the electric field from all other induced dipole moments (see Eq. 6.1). A parametrization of the molecular γ thus includes an atomic γ parameter, γ_P, in addition to the parameters adopted for the molecular polarizability. Equivalently, the solutions of Eq. 6.3 may be expressed with an additional four-atom relay tensor, $B_{IJKL,\alpha\beta\gamma\delta}^{(4)}$, as[92]

$$\mu_{I,\alpha}^{\text{ind}} = \sum_{J}^{N} B_{IJ,\alpha\beta}^{(2)} E_{J,\beta}^{\text{ext}} + \frac{1}{6}\sum_{J,K,L}^{N} B_{IJKL,\alpha\beta\gamma\delta}^{(4)} E_{J,\delta}^{\text{ext}} E_{J,\gamma}^{\text{ext}} E_{J,\beta}^{\text{ext}} \tag{6.4}$$

The resulting molecular polarizability, $\alpha_{\alpha\beta}^{\text{mol}}$, and molecular second hyperpolarizability,

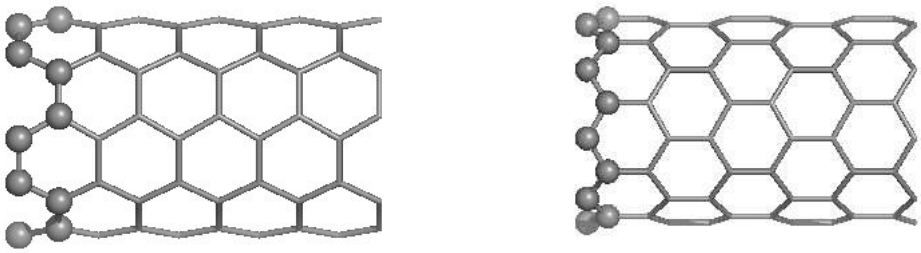

FIGURE 6.1: *(Left) Structure of a [5,5] carbon nanotube with 100 carbon atoms. (Right) Structure of a [9,0] carbon nanotube with 108 carbon atoms. For both carbon nanotubes the bond length of the C-C bond is 1.42 Å. The atoms displayed with ball structure represents the definition of the unit cell used in this work. The unit cell of the [5,5] carbon nanotube contains 20 carbon atoms whereas the unit cell of the [9,0] nanotube contains 18 carbon atoms.*

$\gamma^{\mathrm{mol}}_{\alpha\beta\gamma\delta}$, are given as

$$\alpha^{\mathrm{mol}}_{\alpha\beta} = \sum_{IJ}^{N} B^{(2)}_{IJ,\alpha\beta} \tag{6.5}$$

and

$$\gamma^{\mathrm{mol}}_{\alpha\beta\gamma\delta} = \sum_{IJKL}^{N} B^{(4)}_{IJKL,\alpha\beta\gamma\delta} \ . \tag{6.6}$$

The theoretical background is described in more detail in a previous work. [Ref. 95, Chap. 4]

In this work, it is demonstrated that an atomistic model can be used for calculating a cubic response property, the molecular γ, for carbon nanotubes up to a length where γ scales linearly with the length of the tube. In principle, it is thus possible to use atomistic models to calculate electronic response properties at all relevant length scales. As in many other areas, molecular modelling can thus be adopted for asking and answering questions regarding what happens if specific functional groups are added or modified.

6.3 Results

The parameters, α_C and Φ_C have been obtained in a previous work where α^{mol} is parametrized from Hartree-Fock calculations of α^{mol} for 184 molecules. [Ref. 63, Chap. 3] These parameters were shown to give good results for α^{mol} for nanotubes[100] and fullerene clusters. [Ref. 63, Chap. 3] The last parameter γ_C has been chosen to describe γ^{mol} of C_{60} obtained from Hartree-Fock calculations taken from Ref. 65. The values used in this work are α_C= 9.312 a.u., Φ_C= 0.124 a.u., and γ_C= 1600.0 a.u. These parameters give good results for α^{mol} for fullerenes and nanotubes and for γ^{mol} for small fullerenes,[99] and it is therefore expected that they will give reasonable results also for carbon nanotubes.

It was also demonstrated that the differences for γ^{mol} between quantum chemical calculations and the interaction model are on average around 10% and below 30%. [Ref. 95, Chap. 4] Although, Hartree-Fock calculations by no means represent the true answer, it is encouraging that a simple model like the interaction model can reproduce quantum chemical calculations consistently. It should therefore be relatively straightforward to reparametrize the model when more sophisticated quantum chemical methods become routine for medium-sized molecules. For comparison, most semi-empirical calculations give unrealistic values for γ (see examples in Ref. 95, Chap. 4), and density functional theory still presents difficulties for electric response properties although some recent achievements have been presented.[84]

The molecular γ has been calculated for [5,5] and [9,0] open-ended carbon nanotubes (see Figure 6.1 for structures) as a function of the tube length. The results are given in Figures 6.2 and 6.3 as γ/N, where N is the number of unit cells (see caption of Figure 6.1 for the definition of unit cells). Results are presented for the average $\overline{\gamma}$, defined as

$$\overline{\gamma} = \frac{1}{15} \sum_{\alpha,\beta} \gamma_{\alpha\alpha\beta\beta} + \gamma_{\alpha\beta\alpha\beta} + \gamma_{\alpha\beta\beta\alpha} \tag{6.7}$$

and for the individual components γ_{zzzz}, γ_{xxxx}, and γ_{xxzz}, where the z axis is directed along the tube and the x axis is perpendicular to the tube. The largest tubes of ~ 300 unit cells corresponds to ~ 6000 atoms and a length of ~ 75 nm. All of the results for the molecular

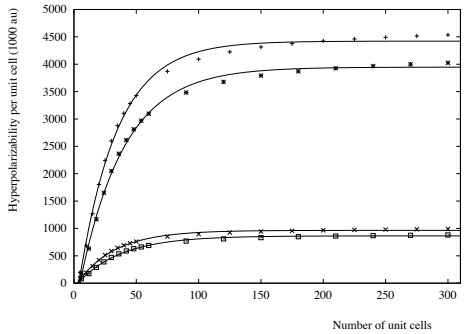

FIGURE 6.2: *Mean and ZZZZ component of the third-order polarizability per unit cell as a function of the number of unit cells for the [5,5] and [9,0] carbon nanotube. All results are in* 10^3 *a.u. (+) and (×) denotes ZZZZ component and mean value, respectively, for the [5,5] nanotube. For the [9,0] nanotube (∗) denotes the ZZZZ component and (□) the mean value. Solid lines are the plot of the corresponding fit.*

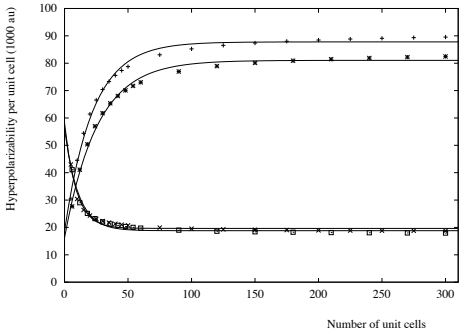

FIGURE 6.3: *XXZZ and ZZZZ component of the third-order polarizability per unit cell as a function of the number of unit cells for the [5,5] and [9,0] carbon nanotube. All results are in* 10^3 *a.u. (+) and (×) denotes XXZZ and XXXX component, respectively, for the [5,5] nanotube. For the [9,0] nanotube (∗) denotes the XXZZ component and (□) the XXXX component. Solid lines are the plot of the corresponding fit.*

γ have been characterized by fitting the results to the expression

$$\frac{\gamma(N)}{N} = \gamma^{\infty} - C\exp\left(-\frac{N}{N^{\mathrm{sat}}}\right) \tag{6.8}$$

used by Schulz *et al.*[101] to characterize the saturation of γ^{mol} of organic oligomers. This allows for a description of γ^{mol} in terms of three parameters which are independent on the chain length. The parameter γ^{∞} represents the asymptotic value and N^{sat} represents the onset of which the saturation starts. The parameters for all the fits are displayed in Table 6.1 and are plotted with solid lines in Figures 6.2 and 6.3. It is found that all the γ components and $\overline{\gamma}$ are well characterized by this model.

	Mean	*zzzz*	*xxzz*	*xxxx*
[5,5]				
N^{sat}	30.47 ± 0.93	30.64 ± 0.94	22.14 ± 0.96	9.13 ± 0.82
γ^{∞}	965.07 ± 5.95	4421.99 ± 28.6	87.79 ± 0.49	19.65 ± 2.96
C	1048.17 ± 18.02	5039.3 ± 86.2	69.10 ± 1.90	-38.50 ± 2.96
[9,0]				
N^{sat}	35.40 ± 1.07	35.58 ± 1.07	25.78 ± 1.13	10.74 ± 0.99
γ^{∞}	864.28 ± 5.45	3947.04 ± 26.15	81.05 ± 0.48	18.81 ± 0.29
C	940.98 ± 15.87	4517.83 ± 75.81	64.80 ± 1.80	-37.21 ± 2.94

TABLE 6.1*: Fitting parameters for characterizing mean value and individual components of the third-order polarizability for [5,5] and [9,0] carbon nanotubes. All parameters are in a.u.*

By comparing the two types of nanotubes, *i.e.* [5,5] and [9,0], it is noted that nearly identical results are obtained. The parameters for the [5,5] nanotube obtained from Eq. 6.8 are $\sim 10\%$ higher than the corresponding parameters for the [9,0] nanotube except for N^{sat} which is $\sim 10\%$ lower. The main reason for this is not due to a different behaviour of the two types of nanotubes but reflects that the unit cell of [5,5] is $\sim 10\%$ longer than the [9,0] unit cell. The saturation parameter, N^{sat}, for $\overline{\gamma}$ is for the [5,5] nanotube ~ 30 unit cells and for [9,0] about ~ 35 unit cell which corresponds to a tube length of ~ 7.3 nm for the [5,5] nanotube and ~ 7.5 nm for the [9,0] nanotube, respectively. As put forward by Schulz *et al.*,[101] a characterization of γ in terms of a power law, *i.e.* $\gamma \sim N^{a}$, is not appropriate since the exponent a varies strongly with N. This can be illustrated by plotting the variation in a defined as $b \equiv \frac{d\ln(\gamma)}{d\ln(N)}$ as a function of N, which is displayed in Figure 6.4. From the Figure, it is seen that b tends slowly towards one for long nanotubes and that the strongest variation in b is found for the small tubes. It is also found that N^{sat} corresponds well with the point were the variation b start to decrease.

As expected, if the results of $\overline{\gamma}$ and the individual components are compared, it is found that γ_{zzzz} has the longest saturation length and the smallest saturation length is found for γ_{xxxx}. For this reason, the saturation of $\overline{\gamma}$ is determined by the saturation of γ_{zzzz}. However, its asymptotic value, γ^{sat}, as obtained from the fit to $\overline{\gamma}$ is $\sim 10\%$ higher

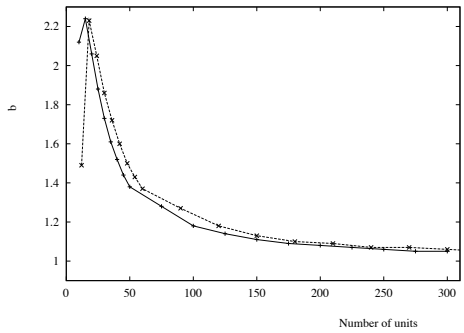

FIGURE 6.4: *The variation,* $b \equiv \frac{d\ln(\gamma)}{d\ln(N)}$*, of a power law representation of the mean third-order polarizability for the [5,5] and [9,0] carbon nanotube as a function of the number of unit cells. (+) denotes [5,5] nanotube and (×) [9,0] nanotube.*

than that obtained from $\gamma_{zzzz}/5$. Therefore, when extrapolating γ to the asymptotic limit by only considering the longitudinal components, which is typically done (see *e.g.* Ref.298), an error of $\sim 10\%$ is introduced as compared with extrapolating the mean value.

Even if it is difficult to strictly define where the scaling of γ becomes linear with tube length, it can be concluded that for tubes shorter than 100 unit cells $\overline{\gamma}$ and γ_{zzzz} behave in a clearly nonlinear way. For example, γ_{zzzz}/N of the [5,5] tube increases by a factor of 20 if the length of the tube is increased from 5 to 100 unit cells, but only with an additional 10% if the tube is extended to 300 unit cells.

The scaling parameters obtained for the nanotubes can be compared with the characterization of a series of conjugated organic oligomers carried out by Schulz *et al.*[101] The saturation lengths obtained for the oligomers are between $\sim 2-8$ nm, in comparison to ~ 7.5 nm obtained for the carbon nanotubes in this work. If γ^{∞}_{zzzz} is considered, a value of $\sim 1.8\times10^6$ a.u/Å is found for both types of nanotubes compared with the values for the conjugated oligomers which vary between $\sim 6\times10^4$ a.u/Å and $\sim 1.2\times10^6$ a.u/Å. If γ^{∞} for polyacetylene of 0.66×10^6 a.u./Å obtained using the semiemperical INDO/S method[101] is compared with the *ab initio* Hartree-Fock result of 1.3×10^6a.u./Å,[298] it is noted that the INDO/S result is about a factor of 2 smaller than the *ab initio* result. Therefore, even if a possible underestimation of γ using the INDO/S method instead of *ab initio* methods is considered, it is found that the magnitude of γ with respect to the length of carbon nanotubes is comparable with that of conjugated polymers. For this reason, carbon nanotubes are demonstrated to be a valid alternative to conjugated polymers for constructing new materials for use in nonlinear optical devices, especially considering the possibilities of enhancing the nonlinearities of carbon nanotubes by means of either endohedral, exohedral or substitutional doping (see *e.g.* Ref. 62, 71).

Acknowledgment

L.J. gratefully acknowledges The Danish Research Training Council for financial support.

Chapter 7

Microscopic and macroscopic polarization in C_{60} clusters

L. Jensen, P.-O. Åstrand, and K. V. Mikkelsen, "Microscopic and Macroscopic Polarization in C_{60} Fullerene Clusters as Calculated by an Electrostatic Interaction Model" **Submitted**, 2003.

7.1 Abstract

The dipole-dipole polarizability, α, and the second hyperpolarizability, γ, as well as the corresponding linear and third-order susceptibilities, $\chi^{(1)}$ and $\chi^{(3)}$, have been calculated for C_{60} fullerene clusters by a point-dipole interaction (PDI) model. The size dependences of a linear chain, a mono-layer film, and a face-centered cubic crystal cluster have been investigated. It is found that the effects of the surrounding molecules on the molecular α and γ are large, in particular for the chain and the film because of the anisotropic surroundings, and that large clusters are required to obtain converged results. A localized PDI model gives the opportunity to divide α and γ into fragment contributions, and it is found that α and γ of molecules in the middle of the chain converge slower than the properties for the end molecules with respect to the length of the chain. Similar results are found for the mono-layer film. Finally, $\chi^{(1)}$ and $\chi^{(3)}$ have been calculated using a modified local-field theory including the induced dipole moments of the surrounding molecules explicitly. The corresponding refractive index and dielectric constant compare well with experiments. On the other hand, the comparison of $\chi^{(3)}$ with experiments is complicated by dispersion and vibrational contributions. Nonetheless, our value of $\chi^{(3)}$ is in good agreement with a recent quantum chemical calculation adopting a self-consistent reaction-field model.

7.2 Introduction

The development of new functional materials exhibiting nonlinear optical (NLO) effects holds great potential for future application in electronics and photonics.[8,9] An important prospect is the utilization of the intensity dependence of the refractive index in all-optical switching devices, an essential element in future information processing technology.[8] Because the refractive index is governed by the linear susceptibility, $\chi^{(1)}$ (at the molecular level the linear dipole-dipole polarizability, α), and the intensity dependence of the refractive index by the third-order susceptibility, $\chi^{(3)}$ (where the molecular second hyperpolarizability, γ, is the corresponding microscopic property), an in-depth understanding of these properties is required.[8,12,13] These new materials will be designed on a molecular scale. Consequently, a detailed understanding of the electronic structure of the molecular building blocks, the dependence of the microscopic optical response properties on the molecular structure, and the differences between the properties of isolated molecules and molecules embedded in the actual macroscopic devices are of fundamental importance. Therefore, it has been conjectured that applied quantum chemistry will play a central role in the development of such new NLO materials.[18,23]

Since the discovery of fullerenes[61] and later carbon nanotubes,[294] they have been strong candidates for the next generation of functional materials.[299–303] Carbon-based materials provide numerous possibilities to design molecular functionality because of the large variety of molecules that can be synthesized in organic chemistry. This is indeed the case in nature where all functionality exists that we can expect that nanotechnology can provide. The particular reason that carbon fullerenes are of interest in NLO applications is their extended π-system and that no absorption occurs due to C-H bonds.[62,71] Recently, the scaling behaviour of the second hyperpolarizability of carbon nanotubes with increasing system size has been investigated theoretically and it was demonstrated that carbon nanotubes can be considered as a valid alternative to conjugated polymers for constructing new materials for use in NLO devices. [Ref. 96, Chap. 6] Since the C_{60} molecule was the first fullerene to be discovered, numerous theoretical and experimental investigations have been performed of its linear and nonlinear optical properties, see *e.g.* [Ref. 62–66, Chap. 3], and references therein.

Recently, accurate experimental results have been presented for the dipole-dipole polarizability of the C_{60} molecule in the gas phase.[204,304] A value of 76.5 ± 8.0 Å^3 was reported for the static polarizability,[204] and a value of 79 ± 4 Å^3 was measured for the polarizability at the frequency 0.0428 a.u. (λ=1064 nm).[304] For both the static and the frequency-dependent polarizability, the results are in good agreement with recent quantum chemical calculations[64,205] and results from a frequency-dependent point-dipole interaction (PDI) model.[166] In contrast, the DFT results of 80.6 Å^3 and 82.4 Å^3[64] for the static and frequency-dependent polarizability, respectively, are slightly higher than the *ab initio* SCF results of 75.1 Å^3 and 76.4 Å^3[205] and the results from the PDI model of 77.5 Å^3 and 78.2 Å^3.[166] The overestimation of the polarizability of C_{60} using conventional density functionals can, however, be improved by using *e.g.* time-dependent current-DFT.[305] Similarly, the overestimation of the polarizability in DFT for linear polymers is considerably large,

in particular for longer chains.[84,306] In addition, comparison between calculated molecular properties and experiments in the gas phase is complicated by vibrational contributions. However, the pure vibrational polarizability for the isolated C_{60} molecule has been calculated using first principles methods and is found to be small, ~ 0.8 Å^3, as compared with the electronic polarizability of around 80 Å^3.[307]

In the condensed phase, experiments are usually carried out on thin films of C_{60} molecules and the molecular polarizability is extracted from measurements of the refractive index or the dielectric constant by means of the Clausius-Mossotti equation and gives results in the range between 80.5 Å^3 and 91.9 Å^3.[206–211] These values are, as expected, slightly higher than the results for the isolated molecule. The contribution to the polarizability from pure vibrational lattice effects has been estimated experimentally to ~ 2 Å^3,[211] and it is therefore too small to account for the difference between the experiments in the gas phase and in the condensed phase. Most theoretical studies have considered the isolated molecule C_{60} and therefore neglect intermolecular interactions. There is, however, a quantum chemical calculation of the polarizability of C_{60}, C_{70} and C_{84} in the condensed phase using self-consistent reaction-field (SCRF) theory.[308] The polarizability of C_{60} was calculated to 93.8 Å^3 compared with 75.1 Å^3 in the gas phase. In addition, the PDI model has been used to calculate the polarizability of fullerene mono-layer films which resulted in 83.9 Å^3 for a C_{60} molecule in the film and 77.5 Å^3 for the isolated molecule [Ref. 63, Chap. 3], also in good agreement with experimental results.

For the second hyperpolarizability, the situation is less clear and the differences between theory and experiment are much larger. In contrast to the polarizability, experiments have been carried out only for the condensed phase, usually for thin films or in solution, and the differences between various measurements are substantial.[62] The third-order susceptibility is very sensitive to the experimental conditions such as the experimental measuring techniques, laser power, frequency-dispersion, condensed phase, and even the sample preparation method.[62,67] Furthermore, most experimental results have been obtained for the resonant third-order susceptibility which is in the region where the frequency-dispersion is the largest. The theoretical results have usually been calculated for the isolated molecule and often for the static case or at non-resonant frequencies. Even if only the theoretical results for the static second hyperpolarizability are compared with each other, the spread of the data is large.[62] In particular, methods using a semi-empirical sum-over-states (SOS) approach seem to give results significantly higher than other theoretical models. Among methods like DFT and SCF the agreement is much better. There has been a study of the static second hyperpolarizability in the condensed phase calculated with SCRF at the SCF level of theory, where a value of 278×10^3 a.u. (140×10^{-36} esu) was found compared with a value of 109×10^3 a.u. (55×10^{-36} esu) in the gas phase.[308] In Ref. 308, the third-order susceptibility was also calculated using a general local field theory obtained from the Onsager-Böttcher relation[31] and good agreement with experiments was claimed. However, the comparison between the experimental and the theoretical susceptibility was carried out without correcting for different conventions adopted.[27]

In this work, we combine the point-dipole interaction (PDI) model with a local-field ansatz resulting in that the linear and third-order macroscopic susceptibilities may be

obtained. Furthermore, adopting a localized PDI model, the (hyper)polarizability of a molecule in a cluster may be calculated. Calculations have been carried out for C_{60} fullerene clusters: linear chains, mono-layer films, and face-centered cubic clusters. The presentation is organized as follows. A theoretical background is given in section 7.3, computational details are given in section 7.4, our results are presented in section 7.5, and, finally, the conclusions are given in section 7.6.

7.3 Theoretical background

7.3.1 The Point-Dipole Interaction Model

An alternative approach to quantum chemical methods is based on representing the molecule as a set of interacting induced point dipoles,[87–89] a model exploited extensively by Applequist and coworkers.[90,91] In a system of N point polarizabilities, $\alpha_{I,\alpha\beta}$, the atomic induced dipole moment of atom I, $\mu^{\mathrm{ind}}_{I,\alpha}$ is given as

$$\mu^{\mathrm{ind}}_{I,\alpha} = \alpha_{I,\alpha\beta} E^{\mathrm{tot}}_{I,\beta} + \frac{1}{6}\gamma_{I,\alpha\beta\gamma\delta} E^{\mathrm{tot}}_{I,\beta} E^{\mathrm{tot}}_{I,\gamma} E^{\mathrm{tot}}_{I,\delta} \ , \tag{7.1}$$

where the total microscopic electric field, $E^{\mathrm{tot}}_{I,\beta}$ is given by[31,33]

$$E^{\mathrm{tot}}_{I,\beta} = E^{\mathrm{loc}}_{\beta} + E^{\mathrm{dip}}_{I,\beta} = E^{\mathrm{mac}}_{\beta} + \frac{4\pi}{3} P_{\beta} + \sum_{J \neq I}^{N} T_{IJ,\beta\gamma} \mu^{\mathrm{ind}}_{J,\gamma} \ . \tag{7.2}$$

Here, E^{loc}_{β} is the local field experienced due to the external electric field, which is given as the sum of the macroscopic electric field, E^{mac}_{β}, and the macroscopic polarization, P_{β}.[31,33] The term, $T_{IJ,\beta\gamma}\mu^{\mathrm{ind}}_{J,\gamma}$, denotes the electric field of the induced dipole moment at site J calculated at atom I, and $E^{\mathrm{dip}}_{I,\beta}$ is thus the electric field at site I from all other induced dipole moments. Greek subscripts denote Cartesian coordinates, x, y, or z and the Einstein summation convention is used for repeated subscripts.

The atoms are regarded as spherically symmetric particles, resulting in that $\alpha_{P,\alpha\beta} = \alpha_P \delta_{\alpha\beta}$, where the isotropic atomic polarizabilities, α_P, are treated as atom-type parameters where one parameter is used for each element. It has been demonstrated that accurate parameters are obtained if they are parametrized from a training set of molecular polarizabilities obtained from quantum chemical calculations instead of experimental data.[94] One reason for that is that experimental polarizabilities often have been converted from macroscopic susceptibilities, which, as demonstrated here, is a non-trivial task.

An improved parametrization is obtained if the contributions from a smeared-out charge distribution is included in terms of a damping of the interaction in Eq. 7.1 by modifying the $T_{IJ,\alpha\beta}$ tensor.[93,309] Consequently, by adopting two parameters for each element, a polarizability, α_P, and a damping parameter, Φ_P, good results have been obtained for example for the polarizability of large molecular clusters [Ref. 63, Chap. 3]. A parametrization of the

molecular γ includes an atomic γ parameter, γ_P, in addition to the parameters adopted for the molecular polarizability [Ref. 95, Chap. 4].

The solutions of the coupled set of linear equations in Eq. 7.1 may be expressed in terms of a two-atom relay tensor, $B^{(2)}_{IJ,\alpha\beta}$, and a four-atom relay tensor $B^{(4)}_{IJKL,\alpha\beta\gamma\delta}$ as[92] [Ref. 95, Chap. 4]

$$\mu^{\mathrm{ind}}_{I,\alpha} = \sum_{J}^{N} B^{(2)}_{IJ,\alpha\beta} E^{\mathrm{loc}}_{J,\beta} + \frac{1}{6} \sum_{J,K,L}^{N} B^{(4)}_{IJKL,\alpha\beta\gamma\delta} E^{\mathrm{loc}}_{L,\delta} E^{\mathrm{loc}}_{K,\gamma} E^{\mathrm{loc}}_{J,\beta} \ , \tag{7.3}$$

where $B^{(2)}_{IJ,\alpha\beta}$ gives the induced dipole moment at atom I from a local electric field on atom J. The two-atom relay tensor is given in the regular way as an inverse of a supermatrix,[90,93]

$$\mathbf{B}^{(2)} = \left(\boldsymbol{\alpha}^{-1} - \mathbf{T}\right)^{-1} \ . \tag{7.4}$$

Analogously, $B^{(4)}_{IJKL,\alpha\beta\gamma\delta}$ gives the induced dipole moment at atom I from a local electric field on atom J, K, and L. The four-atom relay tensor for a system of spherically symmetric particles may be written as [Ref. 95, Chap. 4]

$$B^{(4)}_{IJKL,\alpha\beta\gamma\delta} = \sum_{M}^{N} \gamma_{M,\lambda\mu\nu\xi} \widetilde{B}^{(2)}_{ML,\xi\delta} \widetilde{B}^{(2)}_{MK,\nu\gamma} \widetilde{B}^{(2)}_{MJ,\mu\beta} \widetilde{B}^{(2)}_{MI,\lambda\alpha} \ , \tag{7.5}$$

where $\widetilde{B}^{(2)}_{IJ,\alpha\beta}$ is defined as

$$\widetilde{B}^{(2)}_{IJ,\alpha\beta} = \delta_{IJ}\delta_{\alpha\beta} + \sum_{K\neq I}^{N} T^{(2)}_{IK,\alpha\gamma} B^{(2)}_{KJ,\gamma\beta} = \alpha^{-1}_{I,\alpha\tau} B^{(2)}_{IJ,\tau\beta} \ . \tag{7.6}$$

The resulting molecular polarizability, $\alpha^{\mathrm{mol}}_{\alpha\beta}$, and molecular second hyperpolarizability, $\gamma^{\mathrm{mol}}_{\alpha\beta\gamma\delta}$, are given as

$$\alpha^{\mathrm{mol}}_{\alpha\beta} = \sum_{IJ}^{N} B^{(2)}_{IJ,\alpha\beta} \ , \tag{7.7}$$

and

$$\gamma^{\mathrm{mol}}_{\alpha\beta\gamma\delta} = \sum_{IJKL}^{N} B^{(4)}_{IJKL,\alpha\beta\gamma\delta} \ . \tag{7.8}$$

The theoretical background of the calculation of second hyperpolarizabilities within a PDI model is described in more detail in a previous work [Ref. 95, Chap. 4].

7.3.2 The Localized Point-Dipole Interaction Model

A localized point-dipole interaction model (LPDI) is utilized to calculate the (hyper)polarizability of the individual molecules (or subgroups) in a cluster [Ref. 97, Chap. 5]. The partitioning is carried out by first decomposing the two-atom matrix into a block diagonal form with M

blocks, $\hat{B}^{(2)}_{I,PQ,\alpha\beta}$, corresponding to a relay tensor for the I'th molecule or subgroup, where M is the total number of molecules or subgroups in the cluster. In the decomposition of the relay matrix, the interaction blocks $B^{(2)}_{P\in IQ\in J,\alpha\beta}$, where atom P belongs to molecule I and atom Q to molecule J, is assigned to the diagonal blocks $B^{(2)}_{P\in IQ\in I,\alpha\beta}$ where both atom P and Q belong to molecule I. This assignment is a more or less arbitrary procedure but can be done similarly to the Mulliken population analysis.[98] Therefore, we have for molecule I,

$$\hat{B}^{(2)}_{I,PQ,\alpha\beta} = B^{(2)}_{P\in IQ\in I,\alpha\beta} + \frac{1}{2}\sum_{J\neq I}^{M}\left(B^{(2)}_{P\in IQ\in J,\alpha\beta} + B^{(2)}_{P\in JQ\in I,\alpha\beta}\right) \ . \tag{7.9}$$

The polarizability and second hyperpolarizabilty can subsequently be calculated by Eqs. 7.7, 7.6 and 7.8 using the diagonal blocks of the decomposed relay matrix, $\hat{B}^{(2)}_{I,PQ,\alpha\beta}$. They also give the polarizability and hyperpolarizability of each of the M individual molecules in the molecular cluster.

7.3.3 The linear and nonlinear susceptibility

In a similar way to the induced dipole moment, the macroscopic polarization, P, can be expanded in powers of the macroscopic electric field, E^{mac},[10,31]

$$P_I = \chi^{(1)}_{IJ}E^{\mathrm{mac}}_J + \chi^{(3)}_{IJKL}E^{\mathrm{mac}}_J E^{\mathrm{mac}}_K E^{\mathrm{mac}}_L \tag{7.10}$$

where $\chi^{(1)}_{IJ}$ is the linear susceptibility and $\chi^{(3)}_{IJKL}$ is the third-order suceptibility. The macroscopic polarization is also given in terms of the microscopic induced molecular dipole moments, μ, as[10,31,33]

$$P_I = N_d\left\langle\mu_\alpha\right\rangle_I = N_d\left\langle\alpha^{\mathrm{mol}}_{\alpha\beta}\right\rangle_{IJ}E^{\mathrm{loc}}_J + \frac{1}{6}N_d\left\langle\gamma^{\mathrm{mol}}_{\alpha\beta\gamma\delta}\right\rangle_{IJKL}E^{\mathrm{loc}}_J E^{\mathrm{loc}}_K E^{\mathrm{loc}}_L \ , \tag{7.11}$$

where N_d is the number density and $\langle\rangle$ denotes orientation averaging which relates the molecule-fixed axes, $\alpha,\beta,\ldots$ to the space-fixed axes $I,J,\ldots$.[25] Inserting the definition of the local field, Eq. 7.2, in Eq. 7.11 the polarization in the Z direction due to a electric field in the Z direction can be written as

$$P_Z = N_d\overline{\alpha}^{\mathrm{mol}}\left(E^{\mathrm{mac}}_Z + \frac{4\pi}{3}P_Z\right) + \frac{1}{6}N_d\overline{\gamma}^{\mathrm{mol}}\left(E^{\mathrm{mac}}_Z + \frac{4\pi}{3}P_Z\right)^3 \ , \tag{7.12}$$

where the average molecular polarizability is given by[25]

$$\overline{\alpha}^{\mathrm{mol}} = \left\langle\alpha^{\mathrm{mol}}_{\alpha\beta}\right\rangle_{ZZ} = \frac{1}{3}(\alpha_{xx}+\alpha_{yy}+\alpha_{zz}) \ , \tag{7.13}$$

and the average molecular second hyperpolarizability by[15,25]

$$\overline{\gamma}^{\mathrm{mol}} = \left\langle\gamma^{\mathrm{mol}}_{\alpha\beta\gamma\delta}\right\rangle_{ZZZZ} = \frac{1}{15}\sum_{\alpha\beta}(\gamma_{\alpha\alpha\beta\beta}+\gamma_{\alpha\beta\beta\alpha}+\gamma_{\alpha\beta\alpha\beta}) \tag{7.14}$$

Combining this equation with the power expansion of the polarization in Eq. (7.10), the linear electric susceptibility, $\chi^{(1)}_{ZZ}$ is obtained as

$$\chi^{(1)}_{ZZ} = \left.\frac{\partial P_Z}{\partial E^{\rm mac}_Z}\right|_{E^{\rm mac}=0} = N_d\overline{\alpha}^{\rm mol}(1+\frac{4\pi}{3}\chi^{(1)}_{ZZ}) \ , \tag{7.15}$$

resulting in

$$\chi^{(1)}_{ZZ} = \frac{N_d\overline{\alpha}^{\rm mol}}{1-\frac{4\pi}{3}N_d\overline{\alpha}^{\rm mol}} \ . \tag{7.16}$$

The related refractive index, $n^{(1)}$, and dielectric constant, $\epsilon^{(1)}$, are given as,[33]

$$n^{(1)} = \sqrt{\epsilon^{(1)}} = \sqrt{1+4\pi\chi^{(1)}_{ZZ}} = \sqrt{\frac{1+\frac{8\pi}{3}N_d\overline{\alpha}^{\rm mol}}{1-\frac{4\pi}{3}N_d\overline{\alpha}^{\rm mol}}} \ , \tag{7.17}$$

which is the familiar Lorentz-Lorenz equation or Clausius-Mossotti equation. The corresponding third-order susceptibility, $\chi^{(3)}_{ZZZZ}$, is given as

$$\chi^{(3)}_{ZZZZ} = \left.\frac{\partial^3 P_Z}{\partial E^{\rm mac}_Z E^{\rm mac}_Z E^{\rm mac}_Z}\right|_{E^{\rm mac}=0} = \frac{1}{6}N_d\overline{\gamma}^{\rm mol}(1-N_d\overline{\alpha}^{\rm mol}\frac{4\pi}{3})^{-1}(1+\frac{4\pi}{3}\chi^{(1)}_{ZZ})^3 \ , \tag{7.18}$$

which may be rewritten as[10]

$$\chi^{(3)}_{ZZZZ} = \frac{1}{6}N_d\overline{\gamma}^{\rm mol}(\frac{\epsilon^{(1)}+2}{3})^4 \ . \tag{7.19}$$

Although the equations for $\chi^{(1)}$ and $\chi^{(3)}$ presented here look identical to the standard Lorentz local-field treatment, it should be emphasized that they are different since the electric field from the nearby dipoles, $E^{\rm dip}_{I,\beta}$, is included in Eq. 7.2. In the standard Lorentz local-field approach, this field is ignored since it is zero in a simple cubic lattice and assumed likewise in a completely random situation.[31,33]

7.4 Computational details

The parameters, α_C and Φ_C have been obtained in a previous work where the molecular α was parametrized from Hartree-Fock calculations on 184 molecules [Ref. 63, Chap. 3]. The model gives good results for α for carbon nanotubes,[166] boron nitride tubes,[100] and C_{60} fullerene clusters [Ref. 63, Chap. 3]. The remaining parameter γ_C has been chosen to describe the molecular γ of C_{60} obtained from Hartree-Fock calculations taken from Ref. 65. The values used in this work are α_C= 9.312 a.u., Φ_C= 0.124 a.u., and γ_C= 1600.0 a.u. This set of parameters have previously been used to study the saturation of the second hyperpolarizability of carbon nanotubes with increasing tube-length [Ref. 96, Chap. 6]. The structure of the C_{60} molecule was taken from our previous work.[166] In the solid phase at room temperature, C_{60} exhibits a face-centered-cubic (FCC) structure with a lattice vector

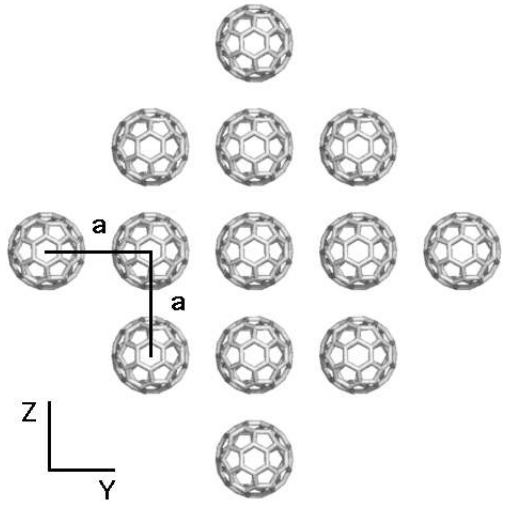

(a) A-Layer: (1 0 0) layer with 13 C_{60} molecules

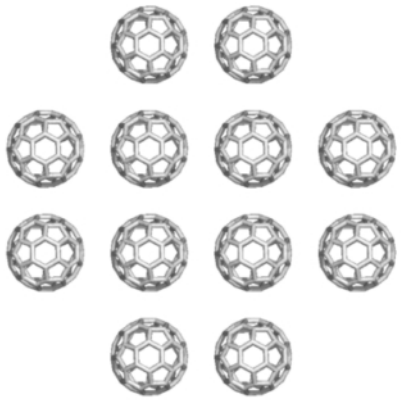

(b) B-Layer: rotated (1 0 0) layer with 12 C_{60} molecules

FIGURE 7.1: *C_{60} films. The nearest neighbour distance is a = 10.02 Å. The films are in the YZ-plane. Figures prepared using the PyMOL program.*[310]

of $a_0 = 14.17$ Å giving a nearest-neighbor distance of $a = 10.04$ Å .[191,211] In this study, we have investigated chains, mono-layers and FCC clusters of C_{60} molecules and all the structures have been constructed using this nearest-neighbor distance. The two different mono-layers (A and B) used in this work are illustrated in Figure 7.1, which correspond to the (1 0 0) surfaces of the FCC crystal. The chains of C_{60} molecules correspond to the diagonal of the A-layer, the mono-layers studied are A-layers and the FCC-clusters are constructed by combinations of A- and B-layers.

7.5 Results

The polarizability and the second hyperpolarizability of a C_{60} molecule in a fullerene cluster have been calculated in three different ways. In the following ξ represent either α or γ. The first method is to calculate the average value per molecule $\overline{\xi}(N)/N$, the second way is the Δ approach,[203] *i.e.*, the difference between the value for N molecules and for $N - X$ molecules $\Delta\xi = (\overline{\xi}(N) - \overline{\xi}(N - X))/X$ where X is the step-size, and finally the localized PDI model $\overline{\xi}^{\mathrm{LPDI}}$ as described in section 7.3.2. In the average approach, the total ξ of the system is distributed evenly between the molecules and for this reason resembles the experimental results. The average approach requires, however, a very large number of molecules in the cluster before ξ/N converges due to a large number of molecules in the outer part of the cluster. For this reason, the Δ approach has been introduced in order to improve the slow convergence by removing the effect of the outlying molecules.[203] As

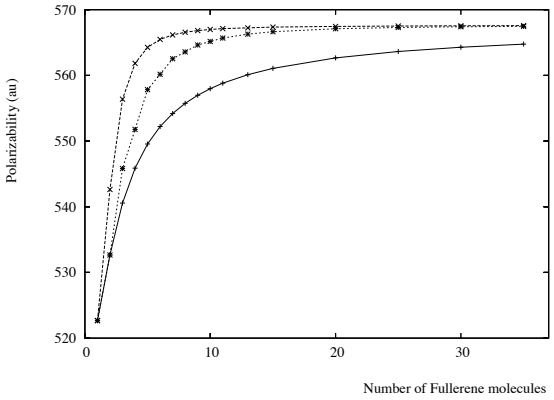

FIGURE 7.2: *Mean static polarizability per molecule for C_{60} chains as a function of the number of C_{60} molecules (in a.u.). (+) $\overline{\alpha}/N$ molecule (×) $\Delta\alpha$, and (∗) $\overline{\alpha}^{\mathrm{LPDI}}$.*

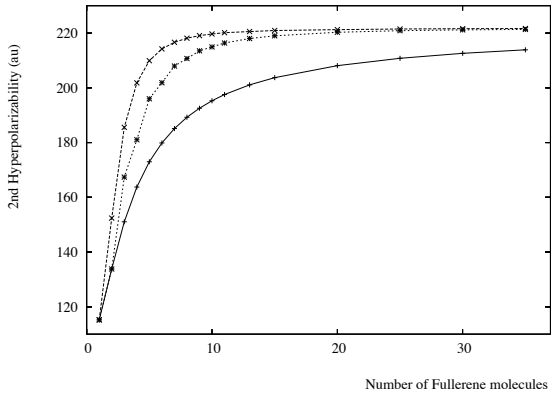

FIGURE 7.3: *Mean static second hyperpolarizability per molecule for C_{60} chains as a function of the number of C_{60} molecules (in 1000 a.u.). (+) $\overline{\gamma}/N$ molecule (×) $\Delta\gamma$, and (∗) $\overline{\gamma}^{\mathrm{LPDI}}$.*

realized from the definition of the Δ approach it is most efficient when the step-size is small compared with the total number of molecules in the cluster, *i.e.* it is identical to the average approach in the limit where X becomes identical with N. Here, these approaches are compared to the LPDI approach [Ref. 97, Chap. 5].

7.5.1 Chains of C_{60} molecules

The dependence of the (hyper)polarizability of a C_{60} molecule in a linear chain of C_{60} molecules on the length of the chain has been investigated. The fullerene chain is not only a suitable model system for investigating this approach but is also considered as a model of the edges of a fullerene crystal. Furtermore, linear chains of C_{60} molecules have also been found inside carbon nanotubes, so-called peapods, with the same spacing between the C_{60} molecules.[311] In Figures 7.2 and 7.3, respectively, the polarizability and second hyperpolarizability of a C_{60} molecule in a chain of C_{60} molecules are presented as a function of the number of molecules in the chain. The longest chain contains 35 C_{60} molecules corresponding to a chain length of $\sim$ 35 nm. For this chain, the polarizability was obtained as $\overline{\alpha}/N = 564.76$ a.u., $\Delta\overline{\alpha} = 567.57$ a.u. and $\overline{\alpha}^{\mathrm{LPDI}} = 567.46$ a.u. In the Δ approach a step-size of one was used until $N = 11$, then a step-size of two until $N = 15$, and for the rest a step-size of five was used. The second hyperpolarizability was calculated to be $\overline{\gamma}/N = 213.89 \times 10^3$ a.u., $\Delta\overline{\gamma} = 221.67 \times 10^3$ a.u., and $\overline{\gamma}^{\mathrm{LPDI}} = 221.34 \times 10^3$ a.u. Good agreement is found between the Δ approach and the LPDI model both for the polarizability and for the second hyperpolarizability, whereas the average approach gives values that are slightly smaller. In Figures 7.2 and 7.3, it is also noted that the Δ approach converges faster than the other approaches. The LPDI approach converges slightly slower but still

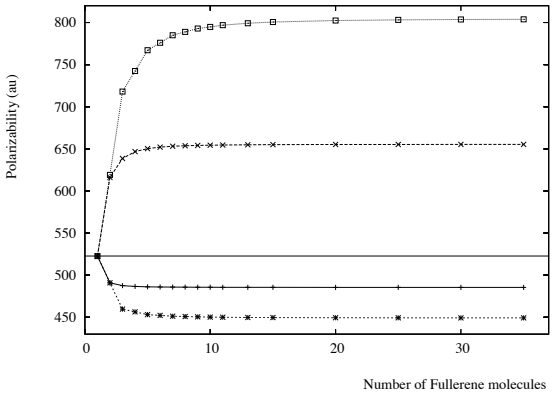

FIGURE 7.4: *Static polarizability in a.u. for a C_{60} molecule in a fullerene chains as a function of the number of C_{60} molecules calculated with LPDI. For a molecule in the end of the chain (+) α_{xx} and (×) α_{zz}. For a molecule in the middle of the chain, (∗) α_{xx}, and (□) α_{zz}. x axis perpendicular to the chain and z axis along the chain.*

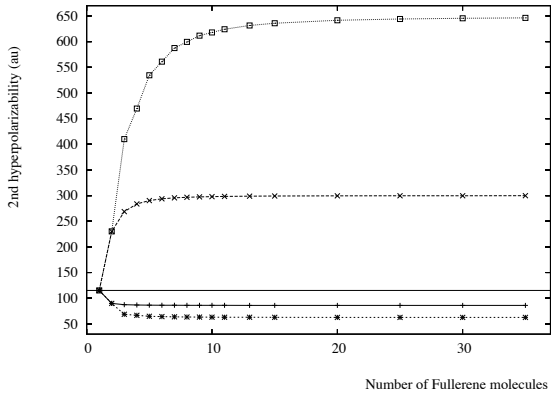

FIGURE 7.5: *Static second hyperpolarizability for a C_{60} molecule in a chains of fullerene molecules as a function of the number of C_{60} molecules in the chain (in 1000 a.u.). For a molecule in the end of the chain (+) γ_{xxxx} and (×) γ_{zzzz}. For a molecule in the middle of the chain, (∗) γ_{xxxx}, and (□) γ_{zzzz}. x axis perpendicular to the chain and z axis along the chain.*

much faster than the average method. If the linear chain of C_{60} molecules is compared with a carbon nanotube with the same diameter, *i.e.* a [5,5] or [9,0] carbon nanotube, $\overline{\alpha}/N_{atom}$ is $\sim$ 9.5 a.u. for the chain whereas it is $\sim$ 14.2 a.u. for the nanotube,[99] where N_{atom} is the number of Carbon atoms. Analogously, $\overline{\gamma}/N_{atom}$ is $\sim 3.7 \times 10^3$ a.u. for the chain and $\sim 48 \times 10^3$ a.u. for the nanotube [Ref. 96, Chap. 6]. Thus, $\overline{\alpha}/N_{atom}$ and in particular $\overline{\gamma}/N_{atom}$ are as expected much larger for the carbon nanotube than for the chain of C_{60} molecules because of the extended conjugated electronic structure. In Figures 7.4 and 7.5, α and γ are presented for a C_{60} molecule in the chain calculated with the LPDI model where the molecule is situated either in the middle of the chain or at the end of the chain. It is found that α_{zz} and γ_{zzzz} increase and α_{xx} and γ_{xxxx} decrease with increasing chain length for both the middle and the end molecules, and that the perturbation is larger along the chain (z-axis) and, therefore, the components in this direction converge slower with respect to the length of the chain. Furthermore, the differences are significant between the middle and the end molecules of the chain. For the chain of 35 C_{60} molecules, we obtained α_{zz}=803.89 a.u. and γ_{zzzz}=646.26 $\times 10^3$ a.u. for the middle molecule and α_{zz}=655.33 a.u. and γ_{zzzz}=299.72 $\times 10^3$ a.u. for the end molecules, respectively. For the end molecules, both α and γ converge much faster with respect to the length of the chain than the molecule in the middle which illustrates clearly why the Δ approach converges much faster than the average method.

7.5.2 Mono-layer films of C_{60} molecules

The second type of system is a C_{60} molecule in mono-layer films of C_{60} molecules. The mono-layer is considered as a model of the (1 0 0) surface of the fullerene crystal.

N	1	5	13	25	41	61
$\overline{\alpha}/N$	522.76	541.05	555.24	566.19	574.58	581.15
$\Delta\overline{\alpha}$	522.76	545.62	564.11	578.06	587.69	594.61
$\overline{\alpha}^{\mathrm{LPDI}}$	522.76	568.74	575.07	586.23	595.05	601.73
$\overline{\gamma}/N$	115.21	150.91	178.06	200.52	218.70	233.55
$\Delta\overline{\gamma}$	115.21	159.83	195.02	224.85	247.12	263.99
$\overline{\gamma}^{\mathrm{LPDI}}$	115.21	196.35	218.63	244.86	265.81	282.22

TABLE 7.1*: Static polarizability and second hyperpolarizability for C_{60} in a monolayer film. N is the number of C_{60} molecules in the film. α in a.u. and γ in 10^3 a.u.*

In Table 7.1, $\overline{\alpha}$ and $\overline{\gamma}$ are presented for a C_{60} molecule in a monolayer film of C_{60} molecules calculated using the average, Δ and LPDI approaches. We find for the largest film, containing 61 C_{60} molecules, a polarizability of $\overline{\alpha}/N = 581.15$ a.u., $\Delta\overline{\alpha} = 594.61$ a.u. and $\overline{\alpha}^{\mathrm{LPDI}} = 601.73$ a.u. For the second hyperpolarizability, we find $\overline{\gamma}/N = 233.55 \times 10^3$ a.u., $\Delta\overline{\gamma} = 263.99 \times 10^3$ a.u., and $\overline{\gamma}^{\mathrm{LPDI}} = 282.22 \times 10^3$ a.u. Compared with the results for the longest chain, $\overline{\alpha}$ is increased by $\sim 3\%$, $\sim 5\%$, and $\sim 6\%$ for the various methods and $\overline{\gamma}$ by $\sim 9\%$, $\sim 19\%$, and $\sim 28\%$, respectively. For the films, the LPDI approach gives the largest $\overline{\alpha}$ and $\overline{\gamma}$ values in good agreement with the expectation that the LPDI model will converge faster than both the Δ and the average approach when the dimension of the system increase. For the mono-layer films, both α and γ show similar trends with increasing system size as was found for the chains.

Using the LPDI model, the results of a C_{60} molecule in one of the corners of the mono-layer film with 61 C_{60} molecules are $\overline{\alpha} = 547.79$ Å^3 and $\overline{\gamma} = 168.66 \times 10^3$ a.u. This is as expected much lower than the values of $\overline{\alpha} = 601.73$ Å^3 and $\overline{\gamma} = 282.22 \times 10^3$ a.u found for the molecule in the middle of the film . Compared with the isolated molecule, the change in $\overline{\alpha}$ and $\overline{\gamma}$ are for the corner molecule only $\sim 5\%$ and $\sim 45\%$, respectively, whereas the changes are $\sim 15\%$ and $\sim 145\%$, respectively, for the molecule in the middle, *i.e.* around three times larger. For the chain with the same number of molecules as on the diagonal of the film (11 C_{60} molecules), the results for an end molecule are $\overline{\alpha} = 541.96$Å^3 and $\overline{\gamma} = 149.96 \times 10^3$a.u. Thus, only small differences are found for the molecule in the corner of the film as compared with the molecule at the end of the chain.

7.5.3 FCC cluster of C_{60} molecules

The final type of system is a C_{60} molecule in a FCC cluster of C_{60} molecules. The smallest FCC structure contains 13 C_{60} molecules and was built as one A-layer with 5 molecules and two B-layers with 4 molecules (see Figure 1), one above and one below the A-layer ($B_4A_5B_4$-cluster). The spacing between two A-layers is 14.17 Å[211] and the spacing between

the B-layers and the A-layer is half of the A-A distance, 7.09 Å. The second structure contains 37 C_{60} molecules ($B_{12}A_{13}B_{12}$-cluster), and the last structure contains 63 C_{60} molecules ($A_{13}B_{12}A_{13}B_{12}A_{13}$-cluster). The results for $\overline{\alpha}$ and $\overline{\gamma}$ for a C_{60} molecule in a FCC

N	1	13	37	63
$\overline{\alpha}$/N	522.76	538.22	545.91	546.05
$\Delta\overline{\alpha}$	522.76	539.50	550.09	548.09
$\overline{\alpha}^{\mathrm{LPDI}}$	522.76	582.71	578.16	571.84
$\overline{\gamma}$/N	115.21	142.17	157.53	158.75
$\Delta\overline{\gamma}$	115.21	144.42	165.85	163.06
$\overline{\gamma}^{\mathrm{LPDI}}$	115.21	182.68	194.66	169.12

TABLE 7.2*: Static polarizability and second hyperpolarizability for C_{60} in a fullerene FCC cluster. α in a.u. and γ in 10^3 a.u.*

crystal is presented in Table 7.2. The difference is small between the results obtained with the average and the Δ approaches. The reason for this is that the step-size, X, is too large relative to the system size in the three-dimensional cluster such that the Δ approach will not be significantly different from the average approach. Secondly, as was the case for the mono-layer films the results obtained with the LPDI model are larger than the results obtained with both the average and the Δ approach. Furthermore, $\overline{\alpha}$ and $\overline{\gamma}$ calculated using the LPDI model are larger for the $N = 13$ and $N = 37$ clusters than for the $N = 63$ cluster. Furthermore, $\overline{\alpha}$ decreases whereas $\overline{\gamma}$ increases when going from the $N = 13$ cluster to the $N = 37$ cluster. On the other hand, both $\overline{\alpha}$ and $\overline{\gamma}$ decrease when going from the $N = 37$ cluster to the $N = 63$ cluster and they also become smaller than the results for the $N = 13$ cluster. Because of these irregularities, it becomes important to have a large cluster for the three-dimensional cluster. In Table 7.3, we present a comparison of $\overline{\alpha}$, $\overline{\gamma}$, and their

	Isolated, N =1	Chain, N = 5	Monolayer, N = 13	FCC cluster, N = 63
α_{xx}	522.76	453.18	363.32	571.84
α_{zz}	522.76	767.12	681.38	571.84
$\overline{\alpha}$	522.76	557.83	575.07	571.84
γ_{xxxx}	115.21	64.74	26.98	169.12
γ_{zzzz}	115.21	534.49	335.22	169.12
$\overline{\gamma}$	115.21	196.00	218.63	169.12

TABLE 7.3*: Comparing the chain, film and crystal of C_{60} molecules. α in a.u. and γ in 10^3 a.u. z-axis is the long axis and x the short axis.*

tensor components α_{xx}, α_{zz}, γ_{xxxx}, and γ_{zzzz} for a C_{60} molecule in a chain, a mono-layer film and a FCC cluster calculated using the LPDI appraoch. The FCC cluster is the cluster with 63 C_{60} molecules, the mono-layer film corresponds to the middle layer of the FCC cluster and contains 13 molecules and the chain corresponds to the diagonal of the film

and contains 5 molecules. From the table, the differences in the anisotropy of the various types of systems may be compared with the gas phase. For the chain, the component (z) along the chain is enhanced whereas the components (x, y) perpendicular to the chain are screened. In the film, the components (z, y) in plane are enhanced and the component (x) perpendicular to the plane is screened. All components for the film are smaller than for the chain but two directions are enhanced and only one direction is screened giving that $\overline{\alpha}$ and $\overline{\gamma}$ are larger for the film than for the chain. In the FCC cluster, α and γ are enhanced in all directions and the properties becomes isotropic as in the gas phase. The enhancements are smaller in the FCC cluster than in the film and chain illustrating the importance of considering a realistic cluster model in order to account both for the enhancement and for the screening of α and γ.

7.5.4 Susceptibilities

For the largest FCC cluster, we have also calculated the linear refractive index and the third-order nonlinear susceptibility and compared with experimental results. The results for the refractive index is $n^{(1)} = 2.0$ ($\epsilon^{(1)} = 4.0$) as calculated from Eq. 7.17 with the number density, $N_d = 4/a^3$ and a lattice constant of $a = 14.17$ Å.[211] Our results are in excellent agreement with the experimental results for the refractive index, $n^{(1)} \sim 2$,[206,208,312] and for the dielectric constant, $\epsilon^{(1)} \sim 4.0 - 4.6$.[207,210,211,313] This good agreement, especially with the refractive index, illustrates the accuracy of the local-field approach used here and indicates that the dipolar term ignored in standard Lorentz local-field theory is required to get good agreement between theory and experiments. If we use the standard Lorentz-Lorenz equation, *i.e.* adopting Eq. 7.17 with the gas-phase value for the polarizability, gives a refractive index of $n^{(1)} = 1.89$ and if we use the standard Lorentz local-field theory, *i.e.* Eq. 7.15 with the gas phase polarizability and the experimental susceptibility, we find a refractive index of $n^{(1)} = 1.94$. Although the differences in the refractive indexes are small, it becomes important when considering the nonlinear susceptibilities as realized from Eq. 7.19.

For the third-order nonlinear susceptibility, a value of $\chi^{(3)} = 3.2 \times 10^{-13}$ esu is obtained using Eq. 7.19 and the dielectric constant calculated here. Only a few experimental studies have been carried out of the non-resonant third-order nonlinear susceptibility for C_{60} films. A third-harmonic generation (THG) experiment at frequency 0.019 a.u. ($\lambda = 2380$ nm) results in $\chi^{(3)} = 4.1 \pm 0.6 \times 10^{-12}$ esu.[312] This value was measured relative to fused silica and a reference value of $\chi^{(3)} = 2.8 \times 10^{-14}$ esu was adopted. However, recently a value for the THG susceptibility for fused silica of $\chi^{(3)} = 1.1 \times 10^{-14}$ esu was found and believed to be more accurate.[314,315] Correcting for this difference in reference values gives a value of $\chi^{(3)} = 16.1 \pm 2.4 \times 10^{-13}$ esu for the C_{60} thin film. The second experiment is a degenerate four-wave mixing (DFWM) study where the static limit of the third-order nonlinear susceptibility was found to be $\chi^{(3)} = 36 \pm 12 \times 10^{-13}$.[316] This value was reported in the so-called "Maker-Terhune"[317] convention and are therefore multiplied by a factor of four in order to compare with the convention used here. They used a reference value for fused silica of $\chi^{(3)} = 1.6 \times 10^{-14}$ at $\lambda = 1064$ nm which is in good agreement with THG

results at the same frequency.[314,315] The two experiments agree within a factor of two which, considering the fact that DFWM can be higher than the corresponding THG due to vibrational contributions,[314] is a good agreement. Theoretically, it has also been found for the isolated C_{60} molecule that the vibrational contribution to γ obtained in a DFWM experiment is of the same order as the electronic contribution.[307]

Comparing our theoretical value for $\chi^{(3)}$ with the experimental results, it is a factor of five smaller than the THG experiment and a factor of ten smaller than the DFWM experiment. Since in this study only the pure electronic contribution to $\chi^{(3)}$ is calculated, we would expect a better agreement with the THG results than with the DFWM results which is indeed the case. There has been one previous theoretical study of the third-order susceptibility where the molecular environment was taken explicitly into account using a general local-field theory obtained from the Onsager-Böttcher relation and the gas-phase α and γ calculated within the Hartree-Fock approximation.[308] They found for the static third-order susceptibility a value of $\chi^{(3)} = 2.7 \times 10^{-13}$ esu which here is divided by a factor of six in order to make the comparison in the convention used here. This value is in very good agreement with our value of 3.2×10^{-13} esu considering the different methods used.

7.6 Conclusion

We have investigated the dependence of α and γ on the size of C_{60} fullerene clusters. It is found that both the Δ approach[203] and the LPDI model [Ref. 97, Chap. 5] give a rapid convergence of α and γ with respect to the chain length and the size of the mono-layer. Furthermore, the LPDI model gives the molecular properties of the individual molecules in a cluster. For a C_{60} chain and mono-layer film, it is found that the surrounding molecules perturb the middle C_{60} molecule much more than the end or corner molecules, which also results in a slower convergence of α and γ for the middle molecule with respect to the system size. In addition, the linear and third-order susceptibilities have been calculated by combining the PDI model with a local-field ansatz. The calculated refractive index and dielectric constant are in good agreement with experiments. The result for $\chi^{(3)}$ is less clear, but a good agreement with a quantum chemical SCRF calculation is found.[308]

Acknowledgment

L.J. gratefully acknowledges The Danish Research Training Council for financial support. P.-O.Å. has received support from the Norwegian Research Council (NFR) through a Strategic University Program (Grant no 154011/420), a NANOMAT program (Grant no 158538/431) and a grant of computer time from the Norwegian High Performance Computing Consortium (NOTUR). K.V.M. thanks Statens Naturvidenskabelige Forskningsråd (SNF), Statens Teknisk-Videnskabelige Forskningsråd (STVF), Danish Centre for Scientific Computing, and the EU-network: MOLPROP for support.

Chapter 8

A discrete solvent reaction field model within DFT

L. Jensen, P. Th. van Duijnen, and J. G. Snijders "A discrete solvent reaction field model within density functional theory" *J. Chem. Phys.* **118**, 514-521, 2003.

8.1 Abstract

In this work we present theory and implementation for a discrete reaction field model within Density Functional Theory (DFT) for studying solvent effects on molecules. The model combines a quantum mechanical (QM) description of the solute and a classical description of the solvent molecules (MM). The solvent molecules are modeled by point charges representing the permanent electronic charge distribution, and distributed polarizabilities for describing the solvent polarization arising from many-body interactions. The QM/MM interactions are introduced into the Kohn-Sham equations, thereby allowing for the solute to be polarized by the solvent and vice versa. Here we present some initial results for water in aqueous solution. It is found that the inclusion of solvent polarization is essential for an accurate description of dipole and quadrupole moments in the liquid phase. We find a very good agreement between the liquid phase dipole and quadrupole moments obtained using the Local Density Approximation (LDA) and results obtained with a similar model at the Coupled Cluster Singles and Doubles (CCSD) level of theory using the same water cluster structure. The influence of basis set and exchange correlation functional on the liquid phase properties was investigated and indicates that for an accurate description of the liquid phase properties using DFT a good description of the gas phase dipole moment and molecular polarizability are also needed.

8.2 Introduction

An interesting theoretical problem is the modeling of molecular properties in the condensed phase. In general, the interactions with the solvent changes the molecular properties considerably when compared with the gas phase. From a quantum chemical point of view the focus is on a single molecule (or a molecular system) and the solvent effects are treated as perturbations of the molecular system. The molecular system of interest is then treated with a quantum mechanical method and the rest of the system is treated by a much simpler method, usually a classical description.[102–116,318]

The methods used for the classical description of the solvent can in general be divided into two groups depending on the detail in which the solvent are considered. The first group of methods are the so-called continuum models[102–104]in which the solvent is treated as a continuous medium characterized by its macroscopic dielectric constants. The continuum models have become a standard approach for modeling solvent effects on molecular properties within computational chemistry and are very efficient models. However, in the continuum model the explicit microscopic structure of the solvent are neglected and therefore provides a poor description of the short range interactions. Also, the results are affected by the choice of the radius and shape of the cavity in which the solute is embedded into.[319]

The second group of methods can be characterized as discrete solvent methods where one or more solvent molecules are treated explicitly. Among these methods are the supermolecular model,[320] frozen density functional approach,[318] *ab initio* molecular dynamics (MD)[321] and the combined quantum mechanical and classical mechanical models (QM/MM).[105–116] In both the supermolecular models and in *ab initio* MD models all molecules are treated at the same level of theory. This gives a highly accurate description of solvent-solute interaction but due to the high computational demand only a few solvent molecules can be included. A problem of these types of models is that there is no unique way of defining properties of the individual molecules[322,323] [Ref. 97, Chap. 5]. The definition of the molecular properties require an arbitrary partitioning of the wave function or the electronic charge density among the molecules much in the same way as defining atomic charges. The molecular properties will depend on the particular partitioning scheme employed as shown in an *ab initio* MD study[322] of ice Ih where it was found that the average dipole moment ranges from 2.3 D to 3.1 D depending on which partitioning scheme used.

In the QM/MM methods[105–116] the system is divided into a quantum mechanical part, the solute, and a classical part, the solvent, and the interaction between the two subsystems are described with an effective operator. The solvent molecules are then treated with a classical force field and the method therefore allows for a greater number of solvent molecules to be included. Like in the continuum model the solute is separated from the solvent molecules and the molecular properties of the solute are therefore well defined. The remaining problem is finding an accurate approximate representation of the solvent molecules and the solute-solvent interactions.[248] The discrete representation of the solvent molecules introduces a large number of solvent configurations over which the solute properties must be averaged. This is typically done using Monte Carlo or MD techniques which

lead to a large number of quantum mechanical calculations. For this reason the QM/MM method is often employed at a semiempirical level of theory.[115]

The force field used in the QM/MM methods are typically adopted from fully classical force fields. While this in general is suitable for the solvent-solvent interactions it is not clear how to model the van der Waals interaction between the solute and the solvent.[324] The van der Waals interactions are typically treated as a Lennard-Jones (LJ) potential and the LJ parameters for the quantum atoms are then taken from the classical force field or optimized to the particular QM/MM method[325] for some molecular complexes. However, it is not certain that optimizing the parameters on small complexes will improve the results in a QM/MM simulation[324] of a liquid.

In recent years the classical force fields have been improved in order to also describe the polarization of the molecules.[165,326–332] The polarization of the classical molecules has also been included in QM/MM studies[105,106,333–339] and shown that it is important to consider also the polarization of the solvent molecules. Since the inclusion of the solvent polarization leads to an increase in computational time most studies ignore this contribution and use the more simple pair potentials. When the solvent polarization is included it is usually treated using either an isotropic molecular polarizability[334,338] or using distributed atomic polarizabilities[333,336,337,339] according to the Applequist scheme.[90] At short distances the Applequist scheme leads to the so-called "polarizability catastrophy" [89,90,93] due to the use of a classical description in the bonding region. Thole[93] avoided this problem by introducing smeared out dipoles which mimics the overlapping of the charges distributions at short distances. Thole's model has been shown to be quite succesful in reproducing the molecular polarizability tensor using model atomic polarizability parameters independent of the chemical environment of the atoms.[93,94,163] This model is used in the Direct Reaction Field model[106,112] which is an *ab initio* QM/MM model. However, so far the inclusion of solvent polarization using Thole's model has not been considered within a Density Functional Theory (DFT) approach.

Therefore, in this work we present an implementation of a QM/MM-type model for the study of solvation effect on molecules within DFT. The model will be denoted the Discrete Reaction Field (DRF) model. In the DRF model the discrete solvent molecules are represented by distributed atomic point charges and polarizabilities. The inclusion of atomic polarizabilities following Thole's model allows also for the solvent molecules to be polarized. The QM/MM interactions are collected into an effective operator which is introduced directly into the Kohn-Sham equations. We will ignore the van der Waals interactions since we adopt supermolecular cluster obtained separately from a MD simulation and the structure is kept fixed during the QM/MM calculations. Therefore, the van der Waals contribution to the energy is a constant independent of the quantum part and can be obtained directly from the MD simulation.

As an initial application we will present dipole and quadrupole moments of water in aqueous solution with focus on choosing the atomic point charges, atomic polarizabilites, basis set and exchange-correlation (xc) potentials.

8.3 Theory

In the QM/MM method the total (effective) Hamiltonian for the system is written as[105–116]

$$\hat{H} = \hat{H}_{QM} + \hat{H}_{QM/MM} + \hat{H}_{MM} \tag{8.1}$$

where $\hat{H}_{QM}$ is the quantum mechanical Hamiltonian for the solute, $\hat{H}_{QM/MM}$ describes the interactions between solute and solvent and $\hat{H}_{MM}$ describes the solvent-solvent interactions. In this work we focus on the description of the quantum part in the presence of a solvent. The solute-solvent interactions are therefore introduced into the vacuum Hamiltonian as an effective operator which are described in more details in the next section.

8.3.1 The Discrete Reaction Field Operator

The Discrete Reaction Field operator at a point r_i contains two terms

$$\upsilon^{DRF}(r_i) = \upsilon^{el}(r_i) + \upsilon^{pol}(r_i) \tag{8.2}$$

where the first term, υ^{el}, is the electrostatic operator and describes the Coulombic interaction between the QM system and the permanent charge distribution of the solvent molecules. The second term, υ^{pol}, is the polarization operator and describes the many-body polarization of the solvent molecules, *i.e.* the change in the charge distribution of the solvent molecules due to interaction with the QM part and other solvent molecules.

The charge distribution of the solvent is represented by atomic point charges, hence the electrostatic operator is given by

$$\upsilon^{el}(r_i) = \sum_s \frac{q_s}{R_{si}} = \sum_s q_s T^{(0)}_{si}, \tag{8.3}$$

where the zero'th order interaction tensor has been introduced and the index s runs over all atoms of the solvent molecules. In general the interaction tensor to a given order, n, can be written as

$$T^{(n)}_{pq,\alpha_1\ldots\alpha_n} = \nabla_{pq,\alpha_1}\ldots\nabla_{pq,\alpha_n}\left(\frac{1}{R_{pq}}\right), \tag{8.4}$$

where R_{pq} is the distance between the interacting entities.

The many-body polarization term is represented by induced atomic dipoles at the solvent molecules and the polarization operator is given by

$$\upsilon^{pol}(r_i) = \sum_s \mu^{ind}_{s,\alpha}\frac{R_{si,\alpha}}{R^3_{si}} = \sum_s \mu^{ind}_{s,\alpha} T^{(1)}_{si,\alpha}. \tag{8.5}$$

where $R_{si,\alpha}$ is a component of the distance vector and μ^{ind}_s is the induced dipole at site s. For Greek indices the Einstein summation convention is employed. The induced dipoles are discussed in more detail in the next section.

8.3.2 The Atomic Induced Dipoles

For a collection of atomic polarizabilities in an electric field, assuming linear response, the induced atomic dipole at site s is given by

$$\mu_{s,\alpha}^{ind} = \alpha_{s,\alpha\beta}(F_{s,\beta}^{init} + \sum_{t \neq s} T_{st,\beta\gamma}^{(2)} \mu_{t,\gamma}^{ind}) \tag{8.6}$$

where $\alpha_{a,\alpha\beta}$ is a component of the atomic polarizability tensor at site s, which for an isotropic atom gives $\alpha_{s,\alpha\beta} = \delta_{\alpha\beta}\alpha_s$. $F_{s,\beta}^{init}$ is the initial electric field at site s and the last term is the electric field from the other induced dipoles. The dipole interaction tensor, $T_{st,\alpha\beta}^{(2)}$, is given by

$$T_{st,\alpha\beta}^{(2)} = \frac{3R_{st,\alpha}R_{st,\beta}}{R_{st}^5} - \frac{\delta_{\alpha\beta}}{R_{st}^3} \tag{8.7}$$

The initial field in Eq. 8.6 is given as a sum of three terms

$$F_{t,\beta}^{init} = F_{t,\beta}^{QM,el} + F_{t,\beta}^{QM,nuc} + F_{t,\beta}^{MM,q} \tag{8.8}$$

where $F_{t,\beta}^{QM,el}$ is the field arising from the electronic charge distribution of the QM part,

$$F_{t,\beta}^{QM,el} = -\int \rho(r_i)\frac{R_{it,\beta}}{R_{it}^3}dr_i = \int \rho(r_i)T_{it,\beta}^{(1)}dr_i \tag{8.9}$$

and $F_{t,\beta}^{QM,nuc}$ is the field arising from the QM nuclei,

$$F_{t,\beta}^{QM,nuc} = \sum_m \frac{Z_m R_{mt,\beta}}{R_{mt}^3} = -\sum_m Z_m T_{mt,\beta}^{(1)} \tag{8.10}$$

and $F_{t,\beta}^{MM,q}$ is the field arising from the point charges at the solvent molecules,

$$F_{t,\beta}^{MM,q} = {\sum_s}' \frac{q_s R_{st,\beta}}{R_{st}^3} = -{\sum_s}' q_s T_{st,\beta}^{(1)} \tag{8.11}$$

The prime in Eq 8.11 indicates that the sum is restricted to sites which do not belong to the same molecule. Since the induced dipole in Eq. 8.6 depends on the induced dipoles at the other sites these equations have to be solved self-consistently. This can be done analytically by rewriting the equations into a $3N \times 3N$ linear matrix equation, with N the number of atoms, as

$$A\mu^{ind} = F^{init} \tag{8.12}$$

and the components of the matrix, $A_{st,\alpha\beta}$, given by

$$A_{st,\alpha\beta} = (\alpha_{s,\alpha\beta}^{-1}\delta_{st} - T_{st,\alpha\beta}^{(2)}). \tag{8.13}$$

This matrix equation can then be solved for the induced dipoles using standard mathematical tools for solving linear equations. The inverse of the matrix A, the so called relay matrix, is a generalized polarizability matrix which describes the total linear response of the discrete solvent molecules.

8.3.3 Damping of the induced dipoles

If F^{init} is an uniform external field the polarizability of the classical system can be written as[90]

$$\alpha_{\alpha\beta}^{\mathrm{mol}} = \sum_{p,q}^{N} B_{pq,\alpha\beta}, \tag{8.14}$$

where $\mathbf{B}$ is the relay matrix defined in a supermatrix notation as

$$\mathbf{B} = \mathbf{A}^{-1} = \left(\boldsymbol{\alpha}^{-1} - \mathbf{T}^{(2)}\right)^{-1}. \tag{8.15}$$

The polarizability parallel, $\alpha_{\parallel}$, and perpendicular, $\alpha_{\perp}$, to the axes connecting two interacting atoms, p and q, are given by Silberstein's equations,[89] which are the exact solutions to Eq. 8.14,

$$\alpha_{\parallel} = \frac{\alpha_p + \alpha_q + 4\alpha_p\alpha_q/r^3}{1 - 4\alpha_p\alpha_q/r^6}, \tag{8.16}$$

$$\alpha_{\perp} = \frac{\alpha_p + \alpha_q - 2\alpha_p\alpha_q/r^3}{1 - \alpha_p\alpha_q/r^6}. \tag{8.17}$$

From Eqs. 8.16 and 8.17 it is seen that when r approaches $(4\alpha_p\alpha_q)^{1/6}$, $\alpha_{\parallel}$ goes to infinity and becomes negative for even shorter distances. In order to avoid this "polarizability catastrophe" Thole[93] modified the dipole interaction tensor using smeared-out dipoles. The dipole interaction tensor was first rewritten in terms of a reduced distance $u_{pq,\beta} = R_{pq,\beta}/(\alpha_p\alpha_q)^{1/6}$ as

$$T^{(2)}_{pq,\beta\gamma} = (\alpha_p\alpha_q)^{1/2} t(u_{pq}) = (\alpha_p\alpha_q)^{1/2} \frac{\partial^2\phi(u_{pq})}{\partial u_{pq,\beta}\partial u_{pq,\gamma}} \tag{8.18}$$

where $\phi(u_{pq})$ is a spherically symmetric potential of some model charge distribution ρ. The screened dipole interaction tensor can be written as

$$T^{(2)}_{pq,\alpha\beta} = \frac{3f^T_{pq}R_{pq,\alpha}R_{pq,\beta}}{R^5_{pq}} - \frac{f^E_{pq}\delta_{\alpha\beta}}{R^3_{pq}}. \tag{8.19}$$

where the damping functions f^T_{pq} and f^E_{pq} have been introduced. If we consider a exponential decaying charge distribution the screening functions in Eq. 8.19 are given by[163]

$$f^E_{pg} = 1 - \left[1 + s_{pq} + \frac{1}{2}s^2_{pq}\right]\exp(-s_{pq}) \text{ and } f^T_{pg} = f^E_{pg} - \frac{1}{6}s^3_{pq}\exp(-s_{pq}), \tag{8.20}$$

where the term s_{pq} is give by $s_{pq} = aR_{pq}/(\alpha_p\alpha_q)^{1/6}$, with a the screening length, and α_p the atomic polarizability of atom p.

8.3.4 The QM/MM interaction energy

The QM/MM interaction energy is given by a sum of three terms,

$$E^{QM/MM} = E^{elst,el} + E^{elst,nuc} + E^{ind} \tag{8.21}$$

where the first two terms are the electrostatic interaction between the QM electrons and the classical point charges

$$E^{elst,el} = -\sum_s q_s \int \rho(r_i) \frac{1}{R_{is}} dr_i \tag{8.22}$$

and the electrostatic interaction between the QM nuclei and the point charges

$$E^{elst,nuc} = \sum_s q_s \sum_m \frac{Z_m}{R_{ms}}, \tag{8.23}$$

respectively. The last term is the induction energy and is given by[31,326]

$$E^{ind} = -\frac{1}{2}\mu^{ind} F^{QM}, \tag{8.24}$$

where F^{QM} is the electric field arising from the QM system, i.e. the field from the QM electrons and nuclei. The induction energy consist of the sum of the energy of the induced dipoles in the electric field and the polarization cost, i.e. the energy needed for creating the induced dipoles.

8.3.5 The effective Kohn-Sham equations

The effective Kohn-Sham (KS) equations which has to be solved for the combined QM/MM system is given by

$$h_{KS}\phi_i(r) = \epsilon\phi_i(r), \tag{8.25}$$

where h_{KS} is the effective KS-operator and ϕ_i is the KS orbital with energy ϵ_i. The effective KS-operator consists of the sum of the vacuum operator, h^0_{KS}, and the reaction field operator, υ^{DRF}, with the vacuum KS-operator given as

$$h^0_{KS} = -\frac{1}{2}\nabla^2 + V_N(r) + V_C(r) + \upsilon_{XC}(r) \tag{8.26}$$

$$= -\frac{1}{2}\nabla^2 - \sum_m \frac{Z_m}{|r - R_m|} + \int \frac{\rho(r)}{|r - r'|} dr' + \frac{\delta E_{XC}}{\delta\rho(r)} \tag{8.27}$$

where the individual terms in the vacuum operator are the kinetic operator, the nuclear potential, the Coulomb potential (or Hartree potential) and the xc-potential, respectively.

The DRF model has been implemented into a local version of the Amsterdam Density Functional (ADF) program package.[131,340] In ADF the KS equations are solved by

numerical integration which means that the effective KS-operator has to be evaluated in each integration point. Since the numerical integration grid is chosen on the basis of the quantum part alone care must be taken when evaluating the DRF operator if the integration points are close to a classical atom. In order to avoid numerical instabilities we introduce a damping of the operator at small distances which is modeled by modifying the distance R_{ij} to obtain a scaled distance S_{ij} [Ref. 63, Chap. 3],

$$S_{ij} = v_{ij} R_{ij} = f(R_{ij}) \ , \tag{8.28}$$

where v_{ij} is a scaling factor and $f(R_{ij})$ an appropriately chosen function of R_{ij}. Furthermore, each component of R_{ij} is also scaled by v_{ij}, so the reduced distance becomes,

$$S_{ij} = \sqrt{S_{ij,\alpha} S_{ij,\alpha}} = v_{ij} \sqrt{R_{ij,\alpha} R_{ij,\alpha}} = v_{ij} R_{ij} \ , \tag{8.29}$$

consistent with the definition in Eq. 8.28. The damped operator can thus be obtained by modifying the interaction tensors in Eqs. 8.3 and 8.5,

$$T^{(n)}_{ij,\alpha_1 \ldots \alpha_n} = \nabla_{\alpha_1} \ldots \nabla_{\alpha_n} \left(\frac{1}{S_{ij}} \right) \ , \tag{8.30}$$

which is equivalent to replacing R_{ij} by S_{ij} and $R_{ij,\alpha}$ by $S_{ij,\alpha}$ in the regular formulae for the interaction tensors. The particular form of the scaling function employed here is [Ref. 63, Chap. 3]

$$f(r_{pq}) = \frac{r_{pq}}{\mathrm{e}r f(r_{pq})}, \tag{8.31}$$

which was obtained by considering the interaction between two Gaussian charge distributions with unity exponents.

8.4 Computational details

All calculations have been performed with the ADF program package. The calculations of the polarizability of water in the gas phase have been done using time-dependent DFT as implemented in the RESPONSE code[57,130,289] in ADF. The ADF program uses basis sets of Slater functions where in this work a triple zeta valence plus polarization (in ADF basis set V), here denoted TZ2P, is chosen as basis. The basis set is then augmented with diffuse functions giving TZ2P+,[289] added s,p and d functions or TZ2P+++,[129] added two s,p,d and f functions. The TZ2P+++ basis set is expected to give results close to the basis set limit for (hyper-)polarizabilities.[129]

We also tested different xc potentials, the Local Density Approximation (LDA), Becke-Lee-Yang-Parr (BLYP),[138,139] the Becke-Perdew (BP),[138,341] and the van Leeuwen-Baerends (LB94)[141] potentials. The BLYP and BP are examples of typical Generalized Gradient Approximations (GGAs) potentials whereas the LB94 is an example of a so-called asymptotic correct potential due to the correct Coulombic decay of the potential at large distances.

The water structure we use in this work was taken from Ref. 338 and consists of 128 rigid water molecule where one molecule, the solute, is treated quantum mechanically. The total structure was obtained from a MD simulation using a polarizable force field[327] and the details about the simulation can be found in Ref. 121. The intra-molecular geometry of the water molecules was that in gas phase, *i.e.* $R_{O-H} = 0.9572$ Å and $\angle_{HOH} = 104.49°$. The solute water molecule was placed in the xz-plane with the z-axis bisecting the H-O-H angle. Results obtained using this structure will be references as "liquid" phase results. We will perform one QM/MM calculation and therefore the molecular properties will not be averaged over different solvent configurations. However, the choice of this particular water structure allows for a direct comparison with results obtained from a similar model within a (Multiconfigurational) Self-Consistent-Field/Molecular Mechanics(MC-SCF/MM)[342] or a Coupled Cluster/Molecular Mechanics (CC/MM)[121] approach. Therefore, it is possible to make a detailed comparison between wave function methods and the DFT method for liquid phase calculations.

8.5 Results

8.5.1 Solvent models

We investigated six different models for representing the solvent molecules using atomic parameters in three non-polarizable and three polarizable models. The atomic parameters used in the different models are given in Table 8.1 along with the molecular dipole moment and polarizability which they reproduce. The first two non-polarizable models, i.e.

Model	q_H	q_O	α_H	α_O	μ	$\overline{\alpha}$	$\Delta\alpha$
MUL	0.3040	-0.6080	0	0	1.71	0	0
VDD	0.1370	-0.2740	0	0	0.77	0	0
SPC	0.3345	-0.6690	0	0	1.88	0	0
Thole-S	0.3345	-0.6690	2.7929	5.7494	1.88	10.06	4.32
Thole-I	0.3345	-0.6690	0	9.7180	1.88	9.72	0
Thole-A	0.3345	-0.6690	0.0690	9.3005	1.88	9.62	0.51

TABLE 8.1: *Atomic parameters for the different solvent models in atomic units and the molecular dipole moment, μ, mean polarizability, $\overline{\alpha}$, and polarizability anisotropy, $\Delta\alpha$, modeled by the atomic parameters. Dipole moment in Debye and mean polarizability and polarizability anisotropy in atomic units. The mean polarizability is defined as $\overline{\alpha} = (\alpha_{xx} + \alpha_{yy} + \alpha_{zz})/3$ and the polarizability anisotropy as $\Delta\alpha = (1/2)^{1/2}[(\alpha_{xx} - \alpha_{yy})^2 + (\alpha_{xx} - \alpha_{zz})^2 + (\alpha_{zz} - \alpha_{yy})^2]^{1/2}$.*

charge only models, where obtained by using different ways of partitioning the electronic charge distribution into atomic charges. The first charge model, MUL, is obtained using the Mulliken population analysis and the second charge model, VDD, using the so-called Voronoi deformation density method, for a descriptions of the partitioning schemes see

Ref. 340. The last charge model, SPC, is adopted from Ref. 327 and is identical to the charge model used in the reference works of Refs. 342 and 121. The point charges in model SPC have been chosen to reproduce the experimental gas phase dipole moment of 1.85 D for the SPC water geometry,[327] however, since we use a different geometry for water the dipole moment will be slightly larger here. The atomic polarizabilities used in the three polarizable solvent models were all obtained using Thole's model, i.e. Eq. 8.14, for reproducing the molecular polarizability. The screening parameter, $a = 2.1304$, used in all three models was taken from Ref. 163. The screening parameter together with atomic model polarizability parameters were obtained by fitting to the experimental mean polarizability of 52 molecules. The model using these atomic polarizability parameters will be denoted Thole-S(tandard). In the second model, Thole-I(sotropic), the atomic polarizability parameters where chosen to reproduce the isotropic mean polarizability of 9.718 a.u. used in the reference works.[121,342] In the third model, Thole-A(nisotropic), the atomic polarizability was chosen so as to reproduce the full molecular polarizability tensor of water calculated using CCSD(T) which was taken from Ref. 343.

Model	μ	$\Delta\mu$	Q_{xx}	Q_{yy}	Q_{zz}
Vacuum	1.86	-	1.83	-1.91	0.08
Without polarization					
MUL	2.34	0.48	1.97	-2.09	0.12
VDD	2.08	0.22	1.90	-1.99	0.10
SPC	2.39	0.53	1.98	-2.10	0.12
With polarization					
Thole-S	2.69	0.83	2.05	-2.16	0.11
Thole-I/Thole-A	2.58	0.72	2.04	-2.17	0.13

TABLE 8.2: *Dipole and quadrupole moments of water in the gas phase and in the "liquid phase" and the induced dipole moment, $\Delta\mu$ in going from the gas phase to the "liquid phase" using different charge and polarization models. Dipole and induced dipole moments in Debye and quadrupole moment in atomic units. All calculations have been made with LDA and the TZ2P basis set.*

The results for the dipole and quadrupole moments for water in the gas phase and in the "liquid" phase and also the induced dipole moment, $\Delta\mu$, in going from the gas phase to the "liquid" phase using the six different solvent models are presented in Table 8.2. We only present results for the diagonal components of the quadrupole moment although off-diagonal elements are present due to the structure of the water cluster. However, these off-diagonal elements will become zero when averaged over more water configurations. The results using the non-polarizable solvent models shows that a 10% change in the atomic parameters, the difference between MUL and SPC, also gives a 10% change in the induced dipole moment. Especially, the VVD charges underestimate the induced dipole moment and illustrates the problem using only point charges without including higher order moments in some way. Therefore, it is important to chose the atomic charges so that they give a good dipole moment and maybe even reasonable higher order moments.

However, for water it is not possible to accurately reproduce both dipole moment and higher order moments using only atomic point charges. We will therefore adopt the SPC model as starting point for the polarizable models.

From the results in Table 8.2 it is seen that including the polarization of the solvent molecules increases the dipole moment and quadrupole moment of the "liquid phase" and therefore it is very important to include this polarization, especially for the dipole moment. This has also been found in previous studies using wave function methods.[121,334] Comparing the three different polarization models we see that there is no difference between Thole-I and Thole-A. Therefore, for water, the effect of distributing the polarizability into atomic contributions is negligible due to the small polarizability anisotropy of the water molecule. In general it is expected that a distributed polarizability approach will give better results than an approach using only a (anisotropic) polarizability located at a single site, especially as the size of the solvent molecule increases.[120] However, as seen from the differences in the results using Thole-S and Thole-A it is important when using distributed polarizability that also the anisotropy is accounted for correctly. In the rest of our work we will use the Thole-A solvent model since it is found that the differences between this solvent model and the one used in the reference work is negligible.

8.5.2 Basis sets

In Table 8.3 we present results for the dipole moment and quadrupole moment both in the gas phase and in the "liquid" phase using the TZ2P, TZ2P+ and TZ2P+++ basis sets. The static mean polarizability in the gas phase is also shown. In the gas phase the dipole moment and quadrupole moment is converged already using the TZ2P basis set. For the polarizability the inclusion of extra diffuse functions are needed in order to achieve accurate results. We see that the inclusion of the first order field induced polarization (FIP) functions of Zeiss et al.[136] in basis set TZ2P+ gives a mean polarizabilty in good agreement with the result using the very large basis set TZ2P+++.

Basis set	μ	$\Delta\mu$	Q_{xx}	Q_{yy}	Q_{zz}	$\overline{\alpha}$
Gas phase						
TZ2P	1.86	-	1.84	-1.91	0.08	8.50
TZ2P+	1.87	-	1.83	-1.90	0.07	10.47
TZ2P+++	1.86	-	1.84	-1.91	0.07	10.55
"Liquid" phase						
TZ2P	2.58	0.72	2.04	-2.17	0.13	
TZ2P+	2.68	0.81	2.07	-2.17	0.10	
TZ2P+++	2.69	0.83	2.08	-2.19	0.11	

TABLE 8.3: *Dipole moment, quadrupole moment and mean polarizability for water in the gas phase and dipole moment, induced dipole moment and quadrupole moment for water in "liquid phase" using the Thole-A solvent model and different basis sets. Dipole and induced dipole moment in Debye. Quadrupole moment and mean polarizability in atomic units.*

In the "liquid" phase the dipole moment is increased considerably by including diffuse functions in the basis set whereas the basis set effects on the quadrupole moment are negligible. The $\Delta\mu$ is increased by 12.5% using TZ2P+ and by 15% using TZ2P+++ compared with the TZ2P basis set. The changes in the $\Delta\mu$ with the basis sets are in good agreement with the changes in the gas phase polarizability. Therefore, for calculating the dipole moment in the liquid phase the inclusion of additional diffuse basis functions, normally associated with calculations of the gas phase polarizability, are required for obtaining good results. This has also been observed in a previous study [344] using a mean field QM/MM approach at the Hatree-Fock level of theory.

8.5.3 xc-potentials

Table 8.4 shows the dipole moment, quadrupole moment and mean polarizability of water in the gas phase and dipole moment, induced dipole moment and quadrupole moment in the "liquid" phase calculated using different xc-potentials. The results are compared with results obtained for the same water structure using a aug-cc-pVTZ basis set and a CCSD/MM[121] approach. In the gas phase the two GGA potentials, BLYP and BP, give

Method	μ	$\Delta\mu$	Q_{xx}	Q_{yy}	Q_{zz}	$\overline{\alpha}$
Gas phase						
LDA	1.87	-	1.83	-1.90	0.07	10.47
BLYP	1.81	-	1.79	-1.85	0.06	10.82
BP	1.81	-	1.80	-1.86	0.06	10.20
LB94	1.97	-	1.72	-1.81	0.09	9.14
CCSD [a]	1.85	-	1.82	-1.90	0.08	-
"Liquid" phase						
LDA	2.68	0.81	2.07	-2.17	0.10	
BLYP	2.63	0.82	2.04	-2.13	0.09	
BP	2.63	0.82	2.04	-2.13	0.09	
LB94	2.65	0.68	1.93	-2.04	0.11	
CCSD/MM[a]	2.71	0.86	2.08	-2.16	0.08	

[a]Results using a aug-cc-pVTZ basis set taken from Ref. 121.

TABLE 8.4: *Dipole moment, quadrupole moment and mean polarizability for water in the gas phase and dipole moment, induced dipole moment and quadrupole moment for water in "liquid phase" using the Thole-A solvent model, TZ2P+ and different xc-potentials. Dipole and induced dipole moment in Debye. Quadrupole moment and mean polarizability in atomic units.*

identical results for dipole and quadrupole moments and compared with LDA slightly lower values. There is very good agreement between the LDA results and the CCSD results for both dipole and quadrupole moments. For a series of small molecules it has been shown that LDA predicts good dipole and quadrupole moments compared with experimental results,

especially for the water molecule.[345,346] The use of an asymptotic correct functional, LB94, increases the dipole moment and lowers the quadrupole moment compared with LDA and made the agreement with the CCSD results less good. For the mean polarizability BLYP gives a larger value, 10.82 a.u., and BP a smaller value, 10.20 a.u., compared with the LDA results of 10.47 a.u. but all values are still larger than the CCSD(T) results of 9.62 a.u. The LB94 results of 9.14 a.u. is much lower than the LDA results and in better agreement with the CCSD(T) result.

The shifts in the dipole and quadrupole moment in going from the gas phase to the "liquid" phase predicted using LDA or one of the GGA potentials are almost identical. The "liquid" phase dipole and quadrupole moments predicted with the GGA's are slightly lower than the LDA results and the differences are identical with the differences found in the gas phase. The solvent shifts for dipole and quadrupole moments predicted with LB94 are smaller than the shifts found using LDA, in agreement with the smaller gas phase polarizability found with LB94 compared with LDA. The "liquid" phase dipole moment found with LB94 compares well with the LDA value but the quadrupole moment is smaller. Also in the "liquid" phase there is a very good agreement between the LDA results and the CCSD/MM results. Since the induced dipole moment correlates well with the gas phase polarizability it indicates that to get a good description of the dipole moment in the liquid phase the gas phase dipole moment and polarizability must also be properly described.

8.5.4 Comparison of theoretical predictions for dipole and quadrupole moments in liquid phase

A comparison between some continuum and discrete models for calculating the dipole and quadrupole moments of "liquid" water is presented in Table 8.5. The continuum models are the CCSD/D.C. model[121] and the LDA/COSMO model[347] and the discrete models are the CCSD/MM and HF/MM models from Ref.[121] and the LDA/DRF model from this work. In all models the same geometry of the water molecules is used and in all discrete models also the same solvent structure is used. From the results in Table 8.5 we see that using a continuum model the dipole and quadrupole moments of the liquid phase are underestimated compared with the discrete models. The induced dipole moment predicted with the continuum models are a factor of two smaller than the results from the continuum model. The agreement between the LDA results and the CCSD results are very good both using the continuum model and the discrete model. Compared with the HF/MM results we find that the LDA/DRF results are in much better agreement with the CCSD/MM results.

There has been put a lot of effort into predicting the average dipole moment of liquid water since there is no way of determining this directly from experiment, although a recent experimental study[348] of liquid water using neutron diffraction predicts a dipole moment of 2.9±0.6 D. The average dipole moment of liquid water estimated using the experimental static dielectric constant is about 2.6 D.[349,350] The most commonly accepted value for the dipole moment of liquid water is 2.6 D[351] arising from an induction model study on ice

Method	μ	$\Delta\mu$	Q_{xx}	Q_{yy}	Q_{zz}
Continuum model					
LDA/COSMO [a]	2.26	0.39	1.92	-2.04	0.13
CCSD/D.C. [b]	2.19	0.34	1.91	-2.09	0.13
Discrete model					
LDA/DRF	2.68	0.81	2.07	-2.17	0.10
HF/MM [c]	2.77	0.79	2.19	-2.01	-0.18
CCSD/MM[c]	2.71	0.86	2.08	-2.16	0.08

[a]Dielectric constant ϵ=78.8 and R_H=1.44 Å and R_O=1.80 Å
[b]Dielectric continuum model using a aug-cc-pVTZ basis set taken from Ref. 121.
[c]Results using a aug-cc-pVTZ basis set taken from Ref. 121.

TABLE 8.5*: Comparison of continuum and discrete models for the prediction of the dipole and quadrupole moments of water in the liquid phase. Dipole and induced dipole moments in Debye. Quadrupole moment in atomic units.*

Ih. However, this study has been repeated recently using more accurate input parameters giving an average dipole moment of 3.1 D.[352] The latter value is in good agreement with an *ab initio* MD simulation of liquid water using maximally localized Wannier functions for describing the molecular charge distribution.[353,354] A different *ab initio* MD simulation of liquid water where the molecular charge distribution is defined using Bader's zero flux surface gives a smaller average dipole moment of 2.5 D.[323] They also reported results for the average dipole moment of ice Ih and found that it is considerably larger than the liquid phase results. The dependency of the molecular results on the partitioning of the charge distribution was clearly shown in a first principle study on ice Ih[322] where the average dipole moment varied between 2.3 D and 3.1 D dependent on the partitioning scheme. This study also showed that the dipole moment obtained using Bader's zero flux surface was smaller than the results predicted with the accurate induction model. To summarize, we believe that the dipole moment of liquid water is smaller than found in ice Ih, therefore 3.1 D is most likely an upper limit. Furthermore, since Bader's zero flux surface underestimates the dipole moment in ice Ih, 2.5 D is probably a lower limit for the average dipole moment in liquid water. Our result for the dipole moment of liquid water of 2.68 D is in good agreement with previously reported studies[121,279,334,342,355,356] and also within the above suggested limits.

8.6 Conclusions

In this work we have presented theory and implementation of a discrete reaction field model within density functional theory. The model combines a quantum mechanical description at the DFT level of theory of the solute and a classical description of the discrete solvent molecules. The solvent molecules are described using atomic point charges for representing the permanent electronic charge distribution and atomic polarizabilities for describing the

solvent polarization arising from many-body interactions. All atomic parameters have been chosen to reproduce molecular gas phase properties, i.e. the atomic charges reproduce the molecular gas phase dipole moment and the atomic polarizabilities reproduce the molecular gas phase polarizability tensor using Thole's model for distributed polarizabilities. The model was tested using a water cluster of 128 water molecules taken from a previous study using a similar solvent model but the solute molecule was treated either at the HF or CCSD level of theory, thereby making it possible to assess the quality of DFT for calculating molecular properties of liquids. The results show that the inclusion of the polarization of the solvent molecules is essential for an accurate prediction of liquid phase properties. Also, surprisingly, a very good agreement was found between the LDA results and the CCSD results for both the dipole and quadrupole moments in the liquid phase. The use of a GGA xc-potential only affected the results slightly whereas using an asymptotic correct functional affected the result more strongly and made the agreement with the CCSD results less well. It was found that the induced dipole moment correlates well with the gas phase molecular polarizability indicating that a good xc-potential must provide both good gas phase dipole moment and molecular polarizability in order to accurately describe the molecular properties in the liquid phase. The results for the dipole moment of 2.68 D are in good agreement with previous theoretical predictions and also with results based on experimental predictions.

Acknowledgment

L.J. gratefully acknowledges The Danish Research Training Council for financial support. We are grateful to Jacob Kongsted, Anders Osted and Dr. Kurt V. Mikkelsen for supplying the water cluster configuration and a preprint of Ref. 121.

Chapter 9

A DRF model for molecular linear response properties in solution

L. Jensen, P. Th. van Duijnen, and J. G. Snijders "A discrete solvent reaction field model for calculating molecular linear response properties in solution" *J. Chem. Phys.* **119**, 3800-3809, 2003.

9.1 Abstract

A Discrete Solvent Reaction Field model for calculating frequency-dependent molecular linear response properties of molecules in solution is presented. The model combines a Time-Dependent Density Functional Theory (QM) description of the solute molecule with a classical (MM) description of the discrete solvent molecules. The classical solvent molecules are represented using distributed atomic charges and polarizabilities. All the atomic parameters have been chosen so as to describe molecular gas phase properties of the solvent molecule, i.e. the atomic charges reproduce the molecular dipole moment and the atomic polarizabilities resproduce the molecular polarizability tensor using a modified dipole interaction model. The QM/MM interactions are introduced into the Kohn-Sham equations and all interactions are solved self-consistent, thereby allowing for the solute to be polarized by the solvent. Furthermore, the inclusion of polarizabilities in the MM part allows for the solvent molecules to be polarized by the solute and by interactions with other solvent molecules. Initial applications of the model to calculate the vertical electronic excitation energies and frequency-dependent molecular polarizability of a water molecule in a cluster of 127 classical water molecules are presented. The effect of using different exchange correlation (xc)-potentials is investigated and the results are compared with results from wavefunction methods combined with a similar solvent model both at the correlated and uncorrelated level of theory. It is shown that accurate results in agreement with correlated wavefunction results can be obtained using xc-potentials with the correct asymptotic behavior.

9.2 Introduction

The calculation of molecular properties of molecules in the condensed phase is a fundamental and important theoretical problem which still remains problematic. Since molecular properties like (hyper)polarizabilities are sensitive to the local environment an accurate calculations of these properties could serve as a test for the molecular models used in describing intermolecular forces. However, accurate calculation of molecular properties require a quantum mechanical treatment which, due to high computational cost, are limited to small systems. Therefore the most successful methods divide the total system into the molecular system of interest which is treated with a quantum mechanical method and another part which contains the rest of the system which is treated by a much simpler method, usually a classical description.[102–116]

Among these methods are the combined quantum mechanical and classical mechanics models (QM/MM).[105–116] In the QM/MM method the solvent molecules are treated with a classical force field and the interactions between the solute and solvent are described with an effective operator, so the problem which remains is to find an accurate approximate representation of the solvent molecules and the solute-solvent interactions.[248] The discrete representation of the solvent molecules requires a large number of solvent configurations over which the solute properties must be averaged. This is typically done using Monte Carlo or MD techniques which lead to a large number of quantum mechanical calculations. For this reason the QM/MM method is often employed at a semiempirical level of theory.[115]

We have recently developed such a method which we denoted the Discrete Solvent Reaction Field model (DRF) [Ref. 117, Chap. 8]. In this model the QM part is treated using Density Functional Theory (DFT). The solvent molecules (MM) are modeled by point charges representing the permanent electronic charge distribution, and distributed polarizabilities for describing the solvent polarization arising from many-body interactions. The QM/MM interactions are introduced into the Kohn-Sham equations and all interactions are solved self-consistently, thereby allowing for the solute to be polarized by the solvent. Furthermore, the inclusion of polarizabilities in the MM part allows for the solvent molecules to be polarized by the solute and by interactions with other solvent molecules. The advantage of including polarizabilities in the MM part is that all parameters can be obtained from gas phase properties. In general it is expected that a distributed polarizability approach will give better results than an approach using only a (anisotropic) polarizability located at a single site, especially as the size of the solvent molecule increases.[120]

The use of Time-Dependent Density Functional Theory (TD-DFT)[37–41] allows for the calculation of frequency-dependent response properties like electronic spectra and frequency-dependent polarizabilities. The use of TD-DFT for calculating molecular response properties in the gas-phase has been shown to be accurate especially using recently developed density functionals[42–48] and the extension of TD-DFT to also treat molecules in solution is of great interest. So far the treatment of frequency-dependent response properties of molecules in solution within a TD-DFT approach has been done within the polarizable continuum model.[357–359] Therefore, in this work we will include the Discrete Solvent Reaction Field model within TD-DFT. This allows for the calculation of response properties

of molecules in solution where the discrete representation of the solvent is retained and electron correlation of the QM part is included in an efficient manner. Within a QM/MM approach the treatment of frequency-dependent properties has been done using both correlated and uncorrelated wavefunction based methods.[122,342,360] As in our previous study on dipole and quadrupole moments of water in aqueous solution [Ref. 117, Chap. 8] we will adopt a single water structure for which there exist wavefunction QM/MM results.[122,342] This will allows us to assess approximate exchange-correlation (xc) potentials for calculating molecular response properties in solution.

9.3 Theory

9.3.1 The Discrete Reaction Field model

In the QM/MM method the total (effective) Hamiltonian for the system is written as[105–116]

$$\hat{H} = \hat{H}_{QM} + \hat{H}_{QM/MM} + \hat{H}_{MM} \tag{9.1}$$

where $\hat{H}_{QM}$ is the quantum mechanical Hamiltonian for the solute, $\hat{H}_{QM/MM}$ describes the interactions between solute and solvent and $\hat{H}_{MM}$ describes the solvent-solvent interactions. The Discrete Reaction Field model has been described in [Ref. 117, Chap. 8] within time-independent DFT. Here, the model will be extended to include the effect of an electric field at frequency, ω, perturbing the QM part.

Within the the Discrete Reaction Field model the QM/MM operator at a point r_i is given by

$$\hat{H}_{QM/MM} = \sum_i v^{DRF}(r_i, \omega) = \sum_i v^{el}(r_i) + \sum_i v^{pol}(r_i, \omega), \tag{9.2}$$

where the first term, v^{el}, is the electrostatic operator and describes the Coulombic interaction between the QM system and the permanent charge distribution of the solvent molecules. The second term, v^{pol}, is the polarization operator and describes the many-body polarization of the solvent molecules, *i.e.* the change in the charge distribution of the solvent molecules due to interaction with the QM part and other solvent molecules.

The charge distribution of the solvent is represented by atomic point charges, hence the electrostatic operator is given by

$$v^{el}(r_i) = \sum_s \frac{q_s}{R_{si}} = \sum_s q_s T^{(0)}_{si}, \tag{9.3}$$

where the zero'th order interaction tensor has been introduced and the index s runs over all atoms of the solvent molecules. In general the interaction tensor to a given order, n, can be written as

$$T^{(n)}_{pq,\alpha_1 \ldots \alpha_n} = \nabla_{pq,\alpha_1} \ldots \nabla_{pq,\alpha_n} \left(\frac{1}{R_{pq}} \right), \tag{9.4}$$

where R_{pq} is the distance between the interacting entities. The many-body polarization term is represented by induced atomic dipoles at the solvent molecules and the polarization operator is given by

$$v^{pol}(r_i,\omega) = \sum_s \mu^{ind}_{s,\alpha}(\omega)\frac{R_{si,\alpha}}{R^3_{si}} = -\sum_s \mu^{ind}_{s,\alpha}(\omega)T^{(1)}_{si,\alpha}. \tag{9.5}$$

where $R_{si,\alpha}$ is a component of the distance vector and $\mu^{ind}_s(\omega)$ is the induced dipole at site s. For Greek indices the Einstein summation convention is employed. The induced dipoles are discussed in more detail in the next section.

9.3.2 The Frequency-dependent Atomic Induced Dipoles

For a collection of atomic polarizabilities in an electric field, assuming linear response, the induced atomic dipole at site s is given by

$$\mu^{ind}_{s,\alpha}(\omega) = \alpha_{s,\alpha\beta}[F^{init}_{s,\beta}(\omega) + \sum_{t\neq s} T^{(2)}_{st,\beta\gamma}\mu^{ind}_{t,\gamma}(\omega)], \tag{9.6}$$

where $\alpha_{a,\alpha\beta}$ is a component of the atomic polarizability tensor at site s, which for an isotropic atom gives $\alpha_{s,\alpha\beta} = \delta_{\alpha\beta}\alpha_s$. Here we neglect the frequency-dependence of the classical part, i.e. the atomic polarizability is frequency independent, but the model can easily be extended to include also this effect.[94] [Ref. 63, Chap. 3]

$F^{init}_{s,\beta}(\omega)$ is the initial electric field at site s and the last term is the electric field from the other induced dipoles. The dipole interaction tensor, $T^{(2)}_{st,\alpha\beta}$, is given by

$$T^{(2)}_{st,\alpha\beta} = \frac{3R_{st,\alpha}R_{st,\beta}}{R^5_{st}} - \frac{\delta_{\alpha\beta}}{R^3_{st}}. \tag{9.7}$$

The initial field in Eq. 9.6 is given as a sum of three terms

$$F^{init}_{t,\beta}(\omega) = F^{QM,el}_{t,\beta}(\omega) + F^{QM,nuc}_{t,\beta} + F^{MM,q}_{t,\beta}, \tag{9.8}$$

where $F^{QM,el}_{t,\beta}(\omega)$ is the field arising from the frequency-dependent electronic charge distribution of the QM part,

$$F^{QM,el}_{t,\beta}(\omega) = -\int \rho(r_i,\omega)\frac{R_{it,\beta}}{R^3_{it}}dr_i = \int \rho(r_i,\omega)T^{(1)}_{it,\beta}dr_i \tag{9.9}$$

and $F^{QM,nuc}_{t,\beta}$ is the field arising from the QM nuclei,

$$F^{QM,nuc}_{t,\beta} = \sum_m \frac{Z_m R_{mt,\beta}}{R^3_{mt}} = -\sum_m Z_m T^{(1)}_{mt,\beta} \tag{9.10}$$

and $F_{t,\beta}^{MM,q}$ is the field arising from the point charges at the solvent molecules,

$$F_{t,\beta}^{MM,q} = \sum_{s}{}' \frac{q_s R_{st,\beta}}{R_{st}^3} = -\sum_{s}{}' q_s T_{st,\beta}^{(1)}. \tag{9.11}$$

The prime in Eq 9.11 indicates that the sum is restricted to sites which do not belong to the same molecule.

The initial field in Eq. 9.8 does not include the electric field perturbing the QM part which means that the field perturbing the QM part is in fact the local field felt by the QM molecule. The reason for this approach is that we are interested in obtaining the properties of a single molecule in solution. This method leads to the identification of the calculated properties as the solute properties, i.e the polarizability of the solute including the solvent effects but not corrected for the difference between the local field and the macroscopic field. For a discussion of these effects and corrections within the dielectric continuum model see e.g. Ref. 29, 280, 281.

Since the induced dipole in Eq. 9.6 depends on the induced dipoles at the other sites these equations have to be solved self-consistently. This can be done analytically by re-writing the equations into a $3N \times 3N$ linear matrix equation, with N the number of atoms, as[31,90]

$$A\mu^{ind}(\omega) = F^{init}(\omega) \tag{9.12}$$

and the components of the matrix, $A_{st,\alpha\beta}$, given by

$$A_{st,\alpha\beta} = (\alpha_{s,\alpha\beta}^{-1}\delta_{st} - T_{st,\alpha\beta}^{(2)}), \tag{9.13}$$

This matrix equation can then be solved for the induced dipoles using standard mathematical tools for solving linear equations. The inverse of the matrix A, the so called relay matrix B, is a generalized polarizability matrix which describes the total linear response of the discrete solvent molecules.

It is well known that if the distance between two polarizable points becomes to small the induced dipoles will grow towards infinity. In order to avoid this "polarizability catastrophe" Thole[93] modified the dipole interaction tensor using smeared-out dipoles. The screened dipole interaction tensor can be written as

$$T_{pq,\alpha\beta}^{(2)} = \frac{3f_{pq}^T R_{pq,\alpha} R_{pq,\beta}}{R_{pq}^5} - \frac{f_{pq}^E \delta_{\alpha\beta}}{R_{pq}^3}. \tag{9.14}$$

where the damping functions f_{pq}^T and f_{pq}^E have been introduced. If we consider an exponential decaying charge distribution the screening functions in Eq. 9.14 are given by[163]

$$f_{pg}^E = 1 - \left[1 + s_{pq} + \frac{1}{2}s_{pq}^2\right]\exp(-s_{pq}) \text{ and } f_{pg}^T = f_{pg}^E - \frac{1}{6}s_{pq}^3\exp(-s_{pq}), \tag{9.15}$$

where the term s_{pq} is give by $s_{pq} = aR_{pq}/(\alpha_p\alpha_q)^{1/6}$, with a the screening length, and α_p the atomic polarizability of atom p.

9.3.3 The Time-dependent Kohn-Sham equation

If one is interested in time-dependent properties within DFT one has to resort to the time-dependent Kohn-Sham equations,[37–41]

$$i\frac{\partial}{\partial t}\phi_i(r,t) = \left[-\frac{1}{2}\nabla^2 + \upsilon_{eff}(r,t)\right]\phi_i(r,t), \tag{9.16}$$

with the effective potential given by

$$\upsilon_{eff}(r,t) = \int dr' \frac{\rho(r',t)}{|r-r'|} + \upsilon^{per}(t) + \upsilon^{DRF}(r,t) + \upsilon_{xc}(r,t), \tag{9.17}$$

where $\upsilon^{DRF}(r,t)$ is the operator defined in Eq. 9.2 and $\upsilon^{per}(t)$ is the perturbing field turned on slowly in the distant past. The last term is the time-dependent xc-potential, given by the functional derivative of the xc-action, which in the adiabatic approximation is given by

$$\upsilon_{xc}[\rho](r,t) \approx \frac{\delta E_{xc}[\rho_t]}{\delta\rho_t(r)} = \upsilon_{xc}[\rho_t](r). \tag{9.18}$$

The time-dependent electronic density is given by

$$\rho(r,t) = \sum_{i}^{occ} n_i |\phi_i(r,t)|^2, \tag{9.19}$$

where n_i is the occupation number of orbital i.

9.3.4 Linear response of the density matrix

Since we are interested in linear response properties we look at the first-order change in the density to a time-dependent perturbation

$$\delta\rho(r,\omega) = \sum_{s,t} P_{st}(\omega)\phi_s(r)\phi_t^*(r) = \sum_{i,a} P_{ia}(\omega)\phi_i(r)\phi_a^*(r) + P_{ai}(\omega)\phi_a(r)\phi_i^*(r), \tag{9.20}$$

where P is the first-order density matrix and a,b indicates virtual orbitals , i,j occupied orbitals and s,t indicates general orbitals. By expanding the KS-equations to first-order in the perturbing potential we find that the first-order density matrix is given by

$$P_{st}(\omega) = \frac{\Delta n_{st}}{(\epsilon_s - \epsilon_t) - \omega}\delta\upsilon_{st}^{eff}(\omega), \tag{9.21}$$

where Δn_{st} is the difference in occupation numbers, i.e. 1 for $st = ai$ and -1 for $st = ia$. The change in the effective potential, $\delta\upsilon_{st}^{eff}$, is dependent on the first order change in the density and is given by

$$\begin{aligned}\delta\upsilon_{st}^{eff}(\omega) &= \delta\upsilon_{st}^{per}(\omega) + \delta\upsilon_{st}^{scf}(\omega) \qquad (9.22)\\ &= \delta\upsilon_{st}^{per}(\omega) + \int dr\phi_s^*(r)\left[\int dr' \frac{\delta\rho(r',\omega)}{|r-r'|} + \upsilon_{xc}[\delta\rho](r,\omega) + \upsilon^{DRF}[\delta\rho](r,\omega)\right]\phi_t(r),\end{aligned}$$

where the self-consistent field, $\delta\upsilon^{scf}$, denotes terms which depend on the first-order change in the density. The contribution from the DRF operator is given by

$$\begin{aligned}\upsilon^{DRF}[\delta\rho](r_i,\omega) &= -\sum_s \mu^{ind}_{s,\alpha}[\delta\rho](\omega)T^{(1)}_{si,\alpha} \\ &= -\sum_s\sum_t B_{st,\alpha\beta}F^{qm.el}_{s,\beta}[\delta\rho](\omega)T^{(1)}_{si,\alpha} \\ &= -\sum_s\sum_t B_{st,\alpha\beta}\int \delta\rho(r_j,\omega)T^{(1)}_{js,\beta}dr_j T^{(1)}_{si,\alpha}, \end{aligned} \tag{9.23}$$

where B is the relay matrix. The DRF contribution arises from the induces dipoles in the MM part due to the first-order change in the QM charge distribution. Inserting the first order change in the density, Eq. 9.20, into Eq. 9.22 allows for the change in the effective potential to be written as

$$\delta\upsilon^{eff}_{st}(\omega) = \delta\upsilon^{per}_{st}(\omega) + \sum_{uv} K_{st,uv}P_{uv}(\omega), \tag{9.24}$$

where the coupling matrix, $\mathbf{K}$, has been introduced. The coupling matrix will be described in more detail later. Inserting Eq. 9.24 into Eq. 9.21 the first-order density matrix can be written as

$$P_{st}(\omega) = \frac{\Delta n_{st}}{(\epsilon_s-\epsilon_t)-\omega}[\delta\upsilon^{per}_{st}(\omega) + \sum_{uv} K_{st,uv}P_{uv}(\omega)]. \tag{9.25}$$

This can be written as a set of coupled linear equations for the first-order density matrix elements using the fact that only elements relating occupied and virtual orbitals are nonzero

$$\sum_{jb}[\delta_{ij}\delta_{ab}(\epsilon_a-\epsilon_i+\omega)+K_{ia,jb}]P_{jb} + \sum_{jb}K_{ia,bj}P_{bj} = -(\delta\upsilon^{per}_{ia}), \tag{9.26}$$

$$\sum_{jb}[\delta_{ij}\delta_{ab}(\epsilon_a-\epsilon_i-\omega)+K_{ai,bj}]P_{bj} + \sum_{jb}K_{ai,jb}P_{jb} = -(\delta\upsilon^{per}_{ai}) \tag{9.27}$$

These equation can be written as one matrix equation using the more common notation $X_{jb} = P_{jb}$ and $Y_{jb} = P_{bj}$ as

$$\left[\begin{pmatrix}\mathbf{A} & \mathbf{C}\\ \mathbf{C}^* & \mathbf{A}^*\end{pmatrix} - \omega\begin{pmatrix}\mathbf{-1} & \mathbf{0}\\ \mathbf{0} & \mathbf{1}\end{pmatrix}\right]\begin{pmatrix}X\\ Y\end{pmatrix} = -\begin{pmatrix}\delta\upsilon^{per}\\ \delta\upsilon^{per*}\end{pmatrix}, \tag{9.28}$$

where the individually matrix elements are defined as

$$A_{ia,jb} = \delta_{ab}\delta_{ij}(\epsilon_a-\epsilon_i) + K_{ia,jb} \tag{9.29}$$

and

$$C_{ia,jb} = K_{ia,bj}. \tag{9.30}$$

In TD-DFT the equality $K_{ia.jb} = K_{ia,bj}$ which allows for that the equations can be reduced to half the size which is not the case in TD-HF where this equality is not valid. From the solution of the linear equations in Eq. 9.28 we have access to the frequency-dependent polarizability or by transforming the left hand side into an eigenvalue equation we can obtain the excitation energies and oscillator strengths.

9.3.5 The coupling matrix

The coupling matrix describes the linear response of the self-consistent field to changes in the density and consist of three terms.

$$\begin{aligned} K_{st,uv} &= \frac{\partial \upsilon_{st}^{scf}}{\partial P_{uv}} \\ &= K_{st,uv}^{Coul} + K_{st,uv}^{xc} + K_{st,uv}^{DRF}. \end{aligned} \tag{9.31}$$

The first term is the Coulomb part given by

$$K_{st,uv}^{Coul} = \int\int dr_i dr_j \phi_s^*(r_i)\phi_t(r_i)\frac{1}{|r_i - r_j|}\phi_u(r_j)\phi_v^*(r_j), \tag{9.32}$$

the second term is the xc part

$$K_{st,uv}^{xc} = \int\int dr_i dr_j \phi_s^*(r_i)\phi_t(r_i)\frac{\delta \upsilon_{xc}(r_i,\omega)}{\delta\rho(r_j,\omega)}\phi_u(r_j)\phi_v^*(r_j) \tag{9.33}$$

and the last term is the DRF part

$$\begin{aligned} K_{st,uv}^{DRF} &= \int dr_i \phi_s^*(r_i)\phi_t(r_i)\frac{\partial \upsilon^{DRF}(r_i,\omega)}{\partial P_{uv}} \\ &= -\int dr_i \phi_s^*(r_i)\phi_t(r_i)\sum_s\sum_t B_{st,\alpha\beta}T_{js,\beta}^{(1)}T_{si,\alpha}^{(1)}\frac{\partial\delta\rho(r_j,\omega)}{\partial P_{uv}} \\ &= -\int\int dr_i dr_j \phi_s^*(r_i)\phi_t(r_i)\sum_s\sum_t B_{st,\alpha\beta}T_{js,\beta}^{(1)}T_{si,\alpha}^{(1)}\phi_u^*(r_j)\phi_v(r_j). \end{aligned} \tag{9.34}$$

9.3.6 Implementation

The DRF model has been implemented into a local version of the Amsterdam Density Functional (ADF) program package.[340,361] The extension to the TD-DFT part has been implemented into the RESPONSE module of ADF.[57,130,289] In the RESPONSE module the functional derivative of the xc-potential in Eq. 9.33 is restricted to the Adiabatic LDA (ALDA) xc-potential. The coupling matrix in Eq. 9.28 becomes very big for large systems and for this reason this matrix is not contructed but the linear equations in Eq. 9.28 are solved iteratively, for details see Ref.[130] This means that the DRF response operator, Eq. 9.23, is never calculated by constructing the relay matrix, B, but the induced dipole moments due to the first-order change in the charge distribution are calculated by solving a set of linear equations like in Eq. 9.12.

In ADF the KS equations and the linear response equations are solved by numerical integration which means that the DRF operator has to be evaluated in each integration point. Since the numerical integration grid is chosen on the basis of the quantum part alone care must be taken when evaluating the DRF operator if the integration points are

close to a classical atom. In order to avoid numerical instabilities we introduce a damping of the operator at small distances which is modeled by modifying the distance R_{ij} to obtain a scaled distance S_{ij} [Ref. 63, Chap. 3],

$$S_{ij} = v_{ij} R_{ij} = f(R_{ij}) \ , \tag{9.35}$$

where v_{ij} is a scaling factor and $f(R_{ij})$ an appropriately chosen function of R_{ij}. Furthermore, each component of R_{ij} is also scaled by v_{ij}, so the reduced distance becomes,

$$S_{ij} = \sqrt{S_{ij,\alpha} S_{ij,\alpha}} = v_{ij} \sqrt{R_{ij,\alpha} R_{ij,\alpha}} = v_{ij} R_{ij} \ , \tag{9.36}$$

consistent with the definition in Eq. 9.35. The damped operator can thus be obtained by modifying the interaction tensors in Eqs. 9.3, 9.5 and 9.23,

$$T^{(n)}_{ij,\alpha_1 \ldots \alpha_n} = \nabla_{\alpha_1} \ldots \nabla_{\alpha_n} \left(\frac{1}{S_{ij}} \right) \ , \tag{9.37}$$

which is equivalent to replacing R_{ij} by S_{ij} and $R_{ij,\alpha}$ by $S_{ij,\alpha}$ in the regular formulae for the interaction tensors. The particular form of the scaling function employed here is [Ref. 63, Chap. 3]

$$f(r_{pq}) = \frac{r_{pq}}{\mathrm{er} f(r_{pq})}, \tag{9.38}$$

which was obtained by considering the interaction between two Gaussian charge distributions with unity exponents.

9.4 Computational details

In this work we use a large even-tempered basis set of Slater-type orbitals with orbital exponent $\zeta = \alpha\beta^i$, $i = 1, \cdots n$, the details of the basis set is presented in Tabel 9.1. We tested different xc potentials, the Local Density Approximation (LDA), Becke-Lee-Yang-Parr (BLYP),[138,139] the Becke-Perdew (BP),[138,341] the van Leeuwen-Baerends (LB94),[141] the statistical averaging of (model) orbital potentials (SAOP),[45,362,363] and the gradient-regulated asymptotic connection procedure applied to the BP potentials (BP-GRAC).[47,48] The BLYP and BP are examples of typical Generalized Gradient Approximations (GGAs) potentials and the LB94 is an example of a so-called asymptotic correct potential due to the correct Coulombic decay of the potential at large distances. Whereas SAOP and BP-GRAC belong to a class of shape-corrected potentials which yield the correct asymptotic behavior. The BP-GRAC potential sets the HOMO level at the first ionization potential (IP) and therefore requires the IP as input. The SAOP xc-potential requires no additional input and the energy of the HOMO corresponds well with the IP.[48,364] For this reason the IP needed as input for the BP-GRAC xc-potential is taken from the SAOP gas-phase calculation, i.e IP = 0.45 a.u.

The parameters needed for the solvent molecules, i.e. point charges and atomic polarizabilities ,where adopted from [Ref. 117, Chap. 8]. The point charges are $q_H = 0.3345$ a.u.

Atom	1s	2p	3d	4f
H(4s3p3d)	0.282564	0.451156	0.407083	
O(8s6p3d4f	0.181199	0.238632	0.530772	0.359191

TABLE 9.1: *Even-tempered basis set for the H, O atoms (in parentheses the number n of 1s, 2p, 3d, 4f) with the orbital exponent* $\zeta = \alpha\beta^i$, $i = 1, \cdots n$, $\beta = 1.7$. *The value of* α *for the most difffuse 1s, 2p, 3d, and 4f is presented.*

and $q_O = -0.6690$ a.u. which generate a molecular dipole moment of 1.88 Debye. The atomic polarizabilities are $\alpha_H = 0.0690$ a.u. and $\alpha_O = 9.3005$ a.u. which reproduced the molecular polarizability tensor with a mean polarizability of 9.62 a.u. and a polarizability anisotropy of 0.52 a.u. The screening parameter, $a = 2.1304$, used in Eq. 9.15, was taken from Ref. 163.

The water structure we used in this work was taken from Ref. 338 and consists of 128 rigid water molecule where one molecule, the solute, is treated quantum mechanically. The total structure was obtained from a MD simulation using a polarizable force field[327] and the details about the simulation can be found in Ref. 122,342 but are summarized here for consistency. The average geometry is obtained from a simulation of a box containing 128 water molecules utilizing periodic boundary conditions with a spherical cut-off distance of 10.0 Å, temperature, 298 K, and a pressure of 0.103 MPa. After equilibration of the sample, the average geometry was obtained from a Boltzmann sampling of 8000 trajectories started from different initial velocity distributions and a simulations time of 20 ps for each trajectory. The intra-molecular geometry of the water molecules was that in gas phase, *i.e.* $R_{O-H} = 0.9572$ Å and $\angle_{HOH} = 104.49°$. The solute water molecule was placed in the xz-plane with the z-axis bisecting the H-O-H angle. Results obtained using this structure will be referred to as "liquid" phase results. We will perform one QM/MM calculation and therefore the molecular properties will not be averaged over different solvent configurations. However, the choice of this particular water structure allows for a direct comparison with results obtained from a similar model within a (Multiconfigurational) Self-Consistent-Field/Molecular Mechanics(MC-SCF/MM)[342] or a Coupled Cluster/Molecular Mechanics (CC/MM)[122] approach. Therefore, it is possible to make a detailed comparison between wave function methods and the DFT method for liquid phase calculations.

9.5 Results

9.5.1 Excitation energies

In Table 9.2 we present excitation energies, ω, and oscillator strengths, f, for the three lowest vertical singlet-singlet excitations of a water molecule in the gas phase calculated using different xc-potentials. The results are compared with results obtained from wave-function methods , i.e. HF,[342] MC-SCF,[342] CCSD,[122] and experimental results taken from Ref. 365. From the results in Tabel 9.2 it is noted that LDA and the GGA potentials

(BP and BLYP) underestimate the excitation energies considerably compared with the experimental results, i.e. for the first excitation ∼1 eV, the second excitation ∼1.5 eV and for the third excitation as much as ∼2 eV. The failure of these common xc-potentials to predict excitation energies for Rydberg-like states (for water the lowest excitations has a high degree of Rydberg character) has been identified as a result of the wrong asymptotic behavior of the xc-potentials.[43,44] This is clearly illustrated by using the xc-functionals (LB94, SAOP, and BP-GRAC) with correct asymptotic behavior, for which the excitations energies are greatly improved compared with the experimental results. Especially the results obtained with the BP-GRAC xc-potentials are in good agreement with the experimental results. Comparing with the wavefunction results we see that HF overestimates the excitation energies compared with the experiments but the MC-SCF and CCSD results are in good agreement with experiment and also with the calculations performed with the asymptotic correct xc-potentials.

	$^1A_1 \rightarrow 1^1B_1$		$^1A_1 \rightarrow 1^1A_2$		$^1A_1 \rightarrow 2^1A_1$	
Method	ω	f	ω	f	ω	f.
LDA	6.47	0.04	7.55	-	7.76	0.00006
BLYP	6.24	0.04	7.33	-	7.53	0.0002
BP	6.57	0.04	7.50	-	7.67	0.00006
LB94	7.89	0.04	9.68	-	9.91	0.09
SAOP	7.72	0.05	9.53	-	9.68	0.09
GRAC	7.33	0.05	9.15	-	9.48	0.09
HF [a]	8.65	-	10.3	-	-	-
MC-SCF[a]	7.85	-	9.56	-	-	
CCSD [b]	7.62	0.05	9.38	-	9.88	0.06
Exp. [c]	7.4	-	9.1	-	9.7	-

[a]Results from Ref. 342 using the aug-cc-pVQZ basis set.
[b]Results from Ref. 122using the d-aug-cc-pVTZ basis set
[c]Results taken from Ref. 365

TABLE 9.2: *Excitation energies (ω) and oscillator strengths (f) of a water molecule in vacuum. ω in eV and f in a.u.*

The excitation energies and oscillator strengths for a water molecule in a cluster of 127 classical water molecules calculated using the different xc-functional are presented in Table 9.3. The results are compared with results for the same water cluster obtained using the HF/MM,[342] MC-SCF/MM[342] and CCSD/MM[122] method. Also presented in Table 9.3 is the solvation shift, $\Delta\omega$, i.e the shift in the excitation energies in going from the gas-phase to the "liquid" phase. Comparing results using LDA with the GGA's (BLYP and BP) results we find good agreement for excitation energies, oscillator strengths and solvation shifts which was also observed for the gas-phase results. Furthermore, comparing the results using the asymptotic correct xc-potentials we also find a good agreement between the results, especially those obtained using SAOP and BP-GRAC. Comparing the LDA/GGA results with the results from the asymptotic correct xc-potentials we find that the agreement is less

good than in the gas-phase. For the first two excitations the excitation energy is underestimated considerably and more than in the gas-phase leading to a too small solvation shift. For the third excitation the excitation energy is still underestimated but the solvation shift is overestimated. Using LDA/GGA this excitation was actual identified lying above other excitations which was not the case for the asymptotic correct xc-potentials. This excitation has a strong Rydberg character and is therefore very sensitive to the asymptotic part of the xc-potential. Comparing the results from the asymptotic correct xc-potentials with the wavefunction results we find that the excitation energies obtained with HF/MM are smaller but there is a good agreement with both the MC-SCF/MM and the CCSD/MM results. If we look at the solvent shift for the three excitations we see that both the wavefunction methods and DFT (except using LDA/GGA) predicts that the excitations are shifted by approximately the same amount, i.e. that the three excitation energies are perturbed by the solvent in the same manner. Also, if we look at the oscillator strengths for the three excitations the first and third excitation are stronger than the second excitation. In the gas phase the second excitation is dipole forbidden. Also, comparing the second and third excitation energy we find, both in the gas phase and in the "liquid" phase, that DFT predicts a smaller difference compared with CCSD.

	$^1A_1 \rightarrow 1^1B_1$			$^1A_1 \rightarrow 1^1A_2$			$^1A_1 \rightarrow 2^1A_1$		
Method	ω	$\Delta\omega$	f	ω	$\Delta\omega$	f	ω	$\Delta\omega$	$f.$
LDA/DRF	6.75	0.28	0.051	7.72	0.17	0.008	8.93	1.17	0.060
BLYP/DRF	6.49	0.25	0.055	7.48	0.15	0.009	8.71	1.18	0.063
BP/DRF	6.80	0.23	0.045	7.64	0.14	0.008	9.03	1.36	0.050
LB94/DRF	8.57	0.68	0.070	10.56	0.88	0.001	10.62	0.71	0.116
SAOP/DRF	8.25	0.53	0.075	10.18	0.65	0.003	10.27	0.59	0.112
GRAC/DRF	8.09	0.76	0.084	10.12	0.97	0.003	10.31	0.83	0.118
HF /MM [a]	9.49	0.84	-	11.3	1.0	-	-	-	
MC-SCF/MM[a]	8.62	0.77	-	10.5	0.9	-	-	-	
CCSD/MM [b]	8.18	0.56	0.079	9.97	0.60	0.006	10.56	0.68	0.113

[a]Results from Ref. 342 using the aug-cc-pVQZ basis set.
[b]Results from Ref. 122using the d-aug-cc-pVTZ basis set

TABLE 9.3: *Excitation energies (ω), solvation shift ($\Delta\omega$), and oscillator strengths (f) for a water molecule in a cluster of 127 classical water molecules. ω and $\Delta\omega$ in eV and f in a.u.*

In the experimental absorption spectrum of liquid water two absorption peaks are found.[366,367] The first peak has a maximum $\sim$ 8.2 eV ($\Delta\omega \sim$ 0.8 eV) and the second peak $\sim$ 9.9 eV ($\Delta\omega \sim$ 0.2 eV). The shifts of the excitation found in ice is even larger. i.e. the first maximum $\sim$ 8.5 eV ($\Delta\omega \sim$ 1.1 eV) and a broad shoulder $\sim$10.4 eV ($\Delta\omega \sim$ 0.7 eV).[367,368] The first peak is assigned to the $^1A_1 \rightarrow 1^1B_1$ (first) excitation and the second peak to $^1A_1 \rightarrow 2^1A_1$ (third) excitation. Comparing the liquid results with the calculated results we find a good agreement for the first excitation both for the excitation energy and for the solvent shift, especially using BP-GRAC. For the third excitation the solvent

shift is found experimentally to be much smaller than the calculated shift. As indicated, experimentally the shifts in the two excitations depend on whether the condense phase is liquid water or ice. This indicates that the solvent shift for the two excitations could behave differently with respect to the local environment of the solvent. Therefore, it could be important to include a more appropriate sampling of the local structure of the solvent, i.e. using a larger number of solvent configurations than the average structure used in this work. This will also provide line broadening of the excitations due to the fluctuations in the local environment of the solvent. However, it should be mentioned that also other effects can account for the difference, e.g. in this approach we neglect the short-range repulsion between water molecules. Also, the solvent effects are introduced as a mean field theory, i.e the solvent feels the mean field from the QM electrons (see e.g. Ref 106, 369, 370).

9.5.2 Frequency-dependent polarizability

In Table 9.4 we present the static and frequency-dependent polarizability for a single water molecule at frequencies $\omega = 0.0428, 0.0570, 0.0856$ a.u.($\lambda = 1064, 800, 532$ nm, respectively) calculated using different xc-potentials. The results are compared with HF,[343] MC-SCF,[342] CCSD[122,371] and experimental results.[372] Also, presented is the mean polarizability, $\overline{\alpha}$, defined as

$$\overline{\alpha} = \frac{1}{3}(\alpha_{xx} + \alpha_{yy} + \alpha zz), \tag{9.39}$$

and the polarizability anisotopy, $\Delta\alpha$, as

$$\Delta\alpha = \sqrt{\frac{1}{2}[(\alpha_{xx} - \alpha_{yy})^2 + (\alpha_{xx} - \alpha_{zz})^2 + (\alpha_{yy} - \alpha_{zz})^2]}. \tag{9.40}$$

From the results in Table 9.4 we see that the LDA/GGA results are larger than the results obtained with the asymptotic correct xc-potentials. Also, the size of the individual components of the polarizability tensor are nearly identical with LDA/GGA resulting in an anisotropy which is much smaller than that obtained with the asymptotic correct xc-potentials. The frequency dispersion is also found to be larger with LDA/GGA for the components and mean polarizability. However, for the frequency dispersion of the anisotropy we find the LDA/GGA predicts an increase in the anisotropy with increasing frequency whereas the asymptotic corrects xc-potentials predicts a decrease. Comparing the results from the three asymptotic correct xc-potentials we find that BP-GRAC predicts the largest components and mean polarizability but the smallest anisotropy. LB94 predicts the largest anisotropy of the functionals due to a small yy component. Comparing with the wavefunction results we find that SAOP is in good agreement with MC-SCF and CCSD. The static CCSD results using the d-aug-cc-pVTZ basis set[371] are in very good agreement with the CCSD(T) result.[343] Comparing with the static CCSD/d-aug-cc-pVTZ results we see that SAOP gives a slightly lower mean polarizability but a larger anisotropy due to a to small yy component. The HF results for the components and anisotropy are the smallest whereas the anisotropy is among the largest. LB94 gives an improved result compared with HF but the yy component is still underestimated compared with CCSD/d-aug-cc-pVTZ and

	ω	LDA	BLYP	BP	LB94	SAOP	GRAC	HF [a]	MC-SCF [b]	CCSD [c]	EXP. [d]
α_{xx}	0.0000	10.59	10.87	10.35	9.89	9.88	10.12	9.18	9.74	9.94 (9.98)	-
	0.0428	10.65	10.93	10.41	9.94	9.93	10.17	-	9.79	9.99	-
	0.0570	10.70	10.98	10.45	9.978	9.97	10.21	-	9.82	10.03	-
	0.0856	10.84	11.13	10.59	10.08	10.08	10.33	-	9.92	10.13	10.31
α_{yy}	0.0000	10.65	11.06	10.30	8.57	8.92	9.68	7.90	9.15	9.05 (9.35)	-
	0.0428	10.78	11.21	10.42	8.63	8.99	9.77	-	9.21	9.13	-
	0.0570	10.88	11.33	10.52	8.68	9.05	9.84	-	9.28	9.19	-
	0.0856	11.21	11.72	10.82	8.84	9.23	10.07	-	9.45	9.37	9.55
α_{zz}	0.0000	10.60	10.88	10.28	9.30	9.52	9.91	8.52	9.36	9.40 (9.61)	-
	0.0428	10.68	10.97	10.36	9.36	9.58	9.98	-	9.41	9.45	-
	0.0570	10.75	11.05	10.42	9.40	9.63	10.03	-	9.46	9.50	-
	0.0856	10.95	11.27	10.61	9.53	9.76	10.19	-	9.58	9.63	9.91
$\overline{\alpha}$	0.0000	10.61	10.94	10.31	9.25	9.44	9.90	8.53	9.42	9.47 (9.65)	9.83 [e]
	0.0428	10.70	11.04	10.40	9.31	9.50	9.97	-	9.47	9.52	-
	0.0570	10.78	11.12	10.46	9.35	9.55	10.03	-	9.52	9.57	-
	0.0856	11.00	11.37	10.67	9.48	9.69	10.20	-	9.65	9.71	9.92
$\Delta\alpha$	0.0000	0.05	0.19	0.06	1.14	0.84	0.38	1.11	0.43	0.78 (0.54)	-
	0.0428	0.11	0.26	0.06	1.13	0.82	0.34	-	0.41	0.76	-
	0.0570	0.16	0.33	0.08	1.12	0.80	0.32	-	0.39	0.74	-
	0.0856	0.33	0.53	0.22	1.08	0.75	0.22	-	0.34	0.67	0.67

[a]Results taken from Ref. 343

[b]Results taken from Ref. 342 using the aug-cc-pVQC

[c]Results taken from Ref. 122 using the aug-cc-pVTZ basis set. In parenthesis results taken from Ref. 371 using the d-aug-cc-pVTZ basis set.

[d]Results from Ref 372 at $\omega = 0.088$ a.u. ($\lambda = 514.5$ nm).

[e]Results taken from Ref. 126

TABLE 9.4: *Frequency-dependent polarizability of a water molecule in vacuum. Frequency (ω) and polarizability in a.u.*

therefore gives a too low mean polarizability and a too high anisotropy. Comparing with the experimental results we see that the BP-GRAC results predict larger values whereas all other results are lower than the experimental results. Since the experimental results also contain a contribution from zero-point vibrations, see Ref. 126 for an estimate of this contribution, a smaller theoretical value is expected. The frequency-dependent polarizablility for a single water molecule in a cluster of 127 classical water molecules calculated using different xc-potentials are presented in Tabel 9.5. The results are calculated for the same frequencies as in the gas-phase and are compared with results for the same water cluster obtained with the MC-SCF/MM[342] and CCSD/MM[122] method. It should be mentioned that for the results in the cluster the off-diagonal components of the polarizability tensor are different from zero. These components are not presented since they will tend to zero if a careful averaging over different solvent configurations representing the isotropic liquid is performed. Since there is a good correlation between the magnitude of the polarizability in the gas phase and in the liquid, i.e. LDA/GGA predict the largest values and MC-SCF the smallest, we will focus on trends for the shifts in the polarizability in going from gas-phase

	ω	LDA	BLYP	BP	LB94	SAOP	GRAC	MC-SCF [a]	CCSD [b]
α_{xx}	0.0000	10.51	10.79	10.25	9.79	9.80	9.91	9.54	9.66 (9.77)
	0.0428	10.57	10.85	10.31	9.84	9.84	9.96	9.58	9.70 (9.82)
	0.0570	10.61	10.90	10.35	9.88	9.88	10.00	9.62	9.74 (9.85)
	0.0856	10.75	11.05	10.48	9.98	9.99	10.11	9.71	9.83 (9.96)
α_{yy}	0.0000	11.55	12.09	11.21	9.14	9.55	10.27	9.72	9.62 (10.01)
	0.0428	11.69	12.26	11.35	9.21	9.63	10.36	9.80	9.70 (10.10)
	0.0570	11.81	12.40	11.46	9.27	9.69	10.44	9.86	9.76 (10.17)
	0.0856	12.17	12.83	11.79	9.43	9.89	10.67	10.0	9.96 (10.39)
α_{zz}	0.0000	10.93	11.28	10.64	9.63	9.85	10.15	9.82	9.82 (10.13)
	0.0428	11.02	11.37	10.72	9.69	9.91	10.21	9.88	9.88 (10.19)
	0.0570	11.08	11.45	10.78	9.73	9.96	10.26	9.92	9.92 (10.24)
	0.0856	11.28	11.66	10.96	9.86	10.10	10.41	10.0	10.05 (10.38)
$\overline{\alpha}$	0.0000	11.00	11.39	10.70	9.52	9.73	10.11	9.70	9.70 (9.97)
	0.0428	11.09	11.50	10.79	9.58	9.79	10.18	9.75	9.76 (10.04)
	0.0570	11.17	11.58	10.86	9.62	9.84	10.23	9.80	9.91 (10.09)
	0.0856	11.40	11.85	11.08	9.75	9.99	10.40	9.93	9.95 (10.24)
$\Delta\alpha$	0.0000	0.90	1.14	0.84	0.59	0.28	0.31	0.25	0.18 (0.32)
	0.0428	0.98	1.24	0.91	0.57	0.26	0.35	0.27	0.18 (0.33)
	0.0570	1.04	1.32	0.97	0.55	0.24	0.39	0.27	0.17 (0.36)
	0.0856	1.25	1.57	1.15	0.50	0.19	0.49	0.29	0.19 (0.43)

[a] Results from Ref. 342 using the aug-cc-pVQC basis set.

[b] Results from Ref. 122 using the aug-cc-pVTZ basis set. In parenthesis results using the d-aug-cc-pVTZ basis set.

TABLE 9.5: *Frequency-dependent polarizability of a water molecule in a cluster of 127 classical water molecules. Frequency (ω) and polarizability in a.u.*

to the cluster. All methods predict a decrease in the yy component and a increase in the xx and zz components leading to an overall increase in the mean polarizability. However, the LDA/GGA methods predicts an increase in the anisotropy in contrast to the other methods. The reason for this is that LDA/GGA predict a shift of ~ 0.9 a.u. in the yy components whereas the rest of the methods predicts a shift ~ 0.6 a.u. The shift in the zz component predicted with CCSD/d-aug-cc-pVTZ and MC-SCF is ~ 0.5 a.u. whereas the DFT methods predicts a shift ~ 0.3 a.u. If we compare the frequency dispersion in the anisotropy predicted with CCSD or MC-SCF we see an increase with increasing frequency, this is also found using BP-GRAC whereas LB94 and SAOP predicts a decrease.

The polarizability of liquid water has also been considered in a few other studies.[279,356,373,374] [Ref. 97, Chap. 5] In general the models[279,374] [Ref. 97, Chap. 5] which calculate the molecular polarizability by averaging over the polarizability obtained from different solvent configuration predict a lowering of the mean polarizability in going from the gas-phase to the liquid phase. The models[356,373] which, like in this work, first average the structure (or the electric field generated by the solvent) and then calculate the molecu-

lar polarizability, predict an increase in the mean polarizability in good agreement with the results of this work. This indicates that it is important to take the local fluctuation of the solvent structure into account when calculating the molecular properties.

An estimate of the frequency-dependent polarizability can be obtained from the refractive index, $n(\omega)$, by using the Lorenz-Lorentz equation[31]

$$\overline{\alpha}(-\omega;\omega) = \frac{3M_w}{4\pi N_a \rho}\frac{n(\omega)^2-1}{n(\omega)^2+2} \tag{9.41}$$

where M_w is the molecular weight, N_a Avogadro's number and ρ the density. Using the refractive index of liquid water at $\omega = 0.0428$ a.u., $n(0.0428) = 1.326$,[375] and $\rho = 0.99707\text{g/cm}^3$ we obtain a polarizaibity of $\overline{\alpha} = 9.74$ a.u. This estimate is in very good agreement with the SAOP and MC-SCF results but in less good agreement with the CCSD or BP-GRAC results. If we instead use the refractive index at $\omega = 0.077$ a.u. ($\lambda = 589.32$nm), $n = 1.33283$[376] we obtain a polarizability of $\overline{\alpha} = 9.93$ a.u again in good agreement with the SAOP and MC-SCF results at $\omega = 0.0856$ a.u. If we compare the liquid results at $\omega = 0.0428$ a.u. with the static results obtained in the gas phase we find a small decrease in the mean polarizability in going from the gas phase to the liquid phase even if we take the frequency dispersion into account.

9.6 Conclusions

We have in this work presented a Discrete Solvent Reaction Field model for calculating frequency-dependent molecular linear response properties of molecules in solution. The model combines a TD-DFT description of the solute molecule with a classical description of the discrete solvent molecules. The classical solvent molecules are represented using distributed atomic charges and atomic polarizabilities. All the atomic parameters have been chosen so as to describe molecular gas phase properties of the solvent molecule, i.e. atomic charges reproduce the molecular dipole moment and atomic polarizabilities resproduce the molecular polarizability tensor using Thole's modified dipole interaction model. As an initial applications of the model we have calculated the vertical electronic excitation energies and frequency-dependent molecular (hyper)polarizability of a water molecule in a cluster of 127 classical water molecules. The effect of using different xc-potentials has been investigated and the results have been compared with the corresponding wavefunction results obtained using combined HF, MC-SCF or CCSD method with a similar solvent model. It was shown that accurate results in agreement with the CCSD and MC-SCF results could be obtained by using xc-potentials which have the correct asymptotic behavior. The use of the shape-corrected functionals like SAOP and BP-GRAC improved the results compared with the asymptotic correct LB94. However, the use of BP-GRAC requires the IP as input and the results are strongly dependent on the input value which therefore limits the usefulness of this functional.

Acknowledgment

L.J. gratefully acknowledges The Danish Research Training Council for financial support.

Chapter 10

A DRF model for the hyperpolarizabilities of molecules in solution

L. Jensen, P. Th. van Duijnen, and J. G. Snijders "A discrete solvent reaction field model for calculating frequency-dependent hyperpolarizabilities of molecules in solution" *J. Chem. Phys.* **119**, 12998-13006, 2003.

10.1 Abstract

We present a Discrete Solvent Reaction Field (DRF) model for the calculation of frequency-dependent hyperpolarizabilities of molecules in solution. In this model the solute is described using Density Functional Theory (DFT) and the discrete solvent molecules are described with a classical polarizable model. The first hyperpolarizability is obtained in an efficient way using Time-Dependent DFT and the (2n+1) rule. The method was tested for liquid water using a model in which a water molecule is embedded in a cluster of 127 classical water molecules. The frequency-dependent first and second hyperpolarizabilities related to the Electric Field Induced Second Hamonic Generation (EFISH) experiment, were calculated both in the gas phase and in the liquid phase. For water in the gas phase, results are obtained in good agreement with correlated wavefunction methods and experiments by using the so-called shape-corrected exchange correlation (xc)-potentials. In the liquid phase the effect of using asymptotically correct functionals is discussed. The model reproduced the experimentally observed sign change in the first hyperpolarizability when going from the gas phase to the liquid phase. Furthermore, it is shown that the first hyperpolarizability is more sensitive to damping of the solvent-solute interactions at short range than the second hyperpolarizability.

10.2 Introduction

Accurate predictions of molecular response properties, like the frequency-dependent (hyper)polarizability, in the condensed phase and in the gas phase are of great interest both from a theoretical and a technological point of view.[8,12,13] However, accurate calculations of molecular properties require a quantum mechanical treatment, which, due to high computational cost, are limited to small systems. Time-Dependent Density Functional Theory (TD-DFT)[37–41] allows for the calculation of frequency-dependent response properties like electronic excitations and frequency-dependent (hyper)polarizabilities. The use of TD-DFT for calculating molecular response properties in the gas-phase has been shown to be accurate for small and medium size molecules, especially if one uses recently developed density functionals.[42–51] Therefore, the extension of TD-DFT to treat also molecules in solution is of great interest.

The calculation of response properties of molecules in condensed phase is a fundamental and important theoretical challenge, which still remains problematic. Since the molecular properties like (hyper)polarizabilities are sensitive to the local environment, an accurate calculation of these properties could serve as a test for the molecular models used in describing intermolecular forces. The most successful methods divide the total system into two parts, one the molecular system of interest which is described with a quantum mechanical method and two the rest of the system which is treated by a much simpler method, usually a classical description.[102–116] Among these methods are the combined quantum mechanical and classical mechanics models (QM/MM).[105–116] In the QM/MM methods the solvent molecules are treated with a classical force field and the interactions between the solute and solvent are described with an effective operator, so the problem that remains is to find an accurate approximate representation of the solvent molecules and the solute-solvent interactions.[248]

An example of such a QM/MM method is the Discrete Solvent Reaction Field model (DRF) which we recently developed. [Ref. 117, 118, Chaps. 8, 9] Although in this model the QM part is treated using Density Functional Theory (DFT) it is not restricted to this approach. The permanent electronic charge distribution of the solvent molecules (MM) is modeled by point charges, while distributed atomic polarizabilities are included to model the solvent polarization arising from many-body interactions. The permanent point charges represent at least the permanent molecular dipole moment, and the distributed atomic polarizabilities the full molecular polarizability tensor. The QM/MM interactions are introduced into the Kohn-Sham equations through an effective operator and all interactions are solved self-consistently, which allows the solute to be polarized by the solvent. An important feature of the model is the inclusion of polarizabilities in the MM part which allows for the solvent molecules to be polarized by the solute and by interactions with other solvent molecules. The advantages of including polarizabilities in the MM part is that all parameters can be obtained from gas phase properties. Furthermore, it is expected that a distributed polarizability approach will give better results than an approach in which one models the molecular polarizability using only a single (anisotropic) polarizability per molecule, especially as the size of the solvent molecule increases.[120] Although standard

DFT methods have problems describing van der Waals interactions, see e.g. Ref.,[377] these problems are not present here since the van der Waals interactions are treated purely classical. The van der Waals interactions are typically treated using a Lennard-Jones (LJ) potential where the LJ parameters are taken from the classical force field or optimized to the particular QM/MM method.[325] However, it is not certain that optimizing the parameters on small complexes will improve the results in a QM/MM simulation[324] of a liquid. So far the DRF model has been applied to study the dipole and quadrupole moments [Ref. 117, Chap. 8] and linear response properties like vertical excitation energies and frequency-dependent polarizability [Ref. 118, Chap. 9] of a water molecule in aqueous solution.

Therefore, as a natural extension, we will apply the Discrete Solvent Reaction Field model to calculate the frequency-dependent hyperpolarizability of a molecule in solution within TD-DFT. This allows for the discrete representation of the solvent to be retained, and electron correlation of the QM part to be included in an efficient manner. The calculation of the frequency-dependent first hyperpolarizability will be achieved efficiently by the use of the (2n+1) rule.[57] Within a QM/MM approach the treatment of frequency-dependent hyperpolarizability has only been considered in one previous study using both correlated and uncorrelated wave function based methods.[360] As in our previous study on dipole and quadrupole moments [Ref. 117, Chap. 8] and linear response properties [Ref. 118, Chap. 9] of water in aqueous solution we will adopt the same water structure for which the wave function QM/MM results exist.[360] This will allow us to asses approximate exchange-correlation (xc) potentials for calculating molecular frequency-dependent hyperpolarizabilities in solution.

10.3 Theory

10.3.1 The Discrete Reaction Field model

In the QM/MM method the total (effective) Hamiltonian for the system is written as[105–116]

$$\hat{H} = \hat{H}_{QM} + \hat{H}_{QM/MM} + \hat{H}_{MM} \tag{10.1}$$

where $\hat{H}_{QM}$ is the quantum mechanical Hamiltonian for the solute, $\hat{H}_{QM/MM}$ describes the interactions between solute and solvent and $\hat{H}_{MM}$ describes the solvent-solvent interactions. The Discrete Reaction Field model is described in [Ref. 117, Chap. 8] within ground state DFT and in [Ref. 118, Chap. 9] within time-dependent DFT for the linear response properties and are therefore only briefly outlined here. Within the Discrete Reaction Field model the QM/MM operator is given by

$$\hat{H}_{QM/MM} = \sum_i v^{DRF}(r_i, \omega) = \sum_i v^{el}(r_i) + \sum_i v^{pol}(r_i, \omega), \tag{10.2}$$

where i runs over all electrons in the QM system. The first term is the electrostatic operator describing the Coulombic interactions between the QM system and the permanent charge

distribution of the solvent molecules and is given by

$$v^{el}(r_i) = \sum_s \frac{q_s}{R_{si}} = \sum_s q_s T^{(0)}_{si}. \tag{10.3}$$

Here the zero'th order interaction tensor has been introduced and the index s runs over all atoms of the solvent molecules. The second term is the polarization operator given by

$$v^{pol}(r_i, \omega) = \sum_s \mu^{ind}_{s,\alpha}(\omega) \frac{R_{si,\alpha}}{R^3_{si}} = -\sum_s \mu^{ind}_{s,\alpha}(\omega) T^{(1)}_{si,\alpha}. \tag{10.4}$$

where $R_{si,\alpha}$ is a component of the distance vector and $\mu^{ind}_s(\omega)$ is the induced dipole at site s. For Greek indices the Einstein summation convention is employed. The polarization operator describes the many-body polarization of the solvent molecules, *i.e.*, the change in the charge distribution of the solvent molecules due to interactions with the QM part and with other solvent molecules.

For a collection of atomic polarizabilities in an electric field the induced atomic dipole at site s is given, in linear response, by[31]

$$\mu^{ind}_{s,\alpha}(\omega) = \alpha_{s,\alpha\beta}[F^{init}_{s,\beta}(\omega) + \sum_{t \neq s} T^{(2)}_{st,\beta\gamma} \mu^{ind}_{t,\gamma}(\omega)], \tag{10.5}$$

where $\alpha_{a,\alpha\beta}$ is a component of the atomic polarizability tensor at site s, which, for an isotropic atom, gives $\alpha_{s,\alpha\beta} = \delta_{\alpha\beta}\alpha_s$. Here we neglect the frequency-dependence of the classical part, *i.e.*, the atomic polarizability is frequency independent, but the model can easily be extended to include also this effect.[94] [Ref. 63, Chap. 3] $F^{init}_{s,\beta}(\omega)$ is the initial electric field at site s and consists of the field arising from the frequency-dependent electronic charge distribution of the QM part, $F^{QM,el}_{t,\beta}(\omega)$, the field arising from the QM nuclei, $F^{QM,nuc}_{t,\beta}$, and the field arising from the point charges at the solvent molecules, $F^{MM,q}_{t,\beta}$. The initial field does not include the electric field perturbing the QM part which means that the perturbing field can be identified as the local field felt by the QM molecule. This leads to the identification of the calculated properties as the solute properties, i.e the (hyper)polarizability of the solute including the solvent effects but not corrected for the difference between the local field and the macroscopic field. For a discussion of these effects and corrections within the dielectric continuum model see e.g. Ref. 29,280,281. The last term is the electric field from the other induced dipoles. It is well known that if the distance between two polarizable points become too small, the induced dipoles become infinit. In order to avoid this "polarizability catastrophe" we modified the dipole interaction tensor using smeared-out dipoles according to the model by Thole.[93] The induced dipole in Eq. 10.5 depends on the induced dipoles at the other sites, and therefore the equation should be solved self-consistently.

10.3.2 The Frequency-dependent (Hyper)Polarizability

The total dipole moment of a molecule in the presence of a time-dependent electric field, $F_\beta = F_\beta^0 + F_\beta^\omega cos(\omega t)$, can be expanded as a Taylor series in the applied electric field[27]

$$\begin{aligned}\mu_\alpha &= \mu_\alpha^0 + \alpha_{\alpha\beta}(0;0)F_\beta^0 + \alpha_{\alpha\beta}(-\omega;\omega)F_\beta^\omega \cos(\omega t) \\ &+\frac{1}{2}\beta_{\alpha\beta\gamma}(0;0,0)F_\beta^0 F_\gamma^0 + \frac{1}{4}\beta_{\alpha\beta\gamma}(0;\omega,-\omega)F_\beta^\omega F_\gamma^\omega \\ &+\beta_{\alpha\beta\gamma}(-\omega;0,\omega)F_\beta^0 F_\gamma^\omega \cos(\omega t) + \frac{1}{4}\beta_{\alpha\beta\gamma}(-2\omega;\omega,\omega)F_\beta^\omega F_\gamma^\omega \cos(2\omega t) + \cdots \quad (10.6)\end{aligned}$$

where $\alpha_{\alpha\beta}$ is the molecular polarizability and $\beta_{\alpha\beta\gamma}$ is the molecular first hyperpolarizability with (α, β, γ) designating Cartesian coordinates. The total dipole moment can be obtained from the trace of the dipole moment matrix, H^α, and the density matrix in the presence of the electric field, $P(F)$,

$$\mu_\alpha = -Tr[H^\alpha P(F)]. \quad (10.7)$$

We can expand the density matrix in a Taylor series,

$$P = P^0 + P^\beta F_\beta + \frac{1}{2!}P^{\beta\gamma}F_\beta F_\gamma + \cdots, \quad (10.8)$$

where P^0 is the unperturbed density matrix, P^β the linear response and $P^{\beta\gamma}$ the quadratic response. Inserting this expansion into Eq. 10.7 and comparing with Eq. 10.6 allows us to identify the dipole moment, the frequency-dependent polarizability, and the frequency-dependent first hyperpolarizabillity as

$$\mu_\alpha = -Tr[H^\alpha P^0] \quad (10.9)$$

$$\alpha_{\alpha\beta}(-\omega;\omega) = -Tr[H^\alpha P^\beta(\omega)], \quad (10.10)$$

$$\beta_{\alpha\beta\gamma}(-\omega_\sigma;\omega_a,\omega_b) = -Tr[H^\alpha P^{\beta\gamma}(\omega_a,\omega_b)], \quad (10.11)$$

where $\omega_\sigma = \omega_a + \omega_b$. In the following we will present how to obtain the linear and quadratic response properties using the (2n+1) rule.

10.3.3 Linear response of the density matrix

In our previous work [Ref. 118, Chap. 9] we showed, using time-dependent response theory,[37–41] how to obtain the first-order change in the density matrix, $P^\beta(\omega)$, from a set of linear equations,

$$P_{st}(\omega) = \frac{\Delta n_{st}}{(\epsilon_s - \epsilon_t) - \omega}\delta v_{st}^{eff}(\omega), \quad (10.12)$$

where Δn_{st} is the difference in occupation numbers, i.e. 1 for $st = ai$ and -1 for $st = ia$, where a denote virtual orbitals and i denote occupied orbitals. This equation now corrects

a misprint in Eqs. 21 and 25 of our previous paper.[118] The change in the effective potential, δv_{st}^{eff}, is dependent on the first order change in the density and is given by

$$\begin{aligned} \delta v_{st}^{eff}(\omega) &= \delta v_{st}^{per}(\omega) \\ &+ \int dr \phi_s^*(r) \left[v_{Coul}[\delta\rho](r,\omega) + v_{xc}[\delta\rho](r,\omega) + v^{DRF}[\delta\rho](r,\omega) \right] \phi_t(r), \end{aligned} \tag{10.13}$$

where the Coulomb term is given by

$$v_{Coul}[\delta\rho](r,\omega) = \int dr' \frac{\delta\rho(r',\omega)}{|r-r'|}, \tag{10.14}$$

the xc part in the adiabatic approximation by

$$v_{xc}[\delta\rho](r,\omega) = \int dr' \frac{\delta v_{xc}(r)}{\delta\rho(r')} \delta\rho(r',\omega), \tag{10.15}$$

and the contribution from the DRF operator by

$$v^{DRF}[\delta\rho](r_i,\omega) = -\sum_s \mu_{s,\alpha}^{ind}[\delta\rho](\omega) T_{si,\alpha}^{(1)}. \tag{10.16}$$

The DRF contribution arises from the induced dipoles in the MM part due to the first-order change in the QM charge distribution. Since the effective potential in Eq. 10.13 depends on the first-order density matrix through the potentials $v_{Coul}[\delta\rho](r,\omega)$, $v_{xc}[\delta\rho](r,\omega)$ and $v^{DRF}[\delta\rho](r_i,\omega)$ a self-consistent solution of Eq. 10.12 is required.

10.3.4 Quadratic response of the density matrix using the (2n+1) rule

In a manner similar to the linear response a set of equations for the solution of the higher order density response can be constructed.[49–51,57,58] However, a more efficient approach is to take advantage of the (2n+1) rule which allows for the quadratic response properties to be rewritten in terms of quantities obtained from the solution of the first order response equations. Within TD-DFT van Gisbergen *et al.* have shown how this is done for the frequency-dependent first hyperpolarizability[57] in an approach similar to the TD-HF approach of Karna and Dupuis.[56] Here we will present the results obtained by van Gisbergen[57] since the inclusion of the DRF operator will not affect the structure of these equations.

The frequency-dependent first hyperpolarizabilty can be rewritten using the (2n+1) rule as[57]

$$\begin{aligned} \beta_{\alpha\beta\gamma}(-\omega_\sigma;\omega_a,\omega_b) &= -Tr[H^\alpha P^{\beta\gamma}(\omega_a,\omega_b)] \\ &= \hat{p}\{(\alpha,\omega_\sigma),(\beta,\omega_a),(\gamma,\omega_b)\} Tr[nU^\alpha(-\omega_\sigma)[G^\beta(\omega_a),U^\gamma(\omega_b)]_-] \\ &+ Tr[g_{xc}(\omega_a,\omega_b)P^\alpha(-\omega_\sigma)P^\beta(\omega_a)P^\gamma(\omega_b)] \end{aligned} \tag{10.17}$$

where $[G^{\beta}(\omega_a), U^{\gamma}(\omega_b)]_-$ denotes the commutator of $G^{\beta}(\omega_a)$ and $U^{\gamma}(\omega_b)$, and $\hat{p}$ the sum of all permutations of $(\alpha, -\omega_\sigma)$, $(\beta, -\omega_a)$, and $(\gamma, -\omega_b)$. The $G^{\alpha}(\omega_a)$ matrix is the first-order KS matrix[57] and is given by

$$G^{\alpha}_{pg}(\omega) = \int dr \phi_p(r) \left\{ v^{\alpha}_{per} + v^{Coul}[\delta\rho^{\alpha}(\omega)] + v_{xc}(r)[\delta\rho^{\alpha}(\omega)](r) + v^{DRF}[\delta\rho^{\alpha}(\omega)](r) \right\} \phi_q(r) \tag{10.18}$$

which is identical to the effective potential matrix, $\delta v^{eff}(\omega_a)$, in Eq. 10.13 due to the α-component of the perturbation. The first-order transformation matrix, $U^{\alpha}(\omega)$, is given by

$$U^{\alpha}_{pq}(\omega) = \frac{G^{\alpha}_{pg}(\omega)}{\epsilon^{(0)}_q - \epsilon^{(0)}_p - \omega} \tag{10.19}$$

and is only nonzero for the occupied-virtual block.[57] The last term in Eq. 10.17 is an additional term in the DFT expression which is not present in the TDHF case and is given by

$$Tr[g_{xc}(\omega_a, \omega_b) P^{\alpha}(-\omega_\sigma) P^{\beta}(\omega_a) P^{\gamma}(\omega_b)] = \int dr \int dr' \int dr'' g_{xc}(r, r', r'', \omega_a, \omega_b) \delta\rho^{\alpha}(r, -\omega_\sigma) \delta\rho^{\beta}(r', \omega_a) \delta\rho^{\gamma}(r'', \omega_b), \tag{10.20}$$

where the xc kernel, g_{xc}, has been introduced,

$$g_{xc}(r, r', r'', \omega_a, \omega_b) = \left. \frac{\delta^2 v_{xc}(r)}{\delta\rho(r', \omega_a)\delta\rho(r'', \omega_b)} \right|_{\rho^{(0)}}. \tag{10.21}$$

Usually the adiabatic approximation is invoked for this kernel,

$$g_{xc}(r, r', r'', \omega_a, \omega_b) \simeq g_{xc}(r, r', r'', 0, 0). \tag{10.22}$$

10.3.5 Implementation

The DRF model has been implemented into a local version of the Amsterdam Density Functional (ADF) program package.[340,361] The extension to the TD-DFT part has been implemented into the RESPONSE module of ADF.[57,130,289] In the RESPONSE module the functional derivative of the xc-potential in Eq. 10.15 and 10.21 is restricted to the Adiabatic LDA (ALDA) xc-potential. The linear equations for the first-order density matrix in Eq. 10.12 is solved using an efficient iterative algorithm,[130] and, for that reason, the DRF response operator, Eq. 10.16, is calculated by solving a set of linear equations like in Eq. 10.5. In ADF the KS equations and the linear response equations are solved by numerical integration and the numerical integration grid is chosen on the basis of the quantum part alone. Therefore, care must be taken when evaluating the DRF operator if the integration points are close to a classical atom. In order to avoid numerical instabilities we introduce a damping of the operators at small distances. This is done by replacing the point charge by a gaussian charge distribution with a unit width and the point dipoles are also smeared out in a similar manner [Ref. 63, 117, 118, Chaps. 3, 8, 9].

10.4 Computational details

The water structure used in this work, taken from Ref. 338, consists of 128 rigid water molecules where one molecule is treated quantum mechanically. The total structure was obtained from a MD simulation using a polarizable force field.[327] Details about the simulation can be found in Ref. 122,342 and will be summarized here for consistency. The average geometry is obtained from a simulation of a box containing 128 water molecules utilizing periodic boundary conditions with a spherical cut-off distance of 10.0 Å, at a temperature of 298 K, and a pressure of 0.103 MPa. After equilibration, the average geometry was obtained from a Boltzmann sampling of 8000 trajectories started with different initial velocity distributions and a simulation time of 20 ps for each trajectory. The intra-molecular geometry of the water molecules was that as in the gas phase, *i.e.* $R_{O-H} = 0.9572$ Å and $\angle_{HOH} = 104.49°$. The solute water molecule was placed in the xz-plane with the z-axis bisecting the H-O-H angle.

The basis set used in this work consists of a large even-tempered basis set of Slater-type orbitals with orbital exponent $\zeta = \alpha\beta^i$, $i = 1, \cdots n$ (details given in [Ref. 118, Chap. 9]). Different xc potentials have been tested: the Local Density Approximation (LDA), Becke-Lee-Yang-Parr (BLYP),[138,139] the Becke-Perdew (BP),[138,341] the van Leeuwen-Baerends (LB94),[141] the statistical averaging of (model) orbital potentials (SAOP),[45,362,363] and the potential obtained from the gradient-regulated asymptotic connection procedure applied to the BP potentials (BP-GRAC).[47,48] The BLYP and BP are examples of typical Generalized Gradient Approximations (GGAs) potentials and the LB94 is an example of an asymptotically correct potential. Whereas SAOP and BP-GRAC belong to a class of shape-corrected potentials, which yield the correct asymptotic behavior. The BP-GRAC potential sets the HOMO level at the first ionization potential (IP) and therefore requires the IP as input. The SAOP xc-potential requires no additional input and the energy of the HOMO corresponds well with the IP.[48,364] For this reason the IP needed as input for the BP-GRAC xc-potential is taken from the SAOP gas-phase calculation, i.e IP = 0.45 a.u.

The parameters needed for the solvent molecules, i.e. point charges and atomic polarizabilities, were taken from [Ref. 117, Chap. 8]. The point charges are $q_H = 0.3345$ a.u. and $q_O = -0.6690$ a.u. which generate a molecular dipole moment of 1.88 Debye. The atomic polarizabilities are $\alpha_H = 0.0690$ a.u. and $\alpha_O = 9.3005$ a.u. which reproduced the molecular polarizability tensor with a mean polarizability of 9.62 a.u. and a polarizability anisotropy of 0.52 a.u. The screening parameter, $a = 2.1304$, was taken from Ref. 163.

From the analytically calculated frequency-dependent first hyperpolarizability in Eq. 10.17 we can obtain the second hyperpolarizability by using finite field differentiation. We have calculated the frequency-dependent second hyperpolarizability associated with the electric field induced second harmonic generation (EFISH) experiments by finite field differentiation of the second harmonic generation (SHG) first hyperpolarizability as

$$\gamma_{\alpha\beta\gamma\delta}(-2\omega;\omega,\omega,0) = \frac{\beta^{F_\delta}_{\alpha\beta\gamma}(-2\omega;\omega,\omega) - \beta^{0}_{\alpha\beta\gamma}(-2\omega;\omega,\omega)}{F_\delta} \tag{10.23}$$

where the field strength $F_\delta = 0.001$ a.u. was used. We will in this work use atomic units (a.u.) but the conversion factor to cgs units are[15] for β: 1 a.u. $= 8.6392 \times 10^{-33}$ esu and for γ: 1 a.u. $= 5.0367 \times 10^{-40}$ esu.

10.5 Results

10.5.1 The first hyperpolarizability

In Table 10.1 we present the static and frequency-dependent first hyperpolarizability, $\beta(-2\omega;\omega,\omega)$, at frequencies $\omega = 0.0428, 0.0570, 0.0856$ a.u.($\lambda = 1064, 800, 532$ nm, respectively) of water in the gas phase calculated with the different xc potentials. The mean first hyperpolarizability, $\overline{\beta}$, defined as[15]

$$\overline{\beta} = \frac{1}{5}\sum_{\alpha}(\beta_{z\alpha\alpha} + \beta_{\alpha z\alpha} + \beta_{\alpha\alpha z}) = \frac{3}{5}(\beta_{zzz} + \beta_{zyy} + \beta_{zxx}) \tag{10.24}$$

is also presented in Table 10.1. The last equality is only valid in the static case or when Kleinman symmetry is adopted as is done in this work. The results are compared with results obtained from different wave function methods, *i.e.*, HF,[360] MC-SCF,[360] CCSD,[371] and CCSD(T) results.[343]

From the results in Table 10.1 it is clear that the LDA/GGA (BLYP and BP) functionals overestimate the first hyperpolarizability as compared to the accurate CCSD and CCSD(T) wave function results. The asymptotically correct (AC) xc-potentials , LB94, SAOP and BP-GRAC, all produce numbers in good agreement with the CCSD and CCSD(T) results. The overestimation of the first hyperpolarizability using LDA and GGA's (BLYP and BP) and the improvement upon this using AC potentials are well established for small molecules.[45,48,129,378] Comparing the HF and MC-SCF results with the CCSD/CCSD(T) results we see that the results are underestimated, especially the HF results are underestimated illustrating the importance of electron correlations. Furthermore, comparing the frequency-dispersion of the mean first hyperpolarizability, we see that the increase in the hyperpolarizability, $\Delta\overline{\beta}_{\mathrm{d}isp}$, with increasing frequency is considerably larger with LDA/GGA than with the AC potentials and the HF and MC-SCF wave function results. The AC potentials predict a larger frequency-dispersion increase than HF and MS-SCF. From the results in Table 10.1 it is also seen that the frequency-dispersion is significant even for the lowest frequencies. It is therefore important to take this into account.

The static and frequency-dependent first hyperpolarizability of a water molecule in a cluster of 127 classical water molecules are presented in Table 10.2. The frequencies used are the same as in the gas phase and the results are compared with results for the same water cluster obtained using the HF/MM[360] and the MC-SCF/MM[360] method. Also presented is the solvation shift, $\Delta\overline{\beta}_{solv}$, i.e. the relative change in the first hyperpolarizability upon solvation. Due to the symmetry of the water cluster components other than the ones presented in Table 10.2 are also nonzero but these components have not been

	LDA	BLYP	BP	LB94	SAOP	GRAC	HF[a]	MC-SCF[a]	CCSD[b]	CCSD(T)[c]
β_{zzz}	-19.70	-20.65	-17.79	-13.11	-13.69	-14.98	-7.30	-10.8	-13.97	-13.8
β_{zyy}	-9.01	-8.35	-7.51	-4.47	-4.78	-5.96	-1.23	-4.27	-5.66	-5.5
β_{zxx}	-11.80	-13.38	-11.59	-10.03	-10.28	-10.41	-9.36	-8.90	-9.92	-9.8
$\overline{\beta}$	-24.31	-25.43	-22.13	-16.57	-17.25	-18.81	-10.73	-14.38	-17.73	-17.5
					$\omega = 0.0428$					
β_{zzz}	-21.97	-23.16	-19.71	-14.21	-14.92	-16.38	-7.81	-11.6	-15.12	
β_{zyy}	-10.08	-9.32	-8.33	-4.82	-5.18	-6.49	-1.25	-4.54	-6.07	
β_{zxx}	-12.86	-14.69	-12.57	-10.69	-10.94	-11.17	-9.83	-9.41	-10.53	
$\overline{\beta}$	-26.95	-28.30	-24.37	-17.83	-18.62	-20.42	-11.33	-15.33	-19.03	
$\Delta\overline{\beta}_{disp}$[d]	10.9%	11.3%	10.1%	7.6%	7.9%	8.6%	5.6%	6.6%	7.3%	
					$\omega = 0.0570$					
β_{zzz}	-24.02	-25.44	-21.43	-15.16	-15.99	-17.60	-8.25	-12.4		
β_{zyy}	-11.04	-10.17	-9.04	-5.11	-5.52	-6.95	-1.26	-4.76		
β_{zxx}	-13.80	-15.83	-13.44	-11.25	-11.55	-11.83	-10.2	-9.84		
$\overline{\beta}$	-29.32	-30.86	-26.35	-18.91	-19.84	-21.83	-11.83	-16.20		
$\Delta\overline{\beta}_{disp}$[d]	20.6%	21.4%	19.1%	14.1%	15.0%	16.1%	10.3%	12.7%		
					$\omega = 0.0856$					
β_{zzz}	-32.01	-34.44	-27.97	-18.55	-19.85	-22.06	-9.73	-15.0		
β_{zyy}	-14.63	-13.23	-11.62	-6.10	-6.70	-8.54	-1.26	-5.69		
β_{zxx}	-17.39	-20.28	-16.67	-13.20	-13.70	-14.17	-11.5	-11.3		
$\overline{\beta}$	-38.42	-40.77	-33.76	-22.71	-24.15	-26.86	-13.49	-19.19		
$\Delta\overline{\beta}_{disp}$[d]	58.0%	60.3%	52.6%	37.1%	40.0%	42.8%	25.7%	33.4%		

[a] Results from Ref. 360
[b] Results from Ref. 371
[c] Results from Ref. 343
[d] $\Delta\overline{\beta}_{disp} = \left(\overline{\beta}(-2\omega;\omega,\omega) - \overline{\beta}(0;0,0)\right)/\overline{\beta}(0;0,0)$

TABLE 10.1: *Static and frequency dependent SHG first hyperpolarizability, $\beta(-2\omega;\omega,\omega)$, for water in the gas phase. All results are in a.u.*

presented, since these components should tend to zero, by considering more solvent configurations, thereby creating a more realistic isotropic solvent environment by averaging over the different solvent configurations.

First it is noted that all methods predict a sign change for the first hyperpolarizability in going from the gas phase to the liquid phase. This sign shift is theoretically well established for methods containing some discrete water molecules in the description.[277,356,360,373,379] As in the gas phase, the LDA/GGA results are larger than those from the AC potentials, but now the MC-SCF/MM results are the largest. The HF/MM results are also larger than the results from the AC potentials. However, the main difference between the wave function results and the DFT results is in $\Delta\overline{\beta}_{solv}$. The wave function methods predict a shift of $\sim 180 - 200\%$ whereas the DFT methods predict a lower solvation shift of $\sim 120 - 150\%$. Part of this difference is not due to differences between the wave function methods and DFT, but it is due to the inclusion of the damping of the DRF operator at short distances. To illustrate this we calculated the mean first hyperpolarizaiblity, using the BP-GRAC xc-potential without the damping of the DRF operator, which increases

	LDA	BLYP	BP	LB94	SAOP	GRAC	HF [a]	MC-SCF[a]
β_{zzz}	10.85	12.83	10.82	4.84	6.51	8.33	9.87	14.9
β_{zyy}	6.68	9.03	7.50	3.57	4.41	5.775	6.45	8.21
β_{zxx}	0.79	0.81	0.14	-2.61	-1.89	-0.78	-1.82	0.56
$\overline{\beta}$	10.99	13.60	11.08	3.48	5.42	7.99	8.70	14.20
$\Delta\overline{\beta}_{solv}$ [b]	145.2%	153.5%	150.1%	121.0%	131.4%	142.5%	181.1%	198.7%
$\omega = 0.0428$								
β_{zzz}	11.63	13.85	11.58	5.05	6.87	8.79	10.4	15.8
β_{zyy}	7.30	10.05	8.24	3.81	4.74	6.20	6.90	8.88
β_{zxx}	1.05	1.10	0.33	-2.66	-1.89	-0.71	-1.82	0.72
$\overline{\beta}$	11.99	15.00	12.09	3.72	5.83	8.57	9.29	15.24
$\Delta\overline{\beta}_{solv}$ [b]	144.5%	153.0%	149.6%	120.9%	131.3%	142.0%	182.0%	199.4%
$\omega = 0.0570$								
β_{zzz}	12.30	14.74	12.24	5.22	7.17	9.18	10.8	16.5
β_{zyy}	7.84	10.99	8.89	4.02	5.03	6.57	7.27	9.47
β_{zxx}	1.29	1.37	0.50	-2.70	-1.88	-0.69	-1.81	0.86
$\overline{\beta}$	12.86	16.26	12.98	3.92	6.19	9.04	9.76	16.10
$\Delta\overline{\beta}_{solv}$ [b]	143.9%	152.7%	149.3%	120.7%	131.2%	141.4%	182.5%	199.4%
$\omega = 0.0856$								
β_{zzz}	14.66	18.00	14.58	5.77	8.16	10.46	12.1	19.2
β_{zyy}	9.90	14.75	11.44	4.72	6.02	7.87	8.56	11.7
β_{zxx}	2.19	2.42	1.16	-2.82	-1.82	-0.36	-1.79	1.41
$\overline{\beta}$	16.05	21.10	16.31	4.60	7.42	10.78	11.32	19.39
$\Delta\overline{\beta}_{solv}$ [b]	141.8%	151.8%	148.3%	120.3%	130.7%	140.1%	183.9%	201.0%

[a] Results from Ref. 360

[b] $\Delta\overline{\beta}_{solv} = \left(\overline{\beta}_{liquid} - \overline{\beta}_{gas}\right)/\overline{\beta}_{gas}$

TABLE 10.2: *Static and frequency dependent SHG first hyperpolarizability, $\beta(-2\omega;\omega,\omega)$, for water in a cluster of 127 classical water molecules. All results are in a.u.*

the first hyperpolarizaiblity from $\overline{\beta} = 7.99$ a.u. to $\overline{\beta} = 11.92$ a.u. in closer agreement with the MC-SCF results. This indicates that the damping, although not optimized to treat this, mimics the short range repulsion due to the overlapping charge densities of the QM part and the MM part. The damping is dependent on the width of the gaussian charge distribution, which in this work was taken to be unit (a.u.). However, both a slightly smaller width[380] and slightly larger width[381] have been suggested. Although further investigation of optimizing this damping to treat the short range repulsion should be carried out, it is expected to be more realistic to retain it in its present form than to ignore it completely. Similar approaches of employing screened charge interactions has also been used in other QM/MM studies.[112,335,380–382]

Furthermore, from the results in Table 10.2, we see that $\Delta\overline{\beta}_{solv}$ is almost independ-

ent of the frequency-dispersion, although the DFT methods predict a slight decrease in the solvation shift with increasing frequency and the wave function methods predict a slight increase with increasing frequency. This apparent frequency independence of $\Delta\overline{\beta}_{solv}$ could results from the neglect of the frequency-dependence of the classical environment in Eq. 10.5. Other theoretical models,[356,373,379] where the molecular properties are calculated at the MP2 level of theory in the presence of a field from effective point charges representing the discrete solvent environment, in general predict a larger mean first hyperpolarizability ~ 25 a.u. (in the gas phase ~ -18 a.u.), but the results are strongly dependent on the actual representation of the local environment.[356,373,379]

10.5.2 The second hyperpolarizability

In Table 10.3 the static and frequency-dependent EFISH second hyperpolarizability, $\gamma(-2\omega;\omega,\omega,0)$, at the frequency $\omega = 0.0428$ a.u. ($\lambda = 1064$ nm) of water in the gas phase calculated using different xc potentials is presented. The mean second hyperpolarizability, $\overline{\gamma}$, defined as[15]

$$\overline{\gamma} = \frac{1}{15}\sum_{\alpha\beta}\gamma_{\alpha\alpha\beta\beta}+\gamma_{\alpha\beta\alpha\beta}+\gamma_{\alpha\beta\beta\alpha} = \frac{1}{5}(\gamma_{xxxx}+\gamma_{yyyy}+\gamma_{zzzz}+2\gamma_{zzxx}+2\gamma_{xxyy}+2\gamma_{yyzz}) \quad (10.25)$$

is also presented, where again the last equality assumes Kleinman symmetry. The results are compared with HF[343] and CCSD(T)[343] wave function results. As was the case for the first hyperpolarizability, the second hyperpolarizability is overestimated by as much as a factor of two using LDA/GGA as compared with the results from the AC potentials. Comparing with the wave function results we see that there is good agreement between the BP-GRAC results and the CCSD(T) results, and that HF considerably underestimates by nearly a factor of two. Also, for the second hyperpolarizability the frequency-dispersion, $\Delta\overline{\gamma}_{disp}$, is overestimated by a factor of about two using LDA/GGA as compared with the results from the AC potentials. The static and frequency-dependent EFISH second hyperpolarizabilities for a water molecule in a cluster of 127 classical water molecules calculated using different xc-potentials are presented in Table 10.4. The frequency used for the EFISH second hyperpolarizability is the same as in the gas phase, i.e. $\omega = 0.0428$ a.u. ($\lambda = 1064$ nm). Also presented in Table 10.4 is the solvation shift, $\Delta\overline{\gamma}_{solv}$. Again, LDA/GGA results overestimate by a factor of two the results obtained using the AC potentials. In comparison with the solvation shift for the first hyperpolarizability the solvation shift in the second hyperpolarizability is much smaller for all xc-potentials. The main reason for this small difference in $\Delta\overline{\gamma}_{solv}$ predicted by LDA/GGA and the AC potentials is the different behavior of the individual tensor components upon solvation. That the xc-potentials predict different behavior upon solvation can be illustrated by considering the solvation shift in γ_{yyyy}, which is $\sim 29\%$ for LDA but only $\sim 19\%$ for BP-GRAC. We also see that $\Delta\overline{\gamma}_{solv}$ is more sensitive to the frequency-dispersion than was the case for the first hyperpolarizability, and that an increase in frequency gives a decrease in the solvation shift. The effect of damping the DRF operator was found to be smaller for the second hyperpolarizability than for the

	LDA	BLYP	BP	LB94	SAOP	GRAC	HF [a]	CCSD(T)[a]
γ_{xxxx}	1425.2	1586.7	1386.2	706.35	786.47	880.23	569	836
γ_{yyyy}	5301.8	6425.7	5163.9	1666.0	2080.6	2793.9	1422	2650
γ_{zzzz}	2573	2545	2222	1103	1316	1553	907	1481
γ_{zzxx}	1275.4	1511.2	1214.4	435.01	526.33	468.24	287	439
γ_{xxyy}	1366.5	1567.2	1268.4	470.51	578.3	683.9	338	633
γ_{yyzz}	1361.9	1526.6	1244	473.9	580.1	751.6	389	711
$\overline{\gamma}$	3461.5	3953.5	3245.1	1246.8	1510.5	1806.9	985	1706
$\omega = 0.0428$								
γ_{xxxx}	1577.2	1768.7	1531.5	752.38	842.05	944.55		
γ_{yyyy}	6404.7	7897.0	6213.4	1849.9	2342.0	3170.5		
γ_{zzzz}	2913	2881	2504	1197	1439	1702		
γ_{zzxx}	1614.6	1954.1	1528.0	495.78	608.61	518.41		
γ_{xxyy}	1581.2	1827.4	1460.0	514.2	637.8	753.5		
γ_{yyzz}	1691	1920.6	1533.1	533.4	661.9	872.7		
$\overline{\gamma}$	4133.7	4790.2	3858.2	1377.2	1687.9	2021.3		
$\Delta\overline{\gamma}_{disp}$ [b]	19.4%	21.2%	18.9%	10.5%	11.7%	11.9%		

[a] Results from Ref. 343

[b] $\Delta\overline{\gamma}_{disp} = \left(\overline{\gamma}(-2\omega;\omega,\omega,0) - \overline{\gamma}(0;0,0,0)\right)/\overline{\gamma}(0;0,0,0)$

TABLE 10.3: *Static and frequency dependent EFISH second hyperpolarizability,* $\gamma(-2\omega;\omega,\omega,0)$ *for water in the gas phase. All results are in a.u.*

first hyperpolarizability, e.g. the static mean second hyperpolarizability calculated with BP-GRAC increased from $\overline{\gamma} = 1908.5$ a.u. to $\overline{\gamma} = 1967.8$ a.u. by ignoring the damping.

Previous results calculated at the MP2 level of theory[356] for the static mean second hyperpolarizability of water in the liquid phase gave $\overline{\gamma} = 2417$ a.u. (in the gas phase $\overline{\gamma} = 1654$ a.u.[356]). This result was obtained by calculating the second hyperpolarizability in the presence of an average electric field representing the discrete molecular solvent environment. The solvation shift both for the first and second hyperpolarizabilities predicted in that work is found to be larger than what we predict in this work.

10.5.3 Comparison with experiment

In the gas phase there have been two EFISH experiments from which the first and second hyperpolarizability of water have been determined; one at $\omega = 0.0428$ a.u. ($\lambda = 1064$ nm)[127] and one at $\omega = 0.0656$ a.u. ($\lambda = 694.3$ nm).[383] In the EFISH experiment the measured quantity is[127]

$$\Gamma(-2\omega;\omega,\omega,0) = \overline{\gamma}(-2\omega;\omega,\omega,0) + \frac{\mu\overline{\beta}(-2\omega;\omega,\omega)}{3kT} \tag{10.26}$$

from which the individual contributions can be extracted if one knows the dipole moment μ by performing the experiment at different temperatures. As discussed and clearified by

	LDA	BLYP	BP	LB94	SAOP	GRAC
γ_{xxxx}	1437.1	1693.0	1325.3	679.4	761.0	821.5
γ_{yyyy}	6479.9	7742.3	6309.1	2002.3	2509.9	3246.8
γ_{zzzz}	2473.0	2827.0	2276.0	1141.2	1345.7	1505.2
γ_{zzxx}	757.7	921.8	691.0	353.0	408.9	453.2
γ_{xxyy}	1479.8	1744.1	1388.2	487.6	596.4	747.2
γ_{yyzz}	1439.0	1704.4	1368.6	525.9	640.1	784.1
$\overline{\gamma}$	3548.6	4200.58	3361.2	1311.2	1581.5	1908.5
$\Delta\overline{\gamma}_{solv}$ [a]	2.5%	6.2%	3.6%	5.2%	4.7%	5.6%
0.0428						
γ_{xxxx}	1592.3	1888.0	1465.0	721.3	812.7	877.3
γ_{yyyy}	7821.4	9531.4	7593.9	2226.5	2830.2	3670.2
γ_{zzzz}	2762.0	3182.0	2532.0	1229.8	1460.2	1629.4
γ_{zzxx}	854.8	1048.5	776.1	382.7	446.6	494.4
γ_{xxyy}	1697.3	2023.4	1585.2	528.7	652.0	818.5
γ_{yyzz}	1754.0	2129.0	1661.9	586.9	724.4	892.6
$\overline{\gamma}$	4157.6	5000.6	3927.5	1434.8	1749.8	2117.6
$\Delta\overline{\gamma}_{solv}$ [a]	5.4%	4.4%	1.8%	4.2%	3.7%	4.8%

[a] $\Delta\overline{\gamma}_{solv} = \left(\overline{\gamma}_{liquid} - \overline{\gamma}_{gas}\right)/\overline{\gamma}_{gas}$

TABLE 10.4: *Static and frequency dependent EFISH second hyperpolarizability, $\gamma(-2\omega;\omega,\omega,0)$ for water in a cluster of 127 classical water molecules. All results are in a.u.*

Willetts *et al.*,[27] different conventions are often used in experiments and in calculations. It is therefore important to bring all results to the same convention before comparing (For the definition of the different conventions see Ref. 27). In this work the Taylor series (**T**) convention is used and all values are converted into this convention (see Ref 27 for details). For clarity all details of the conversion are reported. The first experiment at $\omega = 0.0656$ a.u.[383] reported a value of $\overline{\beta} = -94 \pm 4 \times 10^{-33}$esu $= -11 \pm 0.5$ a.u. measured in the **B** convention. Converting this to the **T** convention gives $\overline{\beta} = (-11 \pm 0.5) \times 2 = -22 \pm 1$ a.u. For the second hyperpolarizability the reported value[383] is $\overline{\gamma} = 194 \pm 10 \times 10^{-39}$esu $= 385 \pm 20$ a.u. in the **B** convention and converting it to the **T** convention gives $\overline{\gamma} = (385 \pm 20) \times 6 = \mathbf{2}310 \pm 120$ a.u. The second experiment at $\omega = 0.0428$ a.u.[127] reported $\overline{\beta} = -19.2 \pm 0.9$ a.u. and $\overline{\gamma} = \mathbf{1}800 \pm 150$ a.u., both values reported in the **T** convention. Comparing these results with the calculated results for the first hyperpolarizability in Tabel 10.1 and the second hyperpolarizability in 10.3, we find good agreement with the SAOP, BP-GRAC, CCSD and CCSD(T) results, showing the ability of these methods to describe the first and second hyperpolarizability of water in the gas phase.

For liquid water there has been one EFISH experiment at $\omega = 0.0428$ a.u.[384] Reported was a value of $\Gamma = 1.44 \times 10^{-36}$esu $= 2859$ a.u. in the **X** convention which, converting to the **T** convention, gives $\Gamma = 2859 \times 4 = \mathbf{1}1436$ a.u. The value was measured relative to a

reference standard for which a quartz crystal was used with a value of $d_{11} = 0.8 \times 10^{-9}$ esu = 0.335 pm/V. However, the currently accepted value for quartz is $d_{11} = 0.30$ pm/V.[385,386] In order to extract the contribution from the first hyperpolarizability they used an estimate for the second hyperpolarizability of $\overline{\gamma} = 0.3 \times 10^{-36}$ esu = 595.6 a.u. in the **X** convention. Converting this to the **T** convention and correcting for the difference in reference values of quartz, gives $\overline{\gamma} = 5.95.6 \times 4 \times 0.30/0.335 = \mathbf{2}133.6$ a.u. This value is in good agreement with our result obtained with the BP-GRAC potential. Furthermore, an estimate of the dipole moment in liquid water, μ_{liquid}, was made by relating it to the gas phase dipole moment, μ_{gas}, and the Kirkwood correlation parameter, g, as $\mu_{liquid} = g \times \mu_{gas}$. Using this, an estimate for the first hyperpolarizability was reported as $\overline{\beta} = 0.46 \times 10^{-31}$ esu = 5.3 a.u. in the **X** convention. Converting it to the **T** convention and correcting for the reference values, gives $\overline{\beta} = 5.3 \times 4 \times 0.30/0.335 = \mathbf{1}9.1$ a.u. This value for the first hyperpolarizability of liquid water is considerably larger than the values obtained in this work, even if the damping of the DRF operator at short distances is ignored, but the sign change found experimentally is reproduced in the calculations. However, previous theoretical studies[356,373,379] indicate that especially the first hyperpolarizability of water in the condensed phase is sensitive to the local environment. An indication of this is also seen in this work, since the first hyperpolarizability is much more sensitive to the damping of the DRF operator than the second hyperpolarizability. Therefore, it can be expected that especially the value for $\overline{\beta}$ will change if a more realistic local solvent environment is used in the calculations. Further investigation of the sensitivity of the first and second hyperpolarizabilty to changes in the local discrete environment has to be made before anything conclusive can be said.

10.6 Conclusions

In this work we presented a Discrete Solvent Reaction Field (DRF)model for the calculation of frequency-dependent hyperpolarizabilities of molecules in solution. The DRF model combines a Density functional Theory (DFT) description of the solute with a polarizable classical description of the discrete solvent molecules. The first hyperpolarizability is obtained in an efficient way within Time-Dependent DFT by using the (2n+1) rule to reformulate the quadratic reponse equations into contributions known from a solution of the linear response equations. The method was tested for a water molecule embedded in a cluster of 127 classical water molecules. Frequency-dependent first and second hyperpolarizabilities related to the Electric Field Induced Second Hamonic Generation (EFISH) experiment were calculated both in the gas phase and in the liquid phase. For water in the gas phase, results in good agreement with high-level correlated wave function methods and experiments were obtained by using the so-called shape-corrected xc-potentials (SAOP and BP-GRAC). In the liquid phase the effect of using asymptotically correct functionals was discussed. It was shown that the first hyperpolarizability was more sensitive to damping of the interactions at short range than the second hyperpolarizability. The experimental change of sign for the first hyperpolarizability in going from gas to liquid was reproduced

with the model.

Acknowledgment

L.J. thanks Professor David P. Shelton for valuable comments on the conventions used in the liquid phase EFISH experiments for water. L.J. gratefully acknowledges The Danish Research Training Council for financial support.

Summary

The subject of this thesis is the modelling of molecular optical response properties and the application of these models to nanostructures. There is a lot of interest in nonlinear optical (NLO) properties of materials both from a technological and a scientific point of view. The technological aspect deals with the construction and application of these new nonlinear materials in future electronic and photonic devices. These new devices could lead to a new generation of information technology. The scientific interest lies in, besides that it is a great challenge to accurately predict NLO effects theoretically, that an understanding of these NLO effects could give a fundamental insight into how bulk properties of condensed phase matter emerge from the properties of its individual atoms or molecules.

Sophisticated quantum chemical methods would in principle be ideal tools to investigate these effects, however, these methods can only be applied on rather small molecules. Therefore, for large molecules and assemblies of molecules, modelling is currently restricted to less sophisticated methods. In this thesis we have developed methods to calculate the nonlinear optical properties of nanostructures, *i.e.*, molecules or assemblies of molecules containing several thousand atoms. As an application of these models we have investigated the NLO properties of fullerenes, carbon nanotubes, large clusters of C_{60} molecules and molecules in solution.

As a general introduction to this thesis we review the basic concepts of nonlinear optics, i.e., the expansion of the total macroscopic polarization in a material in powers of the macroscopic electric field where the expansion coefficients define the macroscopic (nonlinear) susceptibilities. Similarly, the total microscopic polarization is expanded in terms of the total microscopic electric field with expansion coefficients defining the microscopic (nonlinear) polarizabilities. By adopting a local field ansatz we show how to define a set of effective microscopic properties which can be related to the macroscopic properties. This ansatz is based on splitting the total system into a macroscopic region containing a large microscopic virtual cavity, in which the discrete electric field arising from the molecules is considered in detail. Since the discrete electric field depends strongly on the local configuration of the molecules inside the cavity this field should be considered explicitly within the microscopic model adopted for the calculations of the nonlinear properties. Further-

more, the discrete electric field is split into two components. The first part arises from the interactions of the macroscopic electric field with the other molecules in the cavity, i.e. it accounts for the induced polarization of the surrounding molecules due to the macroscopic electric field. The second part accounts for the interactions between the molecules when there is no macroscopic electric field present. However, depending on the theoretical model used for describing the microscopic region, this spitting of the discrete electric field is not always possible nor necessary.

Since the discovery of the C_{60} fullerene there have been numerous investigations of its linear and nonlinear optical properties. Both experiment and theory have shown that the third-order nonlinearity of C_{60} is smaller than first assumed. For this reason the possibilities of enhancing the nonlinearities of fullerenes by means of either endohedral, exohedral or substitutional doping is of considerable interest. We have studied the changes in the second hyperpolarizability (γ) by substituting carbon atoms in C_{60} with B or/and N. The second hyperpolarizability of the doubly substitute-doped fullerenes C_{58}NN, C_{58}BB and C_{58}BN has been calculated using time-dependent density functional theory (TD-DFT) and compared with C_{60}. Using TD-DFT we only find small changes in the γ when doping with either 2B or 2N. Although an increase with 50% was found when doping C_{60} with both B and N the effect of doping was in general found to be very small.

An alternative approach to quantum chemical methods is based on representing the molecule as a set of interacting induced point dipoles. In an external field, atomic dipole moments are induced which interact with each other. An anisotropic molecular polarizability tensor is thus obtained even though isotropic (atom-type) atomic polarizabilities are adopted in the model. The molecular γ^{mol} is obtained analogously by including also an atomic γ in the interaction model. It has furthermore been demonstrated that damping of the interatomic interactions at short distances is crucial. We have developed an point dipole interaction (PDI) model along these lines based on a parametrization of molecular polarizabilities (α^{mol}) obtained from quantum chemical calculations. The model includes the frequency dependence of α^{mol}, an improved damping term, and γ^{mol}. By adopting atomic polarizabilities in addition to atom-type parameters describing the damping and the frequency-dependence, respectively, the model is found to reproduce the molecular frequency-dependent polarizability tensor calculated with *ab initio* methods at the Hartee-Fock level of theory. It is also demonstrated that the differences for γ^{mol} between quantum chemical calculations and the PDI model are on average around 10% and below 30%. Although, Hartree-Fock calculations by no means represent the true answer, it is encouraging that a simple model like the PDI model can reproduce quantum chemical results consistently. It should therefore be relatively straightforward to reparametrize the model when more sophisticated quantum chemical methods become routine for medium-sized molecules.

The PDI model developed can be used to calculate the properties of large molecules and cluster of molecules. Therefore, we can use the PDI model to calculate the effective molecular properties which can be related the measurable macroscopic properties. This can be done by calculating the molecular properties per molecule and extend the cluster until no changes are observed in the properties. However, if one is interested in obtaining

the molecular properties of the individual members of the cluster the total response has to be distributed over the molecules. We have developed a Localized PDI (LPDI) model which enables α and γ to be divided into fragment contributions.

An important concept in the design of new NLO materials is the scaling behaviour of the optical properties with increasing size. In the limit of infinitely long chains, both α^{mol} and γ^{mol}, will scale linearly with the length of the chain. In particular, the so-called saturation length, i.e. where the property (α^{mol} or γ^{mol}) starts to scale linearly with increasing size of the system, is of interest. We have used the PDI model to calculate γ^{mol} of carbon nanotubes on the length scale up to 75 nm. It is demonstrated that an atomistic representation of mesoscale systems like nanotubes can be used to obtain a cubic response property up to the saturation length. It is found that these are comparable to conjugated polymers with respect to the magnitude of γ^{mol} and is therefore promising as a candidate for future NLO materials.

The dipole-dipole polarizability, α, and the second hyperpolarizability, γ, as well as the corresponding linear and third-order susceptibilities, $\chi^{(1)}$ and $\chi^{(3)}$, have been calculated for C_{60} fullerene clusters using the PDI model. The size dependences of a linear chain, a mono-layer film, and a face-centered cubic crystal cluster have been investigated. It is found that the effects of the surrounding molecules on the molecular α and γ are large, in particular for the chain and the film because of the anisotropic surroundings, and that large clusters are required to obtain converged results. Finally, $\chi^{(1)}$ and $\chi^{(3)}$ have been calculated using a modified local-field theory including the induced dipole moments of the surrounding molecules explicitly. The corresponding refractive index and dielectric constant compare well with experiment. For $\chi^{(3)}$ the comparison with experiment is complicated by dispersion and vibrational contributions. Nonetheless, our value of $\chi^{(3)}$ is in good agreement with a recent quantum chemical calculation adopting a self-consistent reaction-field model.

In order to study the molecular properties of molecules in solution we have developed a mixed quantum mechanical and classical mechanics (QM/MM) model which we denoted the Discrete Solvent Reaction Field model. The model combines TD-DFT (QM) description of the solute molecule with a classical (MM) description of the discrete solvent molecules. The latter are represented using distributed atomic charges and polarizabilities. All the atomic parameters have been chosen so as to describe molecular gas phase properties of the solvent molecule, i.e. the atomic charges reproduce at least the molecular dipole moment and the atomic polarizabilities resproduce the molecular polarizability tensor using a modified dipole interaction model. The QM/MM interactions are introduced into the (time-dependent) Kohn-Sham equations and all interactions are solved self-consistently, thereby allowing for the solute to be polarized by the solvent. Furthermore, the inclusion of polarizabilities in the MM part allows for the solvent molecules to be polarized by the solute and by interactions with other solvent molecules. Using time-dependent response theory the linear response properties are caculated by solving a set of linear response equation iteratively. The first hyperpolarizability is calculated efficiently by taking advantage of the $(2n + 1)$ rule which allows for the quadratic response properties to be rewritten in terms of quantities known from the solution of the first order response equations. Finally, the second hyperpolarizability can be obtained by a combination with a finite field

differentiation. Initial applications of the model to calculate the dipole and quadrupole moments, vertical electronic excitation energies and frequency-dependent molecular (hyper)polarizabilities of a water molecule in a cluster of 127 classical water molecules are presented. The effect of using different exchange correlation (xc)-potentials is investigated and the results are compared with results from wave function methods combined with a similar solvent model, both at the correlated and uncorrelated level of theory. It is shown that for all properties investigated accurate results in agreement with correlated wave function results can be obtained using xc-potentials with a correct asymptotic behavior. The model reproduces the experimentally observed sign change in the first hyperpolarizaibility when going from the gas phase to the liquid phase. Furthermore, it is shown that the first hyperpolarizability is more sensitive to damping of the solvent-solute interactions at short range than the second hyperpolarizability.

Samenvatting

Onderwerp van dit proefschrift is het modelleren van moleculaire optische responseigenschappen en de toepassing van deze modellen op nanostructuren. Er bestaat zowel wetenschappelijk als technologisch veel belangstelling voor niet-lineaire optische (NLO) eigenschappen van materialen. Het technologisch aspect ligt in het maken en toepassen van deze nieuwe materialen in toekomstige elektronische en optische apparatuur, die tot een nieuw type informatietechnologie zou kunnen leiden. Het wetenschappelijk belang ligt—nog afgezien van het feit dat het nauwkeurig voorspellen van NLO effecten een grote uitdaging voor de theorie is—erin dat het begrijpen van NLO effecten fundamenteel inzicht kan opleveren in hoe bulkeigenschappen van materie in de gecondenseerde fase naar voren komt uit de eigenschappen van de individuele atomen of moleculen.

Geavanceerde kwantumchemische methoden zouden in principe ideale gereedschappen kunnen zijn om deze effecten te bestuderen, maar zij zijn alleen toepasbaar op tamelijk kleine moleculen. Voor grote moleculen en verzamelingen van moleculen is het modelleren daardoor beperkt tot minder geavanceerde methoden. In dit proefschrift hebben wij methoden ontwikkeld voor het berekenen van NLO eigenschappen van nanostructuren, d.w.z. moleculen en verzamelingen van moleculen die enkele duizenden atomen bevatten. De methoden werden toegepast op fullerenen, koolstofnanobuizen, grote clusters van moleculen en moleculen in oplossing.

In de algemene inleiding tot dit proefschrift wordt een overzicht gegeven van de basisconcepten van de niet-linaire optica, d.w.z. de expansie van de totale macroscopische polarisatie in materie in termen van machten van het macroscopische elektrisch veld, waarbij de expansiecoëfficiënten de macroscopische (niet-lineaire) susceptibiliteiten definiëren. Op dezelfde wijze wordt de totale microscopische polarisatie geëxpandeerd in termen van machten van het totale microscopische elektrische veld, hetgeen analoog leidt tot de definitie van microscopische (niet-lineaire) polariseerbaarheden. Vanuit een lokaal-veldaanpak laten we zien hoe een stel effectieve microscopische eigenschappen te definiëren zijn die gerelateerd kunnen worden aan macroscopische eigenschappen. Deze aanpak is gebaseerd op splitsing van het totale systeem in een macroscopisch gebied waarin zich een grote, virtuele, microscopische holte bevindt, waarbinnen het discrete elektrische veld—afkomstig

van de zich daarin bevindende moleculen—in detail wordt beschouwd. Omdat het discrete veld sterk afhangt van de lokale moleculaire configuratie, moet dit veld expliciet in beschouwing worden genomen in het microscopische model bij het berekenen van de niet-lineaire eigenschappen. Ook het elektrisch veld wordt in twee componenten opgesplitst. Het eerste deel komt voort uit interacties van het macroscopische veld met moleculen in de holte, m.a.w. het gevolg van de polarisatie van de moleculen door het macroscopische veld. Voor het tweede deel zijn interacties tussen de moleculen zonder macroscopische veld verantwoordelijk. Afhankelijk van het theoretisch model gebruikt voor het microscopische gebied, is deze opsplitsing van het discrete elektrische veld niet altijd mogelijk of nodig.

Sinds de ontdekking van het C_{60} fullereen is veel onderzoek gedaan aan de (niet-) lineaire optische eigenschappen. Experimenten en theorie hebben laten zien dat de derde niet-lineaire susceptibiliteit van C_{60} kleiner is dan eerst aangenomen. Om deze reden zijn de mogelijkheden tot het vergroten van de niet-lineairiteiten van fullerenen door middel van endoëdrische, exoëdrische of substituele doping van groot belang. We hebben de veranderingen in de tweede hyperpolariseerbaarheid (γ) door vervanging van C atomen door B en/of N atomen onderzocht. Met de tijdsafhankelijke dichtheidsfunctionaaltheorie (TD-DFT) vonden we kleine veranderingen in γ van C_{60} als gesubstitueerd werd met twee B of twee N atomen. Hoewel een toename van ca. 50% werd gevonden bij substitutie met één B en één N atoom, werd het effect van doping in het algemeen klein bevonden.

Een alternatief voor kwantumchemische methoden is gebaseerd op een voorstelling van moleculen als bestaand uit een stel geïnduceerde, wisselwerkende puntdipolen. In een extern elektrisch veld worden dipolen geïnduceerd die met elkaar wisselwerken. Een (anistrope) moleculaire polariseerbaarheidstensor (α) kan dan verkregen worden, zelfs als isotrope (atoom)polariseerbaarheden worden gebruikt in het model. Analoog kan een moleculaire γ^{mol} verkregen worden als een atomaire γ wordt opgenomen in het model. Verder wordt aangetoond dat dempen van de interatomaire interacties op korte afstand van groot belang is. Langs deze weg hebben we een puntdipoolinteractiemodel (PDI) ontwikkeld, gebaseerd op een parameterisatie van moleculaire eigenschappen verkregen uit kwantumchemische berekeningen. Het model omvat de frequentie-afhankelijkheid van α^{mol}, een verbeterde demping en γ^{mol}. Met atomaire polariseerbaarheden en atomaire parameters voor de demping en de frequentie-afhankelijkheid, reproduceert het model de moleculaire frequentie-afhankelijke polariseerbaarheid zoals verkregen uit ab initio berekeningen op het Hartree-Fock niveau. Ook is aangetoond dat de verschillen in γ^{mol} tussen kwantumchemische berekeningen en het PDI model gemiddeld ca. 10% zijn en kleiner dan 30%. Hoewel Hartree-Fock berekeningen geen correct antwoord geven, is het bemoedigend dat een eenvoudig model als PDI resultaten kan reproduceren die consistent zijn met kwantumchemische berekeningen. Daardoor zal het eenvoudig zijn het model opnieuw te parameteriseren, zodra meer geavanceerde kwantumchemische berekeningen standaard zijn voor grotere moleculen.

Het PDI model kan gebruikt worden voor eigenschappen van grote moleculen en clusters en daardoor voor het berekenen van effectieve, meetbare moleculaire macroscopische eigenschappen. Dat kan gedaan worden door de eigenschap (per molecule) te berekenen voor steeds grotere clusters, totdat geen verandering meer wordt gevonden. Echter, als

men geïnteresseerd is in de moleculaire eigenschappen van de individuele moleculen in het cluster, moet het totale resultaat verdeeld worden over de moleculen. Daarvoor hebben we een gelokaliseerde PDI (LPDI) model ontwikkeld dat het mogelijk maakt α en γ te splitsen in fragmentbijdragen.

Een belangrijk concept van het ontwerpen van nieuw NLO materiaal is het schaalgedrag van optische eigenschappen met toenemende grootte. In de limiet van oneindig lange ketens zullen zowel α^{mol} als γ^{mol} lineair toenemen met de ketenlengte. Van bijzonder belang is de zgn. verzadigingslengte, d.w.z. de lengte waarbij een eigenschap (α^{mol} of γ^{mol}) lineair begint toe te nemen. We hebben het PDI model gebruikt om γ^{mol} van koolstofnanobuizen met een lengte tot 75 nm te berekenen. Aangetoond wordt dat een atomistische representatie van nanobuizen op mesoschaal gebruikt kan worden om een kubische responseigenschap te verkrijgen tot de verzadiginglengte, bijvoorbeeld voor koolstofnanobuizen. Gevonden werd dat die, voor wat betreft γ^{mol}, vergelijkbaar zijn met geconjugeerde polymeren en derhalve veelbelovende kandidaten voor toekomstig NLO materiaal.

Zowel de dipool-dipool polariseerbaarheid en de tweede hyperpolariseerbaarheid (α en γ) als de corresponderende lineaire en derde orde susceptibiliteiten, $\chi^{(1)}$ en $\chi^{(3)}$, zijn met het PDI model berekend voor clusters van C_{60} fullereen. De grootteafhankelijkheid van een rechte keten, een monolaag film en een vlakgecentreerd kubisch kristal werden onderzocht. Gevonden werd dat het effect van de omringende moleculen op de moleculaire α en γ groot is, in het bijzonder in de rechte keten en de film, tengevolge van de anisotrope, en dat grote clusters nodig zijn om convergentie te bereiken. Tenslotte werden $\chi^{(1)}$ en $\chi^{(3)}$ berekend met een aangepast LPDI model waarin de dipoolmomenten, geïnduceerd in omringende moleculen, expliciet worden behandeld. De corresponderende brekingsindex en diëlectrische constante zijn goed vergelijkbaar met experimentele waarden. Deze vergelijking is voor $\chi^{(3)}$ bemoeilijkt door dispersie en vibrationele bijdragen. Niettemin is onze waarde in goede overeenkomst met die van een recente kwantumchemische berekening met een self-consistent reactieveldmodel.

Om moleculaire eigenschappen in oplossing te bestuderen ontwikkelden wij een kwantumchemisch-klassiek (QM/MM) model dat Discrete Solvent Reaction Field (DRF) wordt genoemd. In dit model wordt TD-DFT (QM) gebruikt voor de beschrijving van het opgeloste molecuul ("solute") en een klassieke weergave (MM) van de discrete omringende moleculen van het oplosmiddel ("solvent"). De laatste worden weergeven door gedistribueerde puntladingen en polariseerbaarheden. Alle atomaire parameters worden zo gekozen dat ze de moleculaire eigenschappen in de gasfase beschrijven, d.w.z. de puntladingen reconstrueren tenminste het moleculaire dipoolmoment en de atomaire polariseerbaarheden de moleculaire polariseerbaarheidstensor, waarbij een gemodificeerde dipool-dipoolinteractie wordt gebruikt. De QM/MM interacties worden toegevoegd aan de Kohn-Sham vergelijkingen en alle interacties worden selfconsistent opgelost, waarbij de "solute"gepolariseerd kan worden door de "solvent". Bovendien, door het opnemen van polariseerbaarheden in MM kunnen de moleculen van de solvent gepolariseerd worden door interacties met de solute en met andere solventmoleculen. Onder gebruik van TD-DFT response theorie worden de lineaire respons eigenschappen berekend door een stelsel van lineaire vergelijkingen iteratief op te lossen. De eerste hyperpolariseerbaarheid

wordt efficiënt berekend met de $(2n + 1)$ regel die het toestaat kwadratische responseigenschappen te herformuleren in termen van grootheden die bekend zijn uit de oplossing van de eerste orde responsvergelijkingen. Tenslotte kan de tweede hyperpolariseerbaarheid verkregen worden uit een combinatie met eindige velddifferentiaties. Eerste toepassingen van dit model zijn berekeningen van het dipool- en kwadrupoolmoment, verticale excitaties en frequentie-afhankelijke moleculaire (hyper)polariseerhardheden van één watermolecuul in een cluster van 127 klassieke watermoleculen. Het effect van verschillende exchange-correlatie (xc)potentialen werden onderzocht en de resultaten vergeleken met die van golffunctiemethoden gecombineerd met een soortgelijk solvatatiemodel, zowel op het ongecorreleerde als het gecorreleerd niveau van de theorie. Aangetoond wordt dat voor alle onderzochte eigenschappen goede overeenkomst met resultaten met gecorreleerde golffuncties verkregen wordt als xc-potentialen worden gebruikt met het juiste asymptotisch gedrag. Het model reproduceert de experimenteel waargenomen tekenverandering van de eerste hyperpolariseerbaarheid van water gaande van de gasfase naar de vloeibare fase. Voorts wordt aangetoond dat de eerste hyperpolariseerbaarheid gevoeliger is voor dempen van de solute-solvent korte afstand interacties dan de tweede.

Bibliography

[1] M. A. Ratner and D. Ratner, *Nanotechnology: A gentle introduction to the next big idea*, Prentice Hall, New Jersey, 2003.

[2] G. Stix, Scientific America **285**, 16 (2001).

[3] G. M. Whitesides and J. C. Love, Scientific America **285**, 32 (2001).

[4] M. Roukes, Scientific America **285**, 42 (2001).

[5] C. M. Lieber, Scientific America **285**, 50 (2001).

[6] R. E. Smalley, Scientific America **285**, 76 (2001).

[7] R. P. Feynmann, In *Engineering and Science*, The Caltech Alumni Magazine, 1960.

[8] P. N. Prasad and D. J. Williams, *Introduction to nonlinear optical effects in molecules and polymers*, Wiley, New York, 1991.

[9] J. Jortner and M. Ratner, editors, *Molecular Electronics*, Blackwell Science, Oxford, 1997.

[10] R. W. Boyd, *Nonlinear Optics*, Academic Press, San Diego, 1992.

[11] P. Ball, *Made to Measure, New Materials for the 21st century*, Princeton University Press, Princeton, New Jersey, 1997.

[12] D. R. Kanis, M. A. Ratner, and T. J. Marks, Chem. Rev. **94**, 195 (1994).

[13] J. L. Brédas, C. Adant, P. Tackx, A. Persoons, and B. M. Pierce, Chem. Rev. **94**, 243 (1994).

[14] D. P. Shelton and J. E. Rice, Chem. Rev. **94**, 3 (1994).

[15] D. M. Bishop, Adv. Quant. Chem. **25**, 1 (1994).

[16] Y. Luo, H. Ågren, P. Jørgensen, and K. V. Mikkelsen, Adv. Quant. Chem. **26**, 165 (1995).

[17] I. D. L. Albert, T. J. Marks, and M. A. Ratner, J. Phys. Chem. **100**, 9714 (1996).

[18] S. P. Karna, J. Phys. Chem. A **104**, 4671 (2000).

[19] L. R. Dalton et al., J. Mater. Chem. **9**, 1905 (1999).

[20] R. R. Tykwinski et al., J. Phys. Chem. B **102**, 4451 (1998).

[21] D. R. Kanis, M. A. Ratner, and T. J. Marks, J. Am. Chem. Soc. **114**, 10338 (1992).

[22] L. R. Dalton, J. Phys.: Condens. Matter **15**, R897 (2003).

[23] J. Bernholc, Phys. Today , 30 (1999).

[24] N. Bloembergen, *Nonlinear optics*, World Scientific Publishing, Singapore, 4th edition, 1996.

[25] D. M. Bishop, Rev. Mod. Phys. **62**, 343 (1990).

[26] P. N. Butcher and D. Cotter, *The elements of nonlinear optics*, Cambridge University Press, Cambridge, 1st edition, 1990.

[27] A. Willetts, J. E. Rice, D. M. Burland, and D. Shelton, J. Chem. Phys. **97**, 7590 (1992).

[28] B. J. Orr and J. F. Ward, Mol. Phys. **20**, 513 (1971).

[29] R. Wortmann and D. M. Bishop, J. Chem. Phys. **108**, 1001 (1998).

[30] H. A. Lorentz, *The theory of electrons*, B. G. Teubner, Leipzig, 1st edition, 1909.

[31] C. J. F. Böttcher, *Theory of Electric Polarization*, volume 1, Elsevier, Amsterdam, 2nd edition, 1973.

[32] L. Onsager, J. Am. Chem. Soc. **58**, 1486 (1936).

[33] J. D. Jackson, *Classical Electrodynamics*, John Wiley and Sons, New-York, 2nd edition, 1975.

[34] G. R. Meredith, Phys. Rev. B **24**, 5522 (1981).

[35] M. Malagoli and R. W. Munn, J. Chem. Phys. **107**, 7926 (1997).

[36] F. Jensen, *Introduction to computational chemistry*, Wiley, 1999.

[37] E. Runge and E. K. U. Gross, Phys. Rev. Lett. **52**, 997 (1984).

[38] E. K. U. Gross and W. Kohn, Adv. Quant. Chem. **21**, 255 (1990).

[39] R. van Leeuwen, Int. J. Mod. Phys. B **15**, 1969 (2001).

[40] M. E. Casida, in *Recent Advances in Density-Functional Methods*, edited by D. P. Chong, page 155, World Scientific, Singapore, 1995.

[41] M. E. Casida, in *Recent Developments and Applications of Modern Density Functional Theory*, edited by J. M. Seminario, Elsevier, Amsterdam, 1996.

[42] S. J. A. van Gisbergen et al., J. Chem. Phys. **105**, 3142 (1996).

[43] M. E. Casida, C. Jamorski, M. C. Casida, and D. R. Salahub, J. Chem. Phys. **108**, 4439 (1998).

[44] D. J. Tozer and N. C. Handy, J. Chem. Phys. **109**, 10180 (1998).

[45] P. R. T. Schipper, O. V. Gritsenko, S. J. A. van Gisbergen, and E. J. Baerends, J. Chem. Phys. **112**, 1344 (2000).

[46] M. E. Casida and D. R. Salahub, J. Chem. Phys. **113**, 8918 (2000).

[47] M. Grüning, O. V. Gritsenko, S. J. A. van Gisbergen, and E. J. Baerends, J. Chem. Phys. **114**, 652 (2001).

[48] M. Grüning, O. V. Gritsenko, S. J. A. van Gisbergen, and E. J. Baerends, J. Chem. Phys. **116**, 9591 (2002).

[49] J.-I. Iwata, K. Yabana, and G. F. Bertsch, J. Chem. Phys. **115**, 8773 (2001).

[50] H. H. Heinze, F. D. Sala, and A. Görling, J. Chem. Phys. **116**, 9624 (2002).

[51] P. Salek, O. Vahtras, T. Helgaker, and H. Ågren, J. Chem. Phys. **117**, 9630 (2002).

[52] P. Hohenberg and W. Kohn, Phys. Rev. **136**, B864 (1964).

[53] E. J. Baerends and O. V. Gritsenko, J. Phys. Chem. A **101**, 5383 (1997).

[54] W. Kohn and L. J. Sham, Phys. Rev. **140**, A1133 (1965).

[55] R. McWeeny, *Methods of molecular quantum mechanics*, Academic Press, London, 2nd edition, 1992.

[56] S. P. Karna and M. Dupuis, J. Comp. Chem. **12**, 487 (1991).

[57] S. J. A. van Gisbergen, J. G. Snijders, and E. J. Baerends, J. Chem. Phys. **109**, 10644 (1998).

[58] E. K. U. Gross, J. F. Dobson, and M. Petersilka, in *Density Functional Theory, Topics in current chemistry*, edited by Nalewajski, volume 181, Springer-Verlag Berlin Heidelberg, 1996.

[59] S. R. Marder et al., Science **276**, 1233 (1997).

[60] U. Gubler and C. Bosshard, Adv. Polym. Sci. **158**, 123 (2002).

[61] H. W. Kroto, J. R. Heath, S. O'brian, R. E. Curl, and R. E. Smalley, Nature **318**, 162 (1985).

[62] R.-H. Xie, Q. Rao, and L. Jensen, Optical nonlinearities of fullerenes and carbon nanotubes, in *Encyclopedia of Nanoscience and Nanotechnology*, edited by H. S. Nalwa, American Scientific Publisher, California, 2003, accepted.

[63] L. Jensen, P.-O. Åstrand, A. Osted, J. Kongsted, and K. V. Mikkelsen, J. Chem. Phys. **116**, 4001 (2002).

[64] S. J. A. van Gisbergen, J. G. Snijders, and E. J. Baerends, Phys. Rev. Lett. **78**, 3097 (1997).

[65] D. Jonsson, P. Norman, K. Ruud, and H. Ågren, J. Chem. Phys. **109**, 572 (1998).

[66] G. B. Talapatra et al., J. Phys. Chem. **96**, 5206 (1992).

[67] L. Geng and J. C. Wright, Chem. Phys. Lett. **249**, 105 (1996).

[68] J. Li et al., Chem. Phys. Lett. **288**, 175 (1998).

[69] P. Norman, Y. Luo, D. Jonsson, and H. Ågren, J. Chem. Phys. **106**, 8788 (1997).

[70] S. Wang et al., Phys. Rev. B **63**, 153408 (2001).

[71] R.-H. Xie, in *Handbook of Advanced Electronic and Photonic Materials and Devices*, edited by H. S. Nalwa, Academic Press, New York, 2000.

[72] J. Dong, J. Jiang, J. Yu, Z. D. Wang, and D. Y. Xing, Phys. Rev. B **52**, 9066 (1995).

[73] Q. Xu, J. Dong, J. Jiang, and D. Y. Xing, J. Phys. B: At. Mol. Opt. Phys. **29**, 1563 (1996).

[74] W. P. Su, J. R. Schrieffer, and A. J. Heeger, Phys. Rev. B **22**, 2099 (1980).

[75] L. Jensen, P. T. van Duijnen, J. G. Snijders, and D. P. Chong, Chem. Phys. Lett. **359**, 524 (2002).

[76] R.-H. Xie, G. W. Bryant, L. Jensen, J. Zhao, and V. H. Smith Jr., J. Chem. Phys. **118**, 8621 (2003).

[77] R.-H. Xie, L. Jensen, G. W. Bryant, J. Zhao, and V. H. Smith Jr., Chem. Phys. Lett. **375**, 445 (2003).

[78] R. H. Xie, Phys. Lett. A **259**, 51 (1999).

[79] L. Hultman et al., Phys. Rev. Lett. **87**, 225503 (2001).

[80] R.-H. Xie et al., Phys. Rev. Lett. **90**, 206602 (2003).

[81] D. Jonsson, K. Ruud, and P. R. Taylor, Comput. Phys. Commun. **128**, 412 (2000).

[82] B. Champagne et al., J. Chem. Phys. **109**, 10489 (1998).

[83] S. J. A. van Gisbergen et al., Phys. Rev. Lett. **83**, 694 (1999).

[84] M. van Faassen, P. L. de Boeij, R. van Leeuwen, J. A. Berger, and J. G. Snijders, Phys. Rev. Lett. **88**, 186401 (2002).

[85] M. Grüning, O. V. Gritzenko, and E. J. Baerends, J. Chem. Phys. **116**, 6435 (2002).

[86] P. Mori-Sánchez, Q. Wu, and W. Yang, J. Chem. Phys. **119**, 11001 (2003).

[87] L. Silberstein, Phil. Mag. **33**, 92 (1917).

[88] L. Silberstein, Phil. Mag. **33**, 215 (1917).

[89] L. Silberstein, Phil. Mag. **33**, 521 (1917).

[90] J. Applequist, J. R. Carl, and K. F. Fung, J. Am. Chem. Soc. **94**, 2952 (1972).

[91] J. Applequist, Acc. Chem. Res. **10**, 79 (1977).

[92] K. R. Sundberg, J. Chem. Phys. **66**, 114 (1977).

[93] B. T. Thole, Chem. Phys. **59**, 341 (1981).

[94] L. Jensen, P.-O. Åstrand, K. O. Sylvester-Hvid, and K. V. Mikkelsen, J. Phys. Chem. A **104**, 1563 (2000).

[95] L. Jensen, K. O. Sylvester-Hvid, K. V. Mikkelsen, and P.-O. Åstrand, J. Phys. Chem. A **107**, 2270 (2003).

[96] L. Jensen, P.-O. Åstrand, and K. V. Mikkelsen, Nano Lett. **3**, 661 (2003).

[97] L. Jensen, M. Swart, P. T. van Duijnen, and J. G. Snijders, J. Chem. Phys. **117**, 3316 (2002).

[98] R. S. Mulliken, J. Chem. Phys. **23**, 1833 (1955).

[99] L. Jensen, P.-O. Åstrand, and K. V. Mikkelsen, unpublished results.

[100] J. Kongsted, A. Osted, L. Jensen, P.-O. Åstrand, and K. V. Mikkelsen, J. Phys. Chem. B **105**, 10243 (2001).

[101] M. Schulz, S. Tretiak, V. Chernyak, and S. Mukamel, J. Am. Chem. Soc. **122**, 452 (2000).

[102] J. Tomasi and M. Persico, Chem. Rev. **94**, 2027 (1994).

[103] C. J. Cramer and D. G. Truhlar, Chem. Rev. **99**, 2161 (1999).

[104] M. Orozco and F. J. Luque, Chem. Rev. **100**, 4187 (2000).

[105] A. Warshel and M. Levitt, J. Mol. Bio. **103**, 227 (1976).

[106] B. T. Thole and P. T. van Duijnen, Theor. Chim. Acta **55**, 307 (1980).

[107] U. C. Singh and P. A. Kollman, J. Comp. Chem. **7**, 718 (1986).

[108] P. A. Bash, M. J. Field, and M. Karplus, J. Am. Chem. Soc. **109**, 8092 (1987).

[109] M. J. Field, P. A. Bash, and M. Karplus, J. Comp. Chem. **11**, 700 (1990).

[110] V. Luzhkov and A. Warshel, J. Comp. Chem. **13**, 199 (1992).

[111] R. V. Stanton, D. S. Hartsough, and K. M. Merz, J. Phys. Chem. **97**, 11868 (1993).

[112] A. H. de Vries et al., J. Comp. Chem. **16**, 37 (1995).

[113] I. Tuñón, M. T. C. Martins-Costa, C. Millot, M. F. Ruiz-López, and J. L. Rivail, J. Comp. Chem. **17**, 19 (1996).

[114] J. Gao, Methods and applications of combined quantum mechanical and molecular mechanical potentials, in *Reviews in Computational Chemistry*, edited by K. B. Lipkowitz and D. B. Boyd, volume 7, pages 119–185, VCH, New York, 1995.

[115] J. Gao, Acc. Chem. Res. **29**, 298 (1996).

[116] J. Gao and M. A. Thompson, editors, *Combined Quantum Mechanical and Molecular Mechanical Methods*, volume 712, ACS Symposium Series, 1998.

[117] L. Jensen, P. T. van Duijnen, and J. G. Snijders, J. Chem. Phys. **118**, 514 (2003).

[118] L. Jensen, P. T. van Duijnen, and J. G. Snijders, J. Chem. Phys. **119**, 3800 (2003).

[119] L. Jensen, P. T. van Duijnen, and J. G. Snijders, J. Chem. Phys. **119**, 12998 (2003).

[120] F. C. Grozema, R. W. J. Zijlstra, and P. T. van Duijnen, Chem. Phys. **256**, 217 (1999).

[121] J. Kongsted, A. Osted, K. V. Mikkelsen, and O. Christiansen, Chem. Phys. Lett. **364**, 379 (2002).

[122] J. Kongsted, A. Osted, K. V. Mikkelsen, and O. Christiansen, J. Chem. Phys. **118**, 1620 (2003).

[123] J. Kongsted, A. Osted, K. V. Mikkelsen, and O. Christiansen, J. Chem. Phys. **119**, 10519 (2003).

[124] J. Kongsted, A. Osted, K. Mikkelsen, and O. Christiansen, unpublished results.

[125] S. L. Shostak, W. L. Ebenstein, and J. S. Muenter, J. Chem. Phys. **94**, 5875 (1991).

[126] A. J. Russel and M. A. Spackman, Mol. Phys. **84**, 1239 (1995).

[127] P. Kaatz, E. A. Donley, and D. P. Shelton, J. Chem. Phys. **108**, 849 (1998).

[128] L. Jensen, M. Swart, and P. T. van Duijnen, unpublished results.

[129] S. J. A. van Gisbergen, J. G. Snijders, and E. J. Baerends, J. Chem. Phys. **109**, 10657 (1998).

[130] S. J. A. van Gisbergen, J. G. Snijders, and E. J. Baerends, Comput. Phys. Commun. **118**, 119 (1999).

[131] ADF 2000.01, http://www.scm.com, 2000.

[132] E. J. Baerends, D. E. Ellis, and P. Ros, Chem. Phys. **2**, 41 (1973).

[133] L. Versluis and T. Ziegler, J. Chem. Phys. **88**, 322 (1988).

[134] G. te Velde and E. J. Baerends, J. Comput. Phys. **99 (1)**, 84 (1992).

[135] C. Fonseca Guerra, J. G. Snijders, G. te Velde, and E. J. Baerends, Theor. Chim. Acta **99**, 391 (1998).

[136] G. D. Zeiss, W. R. Scott, N. Suzuki, and D. P. Chong, Mol. Phys. **37**, 1543 (1979).

[137] P. Calaminici, K. Jug, and A. M. Köster, J. Chem. Phys. **109**, 7756 (1998).

[138] A. D. Becke, Phys. Rev. A **38**, 3098 (1988).

[139] C. L. Lee, W. Yang, and R. G. Parr, Phys. Rev. B **37**, 785 (1988).

[140] J. P. Perdew et al., Phys. Rev. B **46**, 6671 (1991).

[141] R. van Leeuwen and E. J. Baerends, Phys. Rev. A **49**, 2421 (1994).

[142] E. Perrin, P. N. Prasad, P. Mougenot, and M. Dupuis, J. Chem. Phys. **91**, 4728 (1989).

[143] E. F. Archibong and A. J. Thakkar, Mol. Phys. **81**, 557 (1994).

[144] S. A. C. McDowell, R. D. Amos, and N. C. Handy, Chem. Phys. Lett. **235**, 1 (1995).

[145] S. P. Karna, G. B. Talapatra, and P. N. Prasad, J. Chem. Phys. **95**, 5873 (1991).

[146] N. Kurita, K. Kobayashi, H. Kumahora, and K. Tago, Phys. Rev. B **48**, 4850 (1993).

[147] S. P. Karna, P. N. Prasad, and M. Dupuis, J. Chem. Phys. **94**, 1171 (1991).

[148] M. Fanti, G. Orlandi, and F. Zerbetto, J. Phys. Chem. A **101**, 3015 (1997).

[149] J. Jiang, J. Dong, X. Wan, and D. Y. Xing, J. Phys. B: At. Mol. Opt. Phys. **31**, 3079 (1998).

[150] J. Olsen and P. Jørgensen, J. Chem. Phys. **82**, 3235 (1985).

[151] K. G. Denbigh, Trans. Faraday Soc. **36**, 936 (1940).

[152] B. C. Vickery and K. G. Denbigh, Trans. Faraday Soc. **45**, 61 (1949).

[153] K. J. Miller and J. A. Savchik, J. Am. Chem. Soc. **101**, 7206 (1979).

[154] Y. K. Kang and M. S. Jhon, Theor. Chim. Acta **61**, 41 (1982).

[155] K. J. Miller, J. Am. Chem. Soc. **112**, 8533 (1990).

[156] J. M. Stout and C. E. Dykstra, J. Am. Chem. Soc. **117**, 5127 (1995).

[157] J. M. Stout and C. E. Dykstra, J. Phys. Chem. A **102**, 1576 (1998).

[158] K. O. Sylvester-Hvid, P. Åstrand, M. A. Ratner, and K. V. Mikkelsen, J. Phys. Chem. A **103**, 1818 (1999).

[159] K. A. Bode and J. Applequist, J. Phys. Chem. **100**, 17820 (1996).

[160] R. R. Birge, J. Chem. Phys. **72**, 5312 (1980).

[161] R. R. Birge, G. A. Schick, and D. F. Bocian, J. Chem. Phys. **2256**, 1983 (79).

[162] A. H. de Vries, P. T. van Duijnen, R. W. Zijlstra, and M. Swart, J. Elec. Spec. Rel. Phen. **86**, 49 (1997).

[163] P. T. van Duijnen and M. Swart, J. Phys. Chem. A **102**, 2399 (1998).

[164] A. A. Chialvo and P. T. Cummings, Fluid Phase Equilibria **150-151**, 73 (1998).

[165] C. J. Burnham, J. Li, S. S. Xantheas, and M. Leslie, J. Chem. Phys. **110**, 4566 (1999).

[166] L. Jensen, O. H. Schmidt, K. V. Mikkelsen, and P.-O. Åstrand, J. Phys. Chem. B **104**, 10462 (2000).

[167] D. M. Bishop, Adv. Chem. Phys. **104**, 1 (1998).

[168] B. Champagne, Int. J. Quant. Chem. **65**, 689 (1997).

[169] A. D. Buckingham, Adv. Chem. Phys. **12**, 107 (1967).

[170] A. D. Buckingham, E. P. Concannon, and I. D. Hands, J. Phys. Chem. **98**, 10455 (1994).

[171] M. J. Grunning and R. E. Raab, Mol. Phys. **91**, 589 (1997).

[172] S. F. Boys, Proc. Roy. Soc. **200**, 542 (1950).

[173] T. Helgaker, P. Jørgensen, and J. Olsen, *Molecular Electronic-Structure Theory*, John Wiley and Sons, Chichester, 2000.

[174] G. A. van der Velde, MC and MD of H_2O. CECAM Workshop Report, 1972, Editor : H. J. C. Berendsen, unpublished.

[175] T. Helgaker et al., Dalton, an electronic structure program, Release 1.0 http://www.kjemi.uio.no/software/dalton, 1997.

[176] H. J. A. Jensen, H. Koch, P. Jørgensen, and J. Olsen, Chem. Phys. **119**, 297 (1988).

[177] H. J. A. Jensen, P. Jørgensen, and J. Olsen, J. Chem. Phys. **89**, 3654 (1988).

[178] A. J. Sadlej, Coll. Czech. Chem. Commun. **53**, 1995 (1988).

[179] The 74 molecules are : borazine, 1,2-dichloro-borazine, 2,4-dichloro-borazine, 1,2-difluoro-borazine, 1,4-difluoro-borazine, 2,4-difluoro-borazine, 1-amino-4-nitro-borazine, 2-amino-1-nitro-borazine, 2-amino-4-nitro-borazine, 4-amino-1-nitro-borazine, 1,3,5-triborane, 1,3-difluoro-1,3,5-triborane, 1-amino-3-nitro-1,3,5-triborane, 2-amino-4-nitro-1,3,5-triborane, cis-2,4-dichloro-1,3,5-triborane, cis-2,4-difluoro-1,3,5-triborane, trans-2,4-dichloro-1,3,5-triborane, trans-2,4-difluoro-1,3,5-triborane, 1,2-dichloro-1,3,5-triborane, 1,2-difluoro-1,3,5-triborane, 1-amino-2-nitro-1,3,5-triborane, 1,4-dichloro-1,3,5-triborane, 1,4-difluoro-1,3,5-triborane, 1-nitro-2-amino-1,3,5-triborane, 1-nitro-4-amino-1,3,5-triborane, 1-amino-4-nitro-1,3,5-triborane, hexahydro-1,3,5-triazine, 1,3-dichloro-tetrahydro-1,3,5-triazine, 1,3-difluoro-tetrahydro-1,3,5-triazine, 2-amino-4-nitro-tetrahydro-1,3,5-triazine, cis-2,4-dichloro-tetrahydro-1,3,5-triazine, cis-2,4-difluoro-tetrahydro-1,3,5-triazine, trans-2,4-dichloro-tetrahydro-1,3,5-triazine, trans-2,4-difluoro-tetrahydro-1,3,5-triazine, 1,2-dichloro-tetrahydro-1,3,5-triazine, 1-amino-2-nitro-tetrahydro-1,3,5-triazine, 2-amino-1-nitro-tetrahydro-1,3,5-triazine, 1,4-dichloro-tetrahydro-1,3,5-triazine, 1-amino-4-nitro-tetrahydro-1,3,5-triazine, 4-amino-1-nitro-tetrahydro-1,3,5-triazine, hexahydro-1,4-dibora-2,5-diazine, 1,3-dichloro-tetrahydro-1,4-dibora-2,5-diazine, 1,5-dichloro-tetrahydro-1,4-dibora-2,5-diazine, 3,5-dichloro-tetrahydro-1,4-dibora-2,5-diazine, 1,3-difluoro-tetrahydro-1,4-dibora-2,5-diazine, 1,5-difluoro-tetrahydro-1,4-dibora-2,5-diazine, 3,5-difluoro-tetrahydro-1,4-dibora-2,5-diazine, 1-amino-3-nitro-tetrahydro-1,4-dibora-2,5-diazine, 3-amino-1-nitro-tetrahydro-1,4-dibora-2,5-diazine, 1-amino-5-nitro-tetrahydro-1,4-dibora-2,5-diazine, 4-amino-2-nitro-tetrahydro-1,4-dibora-2,5-diazine, 2-amino-6-nitro-tetrahydro-1,4-dibora-2,5-diazine, 3-amino-5-nitro-tetrahydro-1,4-dibora-2,5-diazine, 1,2-dichloro-tetrahydro-1,4-dibora-2,5-diazine, 1,6-dichloro-tetrahydro-1,4-dibora-2,5-diazine, 1,2-difluoro-tetrahydro-1,4-dibora-2,5-diazine,

1,6-difluoro-tetrahydro-1,4-dibora-2,5-diazine, 2,3-difluoro-tetrahydro-1,4-dibora-2,5-diazine, 1-amino-2-nitro-tetrahydro-1,4-dibora-2,5-diazine, 1-amino-6-nitro-tetrahydro-1,4-dibora-2,5-diazine, 2-amino-1-nitro-tetrahydro-1,4-dibora-2,5-diazine, 3-amino-2-nitro-tetrahydro-1,4-dibora-2,5-diazine, 3-amino-4-nitro-tetrahydro-1,4-dibora-2,5-diazine, 1,4-dichloro-tetrahydro-1,4-dibora-2,5-diazine, 2,5-dichloro-tetrahydro-1,4-dibora-2,5-diazine, cis-3,6-dichloro-tetrahydro-1,4-dibora-2,5-diazine, trans-3,6-dichloro-tetrahydro-1,4-dibora-2,5-diazine, 1,4-difluoro-tetrahydro-1,4-dibora-2,5-diazine, 2,5-difluoro-tetrahydro-1,4-dibora-2,5-diazine, cis-3,6-difluoro-tetrahydro-1,4-dibora-2,5-diazine, trans-3,6-difluoro-tetrahydro-1,4-dibora-2,5-diazine, 2-amino-5-nitro-tetrahydro-1,4-dibora-2,5-diazine, trans-3-amino-6-nitro-tetrahydro-1,4-dibora-2,5-diazine, 3-nitro-2-amino-tetrahydro-1,4-dibora-2,5-diazine .

[180] IUPAC, *Nomenclature of Organic Chemistry. Sections A,B,C,D,E,F and H.*, Pergamon Press, Oxford, 1979.

[181] M. J. Frisch et al., Gaussian 94, Revision B.3, Gaussian, INC., Pittsburgh, PA, 1995.

[182] R. C. Weast, editor, *Handbook of Chemistry and Physics*, CRC Press, Boca Raton, 62nd edition, 1981.

[183] J. A. Pople and M. Gordon, J. Am. Chem. Soc. **89**, 4253 (1967).

[184] M. L. Olson and K. R. Sundberg, J. Chem. Phys. **69**, 5400 (1978).

[185] J. Applequist, J. Phys. Chem. **97**, 6016 (1993).

[186] L. Jensen, P.-O. Åstrand, and K. V. Mikkelsen, Int. J. Quant. Chem. **84**, 513 (2001).

[187] J. Applequist and C. O. Quicksall, J. Chem. Phys. **66**, 3455 (1977).

[188] S. F. Boys and F. Bernardi, Mol. Phys. **19**, 553 (1970).

[189] E. R. Andrew and D. Hyndman, Discuss. Faraday Soc. **19**, 195 (1955).

[190] P.-O. Åstrand, A. Wallqvist, and G. Karlström, J. Chem. Phys. **100**, 1262 (1994).

[191] P. A. Heiney et al., Phys. Rev. Lett. **66**, 2911 (1991).

[192] M. P. Hodges, A. J. Stone, and E. C. Lago, J. Phys. Chem. A **102**, 2455 (1998).

[193] R. L. Rowley and T. Pakkanen, J. Chem. Phys. **110**, 3368 (1999).

[194] R. L. Jaffe and G. D. Smith, J. Chem. Phys. **105**, 2780 (1996).

[195] D. M. Bishop and M. Dupuis, Mol. Phys. **88**, 887 (1996).

[196] C. E. Dykstra and S.-Y. Liu, J. Mol. Struct. (THEOCHEM) **135**, 357 (1986).

[197] J. D. Augspurger and C. E. Dykstra, Int. J. Quant. Chem. **43**, 135 (1992).

[198] M. Nakano, S. Yamada, S. Kiribayashi, and K. Yamaguchi, Synth. Met. **102**, 1542 (1999).

[199] G. Maroulis, J. Chem. Phys. **113**, 1813 (2000).

[200] J. Perez and M. Dupuis, J. Phys. Chem. **95**, 6525 (1991).

[201] S. Chen and H. A. Kurtz, J. Mol. Struct. (THEOCHEM) **388**, 79 (1996).

[202] B. Kirtman, C. E. Dykstra, and B. Champagne, Chem. Phys. Lett. **305**, 132 (1999).

[203] E. K. Dalskov, J. Oddershede, and D. M. Bishop, J. Chem. Phys. **108**, 2152 (1998).

[204] R. Antoine et al., J. Chem. Phys. **110**, 9771 (1999).

[205] K. Ruud, D. Jonsson, and P. R. Taylor, J. Chem. Phys. **114**, 4331 (2001).

[206] W. Krätschmer, L. D. Lamb, K. Fostiropoulos, and D. R. Huffman, Nature **347**, 354 (1990).

[207] A. F. Hebard, R. C. Haddon, R. M. Fleming, and A. R. Kortan, Appl. Phys. Lett. **59**, 2109 (1991).

[208] Z. H. Kafafi et al., Chem. Phys. Lett. **188**, 492 (1992).

[209] S. L. Ren et al., Appl. Phys. Lett. **61**, 124 (1992).

[210] A. Ritcher and J. Sturm, Appl. Phys. A **61**, 163 (1995).

[211] P. C. Eklund et al., Thin Solid Films **257**, 211 (1995).

[212] C. Sauteret et al., Phys. Rev. Lett. **36**, 956 (1976).

[213] G. P. Agrawal, C. Cojan, and C. Flytzanis, Phys. Rev. B **17**, 776 (1978).

[214] W. Wu, Phys. Rev. Lett. **61**, 1119 (1988).

[215] J. R. Heflin, K. Y. Wong, O. Zamani-Khamiri, and A. F. Garito, Phys. Rev. B **38**, 1573 (1988).

[216] M. Sinclair, D. Moses, K. Akagi, and A. J. Heeger, Phys. Rev. B **38**, 10724 (1988).

[217] W.-S. Fann et al., Phys. Rev. Lett. **62**, 1492 (1989).

[218] H. Thienpont, G. L. J. A. Rikken, E. W. Meijer, W. ten Hoeve, and H. Wynberg, Phys. Rev. Lett. **65**, 2141 (1990).

[219] S. P. Karna, G. B. Talapatra, W. M. K. P. Wijekoon, and P. N. Prasad, Phys. Rev. A **45**, 2763 (1992).

[220] P. Wautelet et al., Macromolecules **29**, 446 (1996).

[221] C. Weder, M. S. Wrighton, R. Spreiter, C. Bosshard, and P. Günther, J. Phys. Chem. **100**, 18931 (1996).

[222] D. Lu, B. Marten, M. Ringnalda, R. A. Friesner, and W. A. Goddard III, Chem. Phys. Lett. **257**, 224 (1996).

[223] X. Zhan, Y. Liu, D. Zhu, W. Huang, and Q. Gong, Chem. Mater. **13**, 1540 (2001).

[224] X. Zhan et al., Chem. Phys. Lett. **343**, 493 (2001).

[225] X. Zhan, M. Yang, G. Xu, X. Liu, and P. Ye, Macromol. Rapid Commun. **22**, 358 (2001).

[226] F. L. Gu, D. M. Bishop, and B. Kirtman, J. Chem. Phys. **115**, 10548 (2001).

[227] Z. Dai et al., Chem. Phys. Lett. **317**, 9 (2000).

[228] M. Yang and Y. Jiang, Phys. Chem. Chem. Phys. **3**, 4213 (2001).

[229] W. J. Blau et al., Phys. Rev. Lett. **67**, 1423 (1991).

[230] R. J. Knize and J. P. Partanen, Phys. Rev. Lett. **68**, 2704 (1992).

[231] Z. H. Kafafi, F. J. Bartoli, J. R. Lindle, and R. G. S. Pong, Phys. Rev. Lett. **68**, 2705 (1992).

[232] S. R. Flom, R. G. S. Pong, F. J. Bartoli, and Z. H. Kafafi, Phys. Rev. B **46**, 15598 (1992).

[233] Z. Shuai and J. L. Brédas, Phys. Rev. B **46**, 16135 (1992).

[234] F. Kajzar, C. Taliani, R. Danieli, S. Rossini, and R. Zamboni, Phys. Rev. Lett. **73**, 1617 (1994).

[235] H. Liu, B. Taheri, and W. Jia, Phys. Rev. B **49**, 10166 (1994).

[236] F. Sun et al., Phys. Rev. B **51**, 4614 (1995).

[237] C. E. Moore, B. H. Cardelino, and X.-Q. Wang, J. Phys. Chem. **100**, 4685 (1996).

[238] G. Gu et al., Chem. Phys. Lett. **289**, 167 (1998).

[239] X. Liu et al., Appl. Phys. Lett. **74**, 164 (1999).

[240] S. Wang et al., Chem. Phys. Lett. **320**, 411 (2000).

[241] W. P. Su, J. R. Schrieffer, and A. J. Heeger, Phys. Rev. Lett. **42**, 1698 (1979).

[242] A. J. Heeger, S. Kivelson, J. R. Schrieffer, and W.-P. Su, Rev. Mod. Phys. **60**, 781 (1988).

[243] J. Yu and W. P. Su, Phys. Rev. B **44**, 13315 (1991).

[244] R.-H. Xie and J. Jiang, Chem. Phys. Lett. **280**, 66 (1997).

[245] R.-H. Xie and J. Jiang, Appl. Phys. Lett. **71**, 1029 (1997).

[246] R.-H. Xie and J. Jiang, J. Appl. Phys. **83**, 3001 (1998).

[247] X. Wan, J. Dong, and D. Y. Xing, Phys. Rev. B **58**, 6756 (1998).

[248] O. Engkvist, P.-O. Åstrand, and G. Karlström, Chem. Rev. **100**, 4087 (2000).

[249] J. Applequist, J. Chem. Phys. **83**, 809 (1985), Erratum in 98, 7664, 1993.

[250] A. D. Buckingham and B. J. Orr, Quart. Rev. **21**, 195 (1967).

[251] T. Zhou and C. E. Dykstra, J. Phys. Chem. A **104**, 2204 (2000).

[252] F. Torrens, J. Sánchez-Marín, and I. Nebot-Gil, J. Mol. Graph. **14**, 245 (1996).

[253] Z. G. Soos, E. V. Tsiper, and R. A. Pascal Jr, Chem. Phys. Lett. **342**, 652 (2001).

[254] J. Applequist, J. Chem. Phys. **58**, 4251 (1973).

[255] J. Applequist, J. Phys. Chem. A **102**, 7723 (1998).

[256] D. F. Bocian, G. A. Schick, and R. R. Birge, J. Chem. Phys. **74**, 3660 (1981).

[257] J. Applequist, K. R. Sundberg, M. L. Olson, and L. C. Weiss, J. Chem. Phys. **70**, 1240 (1979), Erratum in **71**, 2330, 1979.

[258] B. Shanker and J. Applequist, J. Chem. Phys. **104**, 6109 (1996).

[259] J. Applequist and K. A. Bode, J. Phys. Chem. A **104**, 7129 (2000).

[260] J. Applequist, J. Phys. Chem. A **104**, 7133 (2000), Erratum in **104**, 10994, 2000.

[261] B. F. Levine and C. G. Bethea, J. Chem. Phys. **63**, 2666 (1975).

[262] K. R. Sundberg, J. Chem. Phys. **66**, 1475 (1977), Erratum in *J. Chem. Phys.* **67**, 4314, 1977.

[263] T. Bancewicz, J. Chem. Phys. **111**, 7440 (1999).

[264] F. Sim, S. Chin, M. Dupuis, and J. E. Rice, J. Phys. Chem. **97**, 1158 (1993).

[265] C. Adant, J. L. Brédas, and M. Dupuis, J. Phys. Chem. A **101**, 3025 (1997).

[266] G. Maroulis, J. Phys. Chem. A **104**, 4772 (2000).

[267] T. Pluta and A. J. Sadlej, J. Chem. Phys. **114**, 136 (2001).

[268] P. Norman, D. Jonsson, O. Vahtras, and H. Ågren, Chem. Phys. Lett. **242**, 7 (1995).

[269] P. Norman et al., Chem. Phys. Lett. **253**, 1 (1996).

[270] T. Pluta and A. J. Sadlej, Chem. Phys. Lett. **297**, 391 (1998).

[271] O. Quinet and B. Champagne, J. Chem. Phys. **109**, 10594 (1998).

[272] R. Zanasi, Chem. Phys. Lett. **315**, 217 (1999).

[273] The 72 molecules are : 1,2,3-trifluorobenzene, 1,2,3,4-tetrafluorobenzene, 1,2,3,5-tetrafluorobenzene, 1,2,4,5-tetrafluorobenzene, 1,3-dichlortetrafluorobenzene, 1,3,5-trichlorobenzene, 1,3,5-trifluorobenzene, 2,3,5,6-tetrafluoro-1,4-dichlorobenzene, 2,3,5,6-tetrafluorochlorobenzene, 2,4,6-trifluorochlorobenzene, 2,5-difluoro-1,3-dichlorobenzene, 2,6-difluoro-1,4-dichlorobenzene, 2,6-difluorochlorobenzene, 3,4,5-trifluorochlorobenzene, 3,5-difluorochlorobenzene, 4,5-difluoro-1,2-dichlorobenzene, 4,6-difluoro-1,3-dichlorobenzene, benzene, fluorobenzene, hexafluorobenzene, m-dichlorobenzene, m-difluorobenzene, o-dichlorobenzene, o-difluorobenzene, p-dichlorobenzene, p-difluorobenzene, p-fluorochlorobenzene, pentafluorobenzene, pentafluorochlorobenzene, phenol, toluene, ethylamide, methane, ethane, propane, chloromethane, methanol, pentane, hexane, 1,1,1-trichloroethane, aminomethane, aminoethane, aminopropane, acetone, 3-pentanone 4-heptanone N,N-dimethylformamide, N-methylacetamide, N-methylformamide, malonic acid, acetaldehyde, aminobutane, formic acid, nitroethane, nitromethane, butanal, nitropropane, butanol, butanoic acid, trichloromethane, chloroformamide, cyanobutane, cyanoethane, cyanomethane, cyanopropane, pentanol, propanol, 2,3-dichlororbutane, propanamide, 1,1,2,2-tetrachloroethane, tetrachloromethane, acetic acid .

[274] H. Reis, M. G. Papadopoulos, and R. W. Munn, J. Chem. Phys. **109**, 6828 (1998).

[275] N. Matsuzawa and D. A. Dixon, J. Phys. Chem. **96**, 6241 (1992).

[276] D. M. Bishop and P. Norman, Calculations of dynamic hyperpolarizabilities for small and medium sized molecules, in *Handbook of Advanced Electronic and Photonic Materials*, edited by H. S. Nalwa, Academic Press, San Diego, 2000.

[277] K. V. Mikkelsen, Y. Luo, H. Ågren, and P. Jørgensen, J. Chem. Phys. **102**, 9362 (1995).

[278] R. Cammi, M. Cossi, and J. Tomasi, J. Chem. Phys. **104**, 4611 (1996).

[279] Y. Tu and A. Laaksonen, Chem. Phys. Lett. **329**, 283 (2000).

[280] R. Cammi, B. Mennucci, and J. Tomasi, J. Phys. Chem. A **104**, 4690 (2000).

[281] P. Macak, P. Norman, Y. Luo, and H. Ågren, J. Chem. Phys. **112**, 1868 (2000).

[282] K. V. Mikkelsen, P. Jørgensen, and H. J. A. Jensen, J. Chem. Phys. **100**, 6597 (1994).

[283] J. C. Contador, M. A. Aguilar, and F. J. Olivares del Valles, Chem. Phys. **214**, 113 (1997).

[284] C. Cappelli, B. Mennucci, C. O. da Solva, and J. Tomasi, J. Chem. Phys. **112**, 5382 (2000).

[285] J. Cioslowski, Phys. Rev. Lett. **62**, 1469 (1989).

[286] A. Morita and S. Kato, J. Chem. Phys. **110**, 11987 (1999).

[287] M. Moraldi, M. Celli, and F. Barocchi, Phys. Rev. A **40**, 1116 (1989).

[288] M. H. Champagne, X. Li, and K. L. C. Hunt, J. Chem. Phys. **112**, 1893 (2000).

[289] S. J. A. van Gisbergen, J. G. Snijders, and E. J. Baerends, J. Chem. Phys. **103**, 9347 (1995).

[290] C. Fonseca Guerra, J. G. Snijders, G. te Velde, and E. J. Baerends, Theor. Chem. Acc. **99**, 391 (1998).

[291] A. H. Narten, J. Chem. Phys. **56**, 5681 (1972).

[292] A. H. Narten and W. E. Thiessen, Science **217**, 1033 (1982).

[293] M. Swart and P. T. van Duijnen, In preparation.

[294] S. Iijima, Nature **354**, 56 (1991).

[295] I. D. W. Samuel et al., Science **265**, 1070 (1994).

[296] S. Mukamel, A. Takahashi, H. X. Wang, and G. Chen, Science **266**, 250 (1994).

[297] R.-H. Xie, J. Chem. Phys. **108**, 3626 (1998).

[298] B. Kirtman, J. L. Toto, K. A. Robins, and M. Hasan, J. Chem. Phys. **102**, 5350 (1995).

[299] H. Dai et al., J. Phys. Chem. B **103**, 11246 (1999).

[300] M. Terrones, W. K. Hsu, H. W. Kroto, and D. R. M. Walton, Topics Curr. Chem. **199**, 189 (1999).

[301] P. Avouris, Acc. Chem. Res. **35**, 1026 (2002).

[302] P. Avouris, Chem. Phys. **281**, 429 (2002).

[303] G. Brusatin and R. Signorini, J. Mater. Chem. **12**, 1964 (2002).

[304] A. Ballard, K. Bonin, and J. Louderback, J. Chem. Phys. **113**, 5732 (2000).

[305] M. van Faassen, L. Jensen, P. de Boeij, and P. T. van Duijnen, unpublished results.

[306] M. van Faassen, P. L. de Boeij, R. van Leeuwen, J. A. Berger, and J. G. Snijders, J. Chem. Phys. **118**, 1044 (2003).

[307] E. A. Perpéte, B. Champagne, and B. Kirtman, Phys. Rev. B **61**, 13137 (2000).

[308] Y. Luo, P. Norman, P. Macak, and H. Ågren, Phys. Rev. B **61**, 3060 (2000).

[309] R. R. Birge, J. Chem. Phys. **72**, 5312 (1980).

[310] W. L. Delano, The PyMOL Molecular Graphics System, http://www.pymol.org, 2002.

[311] B. W. Smith, M. Monthioux, and D. E. Luzzi, Nature **396**, 323 (1998).

[312] J. S. Meth, H. Vanherzeele, and W. Y., Chem. Phys. Lett. **197**, 26 (1992).

[313] P. L. Hanse, P. J. Fallon, and W. Krätschmer, Chem. Phys. Lett. **181**, 367 (1991).

[314] C. Bosshard, P. Gubler, U. snd Kaatz, W. Mazerant, and U. Meier, Phys. Rev. B **61**, 10688 (2000).

[315] U. Gubler and C. Bosshard, Phys. Rev. B **61**, 10702 (2000).

[316] F. P. Strohkendl et al., J. Phys. Chem. B **101**, 8802 (1997).

[317] P. D. Maker and R. W. Terhune, Phys. Rev. **137**, A801 (1965).

[318] T. Wesolowski and A. Warshel, J. Phys. Chem. **98**, 5183 (1994).

[319] V. Barone, M. Cossi, and T. Tomasi, J. Chem. Phys. **107**, 3210 (1997).

[320] A. Pullman and B. Pullman, Quart. Rev. Biophys. **7**, 505 (1975).

[321] R. Car and M. Parrinello, Phys. Rev. Lett. **55**, 2471 (1985).

[322] E. R. Batista, S. S. Xantheas, and H. Jónsson, J. Chem. Phys. **111**, 6011 (1999).

[323] L. Delle Site, A. Alavi, and R. M. Lynden-Bell, Mol. Phys. **96**, 1683 (1999).

[324] Y. Tu and A. Laaksone, J. Chem. Phys. **111**, 7519 (1999).

[325] M. Freindorf and J. Gao, J. Comp. Chem. **17**, 386 (1996).

[326] J. A. C. Rullmann and P. T. van Duijnen, Mol. Phys. **63**, 451 (1988).

[327] P. Ahlström, A. Wallqvist, S. Engström, and B. Jönsson, Mol. Phys. **68**, 563 (1989).

[328] S. Kuwajima and A. Warshel, J. Phys. Chem. **94**, 460 (1990).

[329] L. X. Dang, J. Chem. Phys. **97**, 2183 (1992).

[330] J.-C. Soetens and C. Milot, Chem. Phys. Lett. **235**, 22 (1995).

[331] L. X. Dang and T.-M. Chang, J. Chem. Phys. **106**, 8149 (1997).

[332] T. A. Halgren and W. Damm, Curr. Opin. Struc. Biol. **11**, 236 (2001).

[333] M. A. Thompson and G. K. Schenter, J. Phys. Chem. **99**, 6374 (1995).

[334] G. Jansen, F. Colonna, and J. G. Ángyán, Int. J. Quant. Chem. **58**, 251 (1996).

[335] P. N. Day et al., J. Chem. Phys. **105**, 1968 (1996).

[336] J. Gao and M. Freindorf, J. Phys. Chem. A **101**, 3182 (1997).

[337] J. Gao, J. Comp. Chem. **18**, 1061 (1997).

[338] T. D. Poulsen, J. Kongsted, A. Osted, P. R. Ogilby, and K. V. Mikkelsen, J. Chem. Phys. **115**, 2393 (2001).

[339] M. Dupuis, M. Aida, Y. Kawashima, and K. Hirao, J. Chem. Phys. **117**, 1242 (2002).

[340] G. te Velde et al., J. Comp. Chem. **22**, 931 (2001).

[341] J. P. Perdew, Phys. Rev. B **33**, 8822 (1986).

[342] T. D. Poulsen, P. R. Ogilby, and K. V. Mikkelsen, J. Chem. Phys. **116**, 3730 (2002).

[343] G. Maroulis, Chem. Phys. Lett. **289**, 403 (1998).

[344] M. L. Sanchez Mendoza, M. A. Aguilar, and F. J. Olivares del Vall, J. Mol. Struct. (THEOCHEM) **426**, 181 (1998).

[345] P. Duffy, D. P. Chong, and M. Dupuis, J. Chem. Phys. **102**, 3312 (1995).

[346] F. De Proft, F. Tielens, and P. Geerlings, J. Mol. Struct. (THEOCHEM) **506**, 1 (2000).

[347] C. C. Pye and T. Ziegler, Theor. Chim. Acta **101**, 396 (1999).

[348] Y. S. Badyal et al., J. Chem. Phys. **112**, 9206 (2000).

[349] S. L. Carnie and G. N. Patey, Mol. Phys. **47**, 1129 (1982).

[350] K. Watanabe and M. L. Klein, Chem. Phys. **131**, 157 (1989).

[351] C. Coulson and D. Eisenberg, Proc. R. Soc. London A **291**, 445 (1966).

[352] E. R. Batisa, S. S. Xantheas, and H. Jónsson, J. Chem. Phys. **109**, 4546 (1998).

[353] P. L. Silverstrelli and M. Parrinello, Phys. Rev. Lett. **82**, 3308 (1999).

[354] P. L. Silverstrelli and M. Parrinello, J. Chem. Phys. **111**, 3572 (1999).

[355] L. X. Dang, J. Phys. Chem. B **192**, 620 (1998).

[356] A. V. Gubskaya and P. G. Kusalik, Mol. Phys. **99**, 1107 (2001).

[357] R. Cammi, B. Mennucci, and J. Tomasi, J. Phys. Chem. A **104**, 5631 (2000).

[358] C. Adamo and V. Barone, Chem. Phys. Lett. **330**, 152 (2000).

[359] M. Cossi and V. Barone, J. Chem. Phys. **115**, 4708 (2001).

[360] T. D. Poulsen, P. R. Ogilby, and K. V. Mikkelsen, J. Chem. Phys. **115**, 7843 (2001).

[361] ADF 2002.03, http://www.scm.com, 2003.

[362] O. V. Gritsenko, P. R. T. Schipper, and E. J. Baerends, Chem. Phys. Lett. **302**, 199 (1999).

[363] O. V. Gritsenko, P. R. T. Schipper, and E. J. Baerends, Int. J. Quant. Chem. **76**, 407 (2000).

[364] D. P. Chong, O. V. Grtisenko, and E. J. Baerends, J. Chem. Phys. **116**, 1760 (2002).

[365] R. J. Buenker and S. D. Peyerimhoff, Chem. Phys. Lett. **29**, 253 (1974).

[366] M. B. Robin, *Higher Excited States of Polyatomic Molecules*, volume 1, Academic Press, New York and London, 1974.

[367] G. D. Kerr, R. N. Hamm, M. W. Williams, R. D. Birkhoff, and L. R. Painter, Phys. Rev. A **5**, 2523 (1972).

[368] M. Michaud, P. Cloutier, and L. Sanche, Phys. Rev. A **44**, 5624 (1991).

[369] B. T. Thole and P. T. van Duijnen, Chem. Phys. **71**, 211 (1982).

[370] J. Kongsted, A. Osted, K. V. Mikkelsen, and O. Christiansen, Mol. Phys. **100**, 1813 (2002).

[371] O. Christiansen, J. Gauss, and J. F. Stanton, Chem. Phys. Lett. **305**, 147 (1999).

[372] W. F. Murphy, J. Chem. Phys. **67**, 5877 (1977).

[373] H. Reis, M. G. Papadopoulos, and D. N. Theodorou, J. Chem. Phys. **114**, 876 (2001).

[374] A. Morita, J. Comp. Chem. **23**, 1466 (2002).

[375] F. Kajzar and J. Messier, Phys. Rev. A **32**, 2352 (1985).

[376] I. Thormahlen, J. Straub, and U. Grigul, J. Phys. Chem. Ref. Data **14**, 933 (1985).

[377] T. van Mourik and R. J. Gdanitz, J. Chem. Phys. **116**, 9620 (2002).

[378] A. J. Cohen, N. C. Handy, and D. J. Tozer, Chem. Phys. Lett. **303**, 391 (1999).

[379] H. Reis, S. G. Raptis, and M. G. Papadopoulos, Chem. Phys. **263**, 301 (2001).

[380] M. Eichinger, P. Tavan, J. Hutter, and M. Parrinello, J. Chem. Phys. **110**, 10452 (1999).

[381] H. Takahashi, T. Hori, H. Hashimoto, and T. Nitta, J. Comp. Chem. **22**, 1252 (2001).

[382] A. Laio, J. VandeVondele, and U. Rothlisberger, J. Chem. Phys. **116**, 6941 (2002).

[383] J. F. Ward and C. K. Miller, Phys. Rev. A **19**, 826 (1979).

[384] B. F. Levine and C. G. Bethea, J. Chem. Phys. **65**, 2429 (1976).

[385] P. Kaatz and D. P. Shelton, J. Chem. Phys. **105**, 3918 (1996).

[386] I. Shoji, T. Kondo, and R. Ito, Optical and Quantum Electronics **34**, 797 (2002).

List of Publications

1. J. Kongsted, A. Osted, L. Jensen, P.-O. Åstrand, K. V. Mikkelsen.
   Frequency-dependent polarizability of boron nitride nanotubes: A theoretical study
   J. Phys. Chem. B, **105**, 10243, 2001
   Reference 100

2. T. L. C. Jansen, M. Swart, L. Jensen, P. Th. van Duijnen, J. G. Snijders, K. Duppen.
   Collision effects in the nonlinear Ramon response of liquid carbon disulfide
   J. Chem. Phys., **116**, 3277, 2002

3. L. Jensen, P.-O. Åstrand, A. Osted, J. Kongsted, K. V. Mikkelsen.
   Polarizability of molecular clusters as calculated by a dipole interaction model
   J. Chem. Phys., **116**, 4001, 2002
   Chapter 3, Reference 63

4. L. Jensen, P. Th. van Duijnen, J. G. Snijders, D. P. Chong.
   Time-dependent density functional study of the static second hyperpolarizability of BB-, NN-and BN-substituted C_{60}
   Chem. Phys. Lett., **359**, 524, 2002
   Chapter 2, Reference 75

5. L. Jensen, M. Swart, P. Th. van Duijnen, J. G. Snijders.
   Medium pertubations on the molecular polarizability calculated within a localized dipole interaction model
   J. Chem. Phys., **117**, 3316, 2002
   Chapter 5, Reference 97

6. L. Jensen, K. O. Sylvester-Hvid, K. V. Mikkelsen, P.-O. Åstrand.
   A dipole interaction model for the molecular second hyperpolarizability
   J. Phys. Chem. A, **107**, 2270, 2003
   Chapter 4, Reference 95

7. L. Jensen, P. Th. van Duijnen, J. G. Snijders.
   A discrete solvent reaction field model within density functional theory
   J. Chem. Phys., **118**, 514, 2003
   Chapter 8, Reference 117

8. L. Jensen, P.-O. Åstrand, K. V. Mikkelsen.
   Saturation of the third-order polarizability of carbon nanotubes characterized by a dipole interaction model
   Nano Lett., **3**, 661, 2003
   Chapter 6, References 96

9. R.-H. Xie, G. W. Bryant, L. Jensen, J. Zhao, V. H. Smith Jr.
   First-principles calculations of structural, electronic, vibrational and magnetic properties of C_{60} and $C_{48}N_{12}$: a comparative study
   J. Chem. Phys., **118**, 8621, 2003
   Reference 76

10. R.-H. Xie, L. Jensen, G. W. Bryant, J. Zhao, V. H. Smith Jr.
    Bonding, (hyper)polarizability and vibrational properties of heterofullerene $C_{48}N_{12}$
    Chem. Phys. Lett., **375**, 445, 2003
    Reference 77

11. L. Jensen, P. Th. van Duijnen, J. G. Snijders.
    A discrete solvent reaction field model for calculating molecular linear response properties in solution
    J. Chem. Phys., **119**, 3800, 2003
    Chapter 9, Reference 118

12. L. Jensen, P. Th. van Duijnen, J. G. Snijders.
    A discrete solvent reaction field model for calculating frequency-dependent hyperpolarizabilities of molecules in solution
    J. Chem. Phys., **119**, 12998, 2003
    Chapter 10, Reference 119

13. L. Jensen, P.-O. Åstrand, K. V. Mikkelsen.
    Microscopic and macroscopic polarization in C_{60} fullerene clusters as calculated by an electrostatic interaction model
    submitted, 2003
    Chapter 7

14. R.-H. Xie, Q. Rao, L. Jensen.
    Nonlinear optics of fullerenes and carbon nanotubes
    in "Encyclopedia of Nanoscience and Nanotechnology", **accepted**, 2003
    Reference 62